REHVA Community of Young Professionals

BOOK OF PAPERS

2019

Bucharest, Romania

HVAC World
Student Competition 2019

REHVA
Student Competition 2019

Our Sponsors

BOOK OF PAPERS

2019

Bucharest, Romania

Table of content

Introduction

Arash Rasooli

The Book of papers is presented by RCYP (REHVA Community of Young Professionals). The RCYP aims to facilitate professional activities and knowledge exchange between young professionals (below 35 years) in the fields of indoor climate, HVAC, building physics, and building services. In the current book, the papers written by the participants of the REHVA Student Competition and the ones from the HVAC World Student Competition are presented. The winners of each competition are also shown at the beginning. At the end of the book, the photos of the events can be found.

REHVA Student Competition

Ever since 2005, REHVA has been organizing a yearly international competition to award the best HVAC students in Europe. REHVA member associations nominate one entry per country to the competition after having organized their national level competitions. The submitted works are based on a Master or Bachelor work and can cover any topic in the fields related to REHVA. The Student competitions are organized during the REHVA Annual Meetings and the Students receive a trophy with their names engraved in it, which is then handed over next year to the next winner. The trophy has been traveling long in the past decade, carrying the names of all the proud winners since 2005.

HVAC World Student Competition

In 2013, REHVA founded a World Student competition with a number of its international partner associations. Ever since 2016, the HVAC World Student Competition has been taking place between students nominated by REHVA (EU), ASHRAE (United States), CAHVAC (China), FAIAR (South America), ISHRAE (India), SAREK (South Korea) and SHASE (Japan). Each association may send one candidate from their region or continent. REHVA's candidate in the HVAC World Student Competition is the winner from REHVA Student Competition. The other MoU partners organise the HVAC World Student Competition according to the same rules around the world with the participation of REHVA in the jury. The first competition was held in 2016 by REHVA in Denmark. REHVA co-finances the participation of the European candidate in these global competitions.

REHVA and HVAC World Student Competitions 2019

The REHVA Student Competition 2019 and the HVAC World Student Competition 2019 were held between the 26th-29th of May at CLIMA Congress 2019. Over 15 students had participated in the event. The 1st place and the trophy were awarded to Janis Müller, from the University of Applied Sciences of Erfurt, Germany, on the topic "Development of an adaptive aero foil contour for use as a fan blade". The two other prizes were won by Laura Nebot Andres from Spain and a joint team from Denmark, Michael Rosenlund and Yanting Li.

The jury team of REHVA Student Competition 2019 was composed by Pedro Vicente Quiles, Jorma Säteri, Murat Çakan, Birgit Mueller, Uwe Schulz , Jiri Hirs, Robert Gavriliuc and chaired by Manuel Gameiro da Silva .

The HVAC World Student Competition 2019 took place the day after the REHVA Student Competition 2019, in which 6 students had participated. The award went out to Yijun Fu from the College of Environment and Building, University of Shanghai for Science and Technology, China (CCHVAC), whom received a first-place prize for the topic: "Research on Heat Transfer Characteristics of Carbon Dioxide in Microchannel Evaporator". The two other awards went to Janis Müller from Germany (REHVA) and Rohit Upadhyay from ASHRAE (USA).

The jury team of HVAC World Student Competition 2019 was composed by Hwataik Han, Shin-ichi Tanabe, William Bahnfleth, Xu Zhang and, was chaired by Manuel Gameiro da Silva.

Both competitions are sponsored by Eurovent Certita Certification.

About RCYP (REHVA Community of Young Professionals)

The RCYP was founded in 2020 by REHVA, coordinated by Arash Rasooli, the first winner of REHVA and HVAC World Student Competition (2016). REHVA seeks the objective of advancing its programs and services for young engineers, helping them build their professional foundations and career. REHVA organises courses for students and young professionals and promotes their participation in the REHVA network event by discounts. REHVA will support the joint activities defined together with the RCYP members and offer advantages relying on the existing REHVA knowledge sources and services, such as free or discounted access to REHVA guidebooks, events and trainings, publication possibility in the REHVA Journal, specific sessions at REHVA events for the community.

The CLIMA World Congresses are inviting young researchers to submit abstracts. If students team-up and purchase REHVA guidebooks they receive a discount. RCYP is building an online community and information hub tailored to the interest of community members.

For any inquiries, feel free to contact us at rcyp@rehva.eu.

Results

HVAC World Student Competition [year]

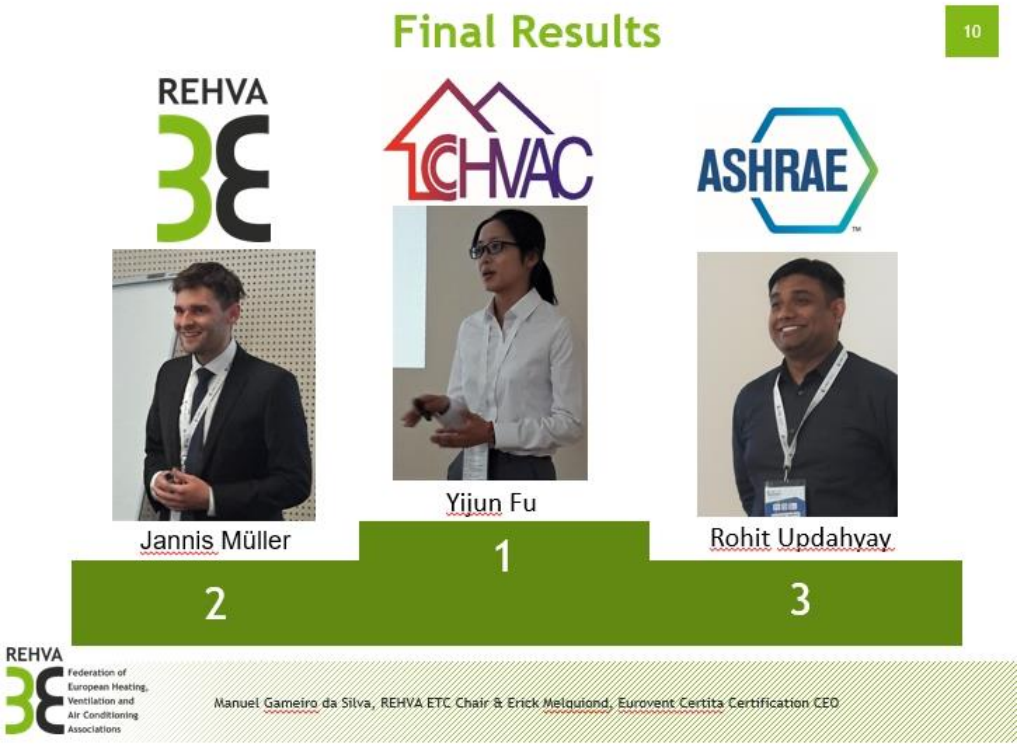

REHVA Student Competition [year]

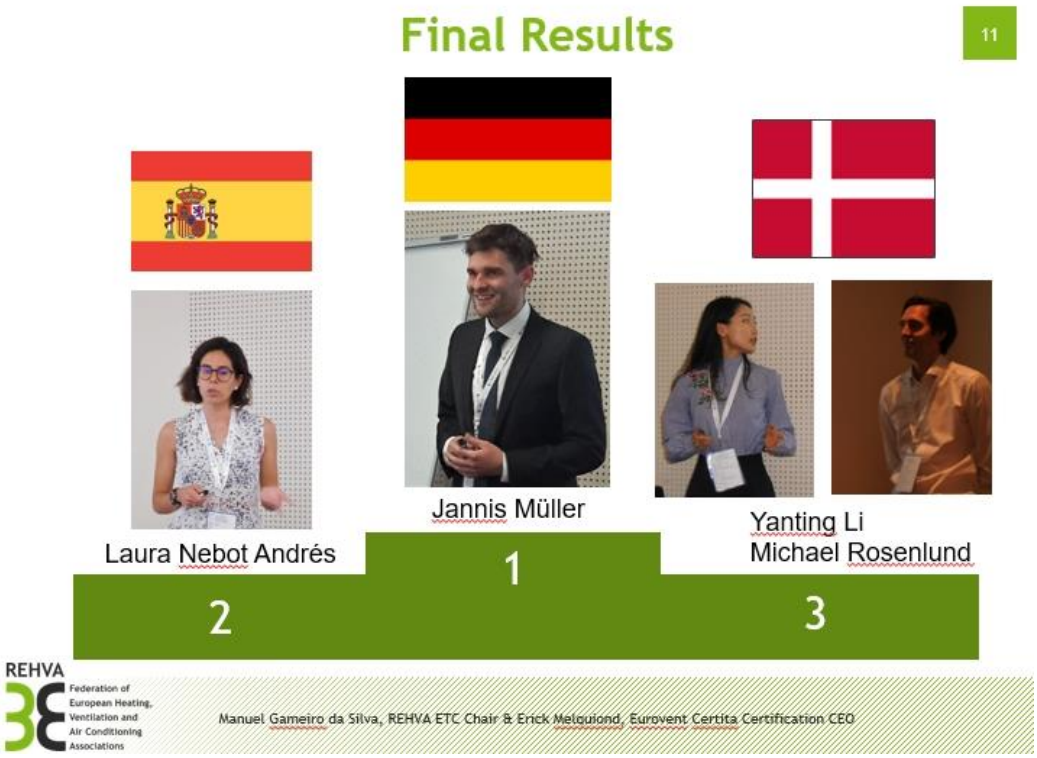

1st Place
HVAC World
Student Competition

Yijun Fu
China

Research on Heat Transfer Characteristics of Carbon Dioxide in Microchannel Evaporator

Fu Yijun Li Guo Lv Jing

(*College of Environment and Building, University of Shanghai for Science and Technology, No. 516, Jungong Road, Yangpu District ,Shanghai, PR. China*. lvjing810@ 163.com.)

***Abstract*—Simulating model based on a specific CO_2 microchannel evaporator was established through controlled volume method in MATLAB, in which both wet and dry conditions for air side, and two-phase and over-heat zones for CO_2 side have been considered during the evaporative process. Simulation results were validated showing good agreement with previous experimental data . And then the heat transfer characteristics in microchannel evaporator were simulated under different inlet air parameters. It was shown that air velocity has the greatest impact on heat transfer effect, followed by air temperature, and air humidity at last. Meanwhile, the dry-out point also has an important impact on heat transfer performance: before the dry out happens, the heat transfer coefficient of the CO_2 increased with higher air temperature, relative humidity and velocity, while after the dry out occurs, there has been a drastic decline of convective heat transfer coefficient. Therefore, the dry-out point should be postponed for better performance. Then, structural optimization has been made by utilizing two-stage series evaporators. Corresponding simulation results showed that 37.5% area of the original experimental device can still achieve 90.5% heat transfer rate of the former one. So this method can greatly improve the heat transfer effect of the CO_2 microchannel evaporator.**

***Index* CO2, Heat transfer characteristics, Microchannel evaporator, Simulation model**

Introduction

The main devices of heat transfer in the refrigerating cycle of CO_2 have been going through the development from the finned tube style to the microchannel style. Compared to traditional heat exchanger, micro-channel heat exchanger is usually more compact and efficient and have a stronger pressure resistance leading to higher heat transfer coefficient. So the combination of CO_2 and micro channel can reduce the size of the evaporator, improve the heat transfer performance, and achieve the effect of complementary advantages[1]. However, when the hydraulic diameter is smaller than 3mm, the two-phase flow and heat transfer regulation differs from the normal size which shows a more evident microscale effect with the narrowing of the channel[2].

Many research institutions have studied on this issue that mainly focus on the boiling heat transfer coefficient of the two-phase field, critical heat flow rate density, dry point, two-phase flow pattern, pressure drop model and some other aspects[3]. Cheng et al. have discovered that the critical dryness of carbon dioxide was generally between 0.5 and 0.7, which was much lower than that of R22 with a critical dryness usually between 0.8 and 0.9[4]. Then, they have considered the characteristics of intermittent flow, annular flow, dry-out inception and mist flow, and modified the boiling heat transfer correlation under the basis research of Wojtan [5]. Zhang has established a two-dimensional distributed parameter model for the CO_2 microchannel evaporator and proposed a modified heat transfer correlation after comparing to the experimental data [6].

Several relevant heat transfer correlations are selected according to the heat transfer characteristics of CO_2 in microchannel evaporator, and comprehensively considered the different heat transfer characteristics of wet and dry conditions on air side along with two-phase region and overheated region of CO_2.. Parameter distribution simulation model of CO_2 microchannel evaporator has been established and through comparison of the experimental results, the simulation model is verified. Finally, through the simulation model, air temperature, humidity and velocity have been analyzed for studying their impact on heat transfer performance in order to make further structural improvement of the device.

I. EXPERIMENT RESEARCH

A. Microchannel Evaporator

This paper is about simulation and experimental investigation on a parallel flow micro-channel evaporator which is composed of 36 parallel flat tubes, each of which has 18 micro-channels with equivalent diameter of 1.096mm. The two-phase CO_2 coming from the collecting pipes flows into the microchannel and exchanges heat and mass with the air in the shutter fin between the micro-channels. Fig. 1 and Fig. 2 show structures of the microchannel evaporator tube and louver fin. The calculated main structural parameters of the microchannel evaporator are shown in Table 1.

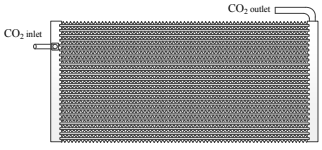

Figure 1. Diagram of the microchannel evaporator

The project was supported by the Hujiang Foundation of China (No. D14003) and Yangtze River Delta Technology Joint Research (10195811000).

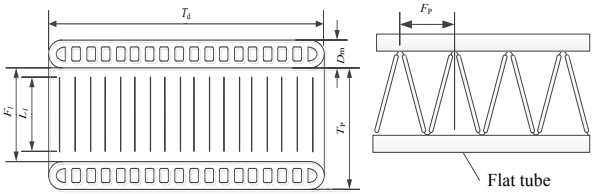

(a) Structure diagram of louver fin

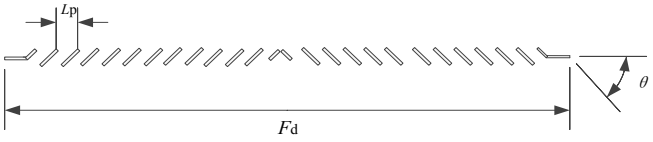

(b) Sectional view of louver fin

Figure 2. Diagram of louver fin of microchannel evaporator

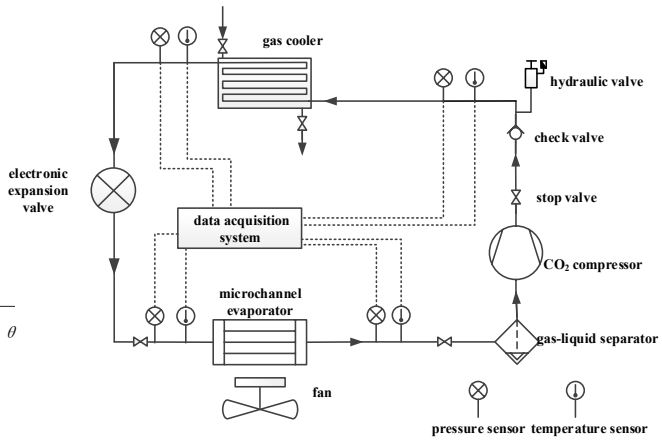

Figure 3. The experiment system diagram

TABLE 1. MAIN STRUCTURAL PARAMETERS OF MICROCHANNEL EVAPORATOR

Upwind surface width	Upwind surface height	Air direction depth	volume	Heat exchange area		Equivalent diameter
				Air side	Refrige-rant side	
L_y/mm	W_y/mm	T_d/mm	V_c/cm^3	A_a/m^2	A_r/m^2	d/mm
810	50	25	7087.5	9.464	2.28	1.096

TABLE 2. EXPERIMENTAL MEASUREMENT VALUES OF CO_2 SIDE

Category	Mass flow（g/s）	Inlet dryness	Inlet pressure (MPa)	Outlet pressure (MPa)	Outlet temperature（℃）
Measured values	15.67	0.28	3.22	3.18	11.58

TABLE 3. DISTRIBUTION OF PARAMETERS

Measuring points	1	2	3	4	5	6	7	8
wind speed (m/s)	1.4	1.9	1.6	1.4	1.8	1.8	1.9	1.8
Outlet temperature (℃)	22.4	22.1	21.7	21.1	19.0	8.2	6.5	5.9
Outlet humidity (%)	26.5	26.8	27.6	28.9	32.7	66.1	60.0	61.1
Wall temperature (℃)	22.8	22.1	21.5	20.5	17.1	6.0	-1.7	-1.9

B. Experimental System

The experimental table of the CO_2 microchannel evaporator was set up (see Fig.3). The conditions of the evaporator side are provided by the Psychometric Room which installed the platinum resistance and pressure transmitter in the evaporator inlet and outlet in order to measure temperature and pressure of CO_2. Thermocouples were fixed on the surface of the evaporator in order to measure wall temperature. The air side state parameters were measured by using temperature and humidity measuring instrument and wind speed measuring instrument. Finally via the electronic expansion valve, the dryness and mass flow rate of CO_2 at the inlet of the evaporator was regulated.

C. Experimental Results

The 18th flat tube was analyzed and divided into 9 sections, which is 90mm with measuring points setting in the center of each section. The experiment measured CO2 mass flow rate, inlet dryness, pressure, evaporation temperature, wall temperature, air temperature, humidity and speed. The convective heat transfer coefficient and heat transfer amount of each section of this flat tube would be calculated according to the experimental data, which are shown in Table 2 and Table 3.The incipient air temperature is set to be 23℃, and relative humidity is 25% ,so the dew point temperature is 2.14℃.

II. SIMULATION MODEL

A. Heat Transfer Correlation of CO_2 Side

1）Overheated Region

According to different evaporator outlet states of CO_2, the refrigerant flow can be divided into two-phase region and overheated region. As for the overheated region, different heat transfer correlations were selected according to the Reynolds number: When $Re \geqslant 2300$, the convective heat transfer coefficient was calculated by Gnielinski formula[7]; Otherwise， the convective heat transfer coefficient was calculated by Sieder-Tate formula[8].

2）Two-phase Region

The currently available CO_2 boiling heat transfer correlations are mainly Shah, Gungor and Winterton, Hwang, Yoon, and Cheng correlations. In Cheng correlation, the whole two-phase region is divided into 3 phases: intermittent flow, annular flow and mist flow, according to the boundary point of intermittent flow and annular flow and the dry-out point. Compared with the experimental data in reference [9], the Cheng correlation was considered to be the most accurate in this experimental

condition. So the Cheng correlation was selected in our simulation on two-phase region.

B. Heat transfer Correlation of Air Side

When the wall temperature is below air dew point temperature, dew will appear on the surface of the flat tube. So when analyzing the heat transfer of the air side, two different working conditions should be considered separately: dry and wet working conditions. Scholars have done more research on dry condition, while the of the *J* factor under wet condition tends to be less. In the wet condition, surface thermal resistance increases, thus, heat transfer coefficient will be much smaller than under dry condition. The correlations developed by Kim and Bullard can predict accurately about the heat and mass transfer performance of the shutters in dry and wet conditions [10]. So their correlation was used in our simulation model on air side heat transfer.

C. Controlling Equation

In order to make the process of calculation easier, the mathematical model of CO_2 microchannel evaporator was assumed as follow:

1) CO_2 is equally divided into each microchannel;

2) of no thermal conduction or heat resistance between micro-channels;

3) CO_2 side and air side are both steady flow;

4) The air on the condensation water surface is saturated and the thermal resistance of the condensed water is negligible;

5) The effect of lubricating oil and non-condensing gas is not considered.

Making the flat tube and the 1/2 louver fin on the upside and underside of it as the research object, the control unit is shown in Fig. 4.

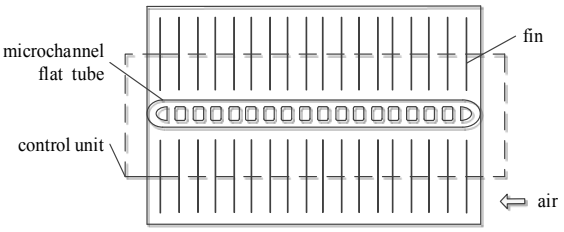

Figure 4. Section view of control unit

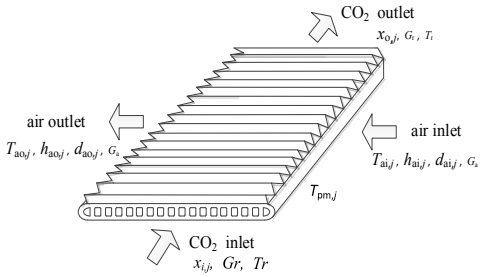

Figure 5. Statistical figure of infinitesimal section

As shown in Fig.5, every infinitesimal section can be regarded as a small cross flow heat exchanger, which was analyzed by energy:

Air side heat exchange:

$$Q_{\mathrm{a},j} = M_{\mathrm{a,d}}\left(h_{\mathrm{ai},j} - h_{\mathrm{ao},j}\right) \tag{1}$$

CO_2 side heat exchange (two-phase):

$$Q_{\mathrm{r},j} = M_{\mathrm{r}}\left(x_{\mathrm{o},j} - x_{\mathrm{i},j}\right) i_{\mathrm{tp}} \tag{2}$$

CO_2 side heat exchange (overheated):

$$Q_{\mathrm{r},j} = M_{\mathrm{r}}\left(h_{o,j} - h_{i,j}\right) \tag{3}$$

Where Q represents heat transfer rate (W), M is mass flow rate (kg/s), h is enthalpy(kJ/kg), *x* is dryness, and *I* is latent heat of vaporization(kJ/kg).

Where subscript abbreviation *a* represents air, *r* refrigerant, *i* inlet, *o* outlet, *tp* two-phase, *j* the *j* infinitesimal section.

Heat transfer between air and pipe wall under dry and wet conditions:

$$Q_{\mathrm{a},j} = \alpha_{\mathrm{ad}}\eta_{\mathrm{ad}}A_{\mathrm{a},j}\left(T_{\mathrm{am},j} - T_{\mathrm{pm},j}\right) \tag{4}$$

$$Q_{\mathrm{a},j} = \beta_{\mathrm{aw}}\eta_{\mathrm{aw}}A_{\mathrm{a},j}\left(h_{\mathrm{am},j} - h_{\mathrm{s,wm},j}\right) \tag{5}$$

Where α represents sensible heat transfer coefficient ($W/m^2 \cdot k$), β is mass transfer coefficient ($kg/m^2 \cdot s$), η is cooling efficiency, *A* is heat transfer area (m^2), and *T* is temperature(K).

Where subscript abbreviation: *d* represents dry air, *w* means water film, *m* means average, and *s* means saturated.

D. Simulation Process Design

Heat transfer process exist both in two-phase region and overheated region in normal heat pump system, because a certain degree of overheated at evaporator outlet is usually required in order to ensure CO_2 enter into the compressor with gas phase. In this condition, the point with dryness equal to 1 of CO_2 was calculated first to divide the heat transfer process into two-phase region and overheated region. The specific calculation process is shown in Fig.6, in which the state parameters of CO_2 and air were obtained from MATLAB by manipulating the REFPROP.

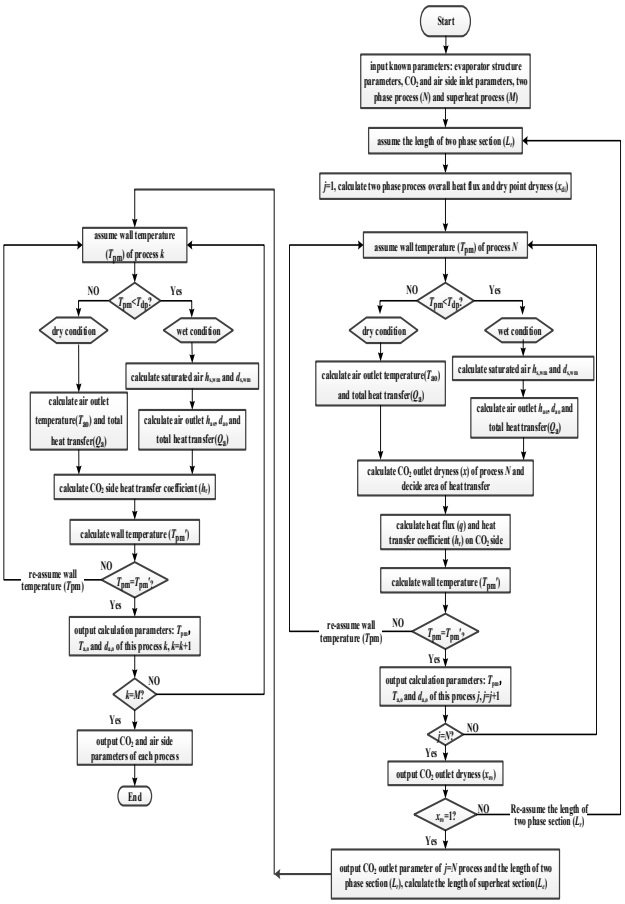

Figure 6. Simulation process of heat transfer

III. RESULTS AND DISCUSSION

A. *Comparison of Experimental and Simulation Results*

Comparing the simulation values with the experimental ones of CO_2 temperature, wall temperature, air inlet and outlet temperature and the convective heat transfer coefficient respectively, as is shown in Fig.7 and Fig.8.

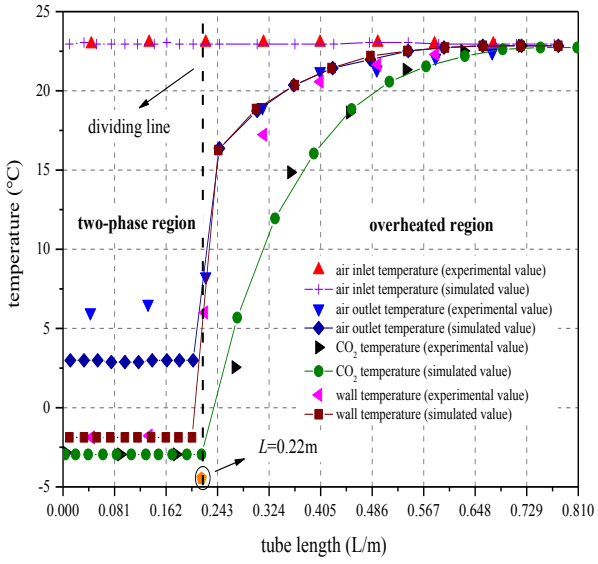

Figure 7. Comparison of CO2 temperature, wall temperature, air inlet and outlet temperature

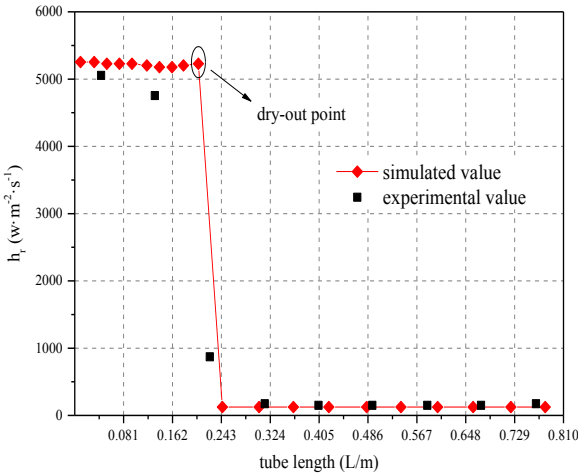

Figure 8. Comparison of the convection heat transfer coefficient

The relative errors between experimental and simulation values of CO_2 temperature, wall temperature, air outlet temperature, convection heat transfer coefficient were calculated. The relative error of CO_2 temperature and wall temperature is 10%, while the relative error of convective heat transfer coefficient is 18.53%. The possible reason might be that micro-channel evaporator tended to have an unequal flow distribution problem. This would cause the CO_2 mass flow rate too low in some single microchannel. The changing trend of simulation values and the experimental values are the same, and their error is also within range of acceptance. So the simulation model is under a higher reliability.

B. *Simulation Analysis*

There are several factors that influence boiling heat transfer of CO_2 in microchannel evaporator. In carbon dioxide side, it includes evaporation pressure, inlet dryness, mass flow rate; while in air side, it includes inlet temperature, humidity, air speed, etc. According to the simulation model of CO_2 microchannel evaporator, impact on heat transfer characteristics of CO_2 was analyzed both for heat transfer coefficient and location of dry-out point. The effect of the air side on the heat transfer characteristics of CO_2, as shown in Fig. 9 to Fig. 11. Different simulating conditions of each figure are shown in Table 4.

Table 4 Simulation conditions

Category	CO_2 inlet dryness	Air inlet temperature ℃	Relative humidity	Air face velocity m/s
Fig.9	0.5	20~30	30%	3
Fig.10	0.5	25	30%~50%	3
Fig.11	0.2	25	30%	2~5

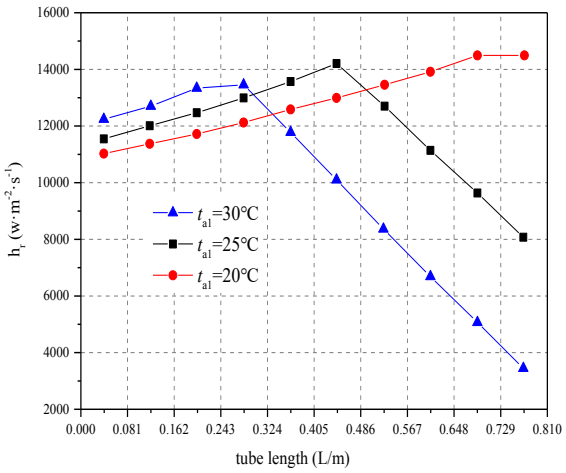

Figure 9. Influence of air temperature on the convection heat transfer coefficient

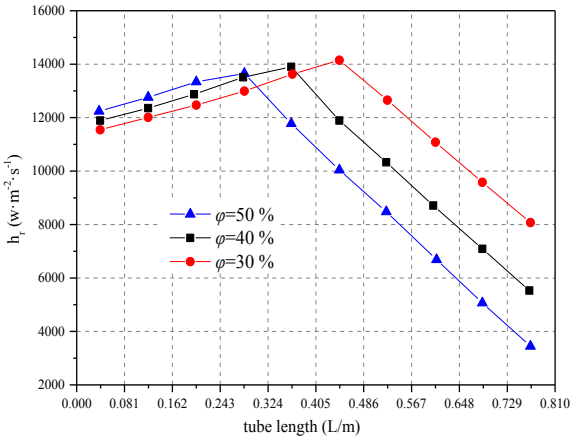

Figure 10. Influence of air relative humidity on the convection heat transfer coefficient

As is shown in Fig.9, with the increase of air inlet temperature, the appearance of dry-out point will be earlier. Because the increase of air inlet temperature leads to increase of average heat flux, which causes decrease of the dryness of dry-out point. Fig.10 shows that with the increase of air relative humidity, dry-out phenomenon also appears earlier. Because that, the greater the relative humidity of air, the greater the dew point temperature, the greater the air enthalpy value will be, the ability of heat transfer increased, and the average heat flux increased. These things all lead to the decrease of the dryness of dry-out point, resulting in the occurrence of dry-out phenomenon sooner. At the same time, it can be found that air temperature has a more significant effect than its relative humidity on heat transfer coefficient for a CO_2 microchannel evaporator under specific structure and operating parameters. When air temperature is 20~25°C and humidity is 30~40%, average heat transfer coefficient has the optimal value.

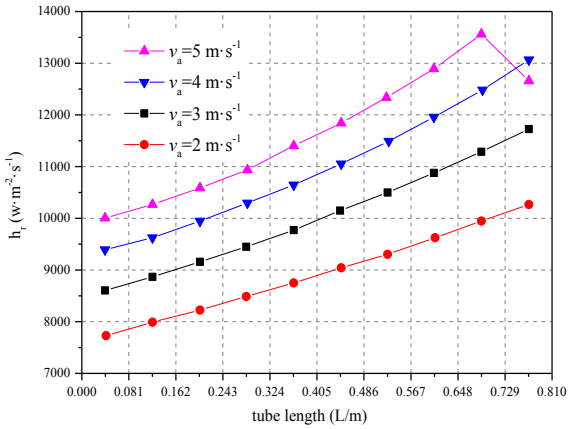

Figure 11. Influence of air speed on the convection heat transfer coefficient

Fig.11 shows that air speed has a significant impact on heat transfer coefficient. With the increase of air speed, thickness of liquid film on the tube surface decreases resulting in bubbles generated by the nucleate boiling escape more easily, which increases heat transfer coefficient and heat flux of the CO_2 side. However, the dryness of dry-out point will decrease which causes the dry-out to occur earlier.

C. *Simulation Improvement*

Considering that the location of drying point is about 1/4 behind the channel inlet in Fig.8, heat transfer efficiency decreases sharply at the latter part of the channel. Therefore, we divide the former one evaporator into two ones with a gas-liquid separator installed between them. The length of the first evaporator is halved to 0.405m, together with halved flat tubes number of 18. Simulation results shows a dryness of 0.68 at the outlet, as is shown in Figure 12. Then the two-phase flow of the first evaporator flows into the gas-liquid separator for liquid separation before it enters the compressor. And the remaining 32% liquid refrigerant enters the next evaporator which also has the length of 0.405 M. The numbers of flat tubes are respectively: 18, 13, 9 and 5. The inlet dryness is assumed to be 0.

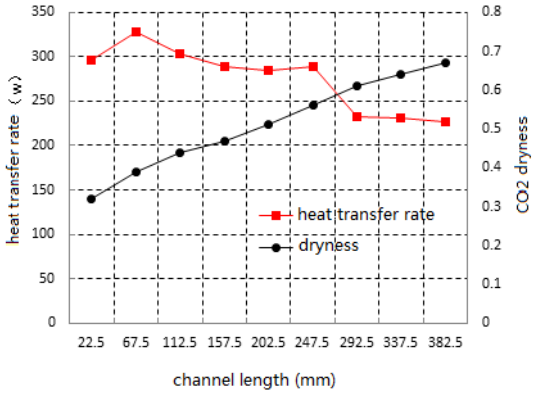

Figure 12. Heat transfer along channel of first-stage evaporator

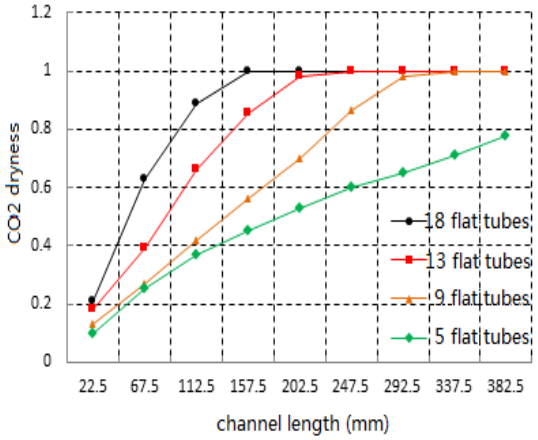

Figure 13. CO_2 dryness of second-stage evaporator under different flat tubes number

Fig.13 shows that when flat tubes number is decreased to 9, CO_2 at outlet of the second stage evaporator is in overheat zone, and when the number is decreased to 5, it changes into two-phase zone. Regardless of refrigerant flow rate change, heat transfer characteristics differences and the overheat extent at the evaporator outlet, considering only the postpone of dry-out point, in order to ensure the over-heated state at the outlet, number of flat tubes should be 9 for optimization of the secondary evaporator which can reduce the heat transfer area to 37.5% of the original one. Former heat transfer capacity of the evaporator was 3.46 KW, and after the optimization, it has become 2.48 KW for the first stage evaporator, and to 0.65 kw for the second stage evaporator, which retains 90.5% of the former one.

IV. Conclusion

Considering dry and wet conditions on air side and different heat transfer characteristics of CO_2 in two-phase region and overheated region, a two-dimensional distributed parameter simulation model of the CO_2 microchannel evaporator was established, in which the heat transfer calculation in the two-phase region was calculated by Cheng correlation. A comparison of experimental values with simulation values, including CO_2 temperature, wall temperature, inlet and outlet air temperature and convective heat transfer coefficient, was performed to verify accuracy of the simulation program. Then the heat transfer characteristics of CO_2 in microchannel evaporator were studied through simulation model. The conclusions are drawn as following:

1) The comparison between experimental and simulation results shows little discrepancy within 18% which verifies the simulation method.

2) The convective heat transfer coefficient reached the maximum at the dry-out point and then decline drastically which causes heat transfer deterioration at CO_2 side. In the overheated region, the heat transfer coefficient is way smaller compared to that of the two-phase region. Therefore, the later the dry-out happens, the better the cooling efficiency of the device.

3) At the air side, air velocity has the most significant impact on heat transfer followed by air temperature, and relative humidity at last. Higher air speed will increase the heat transfer coefficient and heat flux of the CO_2 side. However, the dryness of dry-out point will decrease which causes the dry-out to occur earlier.

4) In order to postpone the dry-out point, structural improvement of the evaporator has been made by separating one evaporator into two with gas-liquid separator between them. Results show that 37.5% area of the original experimental device can still achieve 90.5% heat transfer rate of the former one.

ACKNOWLEDGEMENT

This paper has been admitted by CCHVAC in 2018. L.J. F.Y.J and L.G. thank to the committee members of CCHVAC and sponsor by TICA company, China.

References

[1] Zhao Y and Ohadi M. M, “Experimental study of supercritical CO_2 gas cooling in a microchannel gas cooler”, *ASHRAE Trans*., vol. 110 (1), pp. 291-300. 2004

[2] Zan Wu. “Mechanism and predictive methods for flow boiling in micro/mini-channels and micro-fin tubes.” *Ph. D. Thesis*. Zhe Jiang University, China, 2013.

[3] Yoon S H, Cho E S and Hwang Y. W. “Characteristics of evaporative heat transfer and pressure drop of carbon dioxide and correlation development”, *International. Journal. Refrigerator.*,vol. 27 (2), 2004,pp111-119.

[4] Cheng L, Ribatski G and Wojtan L “New flow boiling heat transfer model and flow pattern map for carbon dioxide evaporating inside horizontal tubes” *Int. J. Heat Mass Transfer,* vol. 49 (21-22), 2006,pp4082-4094.

[5] L Wojtan, T Ursenbacker, J R “Thome, Investigation of flow boiling in horizontal tubes: part II – development of a new heat transfer model for stratified-wavy, dry-out and mist flow regimes”, *Int. J. Heat Mass Transfer,* vol. 48(4), 2005, pp2970-2985.

[6] Haiqing Zhang, Bei Guo, “Numerical simulation of the carbon dioxide microchannel evaporator using distributed parameter model,” *Journal of Xi’an Jiao Tong University*, vol. 46 (1) 2012,pp42-47.

[7] V. Gnielinski, “New equations for heat and mass transfer in turbulent pipe and channel flow”, *Int. Chen. Eng.* vol. 16 (2) 1976,pp401-409.

[8] Sieder E N, Tate G E, Heat transfer and pressure drop of liquids in tubes. Ind Eng Chem., 28 (1936):1429-1435.

[9] Pettersen J, “Flow vaporization of CO2 in microchannel tubes,” *Exp. Therm. Fluid Sci*.,vol. 28 (2-3) ,2004,pp111-121.

[10] Kim M H, Bullard C W, “Air-side thermal hydraulic performance of multi-louvered fin aluminum heat exchangers”, *International Journal Refrigerator*.,vol.25 (3) ,2002, pp390-400.

1st Place
REHVA
Student Competition

Jannis Müller
Germany

2nd Place
HVAC World
Student Competition

REHVA
Federation of European Heating, Ventilation and Air Conditioning Associations

Development of an adaptive aerofoil contour for use as a fan blade

First author: Jannis Müller M.Eng.

Second authors: Prof. Dr.-Ing. H. Hahn
Dipl.-Ing. C. Friebe

***Abstract*— This master thesis represents a contribution to the development of axial fans with adaptive blade profiles. The adaptive blade profiles should be able to be changed in operation so that high efficiency is achieved not only at the design point, but also in the partial load range of the fan operation. Studies on the effectiveness of such blades are held to reduce the complexity of stationary aerofoils.**

In the first part, the basic principles for understanding the work principles of axial fans will be explained.

In the second part, an overview of causes and avoidance strategies of detachment phenomena of the flow around fan blades is provided with the help of literature research. It also evaluates the feasibility of these avoidance strategies on rotating systems.

The search concludes that aerofoils which have a function of adjusting their angle of attack and the additional function of adapting their profile curvature would be particularly suitable for the use on rotating systems. In order to prove this assessment, force measurements are carried out on two reference profiles and finally are compared with an adaptive aerofoil profile developed for this purpose. For these measurements, a separate test rig was set up and validated, which allows equivalent investigations on dormant aerofoil profiles.

The three profiles were developed according to Carolus and designed for the production with a 3D printer using CAD software.

In the final part, investigations are carried out with a laser-optical measuring method in order to reveal potential for improvement in future research.

With an overall assessment of the effect of the adaptive aerofoil, as well as a recommendation for the use of the potentials, this work contributes to the further development of axial fans with adaptive blade profiles.

***Index Terms* — Adaptive aerofoil, axial fan, flow separation, force measurements**

I. INTRODUCTION

A. Basics about fans

Fans are flow machines designed to transport gaseous fluids. They are often used in recooling systems or decentralised ventilation systems. Also, for special applications such as mine ventilation or in wind tunnels, axial fans are used because of their performance in the transport of large volume flows [4]. The task of mass transport fans should meet with a certain volume flow at a given pressure difference. This design point is regularly used to define the type of flow machines. When designing building services, it is common practice to design the fans to peak performance with an additional safety margin to ensure building operation at full capacity. However, it is realistic that the facilities will not work at the design point but mainly in a part load operation. Manufacturer of fans take this into account and therefore develop the blades of a fan in their shape so that they work not at the design point, but at a certain load point with maximum efficiency [6]. However, high efficiency would not be desirable in points, but over a load range between the part load and the design point.

In addition to business economic motivation, environmental policy also plays a role in the design of fans. For example, following the identification of a significant potential for improving the environmental impact of energy-related products, the European Commission also adopted a regulation on the environmentally sound design of fans. Since the regulation (EU) Nr. 327/2011 came into effect, the requirements on the environmentally sound design of fans are according to the directive 2009/125/EG lawfully defined [2]. With a measured system efficiency, axial fans with a power consumption of $125W \leq P_{el} \leq 10kW$ currently has to meet a target efficiency is given by equation (1) with

$$\eta_{target} = 2{,}74 \ln(P) - 6{,}33 + N \qquad (1)$$

where P is the electrical power consumption in kW and N is a prescribed degree of efficiency (static N = 40).

The efficiency tests take place on standardised test setups, whereby the data is recorded with optimal efficiency [2].

It is conceivable that such static test methods will be replaced by methods with dynamic load distribution in the future and thus the target efficiency must be met not at an optimal point, but in different ranges. If the efficiency requirements for fans continue to rise in the future, then the research on fan blades with adjustable curvature while running will be not only very useful, but also an important step in the development of a more efficient generation of flow machines.

This work contributes to the development of adjustable blade contours for use in axial fans. The focus of the work is the development of an adjustable blade and the proof of an improvement of partial load behaviour. For this, a test setup has to be developed and verified. Corresponding examinations and test series should prove the effectiveness of the adjustable blade.

B. Working principle of fan blades

„Every body moving in a fluid experiences a force. Of particular interest are those bodies which - in addition to a low drag force against the direction of movement - have a high lift force perpendicular to the direction of movement. Planar bodies with these properties, whose dimensions in one direction - the "thickness" of the body - are much smaller than in the two perpendicular directions - the "depth" and the "span" - are called "aerofoils". A section

perpendicular to the span direction may be called "aerofoil profile" or "profile" for short.“[10].

During the flow around a profile, different speed and pressure conditions occur along its surface. The air is accelerated when displaced, the dynamic pressure increases and the static pressure decreases according to the energy conservation. The pressure field along the surface is therefore crucial for the resulting lift force.

Fan blades operate on the principle of an aerofoil and typically have an asymmetric curvature. The force resulting from the pressure gradients expresses as lift force on the blades which is necessary for the transportation of the fluid. The one-sided curvature generates a drop in static pressure in front of the fan. A good aerofoil contour is characterised by high lift force with low drag force.

The glide ratio

$$\varepsilon = \frac{W}{A} \quad , \qquad (2)$$

is an indicator for the rating of different contours. The thickening of profiles as well as the increase of its curvature results in an unfavourable glide ratio [5].

C. *Fan-characteristics*

The flow properties of fans are described with fan-characteristics. These describe the possible operating points of a fan from free-air point ($\dot{V} = max\,, \Delta p = 0$) to stagnation point ($\dot{V} = 0\,, \Delta p = max$) at a specific speed. Figure 1 shows a schematic fan-characteristic with loss fractions where the operating point is optimally located at the point of least loss. Often only the static pressures without losses are indicated in the fan characteristics.

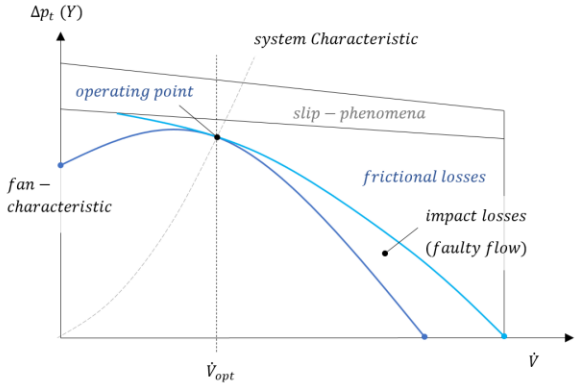

Figure 1. Volume flow total pressure characteristic diagram [7]

For an optimal operation of fans, the sum of hydraulic losses Z_h must be minimised through a net-adapted blade configuration on the impeller. The impellers work Y_{Sch} then transfers to the fluid as much as possible.

$$Y = Y_{Sch} - Z_h = \frac{\Delta p_t}{\rho} \qquad (3)$$

It is:

Y … the spec. Nozzle-work (between suction and discharge nozzles)

Y_{Sch} … the mass-specific work by the fan blades

Z_h … the sum of the hydraulic losses

Δp_t … the increase of total pressure [9]

Unlike fan-characteristics, system characteristic curves describe the resistance to be overcome for transporting fluids generated by friction in the network. Each fluid system has a characteristic which, with

$$\Delta p = \frac{\rho}{2} v^2 \qquad (4)$$

is a quadratic function of velocity. The intersection of the fan characteristic with the line characteristic is the operating point.

A change in the system characteristic can, for example, by actuation of a throttle damper, but also caused by contamination. The connection between the volume flow and the necessary support work in the fluid system then changes and new operating points are created.

Figure 2 shows the fan-characteristic of an axial fan according to BANZHAF [3] at a constant speed and a constant blade angle in a system with a continuously closing throttle damper. With an opened throttle, the fan works at operation point (1) with low pressure loss and high volume flow. With increasing throttling, the operating point on the fan characteristic rises above (2) and (3) to point (4). At point (5) the fan works with maximum pressure increase on the stable part of its characteristic curve. With further throttling the flow separates from the fan blades and the pressure increase suddenly drops. In order to return the fan from the unstable characteristic curve at point (7) to the stable characteristic curve, the throttle must be opened until point (8) has been reached. Only from (9), the flow again can be close on the blades, whereby the fan changes back into its stable characteristic range.

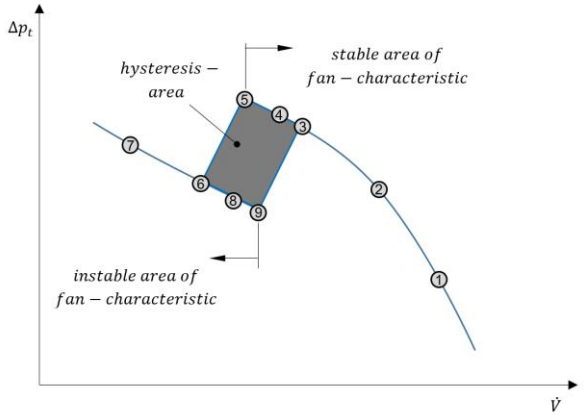

Figure 2. Characteristic of an axial fan [3]; Rotational speed: n = const.; Impeller blade angle: β_s = const.

Instable operating areas of the axial fan lead to so-called pumping which causes an increased oscillatory load. This manifest itself in acoustic problems, damage to the duct system or damage to the suspension, bearings and blades of the fan [3].

D. *Cause of flow separation*

Figure 3 shows the profile section of an impeller blade with its velocity triangles at the operating points (1), (2) and (6) from Figure 2. It is recognisable that the velocity component $\mathbf{c_1}$, which describes the volume flow though the fan decreases as result of a change in the system characteristic; this can be caused by throttling.

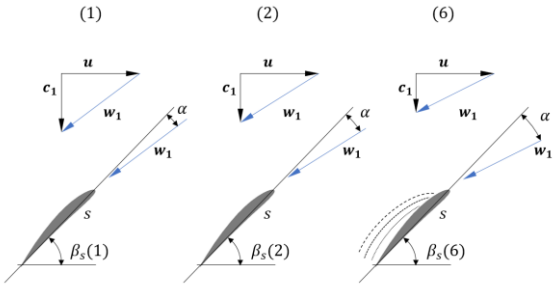

$\beta_s(1) = \beta_s(2) = \beta_s(6)$

$\boldsymbol{u}(1) = \boldsymbol{u}(2) = \boldsymbol{u}(6)$

Figure 3. Flow triangles at the Impeller [3]

The size of the angle of attack α on the profile nose particularly influences the flow pattern on the aerofoils suction surface. If α has a favourable size according to the design of the profile, the air can overflow the profile with low impact. With increasing the angle of attack, it comes first to increase of lift force, but at the expense of worsening the glide ratio. If a maximum value of α is exceeded, the flow on the suction surface separates, which leads to a sudden drop in lift forces and a considerable deterioration in the gliding ratio [3].

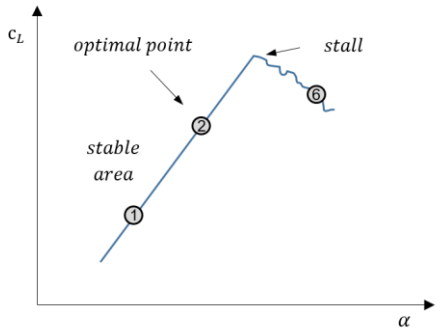

Figure 4. Lift polar schematically according to Figure 2 [3]

Figure 5 shows a brief representation of the characteristics of a system with variable resistance and the characteristics of a fan with variable blade angles. By adjusting the angle of attack of the fan blades, different operating points can be achieved. If the fan design is correct, the operating points are in the range of high efficiency [3].

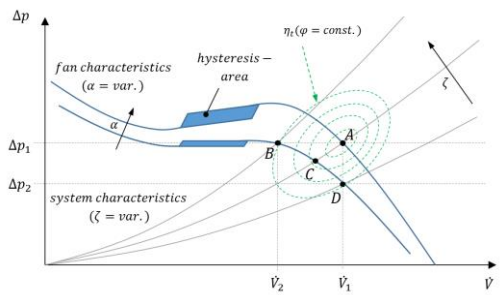

Figure 5. Characteristic diagram with variable impeller blade angles [3]

A→B: Δp = const, $\dot{V}_2 < \dot{V}_1$

A→C: ζ = const, $\dot{V}_2 < \dot{V}_B < \dot{V}_1$, $\Delta p_2 < \Delta p_B < \Delta p_1$

A→D: $\dot{V}$ = const, $\Delta p_2 < \Delta p_1$

When changing the blade angle, the shape of the fan blade is disregarded. The shape of the optimum blade profile depends on the operating point of the fan with the required size volume flow, pressure difference and speed. Usually, this blade profile is not changeable and is picked out for the design point.

As a result, after an adjustment of the angle of attack, the velocity and direction of the flow is less favourable for fan blades with a good glide ratio. The buckle of the blade is then unfavourable because it is not operated at its design point. This produces air impact losses, thereby degrading efficiency and also giving rise to flow separation earlier. An adaptation of the blade profile is therefore crucial for a high efficiency.

Fans with adjustable blade angles are already well developed, but are rarely used because of the complexity and low advantages over speed control [12].

If this blade angle adjustment succeeds in completing a camber adjustment function, the range of high efficiency can be significantly extended. The aim here is to control the adjustment of the profile curvature so that, depending on air speed, pressure and rotational speed, an increase of the range is achieved with high efficiency.

The aim is therefore the development of blades with adjustable blade angle, which have an additional function to change their profile curvature. In Figure 6, the improvement is shown schematically.

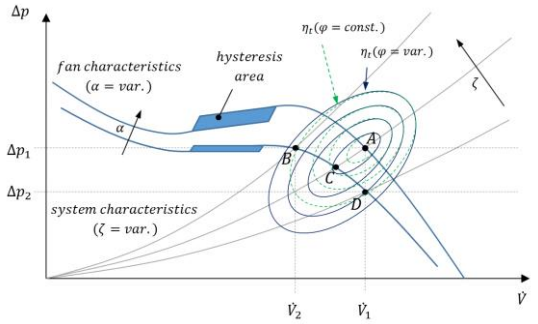

Figure 6. Characteristic diagram schematically [3], extended with a variable blade camber φ(α) = var.

A→B: Δp = const, $\dot{V}_2 < \dot{V}_1$

A→C: ζ = const, $\dot{V}_2 < \dot{V}_B < \dot{V}_1$, Δp2 < ΔpB < Δp1

A→D: $\dot{V}$ = const, Δp2 < Δp1

In order to produce different contours as faithfully as possible with an adaptive aerofoil, a specific subdivision of a profile (4-digit series NACA 4410 [1]) was applied by the superimposition of the parabolic arcs calculated for the construction. It turned out that in the division with three cuts, the shapes of different profiles can be simulated in a favourable approximation (Figure 7). The designed aerofoil consists of four parts, produced by a 3D printing process, which are connected to a common axis. To seal the resulting gaps on the surface of the aerofoil it has been covered with a nitryl-membrane.

Figure 7. Idea for the construction of an adaptive aerofoil

All asymmetrically curved profile shapes have an optimal angle of attack with low impact losses. This corresponds to the $\boldsymbol{w_1}$ at a design-dependent profile curvature. With a mechanical drive, the curvature of the aerofoil adapts itself to its angle of attack, thereby eliminating the increase in the profile angle α with increased work requirements (Figure 8).

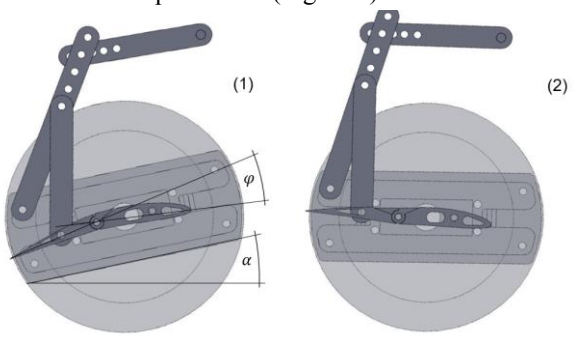

Figure 8. Working principle of adaptive camber drive ($\alpha_1 > \alpha_2, \varphi_1 > \varphi_2$)

II. EXPERIMENTAL INVESTIGATIONS

A. Measurement method

For the measurement of optimal lift-forces, which are determined by minimum values of the glide ratio ε, a test rig was developed. During the development of the test rig, six degrees of freedom of bodies in space were considered. These are the three coordinates of the body's centre of mass x, y, z, as well as the associated angles in space $\gamma, \vartheta, \alpha$ [11]. Figure 9 shows an aerofoil in dimetric exposition with the axial, rotational and pitching forces.

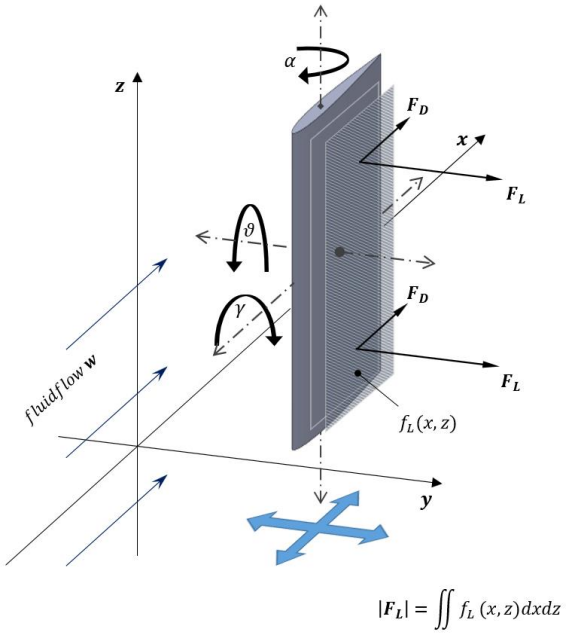

Figure 9. Representation of forces and degrees of freedom

If aerofoils are examined by force measurement in wind tunnels, often one end of the aerofoil, similar to an airplane, is free in the flow. To account for these moments in the measurements, the aerofoil was attached at both ends, eliminating γ and ϑ. At the attachments of the aerofoil, a pair of forces then act accordingly to the priority of $|F_L|$ and $|F_D|$ (Figure 10). Side forces acting in the z −direction will be eliminated through the aerofoil's orientation when the leading edge of the aerofoil is orthogonal to w. Through the setting, the angle of attack α is fixed. The elimination of the degrees of freedom $\alpha, \gamma, \vartheta$ and z, permits force exclusively on the measurement plane $x - y$, which are captured as lift and drag forces.

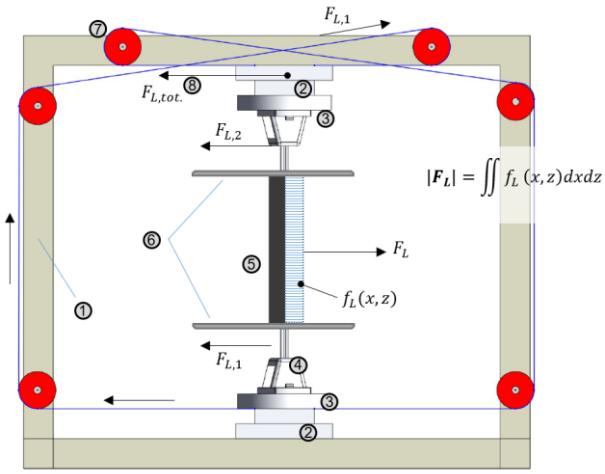

Figure 10. working principle test setup where $F_{L,tot.} = |F_{L,1}| + |F_{L,2}|$

1 Stand
2 Gliding carriage
3 Rotary plate
4 Aerofoil attachment
5 Aerofoil
6 Side plates
7 Deflection roll
8 Position load cell

B. *Force measurements*

Figure 11 shows the measured polars $-F_L/\alpha$ of the three aerofoils A (4410 rigid), B (2410 rigid) und C ([2-4]410 adaptive).

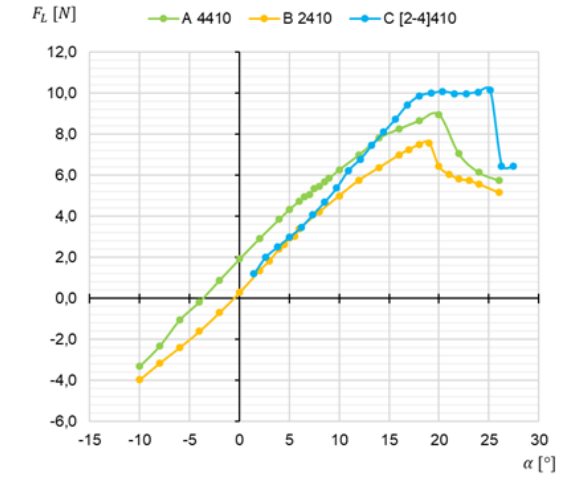

Figure 11. polars $-F_L/\alpha$

The light blue line in the graph describes the polar of the adaptive aerofoil C. Unlike the polars of the rigid aerofoils, which have a slight right curvature, the polar of the adaptive aerofoil having a relatively constant shape over the angle of attack passes.

Under the angles of attack of $1{,}5° \leq \alpha \leq 8°$ aerofoil C develops the same lift values as B. At values $1{,}5° \leq \alpha \leq 8°$, the polar runs between A and B and intersects A at $\alpha \approx 12°$. With a further increase in the angle of attack up to $\alpha \approx 20°$ the lift force increases to 10 N and remains at this value. Only at an angle of $\alpha \geq 25°$ is a very sudden drop in the lift observed.

The polars that can be seen in Figure 12 show the lift values over the associated drag forces. Using a polar tangent through the origin, minimum values for the glide ratio ε can be indicated. Aerofoil A is therefore more efficient for larger lift forces, for smaller B is favourable.

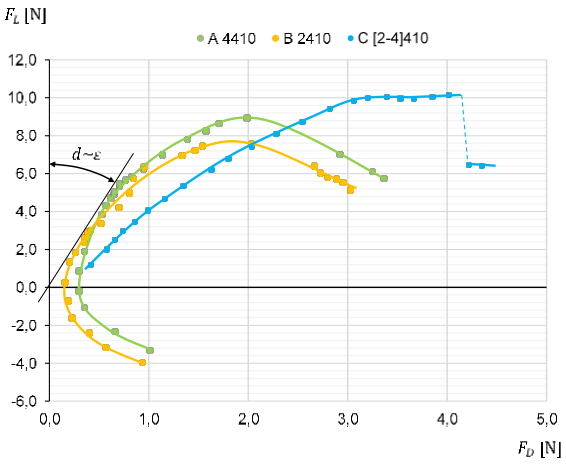

Figure 12. polars $-F_L/F_D$

The polar of aerofoil C is less curved than that of A and B, begins with the first reading at 1,2 N lift force, 0,4 N drag force and runs below the polar A and B. Before the decline of the lift value, a plateau at a force of 10 N can be recognised. It can be seen from the diagram that the drag values of the adaptive aerofoil C are higher than those of the rigid profiles.

C. *PIV-measurements*

For numbering the velocity of flow as well as for the detection of flow separation, the measurements at the adaptive aerofoil were extended with PIV analysis. The measurements also allow an additional assessment of the effects of the nitryl membrane on the surface flow.

Figure 13 shows the aerofoil under the angle of attack of $\alpha = 12{,}4°$ and the related camber of $\varphi = 20{,}9°$. The measurements showed that the stall-phenomena does not lead to flow separation despite an increased camber. The field of high velocities that increases at the leading edge and decreases glidingly with trailing edge indicates a favourable flow. Furthermore, a gap between aerofoil and air can be seen. The cause is that the surface rises due to the suction pressure, which increases the geometric thickness of the profile and can be seen as the reason for the increased drag forces according to Figure 12. Whether this has an influence on the lift distribution in addition to the increase in the form resistance, this must be investigated by future reference measurements.

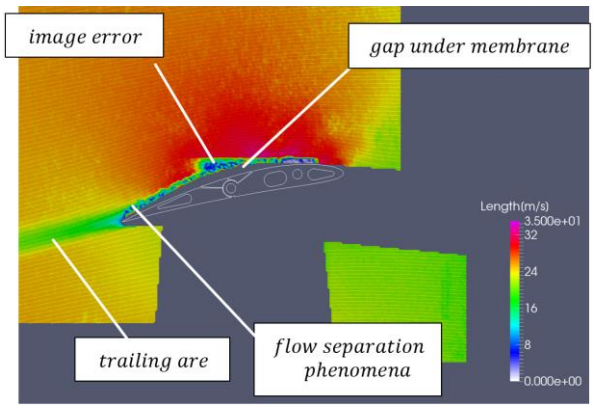

Figure 13. PIV flow mapping α = 12,4°; φ = 20,9°

Air velocities greater than 30 m / s can be detected near the suction surface at an incoming freestream velocity of 20 m/s.

III. CONCLUSION

The development of auto adaptive aerofoils for the use as a fan blade will improve the efficiency of flow machines.

It has been shown, that an aerofoil with a variable camber achieves an improved lift characteristic, especially at requirements outside the design point. This was proven by force measurements.

A high priority in the development of such adaptive aerofoils must be the preservation of a streamlined profile shape with all adjustable cambers. Investigations in the last century have produced many profile shapes, which have been extensively studied, described and optimised for the smallest values of ε. These forms are subject to a calculation method for defining a favourably curved skeleton line. In the adaptive aerofoil constructed in this work, the family of four-digit NACA profiles were chosen.

The uniformly gentle curvature of the skeleton line, which is desired during the change in curvature, is shifted by a division into sections with a common point of rotation. The change in the curvature is transferred as a superposition to the skeleton line as Figure 14 shows.

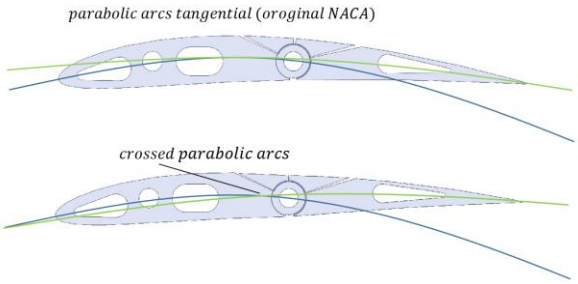

Figure 14. Superposition of the skeleton line

It can therefore be summarised that for the successful construction of an adaptive aerofoil, a low resistance through the flow-optimised contour and a high surface quality are decisive.

Which of the listed criteria outweighs and which effects the simulation of different cambers compared to the rigid original contours, on drag and lift forces, must show a number of further investigations. However, it is advisable to first investigate the effects of different surface materials on the drag forces on the aerofoil.

A. Outlook

The development of a seal for the surface of the adaptive aerofoil with less disruptive effects, for example with the help of a silicone joint or with a perforated membrane, should be strived for further research.

If it were possible to design the surface and shape of the adaptive aerofoil so that the drag force would be similar to that of A and B, the polar– F_L/F_D could look like Figure 15 and achieve optimum values for ε over large areas of F_L.

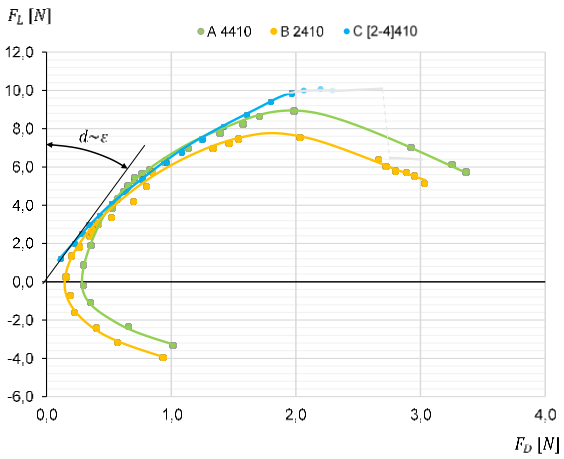

Figure 15. theoretic polar

In the future, acoustic measuring tools for controlling the curvature of impeller blades would be conceivable in order to guide fans on the stable part of the fan characteristic curve. The development of innovative materials, such as shape memory alloy metals or advances in the applicability of elastomers could be an important part of fan design in the future. A replacement of complex mechanisms in the impeller would be conceivable [8].

CONCLUDING REMARK

The research on adaptive aerofoils opens up great potential for the energy-saving use of axial fans. The upcoming challenge is the development of a suitable drive for the required camber control and its integration into the impeller blades.

This would be a large-scale success for a new generation of turbomachinery with dynamic characteristics.

REFERENCES

[1] AIRFOILTOOLS.COM: NACA 4-digit airfoil generator (NACA 4410 AIRFOIL) at http://airfoiltools.com/airfoil/naca4digit.

[2] AMTSBLATT DER EUROPÄISCHEN UNION - DIE EUROPÄISCHE KOMMISSION: VERORDNUNG (EU) Nr. 327/2011(EU) Nr. 327/2011, 6.4.2011.

[3] BANZHAF, Hans-Ulrich (1986): "Stabile und instabile Betriebszustände bei Axialventilatoren" Heidenheim.

[4] BISCHOFF, Walter (2012): "Das kleine Bergbaulexikon" Essen.

[5] CAROLUS, Thomas (2013): "Ventilatoren Aerodynamischer Entwurf, Schallvorhersage, Konstruktion; mit … 42 Tabellen und zahlreichen Übungsaufgaben und Lösungen" Wiesbaden.

[6] EBMPAPST (2017): "A3G630-AQ37-21 Betriebsanleitung Technische Daten" at http://img.ebmpapst.com/products/manuals/A3G630AQ3721-BA-GER.pdf?_ga=2.92730974.21386718.1505986311-1265744298.1505986311.

[7] EPPLE, Philipp (2013): Prof. Dr.-Ing. Philipp Epple "Strömungsmechanische Grundlagen der Turbomaschinen" published.

[8] KIEßLICH, Robert (2017): "Entwurf und Untersuchung einer mittels Formgedächtnislegierungen-Aktoren veränderbaren Oberfläche, 24.04.2017" unpublished.

[9] PFLEIDERER, Carl PETERMANN Hartwig (2005): Strömungsmaschinen, Berlin.

[10] RIEGELS, Friedrich Wilhelm (1958): Aerodynamische Profile Windkanal-Messergebnisse, Munich.

[11] TU-DRESDEN (2007): "Kraftmessungen an umströmten Körpern, in Script (Praktikum)Technische Universität Dresden Institut für Luft- und Raumfahrttechnik" unpublished.

[12] WITT&SOHN AG (2017): "im-lauf-verstellbare-schaufelntechnisches-know-how" at http://www.wittfan.de/de/technisches-know-how/im-lauf-verstellbare-schaufeln

Affiliations: University of Applied Sciences
Altonaer Straße 25, 99085 Erfurt
Mail: gti-dekanat@fh-erfurt.de

ILK Dresden
Bertolt-Brecht-Allee 20, 01309 Dresden
Mail: info@ilkdresden.de

Acceptance date: 17th of November 2017

2nd Place
REHVA
Student Competition

Laura Nebot Andrés

Spain

REHVA
Federation of European Heating, Ventilation and Air Conditioning Associations

Analysis and comparison of subcooling systems in CO_2 refrigeration systems for warm climates

Nebot Andrés, Laura[1]*; Llopis, Rodrigo[1]
ATECYR Representative
[1]Thermal Engineering Group, Mechanical Engineering and Construction Department,
Jaume I University, Spain. 2017
*Corresponding author: lnebot@uji.es, +34 964 718133

Abstract— **Refrigeration with simple CO_2 cycles is undergoing a strong change due to the new European directives and the low performance of these systems in hot climates. Theoretical studies and some experimental trials point to the use of mechanical subcooling cycles to increase the performance and cooling capacity of the base cycles. In this paper, the dedicated mechanical subcooling cycle and the integrated mechanical subcooling cycle are analyzed from a theoretical and experimental view, in order to evaluate their performance and quantify the energy improvements they provide. Firstly, both cycles are studied theoretically, for then sizing and designing the plants in order to perform the experimental tests. The simulations are carried out for the evaporation levels of 0ºC and -10ºC, covering a range of ambient temperatures between 15ºC and 40ºC. In addition, the behavior of both cycles is analyzed over a year in different climatic zones and for different applications. Finally, the feasibility study shows the interest of these applications in hot climates and high plant sizes.**

Index Terms— **CO_2, mechanical subcooling, performance improvement, refrigeration systems.**

Introduction

Refrigeration play a key role in modern life, as it is directly related to food preservation, comfort and aspects related to medicine. The International Institute of Refrigeration (IIR) [1] quantifies that refrigeration and air conditioning represent the 17% of the total electricity consumption in the world. In addition, 2% of the total emissions of greenhouse gases in the world are caused by the emissions to the atmosphere of refrigerants used in these systems [2], also named F-Gas, all of them collected in the Kyoto Protocol [3] and recently in the Montreal Protocol through the Kigali agreement [4]. Taking into account the predominance of vapor compression systems in the refrigeration sector in the last 20 years [5], the industrialized countries must develop efficient and environmentally responsible equipment to reduce these emissions

The latest restrictions approved in Europe to reduce emissions of fluorinated refrigerants condition significantly the current commercial refrigeration market. The European F-Gas Regulation [6] limits the use of these gases in order to reduce the environmental impact they generate, aiming to reduce a 79% the amount of HFCs with high global warming potential (GWP) present in the market by 2030. As a consequence, it is necessary to use refrigerants with low GWP. Although the use of these fluids reduces the direct impact of refrigeration systems (emissions to the atmosphere), it is necessary to take into account the indirect impact: the electrical consumption of the facilities. From these restrictions, CO_2 has taken a step forward, seen as the best refrigerant in many applications, since it has a GWP = 1, it is not toxic, non-flammable and has good heat transmission properties. Its use in commercial refrigeration has become widespread in recent years in the coldest countries in Europe, especially in the Nordic countries, where low ambient temperatures allow the energy efficiency achieved by CO_2 cycles to be even higher than that of the facilities based on HFC.

However, the problem lies in hot climates, where the CO_2 systems used nowadays have lower performance. It is therefore necessary to research for solutions to get new competitive CO_2 equipment in regions whose average annual temperature exceeds 15ºC in order to reduce emissions and adapt the facilities to regulations. In the last years, some researchers have studied the dedicated mechanical subcooling (DMS) system applied to CO2 refrigeration cycles. First, Llopis et al. have studied theoretically this cycle and obtained increments in COP near 23% at high heat rejection temperatures [7] and then Nebot-Andres et al. presented the experimental validation of these theoretical results, where it was observed that the limits of energy improvement are superior to those established in a conservative way by the theoretical simulations [8]. Later, other authors have studied deeply this cycle, testing zeotropic mixtures in the DMS [9]. However, the integrated mechanical subcooling cycle (IMS) has not been studied at the moment.

The purpose of this work is to search and study these solutions, responding to the environmental and technological needs. Specifically, it is based on two alternative cycles, the CO_2 cycle with dedicated mechanical subcooling and the cycle with integrated mechanical subcooling, configured in order to contribute to the implementation of CO_2-based systems in warm zones and allow reducing the emissions to the planet. This work consists of several stages in which a thermodynamic study of each cycles is carried on and their behavior in different conditions is studied. Then, the facilities are designed and tested for an experimental validation, which will allow comparing both systems to each other.

Author acknowledges ATECYR for sponsoring this work in REHVA students competition 2019.

Methods

The two alternative studied cycles in this work are the CO_2 cycle with dedicated mechanical subcooling (DMS) and the CO_2 cycle with integrated mechanical subcooling (IMS). This section briefly describes these cycles and their operation.

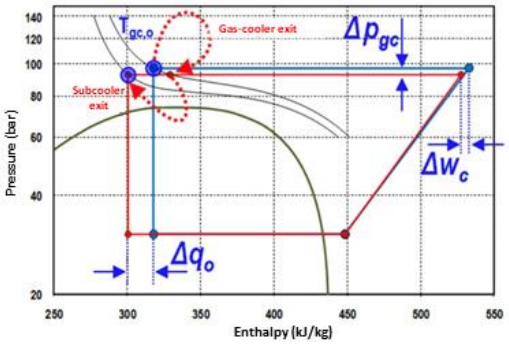

Figure 1. Ph diagram of the CO_2 transcritical cycle with no subcooling (blue) and with DMS (red) and their main effects.

Both systems have the purpose of subcooling the CO_2 at the exit of the gas-cooler in order to increase the specific cooling capacity (q_o) of the cycle. These subcoolings also allow reducing the discharge pressure (p_{gc}), reducing the compression work (W_c), as shown in Figure 1.

Figure 2 shows the DMS cycle in a schematic way and the IMS is represented on Figure 3. Both cycles have an additional heat exchanger (subcooler) located after the gas-cooler, being responsible of the subcooling. In the same way, the two cycles have an additional compressor to favor this subcooling. The big difference between both is that the DMS is a cycle separated from the main cycle, working with any refrigerant, as long as its COP is higher than the global cycle. In contrast, the IMS is part of the main cycle and works with the CO_2 itself, resulting in the simplest cycle configuration of the two and requires less components.

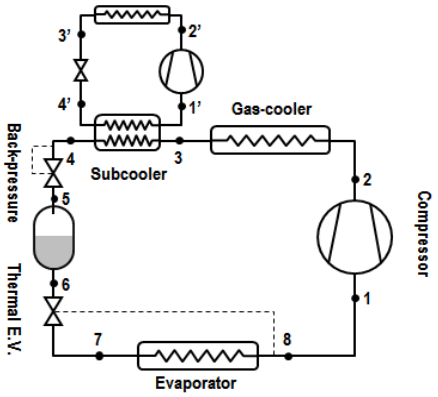

Figure 2. CO_2 cycle with DMS.

The presence of a second compressor means an increase in the electric power consumption. Because of that, it is necessary to find the optimal operating conditions to maximize the COP of the cycle. To achieve these optimal operating conditions it is necessary to regulate the subcooling degree (SUB) calculated with equation (1) and the discharge pressure, as shown by the preliminary theoretical studies: there is a pressure and a degree of subcooling for which the value of COP higher, this being the quotient between the total cooling capacity of the system (Q_o) and the consumption of both compressors (P_c), as shown in equation (4).

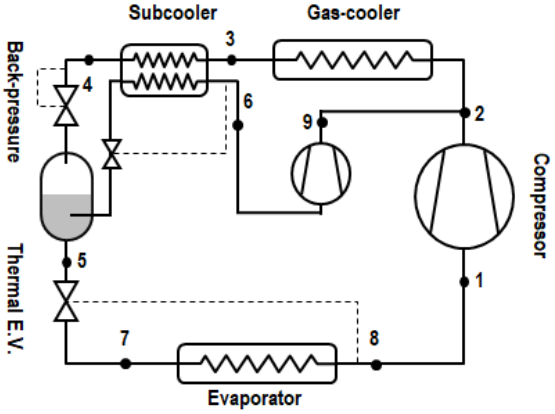

Figure 3. CO_2 cycle with DMS.

$$SUB = T_3 - T_4 \quad (1)$$

$$\dot{Q}_o = \dot{m}_{CO2} \cdot (h_8 - h_7) \quad (2)$$

$$P_c = P_{c,main} + P_{c,aux} \quad (3)$$

$$COP = \frac{\dot{Q}_o}{P_c} \quad (4)$$

Theoretical Results

In first place, the main operating parameters of these cycles are studied and analyzed in a theoretical way, such as the COP or the cooling capacity, among others. These parameters are evaluated for different working conditions: ambient temperatures (T_{amb}) from 15ºC to 40ºC and for evaporation levels (0ºC and -10ºC), always operating in conditions of optimum pressure and optimum subcooling degree, to obtain the maximum COP. The main assumptions in the simulations are:

- Subcritical regime when T_{amb} <25ºC and transcritical regime when T_{amb}> 25ºC.
- Gas-cooler approach of 5K and 10K in the DMS condenser.
- The efficiency considered for the subcooler is 60% (experimental data) and 40% for the internal heat exchanger (IHX).
- Pressure drop and heat losses are not considered.
- Thermodynamic properties are obtained through the REFPROP software v.9.1[10].
- Useful superheat in the CO_2 evaporator is 10K and in the MS evaporators is 5K.
- Behavior of compressors is simulated based on their global (η_g) and volumetric (η_v) efficiency curves obtained from empirical data:

TABLE 1. GLOBAL AND VOLUMETRIC EFFICIENCY RELATIONS.

Main (CO_2)	$\eta_v = 1.017 - 0.112 \cdot t$
	$\eta_g = 0.736 - 0.052 \cdot t$
IMS (CO_2)	$\eta_v = 1.017 - 0.112 \cdot t$
	$\eta_g = 0.736 - 0.052 \cdot t$
DMS (R1234yf)	$\eta_v = 0.972 - 0.053 \cdot t$
	$\eta_g = 0.632 - 0.037 \cdot t$

The obtained theoretical results for each of the cycles are contrasted with those obtained for the base cycle: CO_2 system with internal heat exchanger (IHX), which is considered as the reference cycle. To compare the sub-cooling cycles with the base cycle, the increments obtained with each of them in terms of COP and capacity are calculated from the following expressions:

$$\Delta COP(\%) = \frac{COP_{MS} - COP_{ref}}{COP_{ref}} \times 100 \quad (5)$$

$$\Delta \dot{Q}_o(\%) = \frac{\dot{Q}_{o,MS} - \dot{Q}_{o,ref}}{\dot{Q}_{o,ref}} \times 100 \quad (6)$$

Figure 4 shows the evolution of the COP of each of the studied cycles as a function of the ambient temperature. It can be observed that in all cases, subcooling the CO_2 is beneficial since it always increase the COP. It should also be noted that the higher the ambient temperature is, the greater is the increase achieved. This makes them ideal systems to be implemented in hot climates, where CO_2 has lower performance.

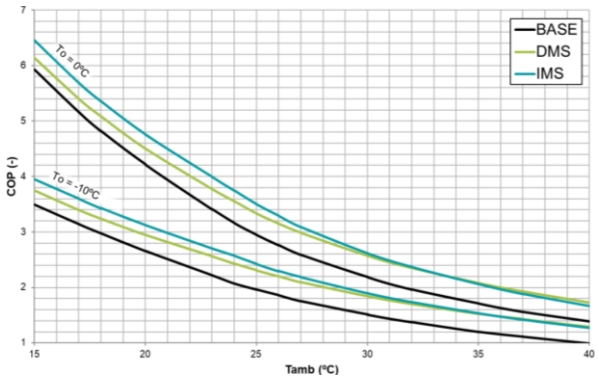

Figure 4. COP evolution for the analyzed systems.

TABLE 2. COP INCREMENTS.

DMS		
Evaporation level	0ºC	-10ºC
Subcritical	3.6% –15.7%	7.1% – 20.8%
Transcritical	12.2% – 25.4%	16.6% – 31.8%
IMS		
Evaporation level	0ºC	-10ºC
Subcritical	8.8% - 21.6%	13.0% - 26.8%
Transcritical	16.8% - 20.4%	22.0% - 28.5%

On the other hand, Figure 5 presents the increases obtained in terms of cooling capacity thanks to the use of DMS system and Figure 6 of IMS. The same trend is observed: greater increase at higher ambient temperatures, and greater benefit when lower the evaporation level is.

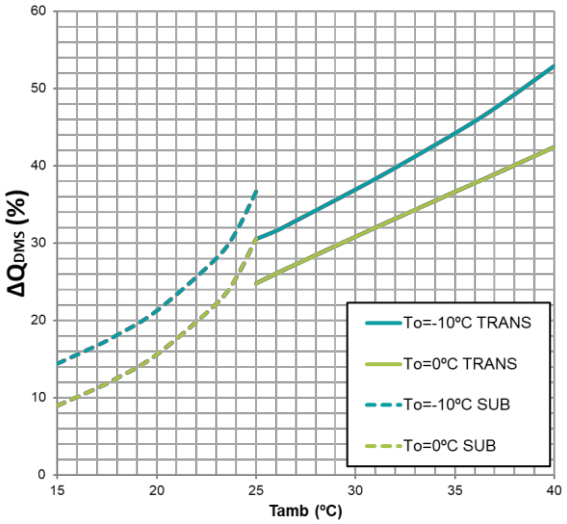

Figure 5. Cooling capacity increments due to the use of the DMS respect to the reference system.

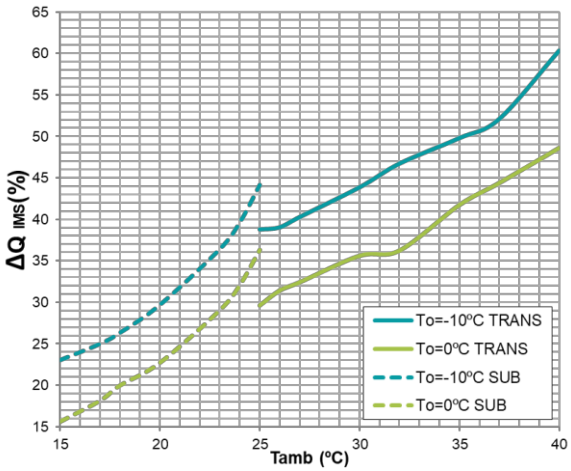

Figure 6. Cooling capacity increments due to the use of the IMS respect to the reference system.

Experimental Data and Discussion

Based on the theoretical calculations, the mechanical subcooling cycles have been dimensioned and designed to apply them to a real laboratory plant. The selection and acquisition of the components has allowed the assembly of the cycles for testing them and to test it to corroborate the results obtained with the simulation. The tested cycle is the dedicated mechanical subcooling system, composed of the main CO_2 cycle and the auxiliary cycle. Two levels of evaporation and 3 heat rejection temperatures between 24 and 40ºC have been tested. The tests were performed in steady state conditions during 15 minutes, in a wide range of gas-cooler pressure going from 74 to 120 bar. The experimental plant is presented in Figure 7. Both compressors have been tested at nominal speed. It is necessary to remark that these are the first tests to understand the behavior of the cycle and therefore the plant has not been evaluated at optimal conditions, to reach the optimum COP, the subcooling degrees must be

optimized, regulating the rotation speed of the secondary compressor.

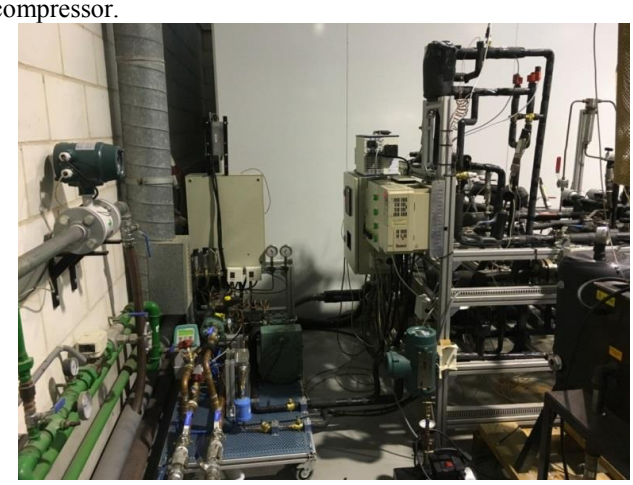

Figure 7. Experimental CO_2 plant with dedicated mechanical subcooling.

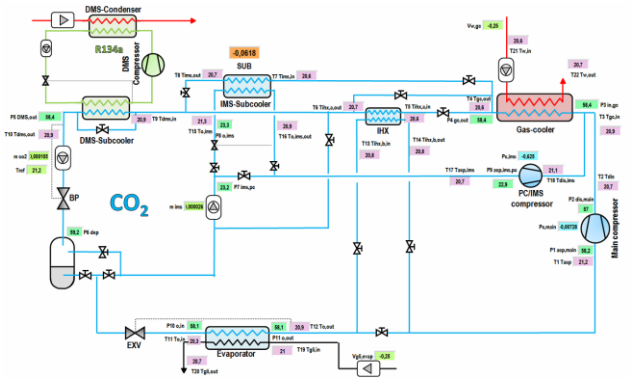

Figure 8. Scheme of the experimental plant and interface of the test monitoring application.

The obtained values of COP for the evaporation level of 0ºC in the experimental tests are represented in Figure 8. In green the behavior of the reference cycle is observed and in red the COP for the plant using the dedicated mechanical subcooling. To quantify the increments, the points with maximum COP are compared, since they would be the points of operation of the machine. The obtained increments are 26.1% at 40.0°C, 22.1% at 30.2°C and 10.9% at 24°C.

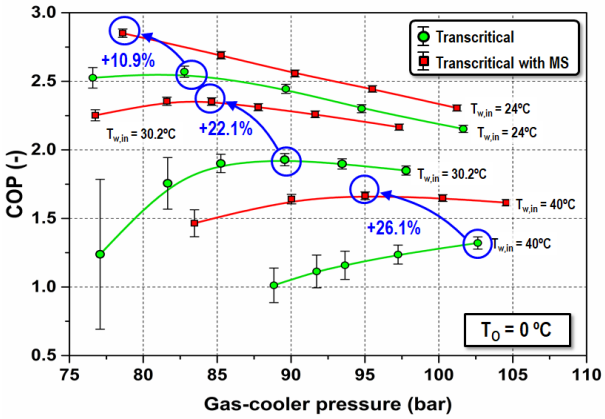

Figure 9. Experimental COP for and evaporating level of 0ºC with and without DMS.

Table 3 summarizes the increments obtained experimentally in terms of COP for both tested evaporation levels.

TABLE 3. EXPERIMENTAL COP INCREMENTS.

Evaporation level	0ºC	-10ºC
$T_{w,in}$=24.0ºC	10.9%	6.9%
$T_{w,in}$=30.2ºC	22.1%	24.1%
$T_{w,in}$=40.0ºC	26.1%	30.3%

Figure 10 presents the cooling capacity obtained for the tested conditions. The measured increments in cooling capacity are 39.4% for 40.0ºC, 34.0% for 30.2ºC and 23.1% for 24.0ºC and table 4 summarizes all the measured increments of capacity.

TABLE 4. EXPERIMENTAL COOLING CAPACITY INCREMENTS.

Evaporation level	0ºC	-10ºC
$T_{w,in}$=24.0ºC	23.1%	24.2%
$T_{w,in}$=30.2ºC	34.0%	41.1%
$T_{w,in}$=40.0ºC	39.4%	55.7%

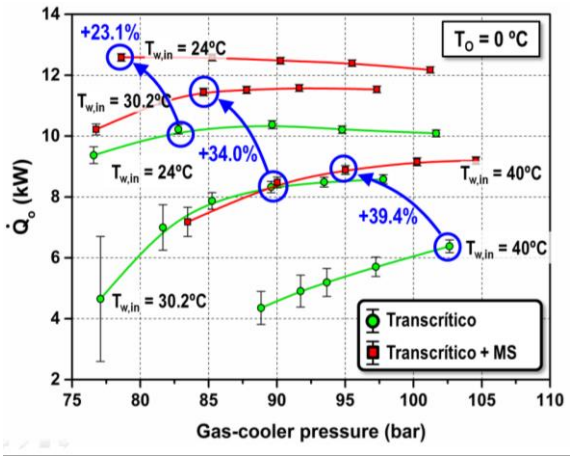

Figure 10. Experimental cooling capacity for and evaporating level of 0ºC with and without DMS.

These experimental results corroborate the results obtained theoretically: the mechanical subcooling is beneficial both in terms of COP and cooling capacity; the increases are higher for lower evaporation temperatures and higher when higher are the ambient temperatures.

Feasibility and economic study

According to the energy parameters we have seen that the integrated cycle was the most beneficial but it is necessary to make a study for a specific application and take into account the economic parameters to know, globally, which of the cycles should be implemented in each case.

For this study the cycles have been evaluated over a climatological year for different climates based on the method of temperature BINs, for four different cities, which climate conditions and location are presented in Figure 11 and Table 5; and for 5 different plant sizes. The cycles have been studied for the application of commercial refrigeration, with constant load requirement, since the plant is placed in an air-conditioned room; and for industrial refrigeration, with variable load, since the system is subject to changes in the environment.

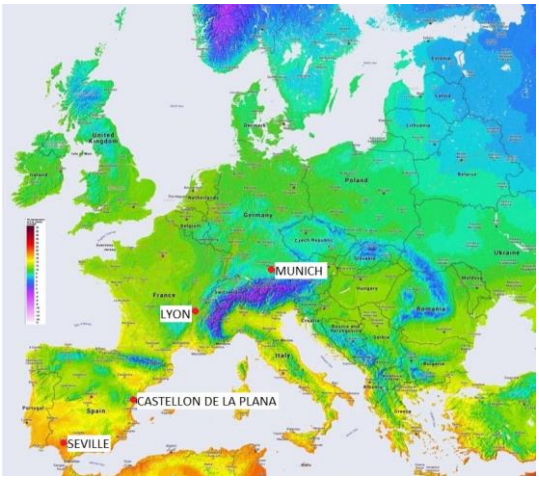

Figure 11. Location of the studied cities.

TABLE 5. CLIMATE CONDITIONS OF THE EVALUATED LOCATIONS.

City	Average temperature	Climate
Seville	18.3ºC	Hot
Castellon de la Plana	16.8ºC	Warm
Lyon	12.0ºC	Tempered
Munich	8.1ºC	Cold

It has been seen that subcooling improves COP and capacity, therefore reducing electricity consumption and achieving energy savings. This savings will depend on the location of the plant, the type of demand and the system used. Annually, the savings achieved with the use of the IMS are higher than the DMS ones and these savings are greater when warmer is the climate.

Table 6 shows the total investment cost of installing the subcooling system to an existing CO_2 plant for different cooling capacities.

TABLE 6. COST OF IMPLEMENTATION OF EACH OF THE SUBCOOLING CYCLES.

	IMS	DMS
	Total inversion (€)	
10kW	1971	2102
20kW	2185	2349
40kW	3209	3204
80kW	4582	4052
100kW	5694	4242

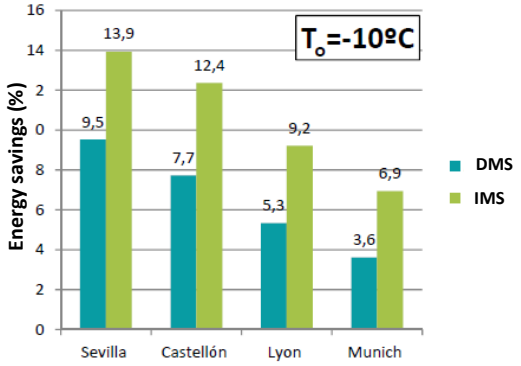

Figure 12. Energy savings for commercial application at -10ºC of evaporating level.

It can be seen that when greater is the plant, proportionally, lower is the inversion that must be done. According to the COP obtained for each cycle and the ambient temperatures of each city during the year, the energy savings are calculated and presented in Figure 12 for commercial refrigeration.

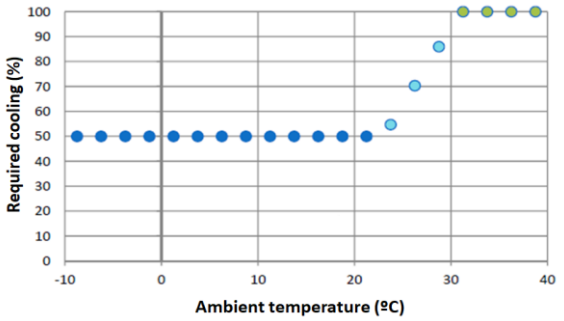

Figure 13. Considered cooling required capacity.

For industrial refrigeration, the required capacity is considered as a function of the ambient temperature, as shown in Figure 13.

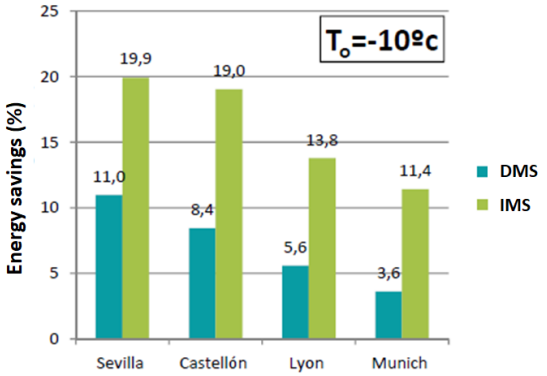

Figure 14. Energy savings for industrial refrigeration (variable load) at an evaporating level of -10ºC.

The energy saving that are reached in this applications are presented in Figure 14. It can be observed that they are greater for hot ambient temperatures and the IMS system gets significantly higher savings. These energy savings imply annual economic savings. Taking into account the price of electrical energy consumption, this economic savings can be calculated. The savings obtained using the IMS for industrial refrigeration at -10ºC are represented in Figure 15. These savings are very significant for big size plants at warm countries.

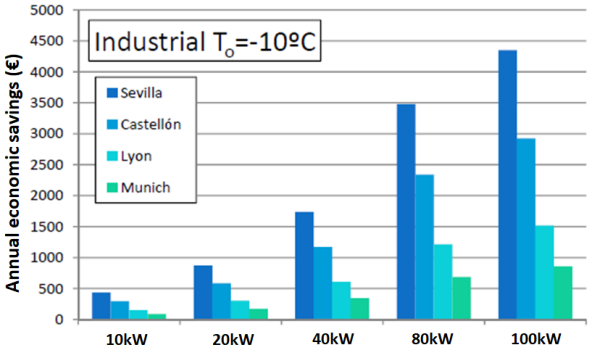

Figure 15. Annual economic savings for industrial refrigeration using the IMS.

For the economic study, energy savings have been translated into annual economic savings but investment cost should be also considered in the study. These extra costs of implementation are compared with the obtained savings to see the profitability of the investment. For this, the profitability, the Payback and the internal rate of return (I.R.R.) have been evaluated.

Figure 16 shows the payback for the 100kW IMS plant in each location. From this study it can be concluded that for cold climates such as Munich, the payback is very high, so it would not be an adequate investment. In hot and warm climates, this parameter is much more reasonable. We also see that the payback is lower for lower evaporation temperatures and for industrial refrigeration the return period is lower.

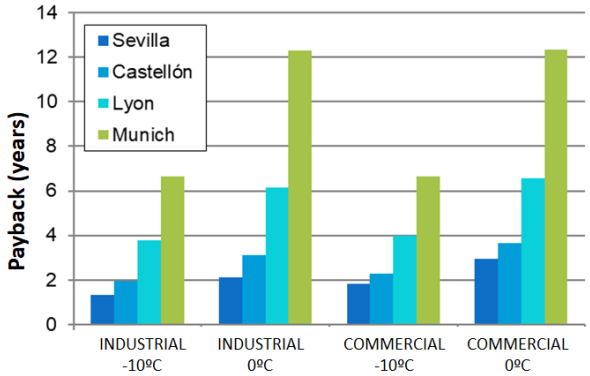

Figure 16. Payback of the IMS system of 100kW of capacity.

Depending on the size of the plant, it is observed that when greater is the capacity of the plant, the return period is lower. In terms of profitability and I.R.R. the obtained values are always positive for the locations of Seville and Castellón, unprofitable values in Munich and a medium term in Lyon, being only a profitable investment in this area for large plants.

TABLE 7. ECONOMIC PARAMETERS FOR THE IMS IN SEVILLE (INDUSTRIAL REFRIGERATION AT -10ºC).

Plant capacity	I.R.R. (%)	Profitability (%)	Payback (years)
10kW	21	19	4.53
20kW	40	33	2.51
40kW	54	46	1.84
80kW	76	65	1.32
100kW	76	64	1.31

Conclusions

In this project the cycles of dedicated mechanical subcooling and integrated mechanical subcooling have been studied both theoretically and experimentally. The study of the cycles has shown that both increase the COP and the capacity of the reference cycle but the IMS does it to a greater extent:

- COP: between 13% and 29% for To = -10ºC and between 9% and 20% for To = 0ºC
- Qo between 23% and 60% for To = -10ºC and between 16% and 49% for To = 0ºC.

Likewise, the dedicated mechanical subcooling has been experimentally tested, verifying the tendencies obtained in the theoretical results.

The study of economic viability allows not to recommend the implementation of these systems in cold climates (Annual average temperature <12ºC). On the other hand, we observe that for plants of size greater than 40kW, both mechanical subcooling systems are a highly recommended alternative, which also allows adapting to the F-Gas regulation, being the IMS the most beneficial system both energetically and economically.

Future lines for this work must be the experimental evaluation of the IMS and the optimization of the control of the plants that can be complex due to the different parameters to be regulated.

ACKNOWLEDGEMENTS

Author gratefully acknowledges Ministerio de Economía y Competitividad of Spain (project ENE2014-53760-R.7), Jaume I University of Spain (project UJI-B2017-06) and Ministerio de Educación, Cultura y Deporte (grant FPU16/00151) for financing this research work. Author gratefully acknowledges R. Llopis for teaching me everything and giving me the opportunity to work on this project.

REFERENCES

[1] International Institute of Refrigeration, 29th Informatory Note on Refrigeration Technologies. The Role of Refrigeration in the Global Economy. 2015, IIR: France.

[2] IPCC, Climate Change 2014: Synthesis Report. Contribution of Working Groups I, II and III to the Fifth Assessment Report of the Intergovernmental Panel on Climate Change [Core Writing Team, R.K. Pachauri and L.A. Meyer (eds.)]. IPCC, Geneva, Switzerland, 151 pp. 2014.

[3] United Nations, The Kyoto Protocol to the Framework Convention on Climate Change. 1997. Available at: <http://unfccc.int/essential_background/kyoto_protocol/background/items/1351.php>. 1997.

[4] UNEP, Report of the Twenty- Eighth Meeting of the Parties to the Montreal Protocol on Substances that Deplete the Ozone Layer. 2016: Kigali, Rwanda.

[5] International Institute of Refrigeration, Refrigeration drives sustainable development. State of the Art - Report Card. . IIR/IIF–UNEP, 2007.

[6] European Commission, Regulation (EU) No 517/2014 of the European Parliament and of the Council of 16 April 2014 on fluorinated greenhouse gases and repealing Regulation (EC) No 842/2006. 2014.

[7] Llopis, R., et al., Energy improvements of CO2 transcritical refrigeration cycles using dedicated mechanical subcooling. International Journal of Refrigeration, 2015. **55**(0): p. 129-141.

[8] Nebot-Andrés, L., et al. Experimental evaluation of a dedicated mechanical subcooling system in a CO2 transcritical refrigeration cycle. in Refrigeration Science and Technology. 2016.

[9] Dai, B., et al., *Energetic performance of transcritical CO2 refrigeration cycles with mechanical subcooling using zeotropic mixture as refrigerant*. Energy, 2018. **150**: p. 205-221.

[10] Lemmon, E.W., M.L. Huber, and M.O. McLinden, *REFPROP, NIST Standard Reference Database 23, v.9.1. National Institute of Standards, Gaithersburg, MD, U.S.A.* 2013.

3rd Place
HVAC World
Student Competition

Rohit Upadhyay
USA

Performance Evaluation of Active Chilled Beam in Real Office Conditions in a High-Performance Building in Heating

Rohit Upadhyay, Rodrigo Mora

Rohit Upadhyay is a graduate student at the British Columbia Institute of Technology, Vancouver, BC, Canada.
Email: rupadhyay@my.bcit.ca
Rodrigo Mora, Ph.D., P.Eng. is a faculty member in the Building Science Graduate Program at the British Columbia Institute of Technology.
Email: Rodrigo_Mora@bcit.ca

The paper is a part of the thesis "Performance evaluation of active chilled beam in cooling and heating operation under actual field boundary conditions." submitted in October 2018 in partial fulfillment of the requirements for the Degree of Master of Applied Science in Building Engineering/Building Science at the British Columbia Institute of Technology (BCIT), Vancouver, Canada.

The British Columbia Institute of Technology is located at 3700 Willingdon Avenue, Burnaby, British Columbia, V5G 3H2, Canada.

Abstract—Active Chilled Beams (ACB) units are air induction units that handle the cooling needs of spaces with a limited amount of primary air. These systems are energy-efficient and are widely adopted worldwide; however, in-depth investigations on the performance of ACB systems under real office conditions are still inadequate. The performance of ACB in heating mode has not been documented and deserves close investigation. The study investigated the operation of 4-pipe ACB under heating mode in a LEED Gold Building at British Columbia Institute of Technology in Vancouver climate under steady state conditions. The air velocity and temperature distribution inside an office under heating mode were studied and found that the ACB system is effective in heating. The Surface temperature distribution was found close to the setpoint temperatures. The supply velocity and supply temperature at both slots of ACB were found different. It was concluded that the difference could be uneven pressure distribution in the primary air plenum and heat exchanger design of the ACB which need further research and investigation in a controlled environment.

***Index Terms*—Active Chilled Beam, ACB, Active Chilled Beam in Heating.**

Introduction

Many types of HVAC indoor terminal units are employed in HVAC applications including diffusers, fan coil units, unit ventilators, active and passive chilled beams, radiant ceiling, etc. Currently, Active Chilled Beam (ACB) terminal unit is considered as one of the leading energy-saving systems because energy is transferred through the water instead of air. ACB was also listed as one of the 15 most promising HVAC related technologies by American Council for Energy-Efficient Economy (ACEEE) in 2009 [1]. Many laboratory experiments have claimed that ACB can offer improved Indoor Environment Quality (IEQ) with great energy savings potentials. The experience with such a unit is growing worldwide, therefore, it is necessary to research and analyze the performance of ACB under real conditions. ACB systems are employed commonly in North America for heating and cooling in commercial buildings especially in a high-performance building where ACB saves fan energy and helps to achieve the optimize energy performance credits under Energy and Atmosphere category for LEED certification. Although many studies have been done in past in cooling mode, the experience of ACB under heating mode is still not studied and require detailed investigation. The purpose of this study was to assess the performance of Active Chilled Beam under real operating conditions in an academic building under heating mode. This study is an initial investigation of ACB performance under heating mode. The study was accomplished by investigating the air velocity and temperature distribution at the outlet of the ACB and inside the office environment under heating mode.

Working Principle of Active Chilled Beam

Active Chilled Beam (ACB) is a device where a specific amount of primary air is supplied through an air handling unit or Dedicated Outdoor Air System (DOAS) to the plenum of the ACB unit. This air is then discharged through induction nozzles in the unit, which induces indoor room air. The induced air flows through the integral water coil (heat exchanger), where it is either heated or cooled based on the water temperature. Then primary air (from air handling unit) and secondary air (induced through the coil) are mixed in the beam and diffused into the room space as supply air through slots located at the bottom of the beam [2]. Operation of an Active Chilled Beam is illustrated in Figure 1. It is to be noted that at the outlet of the nozzle, a low-pressure region is created as the pressure at the nozzle is reduced when air flows through the nozzle. All pressure reduction occurs at the primary air nozzle which results in a low-pressure region immediately at the nozzle outlet. This low-pressure area is slightly lower in pressure than the surrounding room air; therefore, this low-pressure area attracts the surrounding room air, which is at a slightly higher pressure as illustrated in Figure 1 [3]. The efficiency of the induction effect is dependent on the number, size, efficiency of the nozzles and the density and geometry of the secondary cooling coil. This secondary air from the conditioned space is moved across the heat exchanger without the need of any fan energy; therefore, the induction effect is a significant contributor to the energy reduction potential of active beams. Typically, an active beam can induce the secondary air of up to 2 - 5 times the primary air quantity. Usually, the temperature of the water is 14-18°C (57- 65°F) for cooling and 30-45°C (86 - 113°F) for heating application. The water flow rate is regulated for the control of indoor room temperature [4]. Modern ACB is equipped with both the coils, 2-pipe units are capable of either heating or cooling only and 4-pipe units are capable of both cooling and heating.

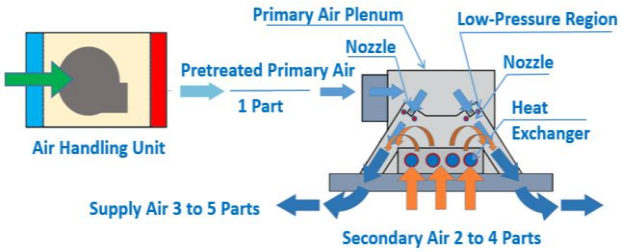

Figure 1. Working Principle of Active Chilled Beam

Methods

The study was carried out in a 3-story high-performance LEED Gold Building at British Columbia Institute of Technology in Burnaby City, province of British Columbia, Canada as shown in Figure 2. The building is located at 49° 14' N and 123° W, 20 km away from the Vancouver International Airport. The office selected for the study was second-floor perimeter office room with a size of 4.60 x 3.00 x 2.95 m (15.1 x 9.84 x 9.7 ft.) high, as shown in Figure 3 & 4. This perimeter office is enclosed by a double façade as shown in Figure 2. The west and north walls are exterior walls, and the east and south walls are the interiors. The exterior walls are made of reinforced concrete. The walls are highly insulated and calculated U values of walls and windows are shown in Table I. The room is illuminated by two ceiling mounted lights. The cooling or heating in the office room is realized with 2 – way flush mounted Active Chilled Beam installed in the acoustic tile ceiling. The ACB details are presented in Table II. The length of the inlet slot is equal to the length of the beam and it is located symmetrically in relation to the centerline of the room and parallel to the window as

illustrated in Figure 4. The primary air is supplied by a central air-handling unit, which is connected to a Water Source Heat Pump (WSHP). The flow and temperature of primary air are recorded in the Building Automation System (BAS). The hot water and chilled water temperature supplied to the chilled beam are also recorded in BAS. The room is exposed to the outside environment only on the west side. The exposed wall has a fixed window of size 2.00 m (6.6 ft.) wide and 2.15 m (7.1 ft.) high with an operable sash of size 1.4 m (4.6 ft.) wide x 0.5 m (1.64 ft.) high.

Figure 2. BCIT Building in Greater Vancouver, BC, Canada

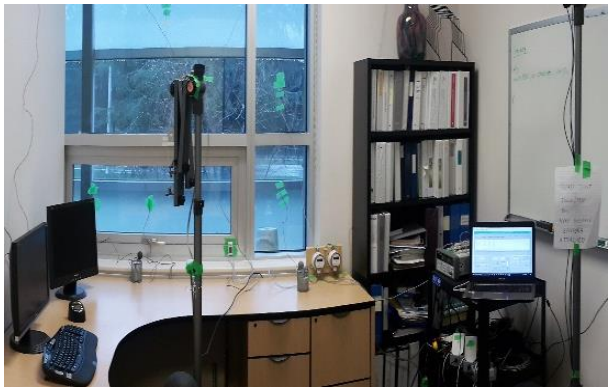

Figure 3. The Perimeter Office on the Second Floor.

TABLE I.
BUILDING DESIGN SUMMARY

Mechanical System	Central Air Handling Units with WSHP
Terminal Units	ACB (Cooling & Heating)
Interior Partitioned Wall	U Value – 0.73 W/m^{2}K
Exposed Wall	U Value – 0.30 W/m^{2}K
Interior Concrete Wall	U Value – 1.86 W/m^{2}K
Slab (Top and Bottom)	U Value – 0.80 W/m^{2}K
Overall Window	U Value – 2.61 W/m^{2}K

Measurements

Room air temperature and velocity were measured at 4 different heights at various locations in the office. Room operative temperature and globe temperature were also measured close to the occupant. Discharge air temperature and velocity at the beam slots were recorded during the experiment, as well as, the induced air temperatures and velocity. Outdoor temperature and surface temperatures were recorded which are described in Table III. Differential pressure (DP) at the ACB plenum, door and window were also recorded. The pressure difference across the door and window was found very low and is not reported in the paper.

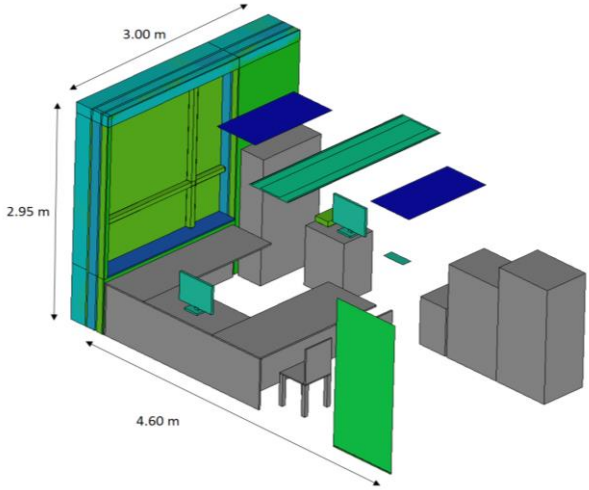

Figure 4. Dimensions and Layout of the Office

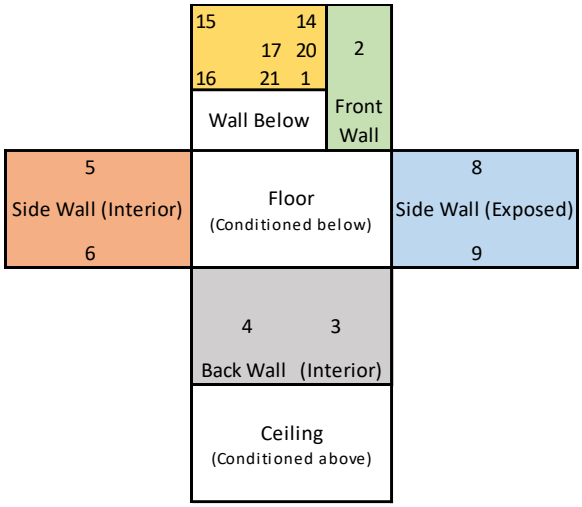

Figure 5. Room Unfolded Surfaces with Temperature Sensors

TABLE II.
SPECIFICATION OF THE ACTIVE CHILLED BEAM

Overall Size	2.40 x 0.60 x 0.21 m	
Number of Beams	1 unit	
Cooling Capacity	1154.0 W	
Heating Capacity	1422.0 W	
	Design	Measured in Office
ACB Plenum Pressure Design	158.0 Pa	140.0 Pa
Supply Chilled Water Temperature	15.8°C	16.0°C
Supply Hot Water Temperature	48.9°C	45.0°C
Primary Air Flow	0.028 m3/s	0.024 m3/s
Primary Air Temperature	18.0°C	18.0°C
Operation Schedule	5.00 AM – 10.00 PM	

TABLE III.
SENSOR SPECIFICATIONS FOR OFFICE EXPERIMENT

Sensor	Application	Type	Range	Accuracy
Temperature	ACB Supply / Return Air Temperature	HOBO MX1101	-20° - 70°C (-4° - 158°F)	±0.21°C from 0° to 50°C (±0.38°F from 32° to 122°F)
Temperature	Air Temperatures	HOBO U12-013	-20° - 70°C (-4° - 158°F)	±0.35°C from 0° to 50°C (±0.63°F from 32° to 122°F)
Temperature	Operative Temperatures	HOBO U12-013 with TMC6-HD	- 40° - 100°C (-40° - 212°F)	±0.25°C from 0° to 50°C (±0.45°F from 32° to 122°F)
Temperature	Outdoor Temperature	HOBO MX2302	-40 to 70°C (-40 to 158°F)	±0.2°C from 0 to 70°C (±0.36 from 32 to 158°F)
Surface Temperature	Wall & Window Temperatures	NXFT15XH103FA2B050 Thermistor	-40°C - 125°C (-40° - 257°F)	±0.2 °C (±0.36°F)
Air Velocity Transducer	Room Air Velocity	SensoAnemo 5100LSF	0.05 - 5 m/s (9.84 – 984 fpm)	±0.02 m/s (3.93 fpm) ±1.5% of readings
Air Velocity Transducer	ACB Supply & Return Velocity	TSI 8475	0 - 2.5 m/s (0 – 492 fpm)	±3.0% of reading

Surface Temperature Measurements

Wall and window surface temperatures were recorded by NTC thermistors. Figure 5 shows the surface labelling of the office and the location of temperature sensors placed on the walls and window. The sensors were placed 0.3 m (1 ft.) below the ceiling for all walls while window temperatures were measured at various locations. Mean radiant temperature was measured by globe thermometer. Data from thermistors and globe were recorded by the Agilent 34972A data logger at every 60 seconds. The details of the sensor used in the experiment are given in Table III.

Room Air Temperature and Velocity Measurements

The measurement of air temperatures and air velocities at different heights were carried out by omnidirectional calibrated anemometers SensoAnemo 5100LSF. The anemometers were placed on a manifold at 0.1 m (0.33 ft.), 0.6 m (2.0 ft.), 1.1 m (3.6 ft.) and 1.7 m (5.6 ft.) heights above the floor as shown in Figure 6, and moved manually at possible occupant's location in the room. The averaging time at each point was 180 seconds. The possible occupant's location is shown in Figure 20. The supply and return air velocity of the beam were measured by TSI 8475 anemometers as shown in Figure 7 and recorded on the Agilent 34972A Data logger at every 60 seconds. The details about anemometers are given in Table III.

Heat Load

Two laptops, data logger and ceiling lights were used as heat sources inside the room. The window of the office at the external wall is shaded by the structure of double façade and partly by trees to protect the office from direct solar radiation and the room temperature is fairly stable at all time, therefore, solar radiation was not considered and measured under the heating mode study of ACB. The details of heat load present during the test are detailed in Table IV. The monthly average outdoor air temperature during the experiment, recorded at the study building was 5.7°C (42°F). The measurements were taken with a real occupant working in the office under heating mode in the month of January 2018. The room temperature was varied between 20°C (68°F) to 24°C (75°F) and measurements were performed.

TABLE IV.
INTERNAL HEAT LOAD AND OTHER CONDITIONS

Lighting Load	10.8 W/m2
Equipment Load	200 W
Occupancy	1 person - 130 W

Figure 6. Local Air Velocity and Temperature Measurement

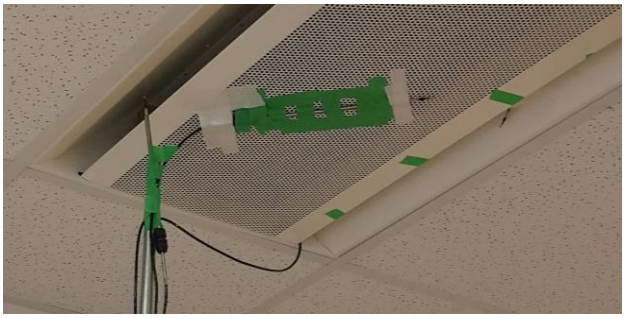

Figure 7. Supply and Return Velocity Measurement of ACB

Results & Discussion

Coanda Effect

The temperature of the air jet discharged through the ACB is different from the ambient (room) air and therefore this experiment illustrated the case of a non-isothermal jet behavior in office. The Coanda effect was seen at the exit of ACB slots. Coanda effect is the tendency of the free jet attached to the ceiling. As soon as the high-velocity jet is discharged from the nozzles and further through the ACB system the air jet is seen attached to the ceiling due to low-pressure region creation above the jet.

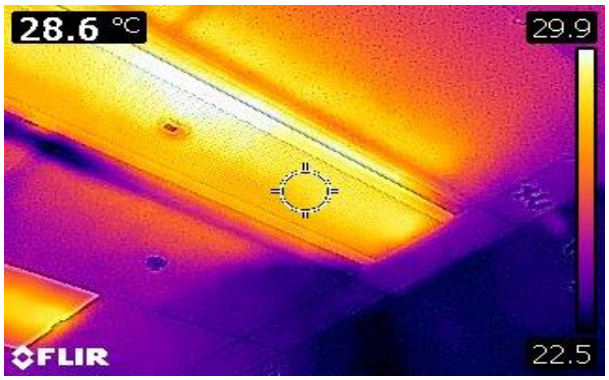

(a)

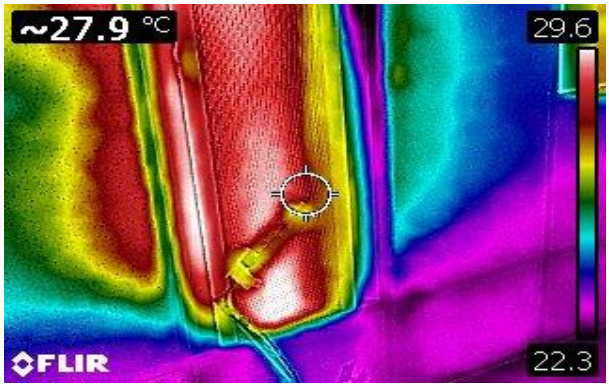

(b)

(c)

Figure 8. Coanda Effect through Thermal Image Camera

This attachment of air jet ensures good thermal comfort and avoid direct throw of cold or hot air to the occupied zone. This effect was visualized in the experiment through a thermal image camera, which nicely captured the air jet attachment to the ceiling. The Coanda effect is shown in Figures 8 (a), (b) & (c).

Difference in Discharge Air Velocities at the Two Slots

The discharge air velocities were recorded during the test at both the supply slots. The velocity at one slot was found always higher than the air velocity at the other slot as shown in Figure 9. This phenomenon is due to the uneven pressure distribution at the nozzles in the ACB primary air plenum box as shown in Figure 10. The primary air supply is connected to the ACB plenum on one side and the airflow is directed towards the other end of the plenum which exerts more pressure at the nozzles at the other end. This causes the uneven air velocity distribution across the beam. The difference in velocities was also shown by Wu et al. [5] in their experiment and further in CFD modelling.

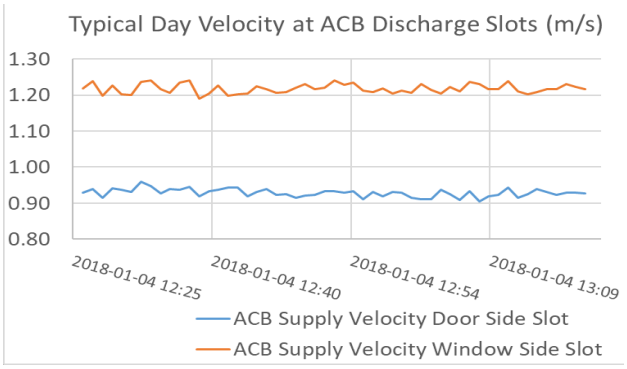

Figure 9. Discharge Air Velocity at the Two Slots

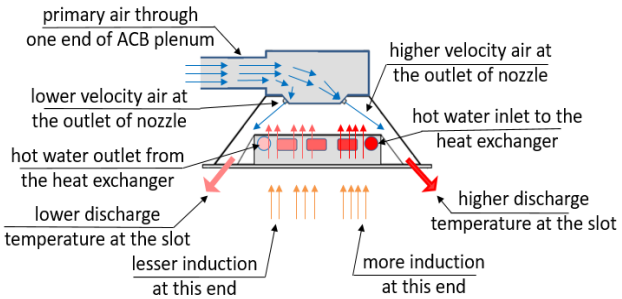

Figure 10. Discharge Velocity & Temperatures

Difference in Discharge Air Temperatures at the Two Slots

The discharge air temperatures were recorded at both the slots and found unequal, which can be seen in Figure 11. This could be due to the design and layout of the heat exchanger. The heat exchanger is placed horizontally in the ACB as shown in Figure 10. The water flowing into the heat exchanger gradually loses its heat while travelling; therefore, the temperature of the air passing through the heat exchanger is uneven, which in turn causes uneven discharge air temperatures. This effect is enhanced by the different discharge velocities at the two slots as explained above which enhances induction at one end and hence more

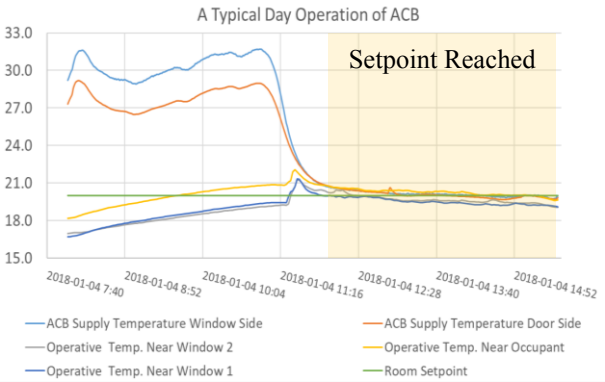

Figure 11. Discharge Air Temperatures at the Two Slots

heat transfer. The hot water inlet to the heat exchanger, higher discharge nozzle velocity (in turn higher induction) coincided at the same side of the tested beam in the experiment and therefore this phenomenon deserves further investigation in a controlled environment with ACB from different manufacturers to compare and analyze. When the room reaches steady state, the non-isothermal jet from ACB turns into an isothermal jet (water flow across the heat exchanger stops or reduced to minimum flow) this phenomenon is then minimized and temperature at both the discharged slots becomes nearly equal as shown in Figure 11.

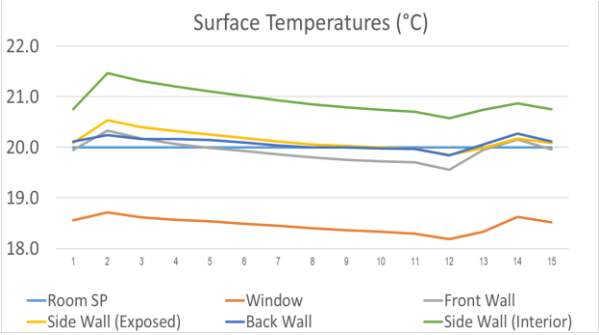

Figure 13. Surface Temperatures

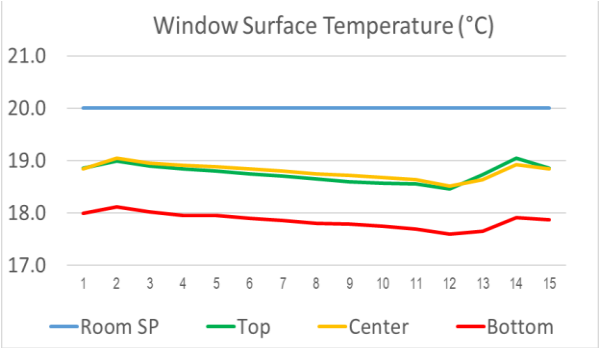

Figure 14. Window Temperatures at the Top, Bottom and Center

Surface Temperature Distribution

Figures 13 & 14 illustrate the surface temperature distribution of room surfaces after attaining the steady state. Each set of temperatures is an average of 15 minutes measured from 12.31 to 4.15 PM. The temperatures of all surfaces were found in line and within ±1°C (±1.8°F) range versus the room setpoint of 20°C (68°F) except the window, which can be seen in Figure 14. The window temperature at the top and center were recorded close to the room setpoint temperature but the bottom of the window was found within -2.5°C (-4.5°F) range of setpoint temperature as shown in Figure 14. The reason of such variation in temperature is the extended aluminum profile of size 0.1 m (0.33 ft.) depth attached to the window as shown in Figure 12 which causes the obstruction to the airflow down the window and destroys the momentum of hot air flowing down.

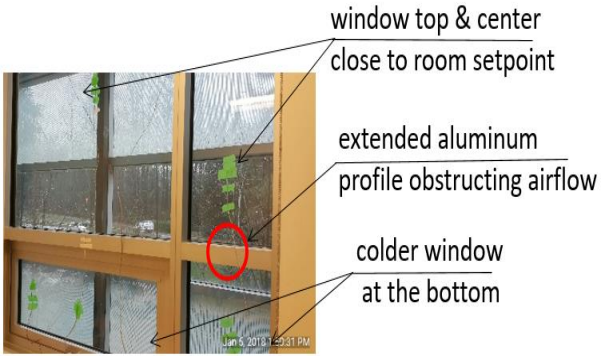

Figure 12. Aluminum Extended Profile Obstructing Airflow at the Bottom Portion of the Window

Room Air Distribution

Figures 15 & 16 illustrate air velocity and air temperature distribution, when room setpoint was 20°C (68°F), at possible occupant's location as shown in Figure 20. The velocities were within the ASHRAE recommended limit in the occupied zone to avoid the draft. It should be noted that this section presented data only for steady state condition. All measurements were taken at the steady state condition with different room setpoints. With the setpoint of 20°C (68°F), the room air is almost uniform and the temperature at a height of 0.6 m (2.0 ft.) can be observed close to the setpoint. Figures 17, 18 & 19 depict the temperature distribution at 4 different heights with different room setpoints near the occupant on different days during the experiment. It can be observed that when the setpoint was raised, to 24°C (75°F), thermal stratification starts to appear.

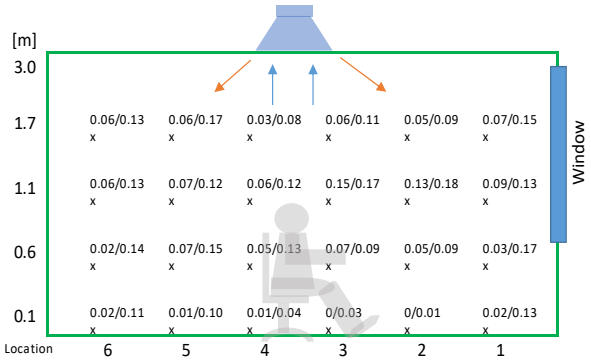

Figure 15. Average / Maximum Air Velocity Distribution (at Setpoint 20°C (68°F))

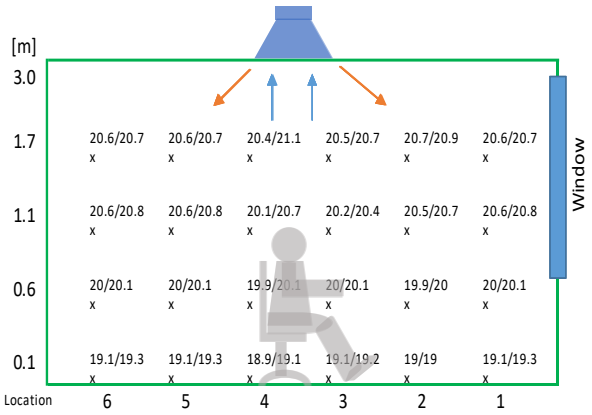

Figure 16. Average / Maximum Temperature Distribution (at Setpoint 20°C (68°F))

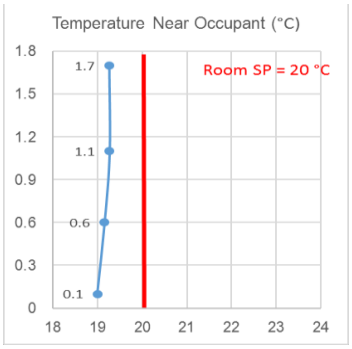

Figure 17. Temperature Distribution at 4 Different Heights at 20 °C Room Setpoint near Occupant

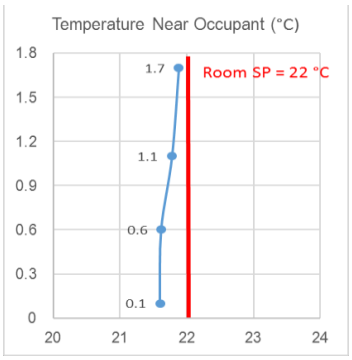

Figure 18. Temperature Distribution at 4 Different Heights at 22 °C Room Setpoint near Occupant

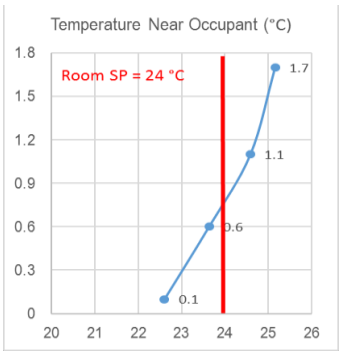

Figure 19. Temperature Distribution at 4 Different Heights at 24 °C Room Setpoint near Occupant

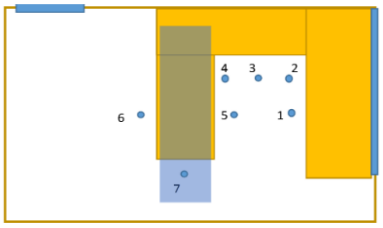

Figure 20. Possible Occupant's Location

Conclusions

The intent of the paper was to obtain field data to help appreciate the real factors that affect the performance of ACB in the heating operation, for the benefit of manufacturers and designers. The temperature and air distribution were found satisfactory which concludes that the ACB is effective in providing cooling as well as heating. Coanda effect was realized which prevents direct throw of cold and hot air to the occupied zone. The velocity and temperature distribution at the supply slots of ACB were found uneven, this could be due to the heat exchanger design and duct connection to primary air plenum which requires a further investigation and CFD analyses to model the chilled beam. The surface temperature distribution was also found close to the setpoint temperatures, except for the window. Further study on the transient operation of the ACB and CFD model is required to gain insight into the system and its limitations.

Limitations and Further Work

The results reported in this paper correspond to a single office, which can be considered representative of many similar offices in this high-performance building. Other factors affecting the performance of ACB have been observed, such as the proximity of light fittings to ACB, the location of ceiling return grille relative to ACB, partition wall layout, and effect of cold or warm enclosure surfaces on ACB throw. A small sample of offices, some with different configurations, are being studied. Experiments in a controlled laboratory environment are being planned. CFD simulations are also being developed. The results will be reported in separate publications.

Acknowledgement

We would like to acknowledge the funding for this project from the BCIT Green Value Strategies Fund.

References

[1] ACEEE emerging technologies report, 2009. Active chilled beam cooling with DOAS.

[2] K. Loudermilk, 2009. Designing Chilled Beams for Thermal Comfort. ASHRAE Journal. p. 58-64.

[3] Dadanco, Active chilled beams, available from http://dadanco.com/.

[4] Virta, M., Kosonen, R., 2005. Chilled Beams in Heating, design criteria and case study. Cold Climate conference, Moscow.

[5] Wu, Bingjie; Cai, Wenjian; Wang, Qinguo; Chen, Can; Lin, Chen; and Chen, Haoran, 2016. The Air Distribution Around Nozzles Based On Active Chilled Beam System. International High-Performance Buildings Conference. Paper 173.

3rd Place
REHVA
Student Competition

Yanting Li &
Michael Rosenlund
Denmark

REHVA
Federation of European Heating, Ventilation and Air Conditioning Associations

Investigating Indoor Environmental Quality Using Virtual Reality in Climate Chambers

Michael Rosenlund, Yanting Li, Steffen Petersen

***Abstract*— Various phenomena defining the perception of indoor environmental quality have been proven to directly or indirectly affect one and another. However, there are no extensive studies on whether there are interactions between occupants' thermal sensation and their perception of the view-out. To investigate this potential interrelationship, a semi-controlled 4 x 4 cross-over experiment involving 51 subjects (25 male, 26 female) was designed. The experiment was conducted in a climate chamber where thermal condition scenarios could be strictly controlled while the view-out scenarios were simulated using virtual reality (VR). A digital interactive questionnaire inside the VR environment was used to record subjects' thermal sensation and view-out satisfaction during the experiment. The results showed that view-out satisfaction may be more sensitive to indoor thermal conditions in rooms with moderate level of glazing compared to rooms with a high level of glazing; in rooms with high level of glazing subjects may be more forgiving towards overheating due to high view-out quality. Overall, the experiment has demonstrated that using VR in climate chambers is a promising approach for investigating interactions between the visual and indoor climate aspects.**

***Index Terms*—Thermal indoor climate, Virtual reality, Climate chamber, Subjective votes, Experimental design.**

I. Introduction

Indoor environmental quality is a subjective human conviction based on a multi-sensory experience of the space. There are many theories on how various visual phenomena and indoor climate aspects affects the perception of indoor environmental quality. These theories are to a wide extent developed under the assumption that an individual phenomenon or aspect can be investigated and theorized upon independently, i.e. assuming that there is no or little interactions between the various phenomena or aspects. Examples of this are thermal comfort models like Fanger's model [1], the adaptive comfort model [2], glare models like daylight glare probability DGP [3], and models for view-out quality and privacy [4]. Investigations on how indoor environmental quality phenomena and/or aspects interacts with one another are relatively rare but not absent. Early examples includes e.g. how room colors may affect the perception of thermal comfort and how air temperature, relative humidity and air movement (three parameters also affecting thermal comfort) may affect the perception of indoor air quality. However, to the best of our knowledge, there has not been any attempts to investigate whether indoor thermal conditions may affect the perception of view-out quality. This paper reports on an experiment investigating whether view-out satisfaction is affected by the indoor thermal conditions, and whether indoor thermal conditions influence the subjective notion of the property price.

II. Method

The experiment was conducted in a climate chamber where thermal conditions could be strictly controlled while the view-out scenarios were simulated inside the climate chamber using virtual reality (VR). The following sections briefly describes the scenarios what was investigated, the setup in the climate chamber and the VR models, the questionnaire used for subjective assessment of the scenarios, and the experimental design.

A. Description of scenarios

A total of four scenarios were defined as depicted in figure 1. The scenarios were combinations of two different thermal conditions where only the operative temperature was different while relative humidity and mean air velocity was were kept constant (RH=40%, mean air velocity=0.1 m/s), and two different window sizes. We also tried to simulate radiation from direct sun using heat lamps but this aspect was disregarded as tests revealed that the functionality of the VR goggles could not withstand the radiation heat. All subjects in the experiment had a clothing insulation level of 0.7 clo and an estimated activity level of 1.2 met. Consequently, the PMV=0.39 for scenario A and C and PMV=1.85 for scenario B and D. Air change rate was set constant at 10 l/s per person.

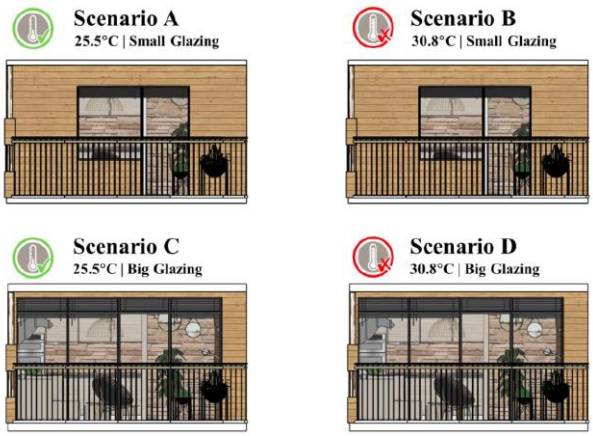

Figure 1. The four investigated scenarios. Two different operative temperatures combined with two different glazing sizes.

B. Climate chamber and VR models

The experiment took place in the two climate chambers located at the department of Public Health at Aarhus University, Denmark. The climate chambers are steel cladded chambers with a high-precision HVAC&R system. Each chamber room was equipped with VR systems to hold two participants at the same time. The setup is illustrated in figure 2.

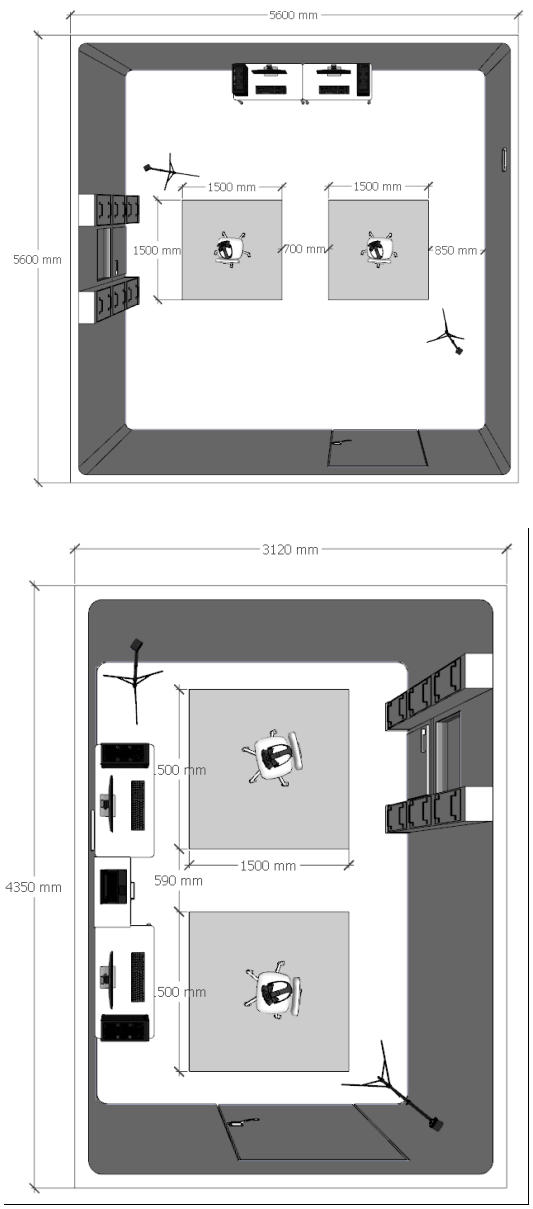

Figure 2. Illustration of climate chamber and VR setup.

The basic 3D model for the virtual reality environment was build and designed in SketchUp. This model was imported into the game development platform Unity, where the surrounding environment was generated, and the questionnaire programming were written. Subjects were sitting down during the whole experiment for security reasons but could move around inside the virtual environment using a teleportation function. Figure 3 depicts examples of the VR environment.

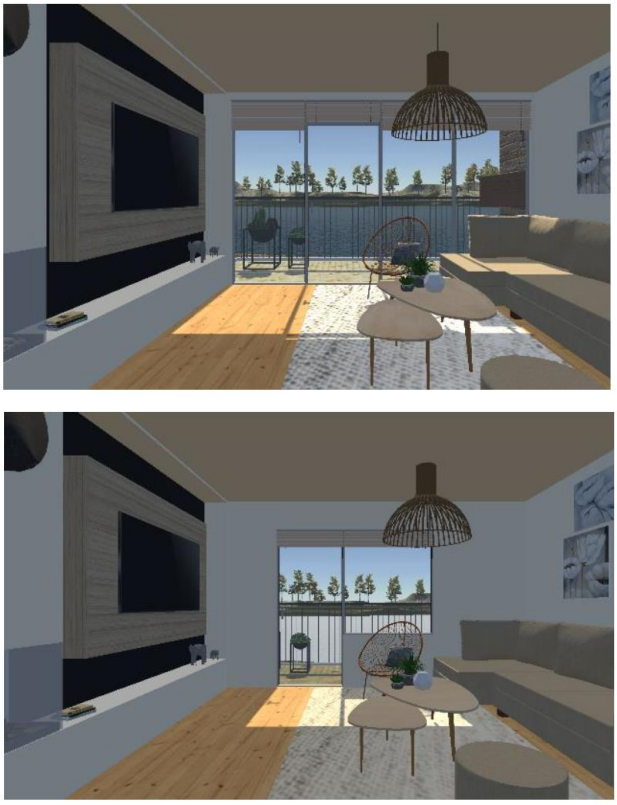

Figure 3. Illustrations from the VR environment. Top: Large glazing area. Bottom: Moderate glazing area.

C. *Questionnaire*

Questions were formulated and votes could be casted by subjects directly in the VR environment using visual analogue scales like the one shown in figure 4. Table 1 summarizes the visual analogue-scaled questions asked in each scenario of the experiment. View-out questions were asked for a VR seating position in the couch near the window and at an office desk in the back of the room.

TABLE I.
QUESTION TYPES AND SCALES USED IN THE EXPERIMENTS

Name	Question types	Voting scale
Thermal comfort	Initial thermal satisfaction	Acceptable/unacceptable: Just - clearly
	Initial thermal sensation	Very cold – very hot
	Adapted thermal satisfaction	Acceptable/unacceptable: Just - clearly
	Adapted thermal sensation	Very cold – very hot
View quality	View quality voted from different positions (desk and couch)	Satisfied/unsatisfied: Just - clearly
	Price estimation	Very cheap – very expensive

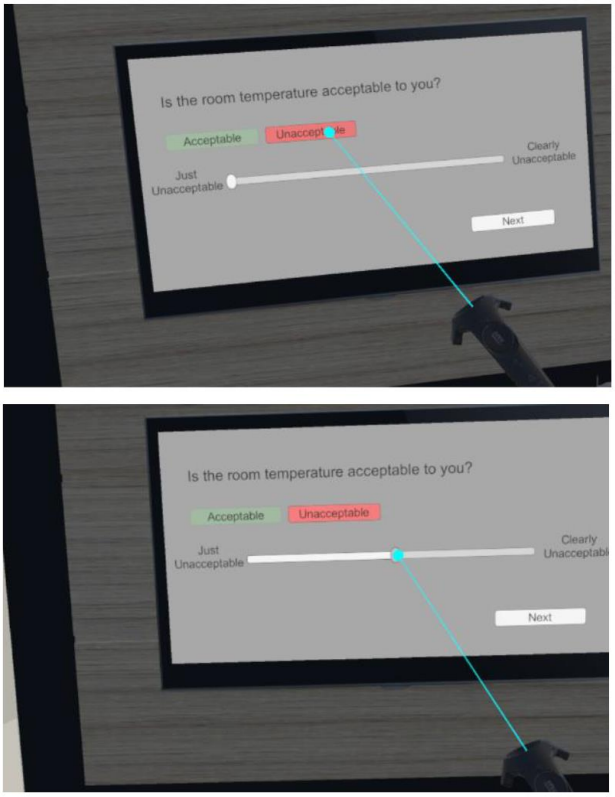

Figure 4. Thermal acceptability question. Top: Pressing 'unacceptable' using the controller pointer. Bottom: Moving unacceptable slider using the controller pointer to determine the degree of unacceptability.

D. Experimental design

A total of 51 subjects (25 males and 26 females) participated in the 4x4 randomized crossover-designed experiment. In this crossover design, subjects will experience all four scenarios described in previous section, and all subjects will be exposed to the same number of scenarios making the experiment balanced. As a part of the randomization procedure, 4x4 sequences of the scenarios was generated using the Williams Latin square. The order of questions that the subjects should answer during the experiments might be a potential bias in the experiment. Therefore, the questions described in the previous section were divided into two categories: questions related to the thermal comfort (T) and questions about to the view-out (V). Two orders of questions were then established, namely "TV" (subjects receiving thermal questions before view questions) and "VT" (subjects receiving view questions before thermal questions). We then assigned VT and TV to two similar scenario sequences leading to eight different sequences.

Each participant was randomly assigned to a certain sequence of scenarios using a lottery system that made sure that all sequences were executed an approximately equal amount of times. Once assigned a sequence, a subject would go through a VR training session in the preparation room to get initial experience with the technology including how to answer questionnaires inside the VR environment before starting the actual experiment. The subject then went to the climate chamber and had to stay there for 15 minutes to adapt to the thermal condition (30 minutes would have been preferred but that would have increased time consumption for the experiments significantly increasing risk of survey fatigue). The subject then used approx. 5 minutes to answer the questionnaire leading to a total session time of 20 per scenario. The subject then went back to the preparation room and spent a washout period of 20 minutes before entering the next scenario in an attempt to reduce any carry-over effect between scenarios.

III. RESULTS

The results regarding the question regarding view-out satisfaction is illustrated in figure 5 and 6. There is a tendency that the hot indoor temperature affected the view-out satisfaction more in the setting with moderate glazing area compared to the setting with large area.

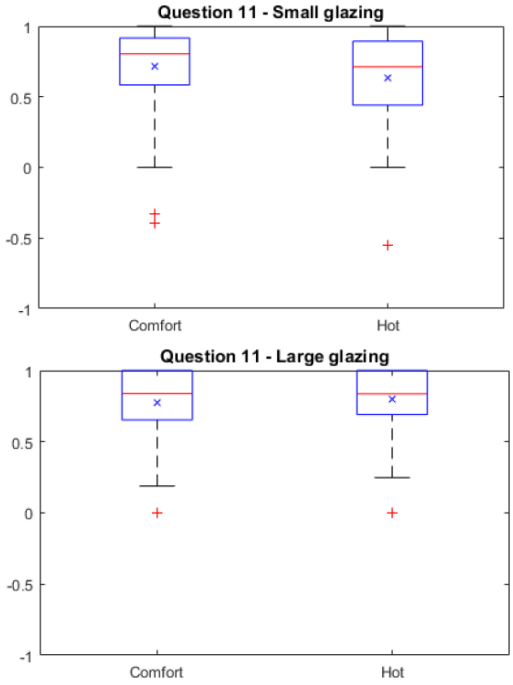

Figure 5. View-out satisfaction from office desk in the back of the room.

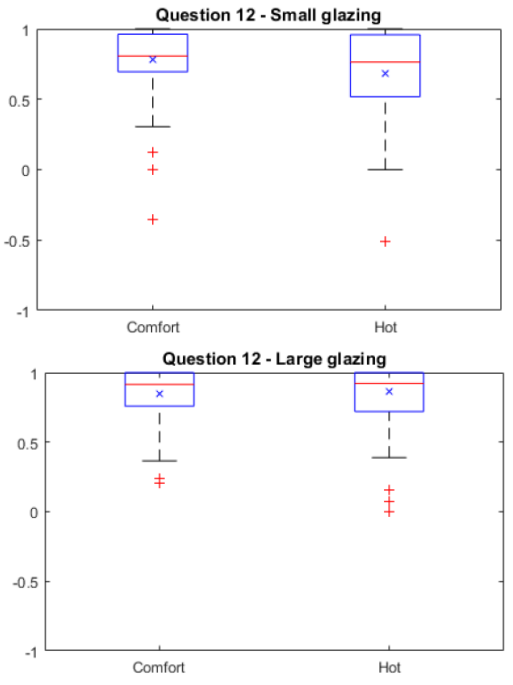

Figure 6. View-out satisfaction from couch near the window.

The votes on the subjective notion of the property price for each scenario is illustrated in figure 7. There is a tendency that the subjects found the apartment with large glazing to be more expensive than the apartment with moderate glazing no matter the thermal condition. For the large glazing area, there is also a tendency that the price was voted higher in the comfort condition.

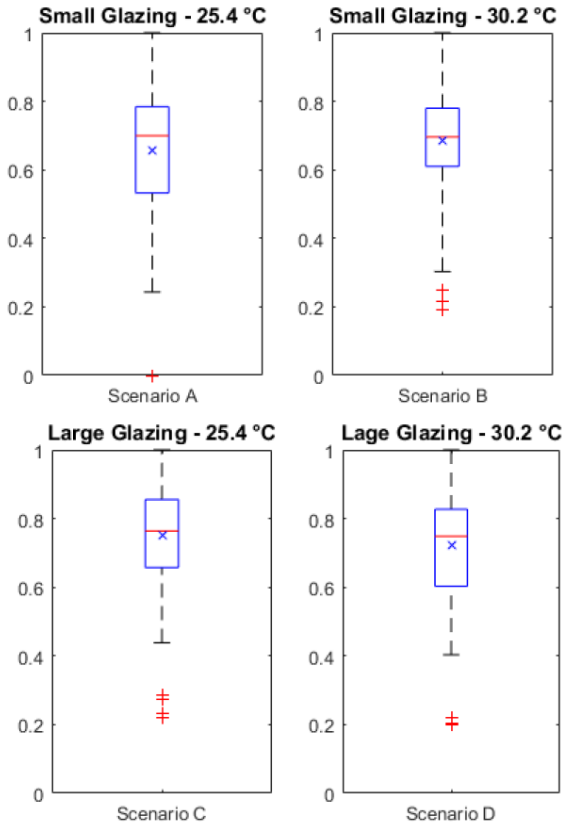

Figure 7. Subjective vote of property price for the four scenarios.

IV. CONCLUSION

The investigation led to the following conclusion: For a moderate glazing size, the subjects tend to be more satisfied with the view in a comfort thermal condition than an overheated condition. The indoor temperature did not seem to affect the perception of view-out in the scenario with large glazing area. None of these tendencies were statistical significant. In addition, the subjective notion of property price seems unaffected by the thermal condition.

Overall, the experiment has demonstrated that VR in climate chambers is a promising approach for investigating interactions between the visual and indoor climate aspects that together defines indoor environmental quality. Future studies should investigate the significance of the quality of the surrounding outdoor environment, as the view in this study in general was rated very high no matter the scenario indicating that the surroundings were too nice to be affected by temperature and/or window size.

ACKNOWLEDGEMENT

1. We would like to thank Torben Sigsgaard and Peter Ravn, Aarhus University, Department of Health, for helping out setting up the climate chamber experiment.

REFERENCES

[1] P. O. Fanger. “Thermal Comfort”, Lyngby, Denmark: Danish Technical Press, 1970 (Republished by McGraw-Hill, New York, 1973).

[2] F. Nicol, “Adaptive thermal comfort: principles and practice”, London New York: Routledge, 2012.

[3] J. Wienold and J. Christoffersen, “Evaluation methods and development of a new glare prediction model for daylight environments with the use of CCD cameras”, *Energy and Buildings,* vol. 38, pp. 743-757, 2006.

[4] P.B. Purup, S.H. Jensen, S. Petersen and P.H. Kirkegaard, “Towards a Holistic Approach to Low-Energy Building Design: Consequences of Metrics for Evaluation of Spatial Quality on Design”, *33th Passive Low-Energy Architecture (PLEA)*, Edinburgh, Scotland, 2017

HVAC World
Student Competition
Other Participants' Contribution

Jun Koyama	Japan
Manish Kumar	India
Yujun Jung	South Korea

REHVA
Federation of European Heating, Ventilation and Air Conditioning Associations

Study on Cool Chair equipped with warming function

Jun Koyama, Doi Yusuke, Masanari Ukai, Tatsuo Nobe

Abstract— **Recent air-conditioning systems aim to provide thermal comfort for an unspecified number of residents. However, office workers may perceive the feeling of comfort differently depending on their clothing, metabolic rate, and personal activity level. This may cause difficulties in maintaining an optimal thermal environment. To address this problem, personal air-conditioning has attracted attention, which is highly versatile and can reduce thermal discomfort and provide comfort to all office workers by enabling individual thermal control. Therefore, the authors focused on developing an office chair, the "Cool Chair", as a chair-type personal air-conditioning system with a cooling function from 2003 to 2016. The authors then added a warming function for year-round operation, creating the "Cool Chair with Warming Function" in 2017. Subjective evaluation results are reported. These experiments using the new chair indicated that the warming function achieves steady state in 30 minutes and the equivalent temperature of the entire body increases by +2℃. In subject experiments, the warming and cooling functions were adjusted according to individual preferences, and the cooling function was used even during winter by some individuals. The authors also confirmed that the feeling of comfort by the subjects improved at both 19°C and 22°C.**

Index Terms—**Cool chair, Isothermal, air flow, Personal air-conditioning system, Thermal comfort.**

I. INTRODUCTION

A. Background

Recently, air-conditioning systems, which have uniform temporal and spatial variations for environments, have caught attention. For example, floor flow air-conditioning and radiation air-conditioning have been introduced into many offices. It is thought that the thermal comfort of office workers is improved because these systems can control planar temperature with less cold draft. On the other hand, evaluation of thermal comfort based on conventional indexes involves considering a single person in a room as a representative of a group of people with common characteristics. However, in offices, employees differ in their degrees of comfort based on their attire, physical condition, and activity level. Therefore, even if the indoor thermal environment is categorized as comfortable, workers who are sensitive to cold or heat will presumably complain of discomfort. As a solution to this problem, personal air-conditioning systems have been attracting significant attention as a means of improving the thermal comfort of office workers. With a personal air-conditioning system, each worker can adjust the thermal environment to his or her desired preference. In addition, it is thought that forming the thermal environment by yourself, like feeling the fan cool and cool, helps to reduce the claims rather than the "self-efficacy"[1].

B. Transition of Cool Chair

The authors have developed a chair-type personal air-conditioning unit, calling it the Cool Chair. Fig. 1 shows the successive development of the Cool Chair. As a background for the development of the chair-type personal air-conditioning, the authors focused on an office chair, which was closest to those typically used by office workers at a major Japanese conglomerate. The authors have continued to try to improve comfort in the office by developing a chair-type personal air conditioning and to have a sense of self-efficacy by operating the air conditioning on an individual basis. In addition, the chair-type personal air conditioning has been developed from 2003 to the present, and personal air conditioning has attracted attention in Japan. Although various personal air conditioning systems have been developed in Japan, chair-type personal air conditioning is the first air conditioning system developed by this laboratory. Cool Chair 2003 was the first experimental model. This model had four air outlets on the movable armrests, and the air velocity at the body surface of an occupant could be adjusted using a fan speed controller. Air intakes were installed on the seat and backrest of the chair. Air inhaled from the seat and backrest was led through the fan and ducts to the outlets on the armrests [2]. Cool Chair 2004 became cordless, with a DC fan and a lead storage battery [3]. Cool Chair 2010 was a practical model. Cool Chair 2010 had three fans installed on the left and right armrests and on the seat of the chair [4]. With the design change to mesh construction, Cool Chair 2013 had only a single fan under the seat compared with the three fans in the other previous models, and the necessary air volume was considerably reduced [5]. The previous model, Cool Chair 2016, featured improved air volume by returning to a three-fan design, which was further improved by miniaturizing the fans. This model contributed to the improved comfort of users in subject experiments by providing users options for speed and direction of airflow [6]. The development of the cool chair from 2003 to 2016 tried to improve the user's comfort by adding a cooling function to the office chair, but there is a thermal complaint about heat in the office, but Thermal dissatisfaction with cold may also be present. Therefore, the authors added warming function to Cool Chair 2016 with the aim of eliminating thermal discomfort due to cold, and tried to improve office comfort throughout the year. Also, chair-type personal air conditioning has also been developed in the United States, and it has been confirmed that the user's comfort has been improved by using the air conditioning system [7]. In this study, the authors report the specifications of the Cool Chair 2017, performance evaluation of the Cool Chair 2017 by utilizing a thermal manikin, and evaluation of real-world operation situation of this chair by a human subject experiment. Additionally, the operation evaluation of the cooling function was carried out in the summer of 2016 [8].

Figure 1. The successive development of the Cool Chair.

C. *Requirements for thermal environment of actual office workers*

Fig. 2 shows the outline of requirements for a comfortable thermal environment. Table 1 shows outline of the authors' investigation. The corresponding paper [9] reported the worker's requirements for the thermal environment in the form of a check sheet that is compiled by the building maintenance managers according to the complaints regarding the thermal environment of the office workers. The authors investigated number of complaints, which included: "Hot", "Cold", "Uncomfortable because of system air-velocity", "Coldness due to air-speed", "Coldness of feet", and "Other". Fig. 3 shows the number of complaints regarding the thermal environment of office workers to the building maintenance managers. The complaints from females accounted for more than 85% of all complaints. It was confirmed that a male requested a change of thermal environment 0.01 times per year on average and a female requested the change of thermal environment 0.12 times per year on average. The total complaints counted were 691 during the six years from 2000 to 2005. Because these complaints included "Cold" and "Coldness due to air-speed", the authors added a warming function to the Cool Chair 2016 and expected to improve the comfort level especially for female chair users.

TABLE I.
OUTLINE OF INVESTIGATION

Place	Minato ward, Tokyo
Architectural area	37000 m^2
Survey period	2000-2005
Number of floors	23 floors and 2 basement floors
Air-conditioning system	Each floor unit CAV + FCU
Declaration method	Air environment check sheet
Declaration contents	Hot, Cold, Uncomfortable by wind, Coldness by wind, Coldness of feet, Other
Standard floor plan	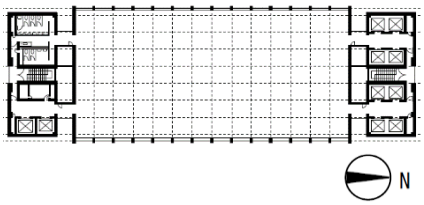

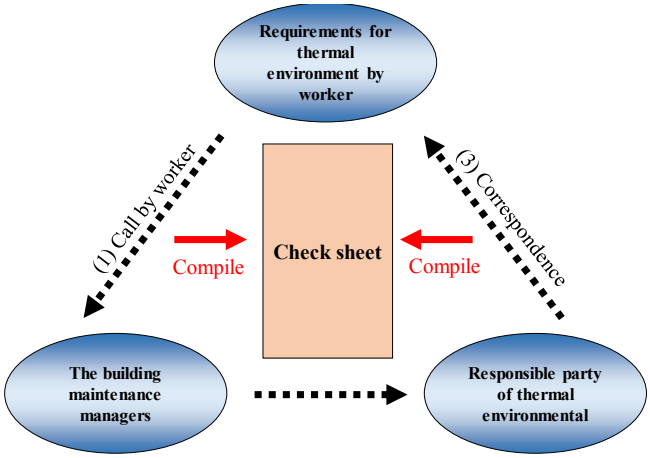

Figure 2. Outline of complaints regarding the thermal environment.

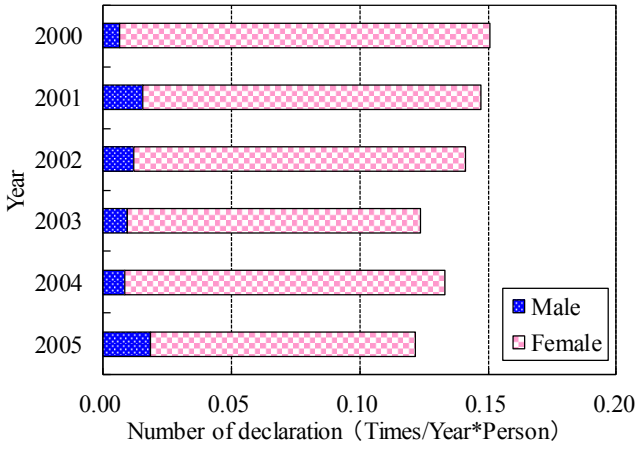

Figure 3. Number of declarations

II. SPECIFICATIONS OF COOL CHAIR 2017 MODEL

In the development of the Cool Chair, the authors did not change its function as a chair, but added a cooling function. In this research, the authors added the warming function in addition to the cooling function of the previous model for expanding the users choise of environment . Table 2 shows the specifications of the Cool Chair 2017.

A. Cooling function

Three fans are installed inside the seat and a 20-mm three-dimensional air-permeable layer covers the seat over the three fans. Air pulled from all over the seat is fed through the fan to flexible hoses, which prevents heat from the human body from building up on the seat. In addition, the Cool Chair 2017 features improved airflow velocity of the fan by 1.6 m/s more than the previous model for users comfort.

B. Warming function

As a heating device, a linear heater was selected in order to maintain the air-permeability of the seating surface, which is necessary for the cooling function. The linear heating elements are installed in the seat on the back, which enables operating each output individually. In order to prevent overheating, a thermal fuse is wired in the liner heater at the seat and the back. This thermal fuse reacts at 72 °C, and when the temperature exceeds this value, the heater stops working. Fig. 4 shows thermal imaging of the liner heating elements. The liner heater of Cool Chair 2017 reaches 40.5 °C at the maximum output. Although there are many studies about low temperature burns, it is thought that these do not occur at a surface temperature of 40.5 °C [10].

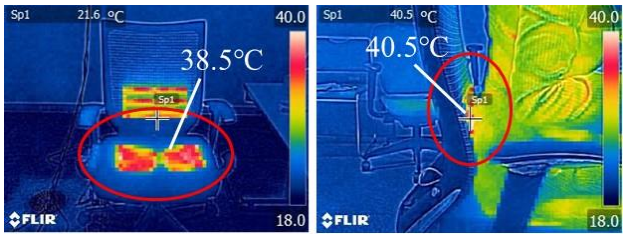

Figure 4. Thermal image of liner heater.

C. Control and operating method

The air flow volume can be gradually adjusted using a dial attached to the right side of the seat. The air flow volume at the side and back can be individually controlled using a no-step dial. The control method employs pulse width modulation because its energy consumption is superior when low air volume is used. To prevent wasteful energy consumption, the fans are also automatically stopped by a seat sensor when the user leaves his or her seat with the power supply switched on.

D. Battery

The battery of the Cool Chair 2017 has a large capacity of 50 Ah. When the battery is fully charged, the fan can move air at the maximum output for approximately 55.6 h and the heater can move air at the maximum output for approximately 26.0 h. Likewise, the controller LED light turns red during operation to prevent malfunction. Moreover, the detachable portion of the battery is placed on the back of the seat in order not to affect the design of the chair.

TABLE II.
SPECIFICATIONS OF THE COOL CHAIR 2017.

Exterior			
Cooling function	Airflow velocity		0-10.8 m/s
	Maximum air volume		Sum of both sides: 46.8 m^3/h Back: 23.4 m^3/h
	Air volume control		No-step dial
	Location of fan		Inside seat
	Power consumption of fan		10.8 W
	Continuous air-movement time		55.6 h
Warming function	Surface temperature	Seat	28.2-38.5°C
		Back	29.0-40.5°C
	Linear heater	Resistance value	25 Ω/m
		Maximum power	Total 23.04 W (12 V)
		Safety device	Thermal fuse (Nominal operating temperature 72 °C)
	Continuous operation time		26.0 h
Controller	Air volume / temperature adjustment		Stepless variable resistor
	Heating / cooling function management		Changeover switch
			LED lamp (cooling: blue heating: red)
	Battery		LiB (12 V, 50 Ah)
	Operating condition		Sensor control by sitting

III. PHYSICAL PERFORMANCES BY THERMAL MANIKIN EVALUATION

A. Outline of evaluation with thermal manikin

By using a thermal manikin, it is possible to conduct a detailed survey for each body part. Figure 5 shows division of each body part. Table 3 shows outline of the survey using thermal manikin. Table 4 shows surface area of each body part. This survey is an experiment assuming winter, and a set temperature of 22 °C. The controller adopted is proportional-integral controller.

TABLE III.
OUTLINE OF SURVEY WITH THERMAL MANIKIN.

Version		Manikin version 3.x
Survey period		January 10-11, 2018
Experimental conditions	Air temperature	22 °C
	Relative humidity	Progress
	Air velocity	0.1 m/s
	Average radiation temperature	Same as air temperature
Thermal manikin	Controller	Proportional-integral controller (PI mode)
	Clothes	Suit (1.0 clo)
	Posture	Sitting straight

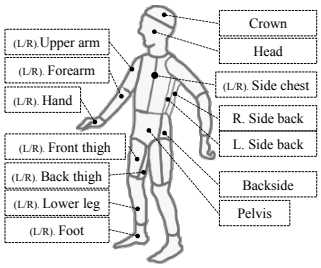

Figure 5. Division of each body part.

TABLE IV.
SURFACE AREA OF EACH BODY PART.

Body part	Surface area [m^2]	Body part	Surface area [m^2]
L. Foot	0.0520	L. Hand	0.0435
R. Foot	0.0520	R. Hand	0.0435
L. Lower leg	0.01140	L. Fore arm	0.0409
R. Lower leg	0.01140	R. Fore arm	0.0409
L. Front thigh	0.0962	L. Upper arm	0.0757
R. Front thigh	0.0962	R. Upper arm	0.0757
L. Back thigh	0.0962	L. Side chest	0.0893
R. Back thigh	0.0962	R. Side chest	0.0893
Backside	0.0736	L. Side back	0.0893
Head	0.0796	R. Side back	0.0893
Crown	0.0524	All	1.6447

B. Sensible heat loss amount by thermal manikin

Fig. 6 shows the sensible heat loss amount. The sensible heat loss amount in the back thigh and back side was decreased by the heating effect. In addition, it reached a steady state in about 30 minutes. By using the chair's heating function for 30 minutes, the sensible heat loss decreased by 39.1 W/m2 in the back thigh, 18.8 W/m2 in the back side, and 7.0 W/m2 in the whole body.

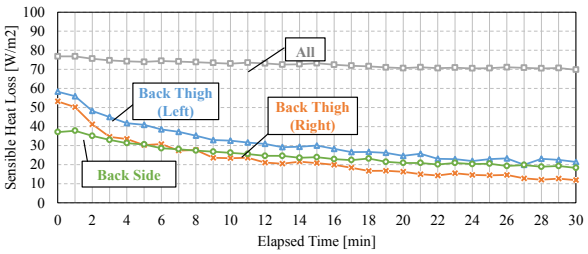

Figure 6. Sensible heat loss amount by thermal manikin.

C. Equivalent temperature by thermal manikin

Fig. 7 shows the equivalent temperature. In the case of heating only, the equivalent temperature increased by about +15 °C in the back thigh and +2 °C in whole body. When adding a blanket on knees, the equivalent temperature increased by about +2 °C more than the case of heating only. With regard to the whole-body,

$$t_{eq} = t_s - (I_{cl} + \frac{I_a}{f_{cl}}) \quad (1)$$

With regard to each part,

$$t_{eqi} = t_{si} - 0.155\,(I_{cli} + \frac{I_{ai}}{f_{cli}})\,Q_t \quad (2)$$

where
t_{eq} = equivalent temperature, °C
t_s = mean skin temperature, °C
I_{cl} = basic clothing insulation, clo
I_a = clothing insulation (at nude), clo
f_{cl} = clothing area factor
t_{eqi} = equivalent temperature of segment, °C
t_{si} = mean skin temperature of segment, °C
I_{cli} = basic clothing insulation of segment, clo
I_{ai} = clothing insulation of segment (at nude), clo
f_{cli} = clothing area factor of segment

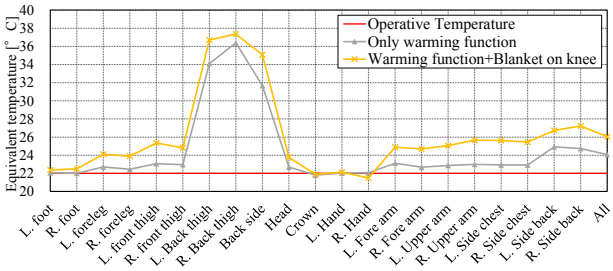

Figure 7. Equivalent temperature by thermal manikin.

IV. SUBJECT EVALUATION

A. Outline of subject evaluation

Fig. 8 shows exterior and plan of experimental building. Table 5 shows the outline of subject evaluation. Subject experiments were verified under two temperature conditions. The first condition was 22 ° C, which is the standard set temperature of Japanese offices. The second condition was 19 °C, which is 3°C lower in temperature than the first condition. The number of subjects was nine males and ten females. As an activity during the experiment, the subjects played puzzles. They used the general chair and the Cool Chair 2017 Model for each room for 30 minutes. In addition, the subjects were allowed to operate either the cooling function or the warming function when seated in the Cool Chair 2017.

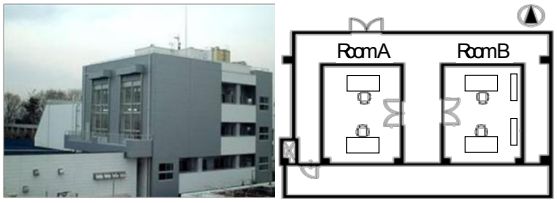

Figure 8. Exterior and plan of experimental building.

TABLE V.
OUTLINE OF SUBJECT EVALUATION.

Place	Kogakuin Twin Chamber Laboratory	
Survey period	December 4-9, 2017 (6 days)	
Air-conditioning system	Floor flow, Ceiling suction	
Number of subjects	Male: 9, Female: 10	
Laboratory	A	B
Air temperature	22°C	19°C
Relative humidity	50%	
Air velocity	0.1 m/s	
Average radiation temperature	Same as air temperature	
Clothes	Male: 1.0 clo, Female: 0.8 clo	
Activity	Puzzle	
Metabolic rate	1.2 Met	

B. Usage rate of cooling and warming function

Fig. 9 shows the usage rate of the cooling and warming functions. At 0 minutes elapsed time, the usage rate was low, because the subjects answered the questionnaire. The use of the cooling function was confirmed in subject experiments assumed in winter. Because the cooling function and the warming function were both used, it is thought that the Cool Chair 2017 with the two functions was operated according to the user's feelings of heat and cold.

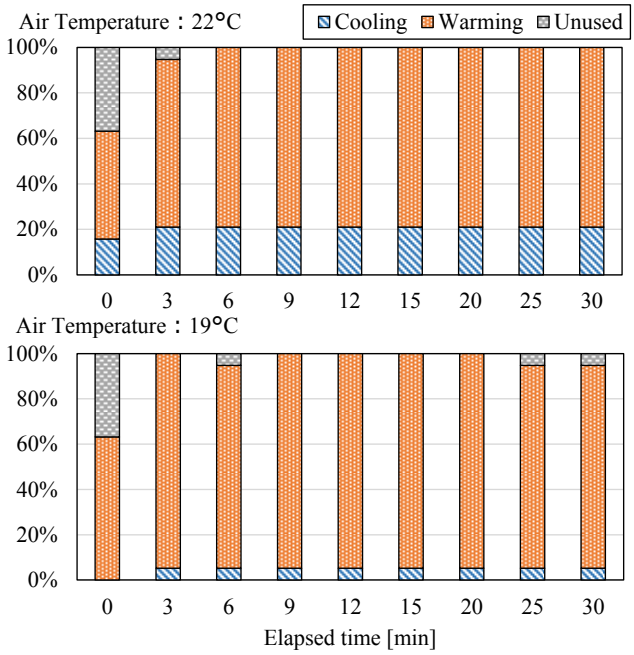

Figure 9. Usage rate of cooling and warming functions.

C. Equivalent cooling and warming temperature

Fig.10 shows the equivalent cooling and warming temperature The calculation was carried out as follows: a) the subjects were asked to recall their thermal sensation vote (TSV) at three- or five-minute intervals while sitting in both chairs, and b) we calculated the predicted mean vote (PMV) temperature, which has the same value as TSV, and defined the difference between this result and indoor temperature (Room A: 22 °C Room B: 19 °C) as the equivalent cooling and warming temperature. At the temperature setting of 22 °C, the equivalent cooling and warming temperature of the normal chair was identified on the warmer side in males, but females identified the temperatures as cooler. However, equivalent cooling and warming temperature for males changed to a perception of cooler when using the Cool Chair's cooling function. On the other hand, equivalent cooling and warming temperatures for females slowly shifted from the cooler side to the warmer side and rose to about +0.8°C after 30 minutes. When the room temperature setting was 19 °C, the equivalent cooling and warming temperatures of males and females indicated a perception of cooler temperatures, in particular, females indicated equivalent cooling and warming temperature -2.2 °C to -3.5 °C. However, this shifted to a warmer perception after 9 minutes of operation by using the Cool Chair 2017.

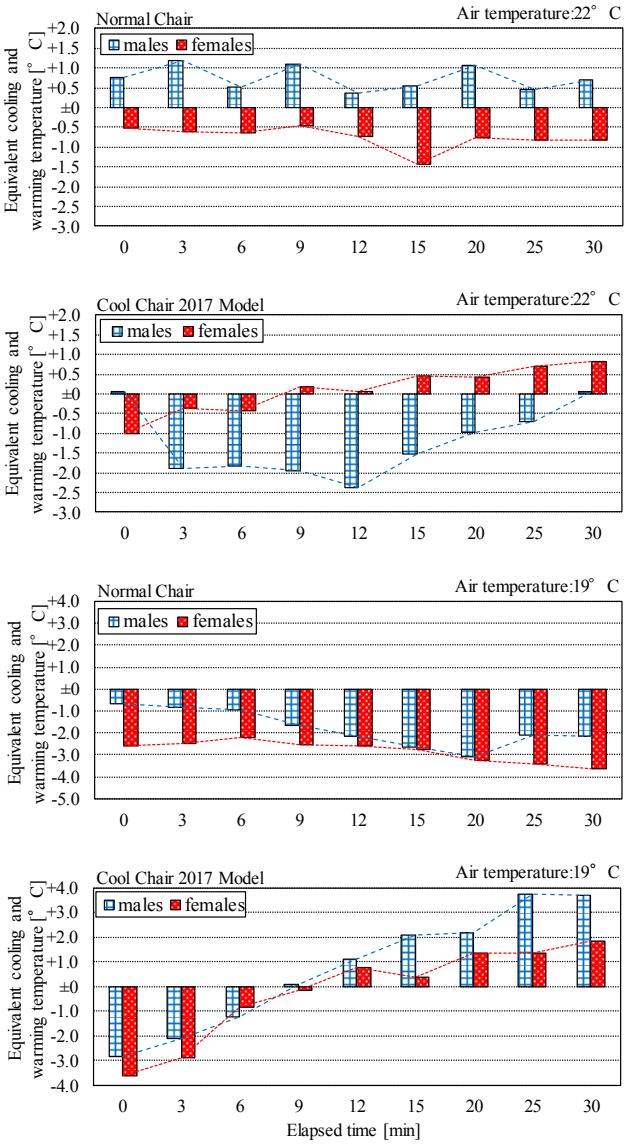

Figure 10. Equivalent cooling and warming temperatures.

D. Evaluation of comfort

In this study, the authors classified the comfort level by using a questionnaire. Fig. 11 shows the comfort level classifications. The authors divided comfort into three levels and introduced them in a questionnaire, which was answered at three- or five-minute intervals while sitting in the chair. The user who answered "Discomfort" at Q.1 is defined as giving an "Discomfort" response. For the subjects who answered "Not uncomfortable" at Q.1, it defined their response as "Comfort" for those who answered " Not pleasant" at Q.2. It lastly defined "Pleasantness" [11] for the subjects who answered "Pleasant" at Q.2. Fig. 12 shows the relationship between the comfort level and elapsed time of using a normal chair and the Cool Chair 2017. Under the temperature environment of 22 °C, the normal chair and Cool Chair 2017 have a low rate of "Discomfort", but "Comfort" is replaced by "Pleasantness" when using the Cool Chair 2017. Under the temperature environment of 19 °C, it was not possible to reduce declarations of "Discomfort" by using the Cool Chair 2017. However, it was confirmed that "Comfort" changed to "Pleasantness". These results indicate that the Cool Chair 2017 can change "Comfort" to "Pleasantness" under the two temperature conditions.

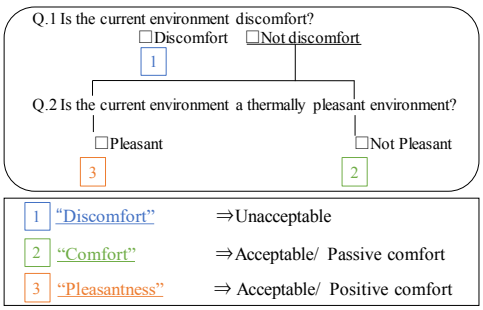

Figure 11. Classification of comfort levels.

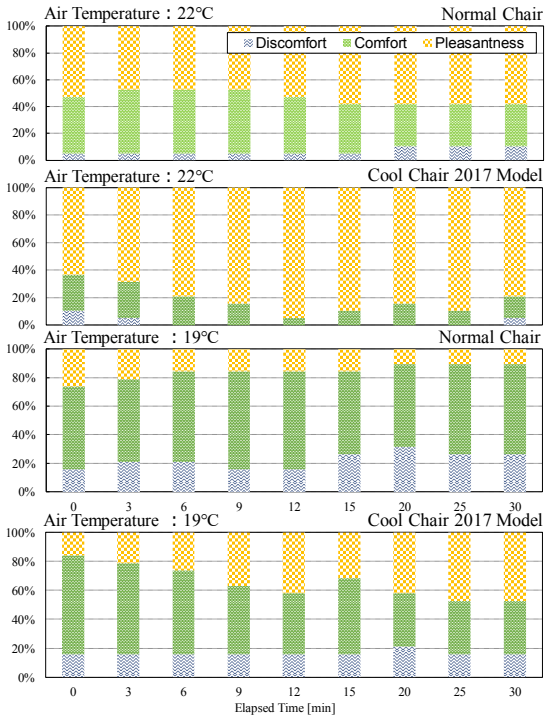

Figure 12. Relationship between comfort and elapsed time.

E. Overall satisfaction

Fig. 13 shows the overall user satisfaction for the Cool Chair 2017. It reveals that the subjects, 90% of men and 80% of women, responded with feelings of satisfaction in the questionnaire. In addition, no subject answered "Dissatisfaction". Hence, through this subject experiment, it is considered that the Cool Chair 2017 was accepted by the users.

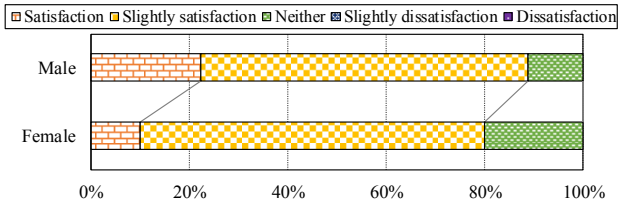

Figure 13. Overall user satisfaction.

V. CONCLUSIONS

In this study, the authors evaluated the Cool Chair 2017 by using a thermal manikin and with a subject experiment. The findings are described below.

1) In a physical performance with thermal manikin, the heating effect of the Cool Chair 2017 Model has a large influence on the back side to the back thigh. And it increases the equivalent temperature by + 2.0 °C in the whole body.

2) In the subject experiment assumed in the winter, use of the cooling function was confirmed under the temperature environment of 22 °C, especially for the male users. Notably, use of the warming effect by subjects was also confirmed.

3) It was observed that the overall comfort of the user shifted from "Comfort" to "Pleasantness" when using the Cool Chair 2017. Finally, the overall user satisfaction indicated that more than 80% of users were satisfied with the Cool Chair 2017.

REFERENCES

[1] T. Nobe, M. Ukai, SHARE, "8 Tries" toward the Next Generation HVAC System – 8 Tries and Human Factors –, vol.3, PP.21-24, September 2016 (Japanese)

[2] T. Nobe, M. Shoji, S. Shimizu, Roomvent, Coimbra, Portugal (2004)

[3] M. Shoji, S. Shimizu, T. Nobe, Summaries of Technical Paper of Annual Meeting Architectural Institute of Japan (2005) (in Japanese)

[4] I. Suzuki, K. Washinosu, T. Nobe, Proceedings of the 7th Windsor Conference (2012)

[5] M. Ukai, T. Yada, T. Nobe, Roomvent (2014)

[6] Y. Doi, M. Ukai, T. Nobe, Roomvent (2018)

[7] P. Wilmer, Z. Hui, A. Ed, Building and Environment, Energy-efficient comfort with a heated/cooled chair: Results from human subject tests, vol.84, pp.10-21, 2015

[8] J. Koyama, Y. Doi, Y. Tanaka, M. Yamada, S. Hanazono, G. Tateyama, M. Ukai, T. Nobe, SHASE (2018) (in Japanese)

[9] A. Onga, Y. Iwasa, T. Nobe, SHASE 12115-1218 (2007) (in Japanese)

[10] A.R. Moritz, F.C. Henriques, Am. J. Pathol. 23(5), 695–720 (1947)

[11] S. Kuno, H. Ohno, N. Nakahara, ASHRAE Trans. 93, Part 2, 396-406 (1987)

REHVA
Federation of European Heating, Ventilation and Air Conditioning Associations

Performance Enhancement of Radiant Heating and Cooling System using Thermoelectric Module

Manish Kumar[1], Jyotirmay Mathur[1]

Department of Mechanical Engineering, Malaviya National Institute of Technology Jaipur, 302017, India
Tel.: +917355038446, E-mail: manishkumar2341.mk@gmail.com
Tel.: +917275696260, E-mail: jmathur.mech@mnit.ac.in
Year of acceptance at home university: 2018

***Abstract*— In the present scenario the polluted environment is the main cause of global warming, which significantly affects the health and well-being of people. So, we need to develop such technologies which provide better performance and minimum environmental pollution. Refrigerant based air conditioners contribute substantially to the pollution problem therefore this study is focused on replacing refrigerant based air conditioning system by thermoelectric module integrated radiant cooling system. Radiant cooling system is a revolutionary change in heating ventilation and air conditioning in recent past years globally. In this study the refrigerant based chiller used for the generation of cold water (to feed the radiant ceiling panels) has been replaced by the thermoelectric module. After he experiment the results show that the average cooling and heating capacity of radiant panel comes out to be approximately 360Watt/m^2 and 175Watt/m^2 respectively in the panel dimension of 0.65×0.65m. There are total 9 active thermoelectric modules of dimension 40×40×3.8 mm have been attached to the radiant panel which operates on direct current. The coefficient of performance in both cooling and heating case comes out to be 4.9 to 7.4 and 1.5 to 3 respectively. The current and voltage required to operate each thermoelectric module are 0.6 to 1.2A and 5 to 7.5V in case of heating while 0.5 to 0.8A and 4 to 6V in case of cooling.**

***Index Terms*— Thermoelectric, Charge Controller, Thermoelectric Radiant Heating and Cooling System (TE-RHCS).**

Introduction

Now a days there are many types of HVAC systems are available for cooling and heating of building space. Most of them use refrigerant causing environmental pollution, because refrigerant used in these systems liberate HFCs (at present) and CFCs (in earlier days). Year by year the average temperature on the earth is increasing due to increasing energy demand by human being for better comfort life and increasing population. Radiant system was the incredible invention in heating and cooling in the industrial sector. Radiant system is energy efficient and provides better thermal comfort over conventional-all air system [14], [19]. In radiant ceiling panel cooling system (RCPCS), water is cooled by chiller in which refrigerant (like R-134a, R410) is used as a working medium and then cooled water is supplied to the aluminum panels through copper tubes embedded on the back side of the panel, also known as radiant panel due to primarily radiation mode of heat transfer [9], [12]. The use of refrigerant based systems causing environmental pollution [2] and some other major issues should be minimized and technologies which are pollution free with same or better thermal comfort and performance should be adopted.

Thermoelectric works on the principle of Seebeck Effect and Peltier Effect, which tells us the conversion of thermal (temperature) gradient into electricity or potential difference and vice-versa. This is a very popular concept and generally used for cooling computer chips and ICs [6], also used for cooling food and beverages, medicines and as a portable refrigerator. So keeping these applications in mind several studies have been already performed [1], [2], [3], [4], [5].

When DC current passes across the terminals of two dissimilar materials then we get the temperature gradient and vice-versa. In thermoelectric radiant system thermoelectric modules (TEM) have been attached in series-parallel combination to the aluminum panel and that is why generally named as Thermoelectric Radiant Cooling and Heating System (TE-RCHS). If battery is used for power supply then arrangement of module depends on the battery size of the system. Solar panel is another good source of power supply which can be used as power source.

Figure1. Thermoelectric module

Figure2. Thermal adhesive

SYSTEM DESCRIPTION

Thermoelectric Radiant Heating and Cooling Test Chamber (TE-RHCS):

Thermoelectric radiant test chamber is designed and fabricated according to the ASHRAE 138 standard for the experiment purpose. Figure (3) shows the front cross-section view of the experimental test chamber which shows the layer wise representation of the system. The ceiling area of the test chamber is 0.4489m^2 after descaling the standard size. Descaling the size depends on the principle of geometric similitude because in radiant system air movement is very slow and static condition exists. So the test chamber dimensions are 0.67(length) ×0.67(width) ×0.58(height) m. Test chamber is completely insulated by XPS insulation sheet of thickness 55mm with thermal conductivity of 0.029W/m-K. The height of the fall ceiling is 42mm from the base. The material used for the test chamber is plywood of thickness 19mm. Table 2 shows the sub components of the test chamber with its geometric parameter and their positioning.

Radiant Panel:

Radiant panel is made of aluminum material with thickness 0.5mm. One face of the panel is facing the indoor space and other face is attached to the copper pipe of non-circular cross section. The actual shape of the pipe is dee (D) shape and it is intentionally created to increase the heat transfer area and the flat face of the pipe is directly attached to the thermoelectric module (fig.1) with the help of thermal adhesive (fig.2). RTD sensors and thermocouples are attached to the panel surface and thermoelectric module to measure the temperatures. For water circulation copper pipes are attached with the CPVC piping circuit and a 500 litre storage tank which is placed at some height above ground level. Nitrile rubber insulation of thickness 9mm has been used at the top surface of the panel to prevent the heat transfer from that surface because aluminum has very good thermal conductivity so heat will be transferred at a faster rate from top surface which is exposed to the ambient.

Charge Controller Circuit:

Since thermoelectric module has been operated on DC (direct current) power supply so we have required a power source which provides DC power. There are some options are available such as use of a battery power or solar photovoltaic system with charge controller or AC (alternating current) to DC converter. In this study we have used AC to DC converter by using SMPS (Switched-Mode Power Supply) and ammeter & voltmeter has been used in series-parallel to check the supply current and voltage.

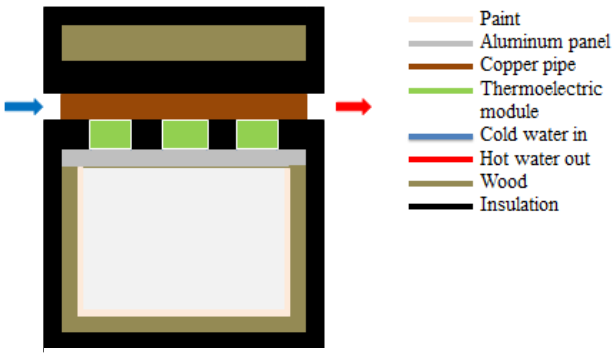

Figure3. Front cross section view of test chamber

TABLE 1 TE-RHCS COMPONENTS

Parameter	Value	Units
Radiant Panel Dimension	0.65×0.65	M
Ratio of Radiant Panel Area to Ceiling Area	1	-
Ceiling Panel Material	Aluminium	-
Radiant Pipe Material	Copper	-
Radiant Pipe Cross Section	D	
Radiant Pipe Spacing	156	mm
Thermoelectric Module	9	-
Incandescent Bulb (3 pieces)	15	Watt

TABLE 2 MEASURED PARAMETERS AND INSTRUMENTS

Experimental Setup Component	Measured Parameter/ Units	Instrument/ Make	Accuracy
Thermoelectric Module	Energy/kWh	Power-Voltage regulator/ Select	-
Charge Controller	Current/A & Voltage/V	Ammeter & Voltmeter/Select	±1.8% & ±1
Radiant Panel surface	Temperature/°C	RTD	±0.2°C
Water	Temperature/°C	Thermocouple/K-type	±1%
Ambient Condition	Temperature	TRh Sensor/Autonics	±0.2°C

EXPERIMENTAL PROCEDURE

Figure (5) shows some of the equipment and measuring instruments used for the experiment.

To measure the temperature at different points RTDs and thermocouples attached to the data logger and input settings were provided data logging automatically.

Specifically two strategies have been followed in this study. One is supply voltage variation and another is supply water temperature variation and these have been described briefly in the next section.

Experiment starts by supplying water to the copper pipes from water tank with certain flow rate. The electrical circuit has been provided power from power source. As the thermoelectric module gets DC it starts functioning and thus the panel gets heated or cooled according to the electrical connection. The opposite face of the module which is in contact with the copper pipes provides heat or to gets cool by water.

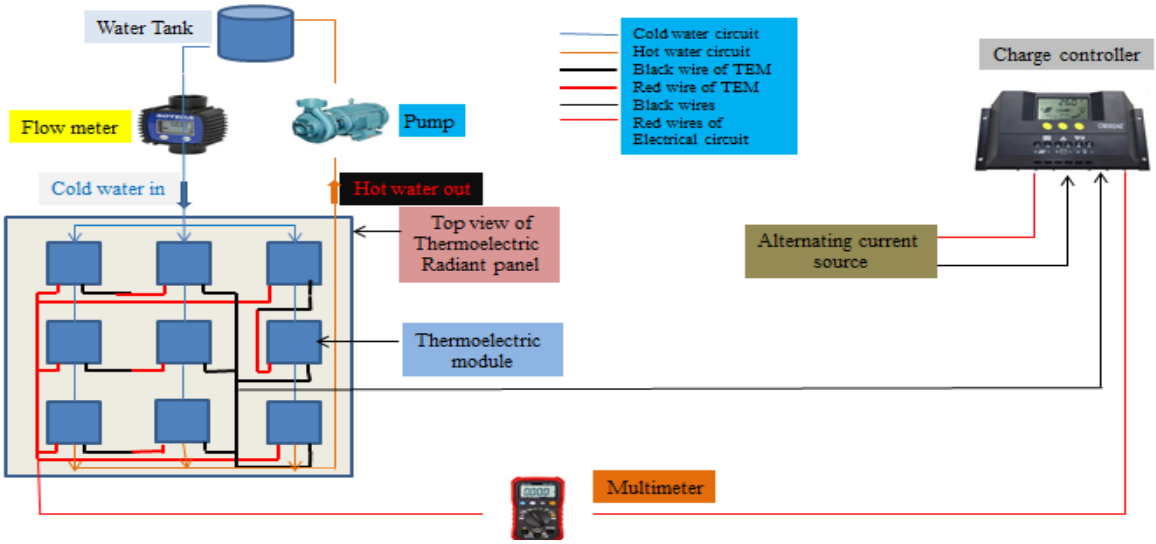

Figure4. Schematic of TE-RHCS

Figure5 TE-RHCS components and measuring instruments

Governing Equations- The equations which are responsible for the heat transfer from the thermoelectric module and its power consumption have been describes earlier by Limei Shena et al. (2013) [2]. In a thermoelectric cooling and heating process, there are four types of heat involved. They are the Peltier cooling, Peltier heat, Joule heat and Fourier heat.

The Peltier cooling (Q_{mC}) transferred at the cold side of a TEM can be defined by T_c

$$Q_{mC} = \propto IT_c \quad \text{……..…...(1)}$$

The Peltier heat (Q_{mH}) transferred at the hot side of a TEM is defined by

$$Q_{mH} = \propto IT_h \quad \text{…….....…...(2)}$$

Where, T_h and T_c are temperature of TEM at hot and cold side respectively.

When current (I) flows through a TEM, Joule heat (Q_J), defined by the following is generated inside the TEM due to the electrical resistance (R). It can be assumed that 50% of the Joule heat goes to the cold side and the other 50% goes to the hot side

$$Q_J = I^2R \quad \text{……..…..……...(3)}$$

The Fourier heat is the heat conducted from the hot side to the cold side due to the thermal conductivity (K) of the thermoelectric material and the temperature gradient. The conduction heat flow (Q_k) is given by

$$Q_k = K(T_h - T_c) \quad \text{…….……(4)}$$

Considering heat balance of the four types of heat as the heat absorption rate at the cold side, i.e. Q_c, and the heat rejection rate at the hot side of TEM, i.e. Q_h, can be obtained by use of following equations respectively:

$$Q_c = \propto IT_c - 0.5I^2R - K(T_h - T_c) \quad \text{……...(5)}$$

$$Q_h = \propto IT_h + 0.5I^2R - K(T_h - T_c) \quad \text{……..(6)}$$

The input electrical power (W) of the TEM is given by

$$P = \propto I(T_h - T_c) + I^2R \quad \text{……..……...(7)}$$

The coefficient of performance of the TEM in the cooling mode (COP_c) is given by

$$COP_c = \frac{Q_c}{P} \quad \text{……..…..(8)}$$

The coefficient of performance of the TEM in the heating mode (COP_h) is given by

$$COP_h = \frac{Q_h}{P} \quad \text{.....(9)}$$

Panel Capacity- According to ASHRAE 138 the radiant panel capacity of the RHCS is given by the following equation

$$q_{P=}\frac{\dot{m}_{wi}*C_{Pw}*(T_{wi}-T_{we})}{A_P} \quad W/m^2 \quad \text{.....10}$$

Where, q_P is in W/m^2 , $\dot{m}_{wi}$ is inlet water mass flow rate (unit- l/min), C_{Pw} is specific heat of water (unit- KJ/kg-K), T_{wi} & T_{we} are water inlet & exit temperature (unit- ^oC) from tube and A_P is area of radiant panel (unit- m^2)

RESULTS AND DISCUSSION

In radiant panel the thermoelectric module is permanently attached to the aluminum sheet. The connections of the electrical circuit are made in such a way that the bottom surface of the thermoelectric module gets heated or cooled as per the requirement. There are two strategies in each case of experiment. These are as following-

1. As we increase/decrease the supply voltage within its working range then cooling and heating effect increases/decreases gradually, provided its non-active surface should be maintained at the temperature for which system has been designed.
2. Both heating and cooling effect can be controlled by controlling the water supply temperature which indirectly circulates on the non-active face of the thermoelectric module.

The main concern is that for cooling active surface excessively we need extra energy that means extra cost. So we have optimized the system for better performance and energy savings. Therefore we performed the experiment under the condition when water is available at 20°C and 22°C in both heating and cooling which we generally get in Indian summer and winter condition.

Effect of supply voltage on active surface temperature and air temperature during heating

When heating mode of experiment was performed for winter condition, the flow rate of water supply is kept close to 1 liter per minute which is determined using load removal calculations from the test chamber as per the ASHRAE 138 standard. In heating mode, at 8V supply the energy consumption is low but the response time of the system was very long (more than an hour) so this set has been ruled out. Therefore we performed the experiment for 10V, 12V and 15V supply with water temperatures at 20°C and 22°C. Panel heating capacity has been determined by equation (10), which comes out to be around 170 W/m^2 for the given panel. The COP of the system has been determined by eq. (9) and it comes out in the range 1.5 to 3.

In the above figures (6 & 8) the temperature profile is increasing continuously as time passes but the rate of temperature increase is higher for 22°C water supply as compare to that of 20°C because at 22°C availability of heat is more that of 20°C. Also we can see that as the voltage supply is increased the heating effect is increased with faster response because at higher supply voltage the movement of electrons and holes inside the thermoelectric module becomes faster causing the surface of the TEM getting heated at a fast rate and thus heating the radiant panel.

From figures (7 & 9) as we increase the supply voltage the rate of increase in room air temperature becomes high initially and after some time it decreases for both 20°C and 22°C water supply. The effect of increase in water supply is same for both the cases has not been seen yet.

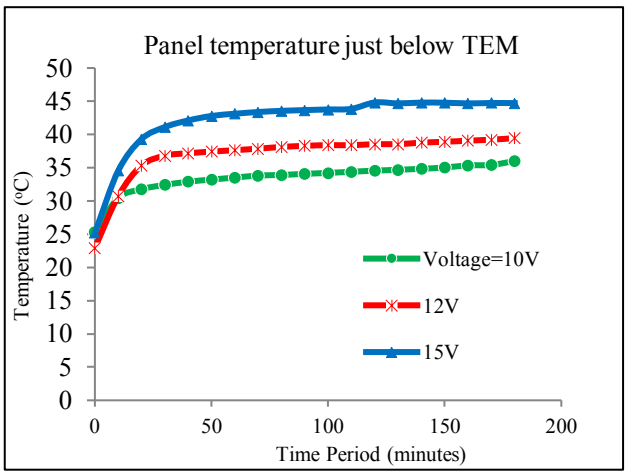

Figure6. Variation of room air temperature with time when water supplied at 20°C

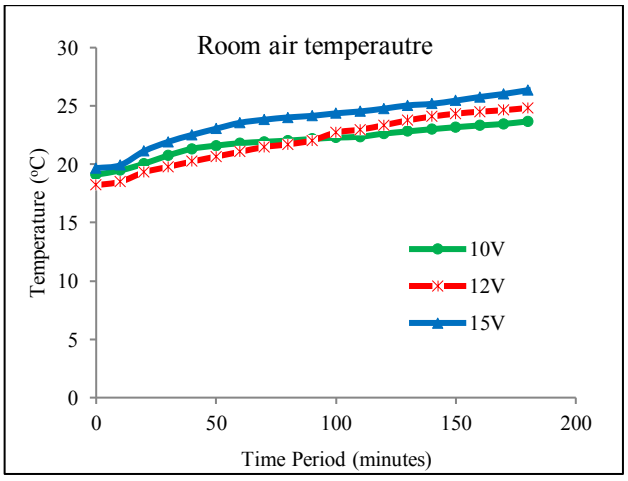

Figure7. Variation of room air temperature with time when water supplied at 20°C

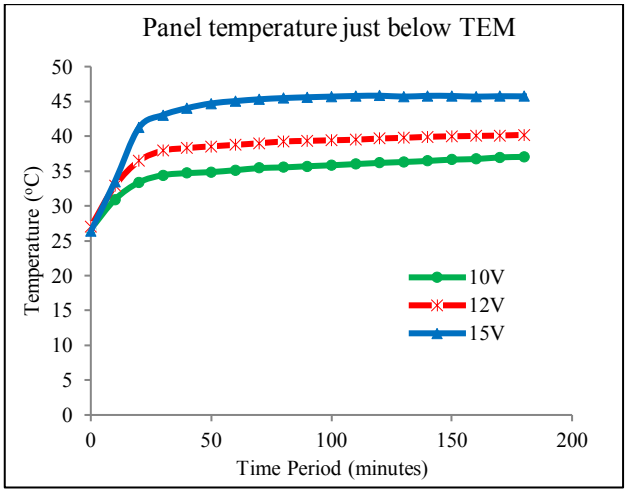

Figure8. Variation of panel temperature below TEM with time when water supplied at 22°C

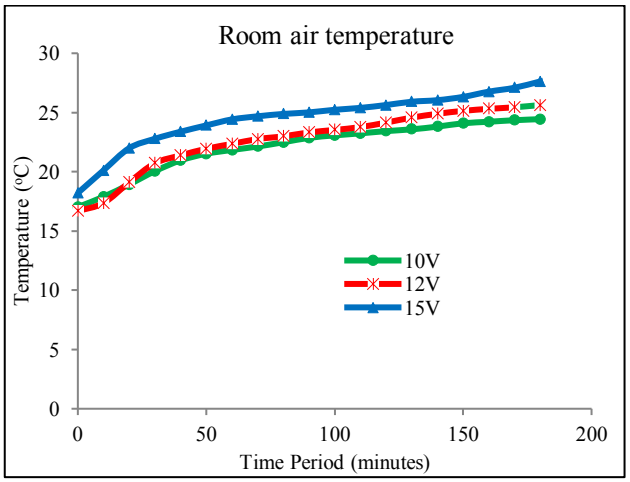

Figure9. Variation of room air temperature with time when water supplied at 22°C

Effect of supply voltage on active surface temperature and air temperature during cooling

For cooling condition the experiment of TE-RHCS was performed with the cold water supplied through the copper pipe (placed above non-active surface of module) to extract the heat from the hot surface (non-active surface) of the TEM. Supply voltage of 10V and 12V have been considered in this strategy because another 8V and 15V is not suitable in case of cooling. At 8V supply the response time for temperature change is very slow and at 15V heat may accumulate inside the TEM after some time if the hot side surface temperature is not maintained at a particular designed value. So 10V and 12V has been taken with water supply temperature at 20°C and 22°C.

In the following figures (11 & 13) we have seen that as the supply voltage increased the rate of change of room air temperature and panel temperature just below the TEM is also increased with cooling effect at faster response and same trend appears for the figures (10 & 12). Also if we decrease the water supply temperature the cooling response becomes faster along with cooling effect.

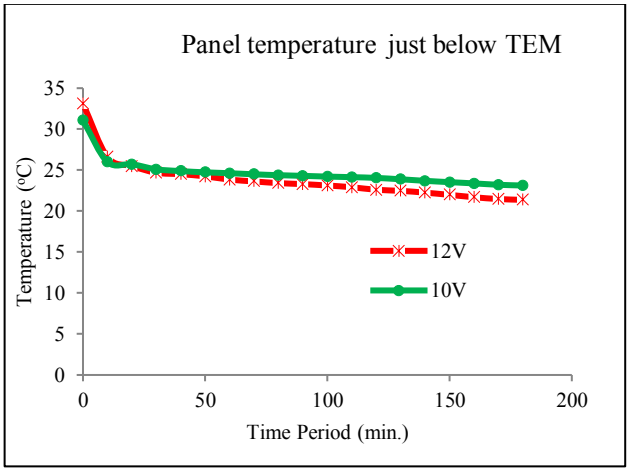

Figure10. Variation of panel temperature below TEM with time when water supplied at 20°C

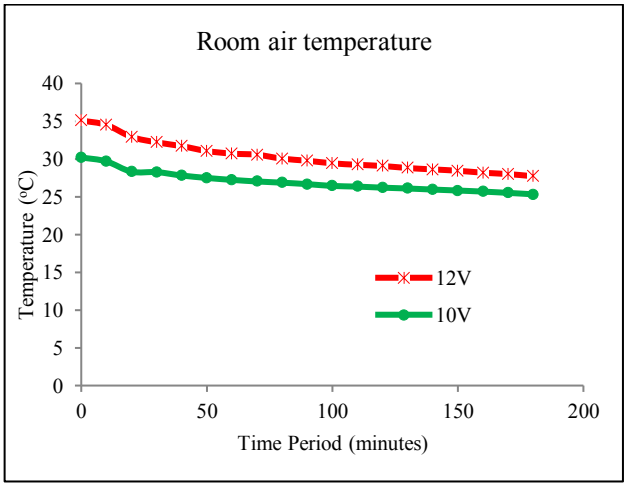

Figure11. Variation of room air temperature with time when water supplied at 20°C

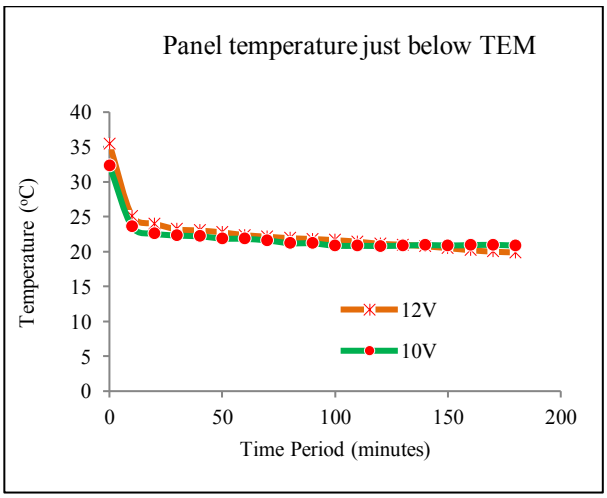

Figure12. Variation of panel temperature below TEM with time when water supplied at 22°C

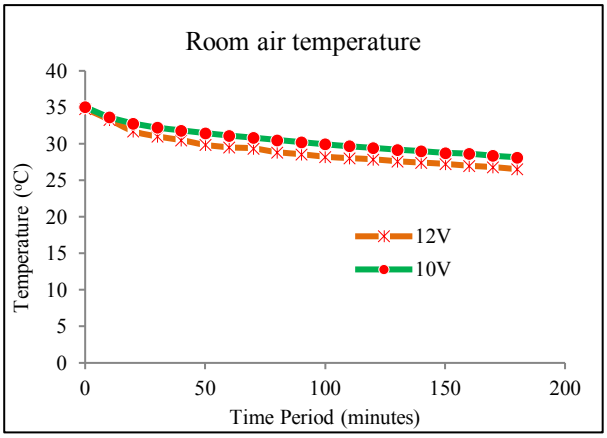

Figure13. Variation of panel temperature below TEM with time when water supplied at 22ºC

CONCLUSION

In this study we found that the thermoelectric module is working successfully for cooling and heating of a building space. The required voltage for each TEM lies in the range of 5V to 7.5V and the current corresponding to this voltage supply is in the range of 0.6A to 1A in heating condition which also depends on the resistance of the TEM while for cooling condition the supply voltage varies from 4V to 6V and the current lies from 0.45A to 0.8A. The heating and cooling effect of each TEM is 12W and 6W respectively when hot side temperature is maintained at 27ºC or closer to it and there is a temperature difference of 10ºC between the hot and cold side surface temperature of thermoelectric module. In case of cooling and the average cooling capacity of the panel is approximately 360W/m^2 and the average heating capacity of the panel is near about 175W/m^2 in case of heating. Above governing equations have been described the system performance and used to determine the different output parameters. The mass flow rate of water is kept constant in this study which is 1lpm for heating and 2lpm for cooling condition. There are total nine thermoelectric module has been used in the panel of size 0.65×0.65m. After performing the experiment of both heating and cooling we conclude that this study will help us to eliminate the use of refrigerant, used in the chiller for cooling water successfully. Using this concept we can create a better environment for the coming generations.

ACKNOWLEDGEMENT

The authors gratefully acknowledge the financial support provided by home university Project Grant 2018.The authors are also thankful to Department of Mechanical Engineering, MNIT Jaipur for providing instruments and infrastructural support.

REFERENCES

1. Limei Shena, Fu Xiaob, Huanxin Chena, Shengwei Wangb “Investigation of a novel thermoelectric radiant air-conditioning system” Energy and Buildings 59 (2013) 123–132.
2. Hansol Lim, Yong-Kwon Kang, Jae-Weon Jeong “Thermoelectric radiant cooling panel design: Numerical simulation and experimental validation” Applied Thermal Engineering (2018)
3. Limei Shen, Zhilong Tu, Qiang Hu, Cheng Tao, Huanxin Chen “The optimization design and parametric study of thermoelectric radiant cooling and heating panel” Applied Thermal Engineering 112 (2017) 688–697
4. Yongqiang Luo, Ling Zhang , Zhongbing Liu, Yingzi Wang , Fangfang Meng, Lei Xie “Modeling of the surface temperature field of a thermoelectric radiant ceiling panel system” Applied Energy 162 (2016) 675–686
5. Yongqiang Luo, Ling Zhang , Zhongbing Liu , Yingzi Wang, Jing Wu, Xiliang Wang “Dynamic heat transfer modelling and parametric study of thermoelectric radiant cooling and heating panel system” Energy Conversion and Management 124 (2016) 504–516.
6. Olga Bubnova, Zia Ullah Khan, Abdellah Malti, Slawomir Braun, Mats Fahlman, Magnus Berggrenand Xavier Crispin “Optimization of the thermoelectric figure of merit in the conducting polymer poly(3,4-ethylenedioxythiophene) ” Nature Materials, vol 10 june 2011.
7. Matthieu Cosnier, Gilles Fraisse, Lingai Luo, “An experimental and numerical study of a thermoelectric air-cooling and air-heating system” Int. J. Refrig. 31 (2008) 1051-1062
8. Stetiu C. “Energy and peak power potential of radiant cooling systems in US commercial buildings.” Energy and Buildings 1999;30: 127–38.
9. Feustel HE, Stetiu C. “Hydronic radiant cooling—preliminary assessment.” Energy and Building 1995;22:193–205. [5] Yost PA, Barbour CE, Watson R.
10. “An evaluation of thermal comfort and energy consumption for a surface mounted ceiling radiant panel heating system.” ASHRAE Transactions 1995;101(1):1221–35.
11. Feustel H, Stetiu C. “Hydronic radiant cooling—preliminary assessment.” Energy Build 1995;22:193–205.
12. Imanari T, Omori T, Bogaki K. “Thermal comfort and energy consumption of the radiant ceiling panel system: comparison with the conventional all-air system.” Energy Build 1999;30:167–75.

REHVA
Federation of European Heating, Ventilation and Air Conditioning Associations

Investigation of optimum thermal energy management for future high energy density batteries with integrated phase change heat transfer package

Yujun Jung, Ukmin Han, Hoseong Lee*

Department of Mechanical Engineering, Korea University
409 Innovation Hall Bldg., Anam-Dong, Sungbuk-Gu, Seoul, Republic of Korea
*: Corresponding Author, Tel: (02) 3290-3355, Email: hslee1@korea.ac.kr

***Abstract*—As response to climate change and strengthened environmental regulations, interests in developing various renewable energy systems is grown. Electric vehicles and plug-in hybrid vehicles, in particular, are anticipated as the next generation vehicles, and many studies on them have been under way for a long time. As electric vehicles use secondary batteries, there is a problem with battery heat generation. As the energy density of a battery is expected to continuously increase, more efficient battery thermal management system is needed to ensure its performance and safety. In this study, various BTMS systems that have been studied so far have been analyzed in advance the integrated phase change heat transfer package composed of three main thermal management systems are newly designed.**

***Keywords*—next generation battery, pouch cell battery, battery thermal management system, integrated phase change heat transfer package**

Nomenclature

Abbreviation

BTMS	battery thermal management system
CFD	computational fluid dynamics
CNT	carbon nanotube
EV	electric vehicle
ESS	energy storage system
IPH	integrated phase change heat transfer package
MSMD	multi-scale multi domain
OHP	oscillating heat pipe
PCM	phase change material
PHEV	plug in hybrid electric vehicle

1. Introduction

In response to climate change and energy problems, the developments of renewable energy systems and EVs (electric vehicles) have been continuously expanded. ESS (energy storage system), which is applied to compensate an imbalance in demand and supply of renewable energy, is the key component technology that determines the efficiency of the energy systems. The development and design of effective battery systems have attracted a significant attention in automotive industry as the secondary battery is become exceptionally crucial for the present-future EVs and PHEVs (plug-in hybrid electric vehicles). Nowadays, most EVs (electric vehicles) use the lithium-ion battery, which shows the highest energy density among several secondary batteries. However, research is still widely carried out to increase the energy density of the battery in order to solve the current problem of a short mileage of EVs compared to conventional internal combustion engine vehicles. The status and prospects of automotive future battery are shown in Fig. 1, implying the energy density of batteries will continue to increase [1]. Therefore, future lithium-ion batteries are expected to have a higher energy density of over 400 Wh/L, and the development of a new and proper battery thermal management system (BTMS) is inevitably required accordingly.

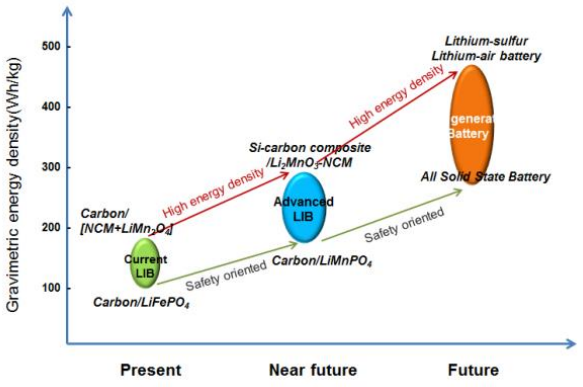

Figure 1. Status and prospects of automotive next generation battery [1]

The highly reliable BTMS are needed to installed within the battery modules/packs to insure its performance and reliability. Generally, lithium-ion battery has its proper operating temperature range between 15℃ and 25℃ [2] as shown in Fig 2. The batteries are faced to some critical problems of their performance and safety if their operating temperatures are out of this proper range. As its energy

density increases continuously, the battery is operated under the much higher voltage and current for fast charging. This results in a locally large heat generation within the battery cell during the charging and discharging process, increasing the average and maximum temperature of the battery cell and inducing a large temperature distribution within the battery cell.

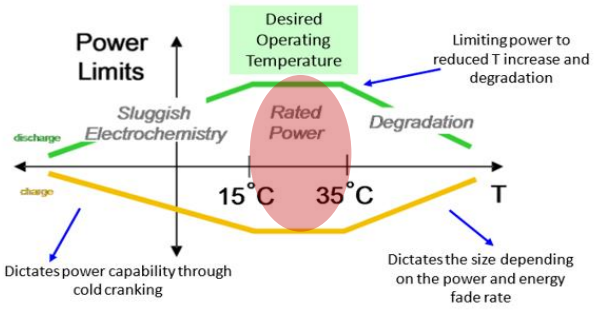

Figure 2. Proper temperature range of Li-ion battery [2]

It is difficult to efficiently manage the high energy density batteries with the existing thermal management systems. To find out the appropriate solution for future battery system, some representative conventional BTMSs are compared in advance from several points of views: integration to automotive system, energy efficiency, temperature changes, maintenance and their lifetime with operating costs. Each system has its own distinct advantages and disadvantages, so it is carefully required to select a suitable system in consideration of the its operating environment. However, this is not a fine way to prevent the degradation of the battery's performance and ensure its safety. Therefore, another new or integrated BTMS is needed that incorporates the advantages of current BTMSs to manage the heat generation of the battery. In this study, the integrated phase change heat transfer package is designed and investigated to manage the heat generation within the battery cell. The newly designed package is consisted of pouch type battery cell with three main thermal management parts: oscillating heat pipe, roll-bond heat exchanger, and carbon nanotube-phase change material. All of them are bonded together in one cube-shaped package and tried to operate individually to stabilize the battery cell's temperature to the desired range.

TABLE I.
COMPARISON OF CONVENTIONAL BATTERY THERMAL MANAGEMENT SYSTEM

	Air forced	Liquid	Cold plate	PCM	Heat pipe	Thermoelectric
Ease of use	Easy	Difficult	Moderate	Easy	Moderate	Moderate
Integration	Easy	Difficult	Moderate	Easy	Moderate	Moderate
Efficiency	Low	High	Medium	High	High	Low
Temperature drop	Small	Large	Medium	Large	Large	Medium
Temperature distribute	Uneven	Even	Moderate	Even	Moderate	Moderate
Maintenance	Easy	Difficult	Moderate	Easy	Moderate	Difficult
Life	≥20 years	3-5 years	≥20 years	≥20 years	≥20 years	1-3 years
First cost	Low	High	High	Moderate	High	High
Annual cost	Low	High	Moderate	Low	Moderate	High

2. Battery model development

In this chapter, the mathematical modeling on pouch type battery cell to analyze its thermal behavior during the charging and discharging process is introduced. The total heat generation rate from the battery cell and required cooling capacity are determined. This mathematical modeling and calculated boundary conditions is referred to develop the CFD simulation model.

2.1. Pouch type battery cell

In this research, the pouch type battery cell shown in Fig. 3 is considered for the battery type used for the novel heat transfer package.

Figure 3. Pouch type battery cell

The pouch type battery cell has the advantages of relatively high energy density and low weight. The pros and cons for some common types of battery cell are listed in Table 2. Under the same energy density, the volume of pouch type battery cell is overwhelmingly lower than other types of batteries. It is also expected to be comfortable to combine with other thermal management systems such as heat pipes and PCM. For those advantages, the pouch type battery cell is selected for the type of battery for the novel thermal management package.

TABLE II.
COMPARISON OF TYPES OF BATTERY CELL

	Advantages	Disadvantages
Cylindrical	Low manufacture price	Strict limitation in energy density
	Ease of manufacture and supply	Memory effect problem
Prismatic	Low price	High weight and
	High durability	Low energy density
Pouch	High energy density	Hard to produce
	Low weight and ease of control	Low speed in fabrication

2.2. Thermal behavior modeling

To calculate the heat generation from the battery cell, the mathematical modeling to describe the general thermal behavior of the battery is carried out. Referring the same specification of battery and modeling process studied earlier by Kim et al. [3], the total heat generation rate from the battery cell is described in Eqn. (1).

$$q = aJ[V_{oc} - V_{cell}] - T\frac{dV_{oc}}{dT} + a_p\frac{|\nabla V_p|^2}{r_p} + a_n\frac{|\nabla V_n|^2}{r_n} \quad (1)$$

where $\boldsymbol{a}$ is the specific area of the battery (m^{-1}), J is the current density ($A\ m^{-2}$), V_{oc} and V_{cell} is the open-circuit potential of the cell (V) and the cell voltage (V) respectively. Rest of right-hand side describes the specification of positive and negative electrodes. The cooling capacity of the novel heat transfer package, especially for the roll-bond heat exchanger is described in Eqn. (2).

$$q_{cooling} = \dot{m}c_p\Delta T \quad (2)$$

Where $\dot{m}, C_p$, and ΔT is the mass flow rate, heat capacity, and temperature difference between the inlet and outlet pipes of the cooling refrigerant.

2.3. CFD model development

The CFD model to simulate the battery thermal behavior and to analyze the performance of each three thermal management systems within the heat transfer package are developed. The heat is mainly generated by the Joule heating process in which heat is generated by the current flow in a conductor. It is caused by the interaction between the moving electrons that make up the current and the atomic ions that compose the conductor. To simulate this process in CFD, the FLUENT® from ANSYS® are selected for the battery simulation tool using the multi-scale multi domain (MSMD) module. Fig. 4 indicates the temperature difference within the battery cell during the charge/discharge process. The specific temperature distribution is discovered as the positive and negative electrodes are positioned on the upper side of the battery cell for the case of the pouch type battery cell. Therefore, unlike the cylindrical battery cell, the paths designs of OHP and roll-bond heat exchanger should be considered by analyzing the temperature distribution of the battery cell.

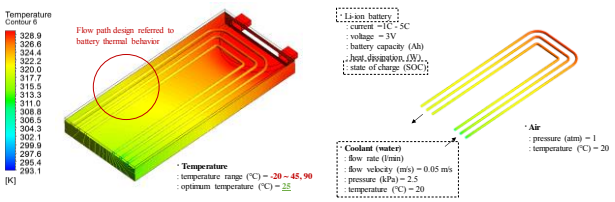

Figure 4. CFD model development

3. Integrated phase change heat transfer package

The newly developed integrated phase change heat transfer package is consisted of each two OHPs, PCMs and roll-bond heat exchangers in the form of thin film. Total six thin films are attached together side by side of the battery cell. The functions of those thermal management systems are described in following sub-sections specifically with their distinctions from the conventional thermal management systems.

3.1 Oscillating heat pipe

During the process of charging, batteries generate the heat. For the case of batteries with high energy density, such as lithium-ion batteries, the heat is generated much more intensely and locally during the charging and discharging, resulting in severe temperature differences within the battery cells. Such temperature differences can adversely affect the performance and longevity of the batteries. In addition, higher battery temperatures reduce the efficiency and reliability of the battery. To solve this problem, thin film with heat pipes are used for our first thermal management system. This thin films with heat pipes, which require no external heat exchangers, can transfer the heat from the high to low temperature of the battery without the use of extra energy. Furthermore, thin-film structures can make up less volume and lighter than conventional heat pipes, which can help to make the vehicle lighter by minimizing the volume and weight of BTMS mounted on the vehicle. The design concepts of this oscillating heat pipes are shown in Fig. 5.

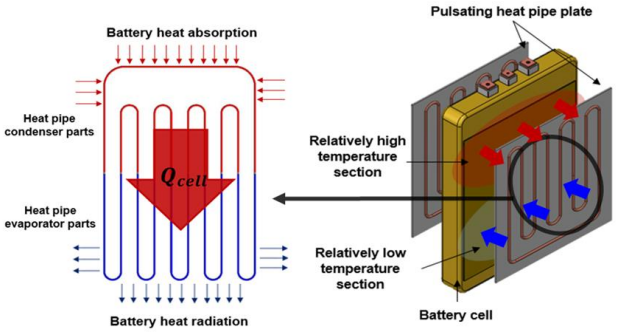

Figure 5. Thin film with oscillating heat pipe

3.2 Carbon nanotube-phase change material

The phase change material part is filled between the thin film heat pipe and the roll-bond heat exchanger as shown in Fig. 6. The interior includes the PCM capsule, from which the phase change materials are filled in, and polyurethane fillers.

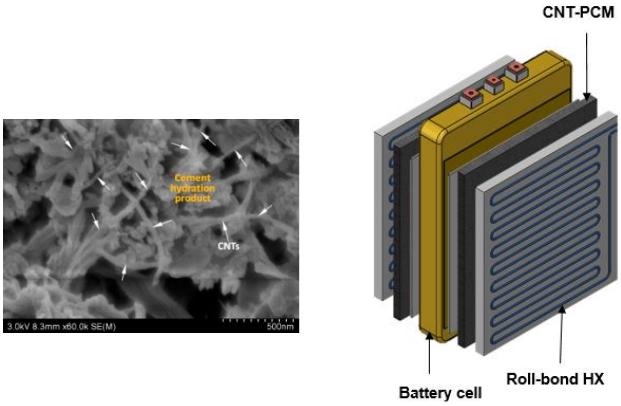

Figure 6. Carbon nanotube-phase change material composite plate

Formed by the melting PCM capsules and filler, foam insulation sheets are made to match the geometry of thin film heat pipes with roll-bond heat exchangers. This foam insulation sheet acts as a thermal buffer in the idling state of the vehicle. The heat generated from the battery is absorbed by the latent heat of the carbon nanotube (CNT)-PCM, reducing the energy consumption due to rapid heat generation response and delayed supply of refrigerant. Furthermore, the heat transfer performance of the heat pipe and the heat exchanger can be increased by filling the empty space between the them

3.3 Roll-bond heat exchanger

For the last part of the heat exchanger, roll-bond heat exchangers are used and refrigerant is circulated via the automotive air conditioning systems. It is closely connected to the outer face of the CNT-PCM composite plate, absorbing and cooling the heat generated from the PCM. When conventional cooling system is used, the temperature of the coolant at the inlet and outlet are varied due to the single-phase heat exchange, which cools the battery temperature unevenly. However, the two-phase heat transfer of refrigerant is used to reduce the temperature distribution. This also improves the cooling performance of the roll-bond heat exchangers at lower flow rates.

3.4 Distinctions from earlier research

The BTMS using the high thermal conductivity plate to extract the heat from the battery cell combining with PCM and heat pipes [4] shown in Fig. 7 was developed earlier in 2012. However, it didn't consider the temperature distribution within the battery cell. As mentioned above, the severe temperature distribution could lead to a drastic degradation on the battery capacity and performance, it is very important to make a uniform temperature on the battery cell. Therefore, the novel integrated phase change heat transfer package is designed not only to reduce the average and maximum temperature, but also to stabilize the temperature distribution during the charging/discharging process [5].

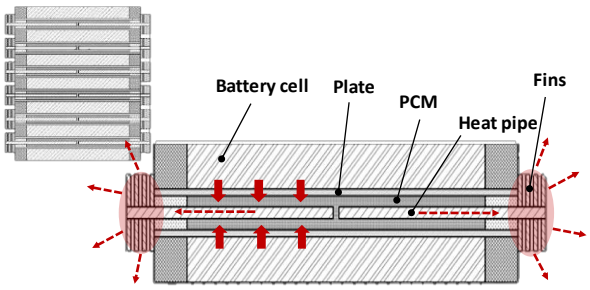

Figure 7. BTMS using the heat pipe and PCM [4]

4. Optimization

The design concept and configuration on newly developed integrated phase change heat transfer package is shown in Fig. 8. After designing the final configuration of each three thermal management systems, we lastly consider to find the optimum design point. The optimization is carried out by simulating numerous cases of various design points within the design space based on the design of experiments. Following the multi-objective genetic algorithm, the trade-off between the total energy consumption for the battery thermal management and cooling performance are investigated. The simulation is conducted under the transient analysis, simulating the thermal behavior during the charging and discharging. The final optimum point is used to build the real size of this heat transfer package and planned to be verified through the experiment.

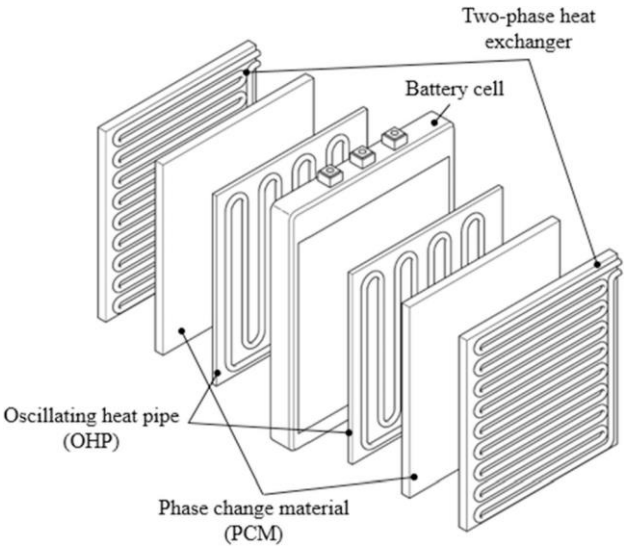

Figure 8. Integrated phase change heat transfer package (IPH) [5]

5. Conclusion

The objective of this study is to carry out an optimization study on the composite phase change heat transfer package composed of thin film oscillating heat pipe, CNT-PCM nano capsule, direct refrigerant cooled roll-bond heat exchanger. Started from the comparison of existing BTMS, the analytical models and CFD simulation models are developed to analyze the thermal management performance of the integrated phase change heat transfer package. The design concepts on three main thermal managements systems are derived with their specific functions. In summary, it is expected that the newly developed heat transfer package utilizing both the thin film heat pipes and the PCM phase change parts can reduce the total energy. This also increase the cooling performance of the package while reducing the complexity of package systems by utilizing refrigerant instead of the cooling water. In addition, the thin film oscillating heat pipes and roll-bond heat exchangers can minimize the volume and reduce the weight of the BTMS system dramatically.

ACKNOWLEDGEMENT

1. This research was supported by the Society of Air-Conditioning and Refrigerating Engineers of Korea.

REFERENCES

[1] Kim KS. “Automotive, next-generation battery technology applications (presentation),” Hanon System Seminar in Korea Electronics, Technology Institute(KETI), 2017.

[2] Pesaran, Ahmad, S. Santhanagopalan, and G. H. Kim, “Addressing the impact of temperature extremes on large format li-ion batteries for vehicle applications (presentation),” National Renewable Energy Lab.(NREL), No. NREL/PR-5400-58145, 2013.

[3] Kim US, Yi J, Shin CB, Han T, Park S. Modeling the thermal behaviors of a lithium-ion battery during constant-power discharge and charge operations. Journal of The Electrochemical Society. 2013 Jan 1;160(6):A990-5.

[4] Hyundai motor, Heat control plate for battery cell module and battery cell module having the same. KR. Patent No. 10-1470072-0000. 2012.

[5] Kim, Jaewan, Jinwoo Oh, and Hoseong Lee. "Review on battery thermal management system for electric vehicles," Applied Thermal Engineering, vol. 149, 2019, pp192-212.

[6] H.S. Lee, J.W. Kim, Battery cooling unit and battery module including the same. KR. Patent No. 10-2018-0029056. 2018.

REHVA
Student Competition
Other Participants' Contribution

Luis Costa	Portugal
Matthias Van Hove	Belgium
Dominika Juhosova	Slovakia
Aleksi Mäki	Finland
Alice Geber	France
Jan Vitous	Czech Republic
Gregor Jeker & Timotheus Zehnder	Germany
Cristina Jurado Lopez	The Netherlands
Karl-Villem Vosa	Estonia
Danijel Todorovic	Serbia
Daniel Butucel	Romania
Manuela Baracani	Italy

REHVA Student Competition, 26 – 29 May, Bucharest, Romania

Cost of thermal comfort in buildings located in Portugal

Luís M.T.M. Costa* and *António M.M.* Raimundo

[1] University of Coimbra, Faculty of Science and Technology, Department of Mechanical Engineering, 3030-788 Coimbra, Portugal

Abstract. The main purpose of this study was to evaluate the relationship between the level of thermal comfort in buildings located in Portugal and the value of the Equivalent Annual Cost (*EAC*) of the complete lifetime cycle (construction + exploration + demolition) of the building.

The evaluation of the energy behaviour of the buildings and the determination of the *EAC* of its complete life cycle was made using a dynamic simulation software based on the monozone model of ISO 13790 [1] and in economic evaluation algorithms [2, 3], the SEnergEd program developed by the supervisor of this work [4]. This software was prepared to control the operation of the HVAC equipment by temperature and/or relative humidity setpoints, which was not suitable for this work. Thus, it was necessary to complement this software with a new module, to made possible the control of the HVAC systems also through setpoints of a thermal comfort indicator, the PMV index.

Five buildings were analysed, representing four types of use: apartment, detached house, private clinic with hospitalization, secondary school and supermarket of medium size. These buildings were considered located in three climatic regions, representative of the Portuguese climate. Several levels of thermal insulation of the opaque constructive solutions were evaluated and 6 thermal comfort classes were created.

The cost of thermal comfort, represented by the building's *EAC*, depends essentially on the class of comfort that is intended to be ensured and the severity of the climate. On the other hand, the use of thermally insulated opaque constructive solutions is only important in zones with a more intense climate and, even so, only in the case of residential buildings.

1. Introduction

Traditionally, air conditioning systems dedicated to a space are programmed to maintain fixed temperature ranges, usually between 21ºC and 24ºC [5]. Keeping the air temperature of interior spaces between the previous setpoints entails costs for the building holder (owner, renter, ...). What is the value of these costs? What is their relationship with the class of thermal comfort to be maintained, the type of climate, usage of the building and quality of its opaque constructive solutions? These costs are not only relevant in zones with a very cold or very hot climate, but also in zones with a moderate climate, such as Portugal. This is because buildings located in zones with a moderate climate have both heating (winter) and cooling (summer) needs, so, their energy consumption for air conditioning can also reach high values. Another question also arises: Would it be advantageous to control the HVAC system's operating schedule based on the thermal comfort of the occupants instead of traditional temperature setpoints?

The focus of this study is on the assessment of the use of energy and economic resources for air conditioning of interior spaces with human occupation in regions with a moderate climate, like Portugal. For this, the level of thermal comfort in buildings located in these regions must be related with the value of the Equivalent Annual Cost (*EAC*) due their use by humans.

Other purpose of this study is the evaluation of the relation between the *EAC* stemming from the use of each type of building and the quality and price of the passive constructive solutions used.

2. Thermal comfort classes

The predicted mean vote (PMV) index [8] is probably the most commonly used parameter to account for the average thermal comfort of a group of people. Its value is obtained from a human body heat balance, which involves the individual metabolic activity and clothing, as well as the air temperature, humidity and velocity, and the mean radiant temperature in the space.

The PMV index is characterized by a scale of 7 values, centred on 0, between -3 and +3, depending on whether the human being feels thermal discomfort due to cold (negative values) or due to heat (positive values).

The ISO 7730 [8] norm also presents a relation between the value of this index and that of another parameter, the PPD (predicted percentage dissatisfied), which estimates

* Corresponding author: luismanueltmc@gmail.com

the percentage of people thermally dissatisfied with the thermal environment.

For the purposes of this work, 6 thermal comfort classes were defined, from worst to best, by D, C, B, A, A+ and A++, for which the values of the setpoints considered in the simulations are presented in Table 1.

Table 1. Classes of thermal comfort considered.

Class	PMV	PPD
A++	-0.25 ≤ PMV ≤ +0.25	6%
A+	-0.50 ≤ PMV ≤ +0.50	10%
A	-1.0 ≤ PMV ≤ +1.0	26%
B	-2.0 ≤ PMV ≤ +2.0	77%
C	-3.0 ≤ PMV ≤ +3.0	99%
D	Without an air conditioning system	

Class D corresponds to a situation in which the building does not have any air conditioning system installed, although it has a ventilation system capable of guaranteeing the indoor air quality requirements imposed by Portuguese regulation [9]. If air conditioning systems are not installed, the costs of acquisition and installation are also not considered.

It should be noted that the PMV range corresponding to the A+ class of this work appeared in previous versions of ISO 7730 [8] as the threshold from which the environment ensures a good level of thermal comfort. Therefore, this class will be assumed as a sort of reference plateau.

3. Calculation tool

The evaluation of the energy behaviour of the buildings and the determination of the *EAC* for its complete life cycle was made using a dynamic simulation software, the SEnergEd program, developed by the supervisor of this work [4]. As the available version of this software was prepared to control the operation of the HVAC equipment by temperature and/or relative humidity setpoints, which was not suitable for this work, it was necessary to complement it with a new module, to made possible the control of the air conditioning systems also through setpoints of the PMV index.

3.1. Calculation methodologies

To simulate the thermal behaviour of each building, the SEnergEd software uses the 5R1C monozone dynamic model (5 thermal resistances and 1 thermal capacitor) described in ISO 13790 norm [1] and to additional models to obtain the other energy needs of the building (lighting, non-HVAC equipment, not air-conditioned spaces, ...). After this, the building energetic needs are converted into energy consumption. Knowing the tariffs to pay for each type of consumer (domestic, business, ...) for each type of energy (electric, natural gas, ...), the consumptions are converted into expenses.

The cost related to the use of the building is represented by the equivalent annual cost (*EAC*), which is a parameter that considers all expenses associated with the building during its lifetime (construction, utilization, taxes, maintenance, demolition, ...). The *EAC* is obtained from the knowledge of the building net present value (*NPV*). These parameters are obtained through the following generic expressions [3]:

$$NPV = \frac{RV}{(1+r)^n} - I_0 + \sum_{k=1}^{k=n} \frac{CF_k}{(1+r)^k} \quad (1)$$

$$EAC = -NPV \cdot \frac{r \cdot (1+r)^n}{(1+r)^n - 1} \quad (2)$$

where n is the time period considered in the analysis, k is the year under appreciation, I_0 is the value of the initial investment, CF is the annual value of the economic-financial cash-flow, RV is the building residual value at the end of the analysis period and r is the financial discount rate (the cost of capital).

3.2. Control of HVAC systems by PMV setpoints

The SEnergEd software is programmed as a set of interconnected MS Excel worksheets. So, for a good running of the new module, to control the operation of the AVAC systems by PMV setpoints, it was necessary to program in MS VBA two subroutines (one for the PMV and one for the PPD), which were incorporated into the MS Excel, so that they can be applied in the same way as any other implicit function of this program. It was also necessary to prepare the fields for entry of the new data on the occupants: metabolic activity, thermophysical characteristics of the clothing used and indoor air velocity.

As an example, the annual evolution of outdoor air temperature and the one foreseen for indoor air, in the case of one of the buildings in question (the Clinic with hospitalization), is shown in Figure 1, in which the HVAC systems are controlled by temperature setpoints (Figure 1.a) and by PMV setpoints (Figure 1.b). As can be seen, the control of the HVAC systems by PMV setpoints improves the thermal comfort of the occupants and presents a significant potential for energy savings.

4. Cases in study

The climate of Portugal is moderate, without a clear predominance of heating needs over cooling ones or vice-versa. Even so, the Portuguese system of building energy certification [9] divides it into three winter climatic zones (I1, I2 and I3) and three summer climatic zones (V1, V2 and V3), in which the index 1 indicates a mild climate, 2 an average climate and 3 an intense climate. The assignment of a given category (1, 2 or 3) depends on the geographical location and of the site

altitude, so there are nine possible climatic zones (I1-V1, I1-V2, ..., I3-V3).

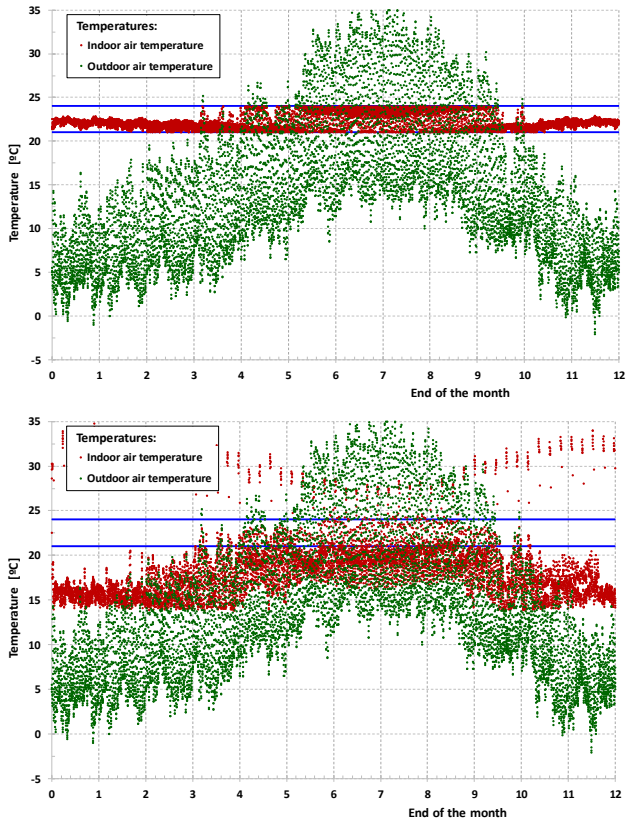

Fig. 1. Annual evolution of air temperature at outdoors (green) and at indoors (red) in the case of the Clinic with hospitalization, when located in a zone of moderate intense climate (Portuguese zone I3-V3) - control of the HVAC systems by setpoints: (a) of temperature [21 ≤ Tair ≤ 24 ºC]; and (b) of PMV [-0.5 ≤ PMV ≤ 0.5].

To represent the climate of Portugal, the buildings were supposedly located in three sites belonging to different climatic zones: Odemira (I1-V1); Ansião (I2-V2) and Mirandela (I3-V3). It is thought that the six possible climatic zones are well represented by these three.

In an attempt of a good representation of the Portuguese reality, buildings presenting 4 different types of use were selected: residential, services with permanent occupation, services with intermittent occupation and commerce. For this purpose, 5 buildings with different climatized areas, occupation, internal thermal loads and types of usage were considered: (i) apartment at mid-level of a multi-story building; (ii) detached house; (iii) private clinic with hospitalization; (iv) secondary school; and (v) medium-sized supermarket. Figure 2 shows a sketch of the layout of the 5 buildings considered and Table 2 reveals a summary of the characteristics of these buildings.

(*a*) Apartment at mid-level of a multi-story building

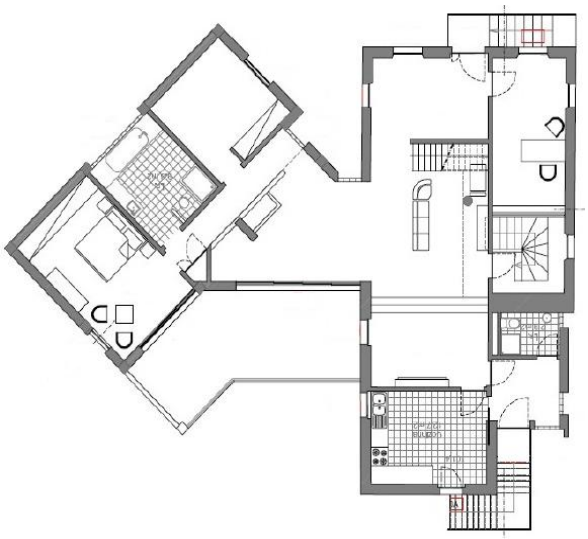

(*b*) Detached house

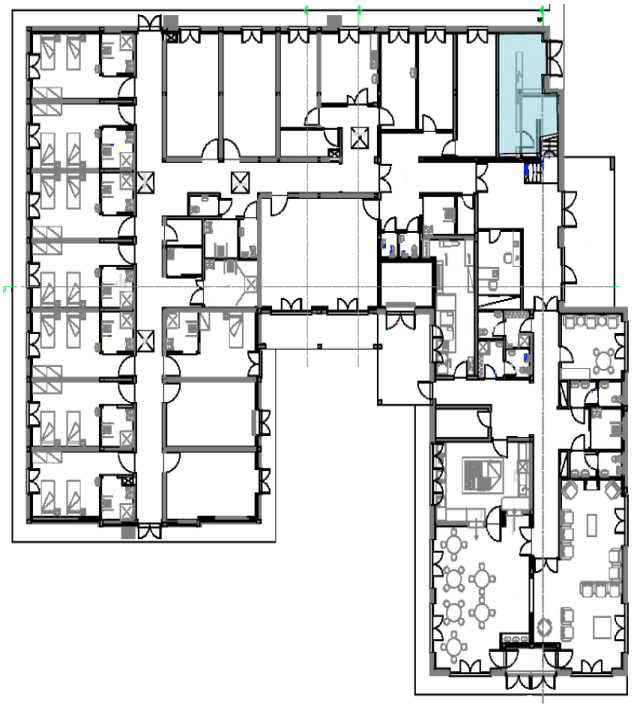

(*c*) Private clinic with hospitalization

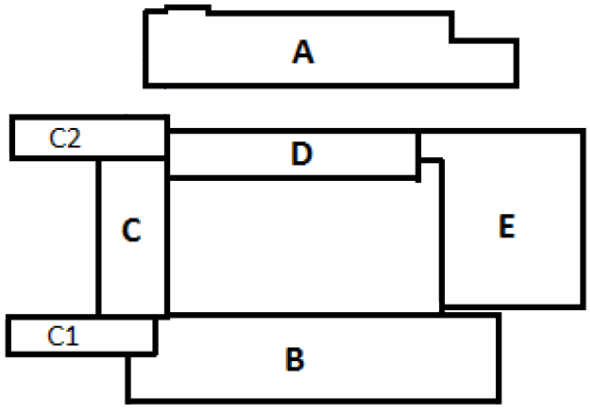

(*d*) Secondary school

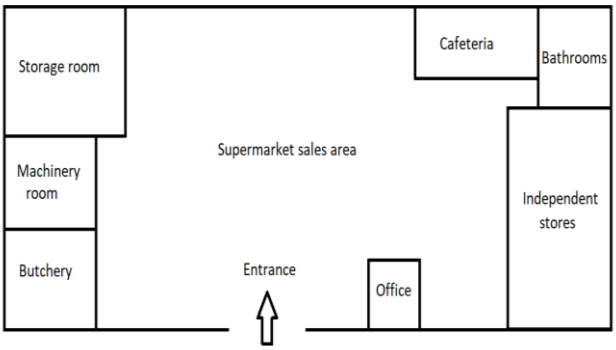

(*e*) Medium-sized supermarket

Fig. 2. Sketch of the main floor layout of the buildings.

It was considered that all buildings are constructed using the same solutions and are equipped with HVAC and DHW systems of the same type, which have comparable energetic efficiencies. It was considered that the air renewal is assured by air handling units, with a ventilation efficiency of 70%, and that the air conditioning is ensured by an air-air Chiller-Heat pump system with COP = 4 in heating mode and EER = 3 in cooling mode. The existence of rejection air heat recovery or of free-cooling were not considered. It was assumed that the DHW are guaranteed by a system of solar thermal panels, with an area suitable for the building in question, assisted by a natural gas boiler with an efficiency of 90%.

The same 5 buildings have already been the subject of previous studies in order to identify the best system for the transparent envelope [10] and to determine the optimal thermal insulation for the opaque envelope [11].

Rebelo [10] identified as the economically more viable solution for the glazing of buildings located in Portugal the application of single windows, with 2 normal glasses separated by an air space of 11 mm, with aluminium frame with a thermal barrier and externally protected by blinds of metallic horizontal strips with thermal insulation by its interior (U_{wdn} = 2.06 W/m^2.K, $g_{\perp glass}$ = 0.71 and $g_{\perp blind}$ = 0.05).

Table 2. Summary of the characteristics of the 5 buildings considered in this study.
Occupation: *Np* - maximum number of occupants [persons];
Building: *Nf* - number of floors, *Vol* - climatized volume [m^3], *Acl* - climatized area [m^2],
Aenv - envelope (opaque + glazed) area [m^2], *Aglz* - envelope glazed area [m^2], *AR* - aspect ratio (= *Aenv* / *Vol*) [m^{-1}],
EA - envelope area ratio (= *Aenv* / *Acl*), *GA* - glazed area ratio (= *Aglz* / *Acl*);
Time: D - during the day, N - during the night, Wi - winter, Su - summer, Sp - spring, Au - autumn.

Building	***Np*** [persons] ***Nf***	***Acl*** [m^2] ***AR*** [m^{-1}]	***EA*** ***GA***	**Utilization profile** **Internal thermal loads**	**Activity level** [met]	**Clothing insulation** [clo]
Apartment at mid-level of the building	4 1	110 0.33	0.87 0.20	Residential Small loads	D - 1.2 N - 0.8	Wi - 1.1/1.1 Su - 0.7/1.1 Sp & Au - 0.9/1.1
Detached house	4 3	167 0.96	2.86 0.30	Residential Small loads	D - 1.2 N - 0.8	Wi - 1.1/1.1 Su - 0.7/1.1 Sp & Au - 0.9/1.1
Private clinic with hospitalization	152 2	927 0.54	2.07 0.27	Permanent High loads	D - 1.6 N - 0.8	Wi - 1.1/1.1 Su - 0.7/1.1 Sp & Au - 0.9/1.1
Secondary school	1 100 4	11 246 0.74	2.77 0.18	Intermittent Small loads	D - 1.2 N - --	Wi - 1.3/-- Su - 0.7/-- Sp & Au - 1.0/--
Medium-sized supermarket	194 1	1 035 0.40	1.46 0.09	Intermittent High loads	D - 1.6 N - --	Wi - 1.5/-- Su - 0.7/-- Sp & Au - 1.1/--

Saraiva [11] identified the application of EPS (expanded polystyrene) in the air box of the walls, in the lower side of the ceilings and in the upper side of the floors, as the economically more viable solutions for the thermal insulation of the opaque envelope of buildings located in Portugal. The EPS thicknesses identified as optimal vary according to the climatic zone, the building utilization and the type of element.

The constructive solutions identified by Rebelo [10] and Saraiva [11] as the most economically viable were considered for this work's purposes. In addition, the use of non-insulated constructive solutions is also analysed. This is to verify the impact of thermal insulation of the opaque envelope on the building's *EAC*.

In the building's dynamic simulations, time intervals of one hour were considered. This means calculations were made for 8 760 time-steps for the simulation of each year of operation.

For purposes of the present study, the costs related to the passive and active constructive solutions were obtained from the works of Rebelo [10] and Saraiva [11] and from the "price generator" of Cype building simulation software [12].

It was considered that all buildings had a useful life of $n = 50$ years [2, 13, 14] and that the increasing of costs due to inflation, including those of energy resources, equals $if = 3\%$/year [13, 14]. A real interest of $r = 3\%$/year was assumed for the financial discount rate [13, 14]. Both the values of *if* and *r* were presumed constant during the entire period of analysis.

The tariffs of the purchase of energy (electric and natural gas), by type of consumer (domestic, commercial and services) were obtained by consulting the European Union energy price statistics explained website [15].

5. Results

Figure 3 graphs show the building's annual *EAC*/m^2 (equivalent annual cost per m^2 of floor area of the building climatized spaces) as function of the class of thermal comfort to be guaranteed and of the climatic zone in which the building is supposed to be located. In this figure the solid lines refer to situations where the opaque constructive solutions incorporate the optimum thermal insulation thickness, identified by Saraiva [11], and the dashed lines refer to cases in which these elements do not include thermal insulation.

Figure 3 shows that in the residential buildings the difference between the *EAC*/m^2 relative to the Detached house and to the Apartment is evident. Independently of the situation, the Detached house presents an *EAC*/m^2 around 50% greater than the Apartment.

In terms of annual equivalent cost per square meter of climatized area, from the ordering of the buildings under analysis, from the cheapest to the most expensive, results: School, Supermarket, Apartment, Detached house and Clinic. Relatively to the cheapest building (the School), the others have an *EAC*/m^2 higher in about: 2.5 times the Supermarket, 2.9 times the Apartment, 4.2 times the Detached House and 4.9 times the Clinic.

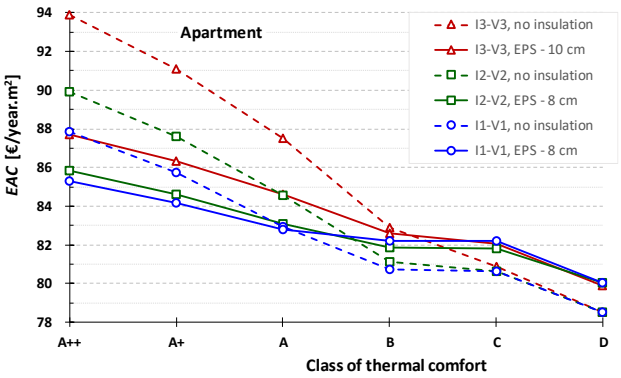

(*a*) Apartment at mid-level of a multi-story building

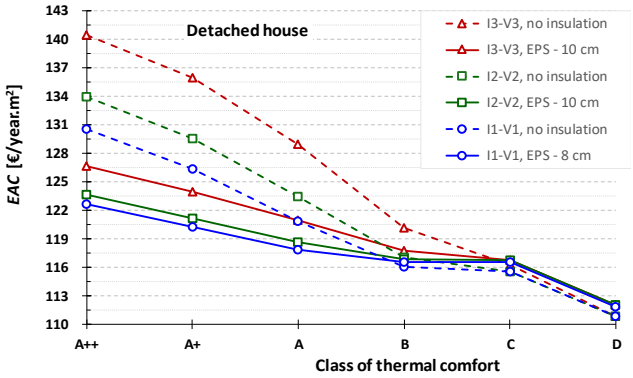

(*b*) Detached house

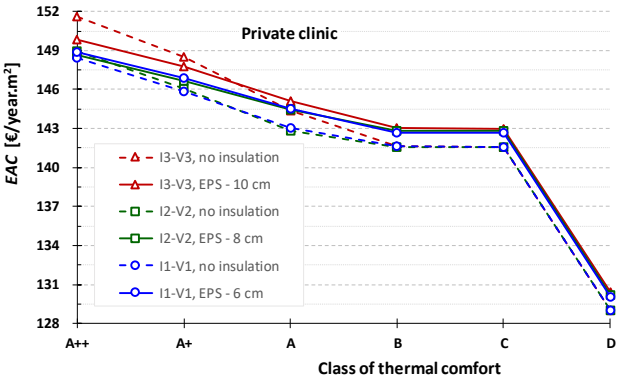

(*c*) Clinic with hospitalization

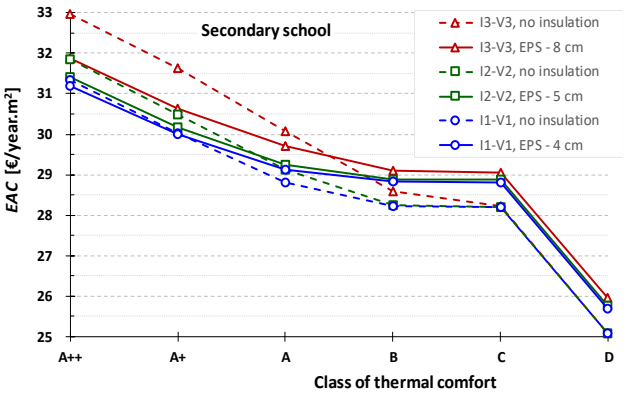

(*d*) Secondary school

* Corresponding author: luismanueltmc@gmail.com

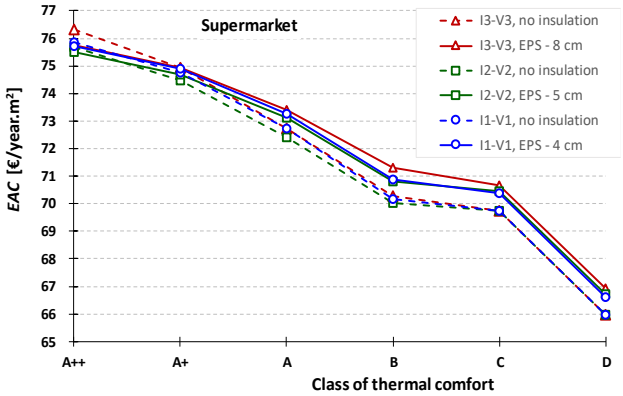

(*e*) Medium-sized supermarket

Fig. 3. Relationship between the building's *EAC* [€/(year.m^2)] and the thermal comfort class to be guaranteed and the climatic zone. Solid lines → opaque elements of the building's envelope with the optimum thermal insulation thickness; Dashed lines → opaque elements without thermal insulation.

It is noticeable in Figure 3 that the importance of insulating the opaque elements of the building's envelope is much greater in the case of residential buildings. For the non-residential buildings considered, there are no significant cost differences between thermally insulating or not the opaque elements of the building envelope. It should however be highlighted that buildings that do not have thermal insulation on its opaque envelope always present energy consumptions much higher than those that occur when these opaque elements incorporate the recommended EPS thickness.

Another highlight is that the application of thermal insulation, in the opaque elements of the building's envelope has a major importance in the building's utilization costs. These grow with the increase of the thermal comfort level required.

Generally, for all building typologies and climatic zones, if the intention is to ensure only the lower thermal comfort classes (D, C or B), then the usage of opaque elements without thermal insulation is the solution that leads to lower EAC values. On the other hand, if the objective is to guarantee classes of higher thermal comfort (A, A+ or A++) then the economically more favourable solution is to insulate the opaque elements of the building's envelope with the optimum EPS thicknesses recommended for the climatic region in question and building typology.

The climate of the region in which the building is located also has a high influence. As the intensity of the climatic conditions increases, the insulation of the opaque elements of the building's envelope becomes more relevant.

Table 3 shows a summary of the *EAC*/m^2 values for the situation of sustenance of the A+ class of thermal comfort ($-0.50 \leq PMV \leq +0.50 \rightarrow PPD = 10\%$), as function of building type of use, of thermal insulation of its envelope opaque elements and of the climatic region.

Table 3 shows that if the goal is to keep an A+ comfort class, and the Clinic or the Supermarket are placed in a mild climate zone (e.g. Odemira: I1-V1) or a medium climate one (e.g. Ansião: I2-V2), the opaque constructive solutions that lead to the lowest *EAC*/m^2 are those that didn't include thermal insulation. However, if this analysis is carried out in energetic terms, the recommended solution is the application of thermal insulation in these elements of the building envelope.

Although not always the most economically profitable, the application of thermal insulation in opaque constructive solutions of the building envelope is always advantageous from the point of view of environmental sustainability, leading to a lower energy consumption by the HVAC systems and, therefore, to a more reduced ecological footprint.

6. Conclusions

The thermal insulation thickness, to apply in the opaque elements of the building's envelope, which leads to lower costs for the use of buildings located in regions with moderate climates (e.g. Portugal) depends of the typology of use of the building, of the specific climatic region and of the thermal comfort level to be guaranteed.

The *EAC*/m^2 of residential buildings is always more dependent on the class of thermal comfort to be assured, on the climate and on the thickness of thermal insulation of the opaque envelope than the buildings destined for the other kinds of use.

Even for Portugal, a region with moderate climate, the differences between the different climatic zones were very relevant. For the same typology of use and class of thermal comfort to be assured, the buildings located in more intense climates always have higher *EAC* values.

As final remark, it is emphasized the advantage that would exist if the operation of the HVAC equipment were controlled by setpoints of the thermal comfort index PMV instead by setpoints of air temperature and/or humidity.

References

1. ISO 13790 (2006), Energy performance of buildings - calculation of energy use for space heating and cooling.
2. EU (2012). European Union Regulation (EU) 244/2012 of 16 January 2012 supplementing Directive 2010/31/EU by establishing a methodology framework for calculating cost optimal levels of minimum energy performance, Official Journal of the European Union (2012) L81/18.
3. A.M. Raimundo (2015). Support elements of the curricular unit Business and Industrial Management, DEM, FCTUC, University of Coimbra, Portugal.

Table 3. *EAC*/m^2 in the situation of guarantee of a A+ class of thermal comfort ($-0.50 \leq PMV \leq +0.50 \rightarrow PPD = 10\%$),

as function of building type of use, thermal insulation and climatic region.
Occupation: *Np* – maximum number of occupants [persons]; Building: *Acl* - climatized area [m^2]

Building	***Np*** / ***Acl*** [m^2]	**Insulation of opaque elements**	***EAC*/m^2 of climatized spaces floor area** [€/(m^2.year)]		
			Odemira **(I1-V1)**	Ansião **(I2-V2)**	Mirandela **(I3-V3)**
Apartment	4	Optimum thickness	EPS - 8 cm 84.2	EPS - 8 cm 84.6	EPS - 10 cm 86.4
	110	Without insulation	85.7	87.6	91.1
Detached house	4	Optimum thickness	EPS - 8 cm 120.3	EPS - 10 cm 121.1	EPS - 10 cm 123.9
	167	Without insulation	126.4	129.6	136.0
Clinic with hospitalization	152	Optimum thickness	EPS - 6 cm 146.9	EPS - 8 cm 146.6	EPS - 10 cm 147.8
	927	Without insulation	145.8	146.1	148.5
Secondary school	1 100	Optimum thickness	EPS - 4 cm 30.0	EPS - 5 cm 30.2	EPS - 8 cm 30.6
	11 246	Without insulation	30.0	30.5	31.6
Medium-sized supermarket	194	Optimum thickness	EPS - 4 cm 74.9	EPS - 5 cm 74.7	EPS - 8 cm 74.9
	1 035	Without insulation	74.8	74.5	74.9

4. A.M. Raimundo (2017). SEnergEd – software for buildings monozone dynamic energetic simulation and calculation of their life-cycle equivalent annual cost, DEM, FCTUC, University of Coimbra, Portugal.
5. H.B. Gunay, W. Shen, G. Newsham, A. Ashouri (2018). Modelling and analysis of unsolicited temperature setpoint change requests in office buildings, Building and Environment **133**: 203-212.
6. D.H. Kang, P.H. Mo, D.H. Choi, S.Y. Song, M.S. Yeo, K.W. Kim (2010). Effect of MRT variation on the energy consumption in a PMV-controlled office, Building and Environment **45**: 1914-1922.
7. L. Zampetti, M. Arnesano, G.M. Revel (2018). Experimental testing of a system for the energy-efficient sub-zonal heating management in indoor environments based on PMV, Energy & Buildings **166**: 229-238.
8. ISO 7730 (2005), Ergonomics of the thermal environment – Analytical determination and interpretation of thermal comfort using calculation of the PMV and PPD indices.
9. SCE (2013). Support legislation of the Portuguese System of Energy Certification of Buildings, in force after December 1, 2013.
10. A.C. Rebelo (2016). Economical optimum point of energy performance of windows applied into buildings located in Portugal (in Portuguese), Masters dissertation, University of Coimbra, Portugal, February 2016.
11. N.B. Saraiva (2017). Economical optimal point of energy performance of opaque constructive solutions of buildings located in Portugal (in Portuguese), Masters dissertation, University of Coimbra, Portugal, July 2017.
12. Cype (2018). Price generator of Cype building simulation, accessed in April 2018, site: http://www.geradordeprecos.info/
13. C. Baglivo, P.M. Congedo, D. D'Agostino, I. Zacà (2015). Cost-optimal analysis and technical comparison between standard and high efficient mono-residential buildings in a warm climate, Energy **83**: 560-575.
14. P.M. Congedo, C. Baglivo, D. D'Agostino, I. Zacà (2015). Cost-optimal design for nearly zero energy office buildings located in warm climates, Energy **91**: 967-982.
15. Eurostat (2018). European Union energy price statistics explained, accessed in May 2018, site: http://ec.europa.eu/eurostat/statisticsexplained/index.php/

Design and operation of domestic hot water systems: optimisation using building energy simulation

Matthias Van Hove[1], Elisa Van Kenhove[1], Lien De Backer[1], Jelle Laverge[1], Arnold Janssens[1]

[1] *Research group Building Physics, Department of Architecture and Urban Planning, Ghent University, Sint Pietersnieuwstraat 41 B4, 9000 Ghent, Belgium*

***Abstract* — Achieving energy savings in buildings is important to restrain global warming and attain the targeted reduction of CO_2-emissions. Nowadays, in well insulated and airtight buildings, Domestic Hot Water (DHW) production accounts for 50% of the total energy demand, due to unaltered high production temperatures which ensure *Legionella*-poor DHW systems. In order to address and study this issue, Dymola simulations models, representing a BBRI test facility and a chosen case-study apartment site, are developed, which allow to examine *Legionella pneumophila* proliferation risks in DHW systems. The findings are utilised to quantify the effect of renovation measures on infected systems.**

Keywords: Legionella pneumophila, Domestic Hot Water, Building Energy Simulation & Validation, Energy saving potential and biologic analysis

INTRODUCTION

Legionella bacteria are innately present in water, albeit often unaltered in nearly undetectable concentrations due to mainly detrimental outdoor conditions. In hydraulic installations however (*e.g.*, DHW systems), favourable conditions occur which stimulate *Legionella* growth. Therefore, DHW is generally produced, stored and distributed at temperatures above 55-60 °C to mitigate the risk of *Legionella* contamination of DHW systems (Stout *et al.*, 1986 [1]). Individuals, exposed to high *Legionella* concentrations can suffer from severe pneumonia and even death can occur.

Accordingly, high energy use for DHW is required, which start to represent an important share in the total energy demand of well insulated and airtight buildings (*Figure 1*). So far on building level, research focussed on the building envelope (*e.g.*, insulation, water-tightness, air-tightness), technical installations (*e.g.*, ventilation, heating, cooling, renewable energy, energy recovery, water (re-)use and recyclability) and architectural design principles. Energy use for DHW systems in residential buildings remained nearly unaltered and has experienced little innovation in the past decennia.

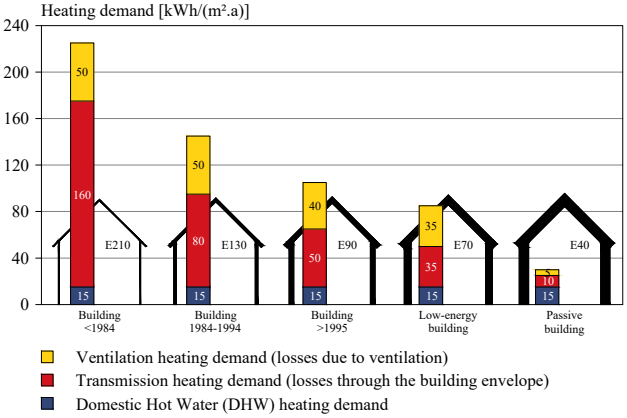

***Figure 1** - Comparison of the heating demand (ventilation, transmission and domestic hot water) for residential buildings of different age and energy efficiency level (adapted from IKZ-HAUSTECHNIK [2]). Data are obtained in Germany for a one-family house with 3 to 4 occupants, with a surface area of 150 m² (A/V = 0.84), which amounts to 15 kWh/m² a year.*

Building Energy Simulation (BES) models can be of importance in the design and optimisation of such buildings. System simulation models are developed, by which energy-saving measures can be compared, based on decreasing *Legionella pneumophila* contamination risk and improving comfort. The aim is to enable utilisation of such models in the design stage as well as to assess various optimisation measures during the operational stage of sanitary systems (*i.e.*, renovation measures). DHW system designers will be able to reduce energy demand for DHW production, while keeping an equilibrium between energy efficient, comfortable and healthy buildings.

METHODOLOGY

This research is divided into two work packages. First and foremost, experience in BES and sensitivity analyses is gained by composing accurate simulation models, representing a BBRI test facility, in Modelica Dymola. A Modelica simulation model is compared with measured data of a BBRI test facility (*Figure 2*) in order to examine how domestic hot water systems can be composed, calibrated and validated based on temperature and flow rate measurements (including temperature stratification of the boiler). Afterwards a second calibration and validation is executed, based on provided *Legionella pneumophila* concentrations, by the addition of a *Legionella* growth model in Modelica (Van Kenhove *et al.*, 2018 [3]). In the end, a better understanding of temperature and *Legionella* behaviour in DHW systems was obtained.

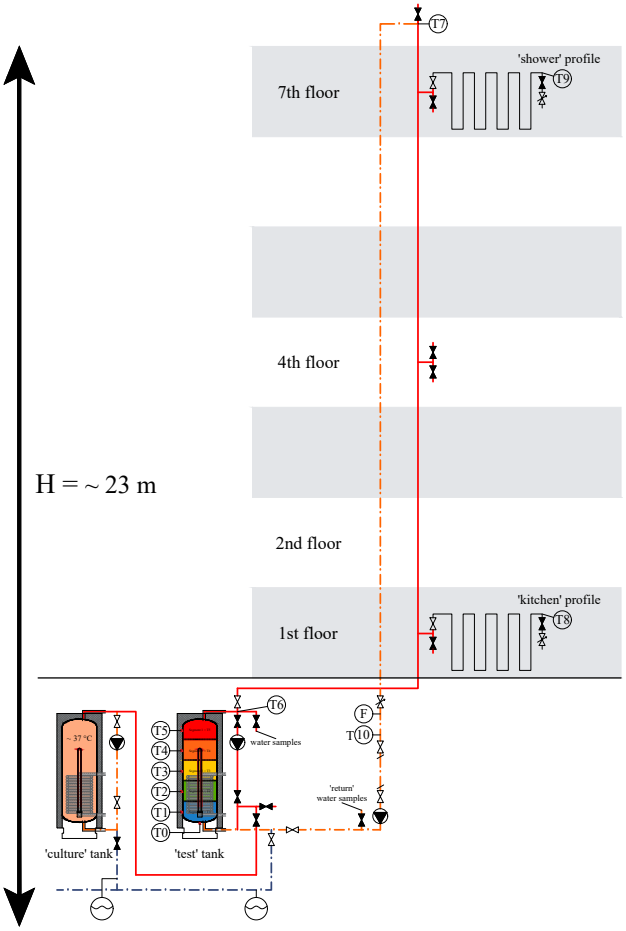

Figure 2 *- Hydraulic scheme of the Legionella test facility (at BBRI [4]).*

Secondly, the validated growth model is used to optimise existing DHW systems in residential buildings. Case study buildings are chosen with occurring *Legionella* issues.

The case study project consists of 4 apartment buildings (block I-IV) with 520 apartments (*Figure 3*) of which both hot and cold water are infected with *Legionella* (*e.g.*, measured DHW temperatures demonstrated in *Figure 4*). A system simulation model of these case-study buildings is developed in Modelica Dymola, based on previously executed water temperature, mass flow rate and *Legionella pneumophila* concentration measurements.

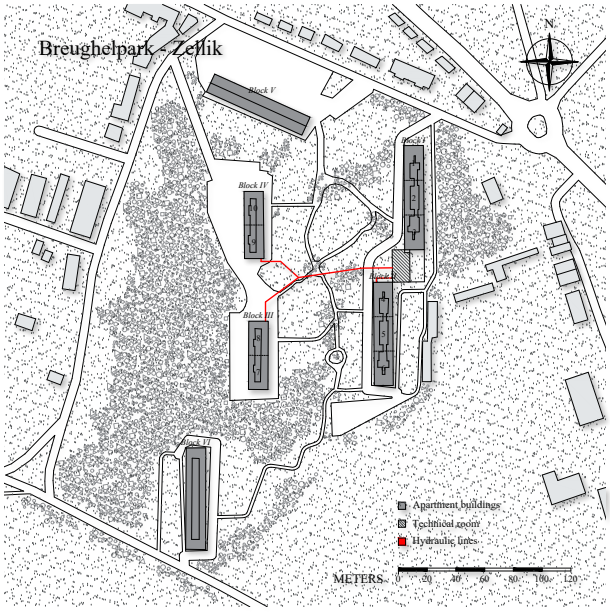

Figure 3 *- Site plan of the apartment blocks, which are located at Breughelpark. The DHW pipes in between the apartment buildings are illustrated by the red lines and verified with a thermography camera.*

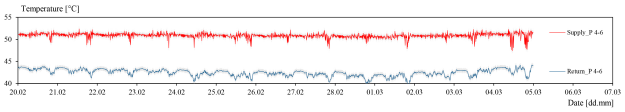

Figure 4 *- Supply and return water temperature to block II (pavilion 4-6). Return temperatures are below 45 °C so Legionella will occur in the system. The accuracy of the logger is 0.21 °C.*

Subsequently, the model is utilised to assess various optimisation measures during the operational stage. The causes of infection of the hot and cold water system and the most effective optimisation/renovation measures, to keep it healthy and energy efficient on the long term, are investigated by simulation. Ultimately, the best suitable measures to adapt the DHW installation are proposed by which energy-saving measures can be compared based on decreasing *Legionella* contamination risk and improving comfort.

RESULTS

For the BBRI test facility, RMSE-values between 0.51 and 2.15 K, MBE-values between -0.010 and 1.199% and CV(RMSE) between 0.158 and 0.734% are achieved for the validation of the thermohydraulic Modelica system simulation model. Furthermore for the *Legionella pneum*. growth model RMSE-values between 435 and 714 cfu/l, MBE-values between -0.000527 and -0.000561% and CV(RMSE) between 0.00069 and 0.00133% are achieved.

Verification of the obtained validation results with calibration acceptance criteria (*Table 1*) justifies that the simulation model can be considered calibrated.

Standard/ Guideline	Monthly criteria [%]		Hourly criteria [%]	
	MBE	CVRMSE	MBE	CVRMSE
ASHRAE [6]	5	15	10	30
IPMVP [7]	20	-	5	20
FEMP [8]	5	15	10	30

Table 1 *- Acceptance criteria for calibration of building energy performance simulation models (Coakley et al., 2014 [5]).*

Given that DHW installations are able to be accurately modelled in Modelica Dymola software as well as calibrated and validated both thermo-hydraulically (*i.e.*, water temperature and flow rate) and biologically (*i.e.*, concerning *Legionella pneumophila* growth), the DHW models can be utilised for existing buildings to determine appropriate renovation strategies.

Three main objectives are explored in the case-study by means of Modelica simulations:

1) Renovation measures to optimise water temperatures throughout the DHW system
2) Renovation measures to keep CW temperatures below 20 °C
3) Verifying if previous best-case renovation measures resolve occurring *Legionella* issues in both domestic water systems

Objective 1

Since only 35% of the 2.8 km of DHW pipes is well or sufficiently insulated, an energy-saving-potential and water temperature analysis by means of adding insulation to uninsulated areas is executed. The obtained results, demonstrated in *Figure 5*, represent the energy savings by decreasing thermal energy losses.

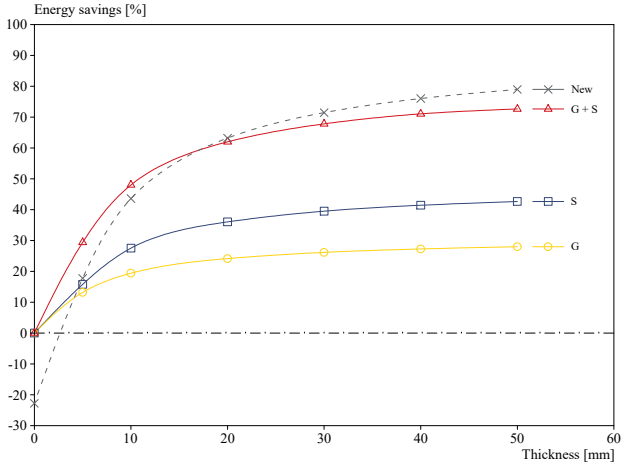

Figure 5 *- Energy savings by adding pipe insulation in the technical shafts (S) of block III/IV (pavilion 7-10), to the uninsulated pipes in the underground (G) or both renovation measures combined (G+S). The grey dotted line represents a scenario in which all existing insulation (35%) is removed and re-insulation is started from scratch (New). The thermal energy savings graph indicates that for 3 cm of pipe insulation, the greater part of potential thermal energy savings is obtained and 3 cm still is a feasible pipe insulation thickness.*

Subsequently, mass flow rates are examined and a system design analysis is executed, which takes the previous findings into account in order to obtain a well considered DHW system design. Simulation results are demonstrated in *Figure 6*.

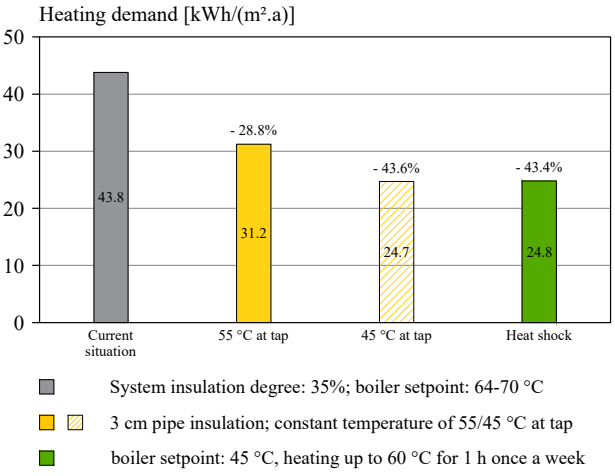

Figure 6 *- Comparison of simulated system optimisation scenarios. Coloured bars (i.e., yellow and green) take 3 cm of pipe insulation, new mass flow rate settings and other boiler recirculation settings into account. Three centimeters of pipe insulation and an improved system design (i.e., the conventional scenario, represented by the yellow bar) account for 28.8% energy savings in comparison to the current situation, higher distributed DHW temperatures and higher temperatures at tapping points. The heat shock regulation (i.e., green bar) accounts for another 20% of energy savings in comparison to the conventional scenario*

Objective 2

DHW and CW pipes are situated together in uninsulated and unventilated shafts (*i.e.*, one shaft supplying the kitchens and one shaft supplying the bathrooms), surrounded by the ambient conditions of two apartments on every floor. The aim of this research question is to make sure cold water temperatures never exceed 20 °C. An additional ventilation flow rate (to keep CW pipes below 20 °C) is utilised to compare the various simulation scenarios in order to find the most cost and energy efficient renovation measure(s) and thus an overall best optimisation scenario. In the new BBT [9] concerning *Legionella*, the BBRI states DHW and CW pipes need to be insulated and located in separate shafts.

Three scenarios were studied, compared and further developed (*Figure 7*).

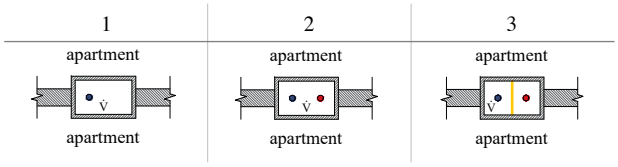

Figure 7 *- Three basic start scenarios, which are studied, compared and further analysed in a CW system optimisation analysis. CW and DHW pipes are displayed, respectively in blue and red. The yellow line represents 3 cm of insulation.*

A summary of the obtained results (in winter conditions) is demonstrated in *Figure 8* and *9*. In *Figure 9*, temperatures in a kitchen shaft at floor level 12 are illustrated since this is the worst-case scenario (*i.e.*, ambient shaft temperatures 'Sh_' and CW temperatures 'L12_') and compared to the tappings of the whole building block to clarify the temperature curves.

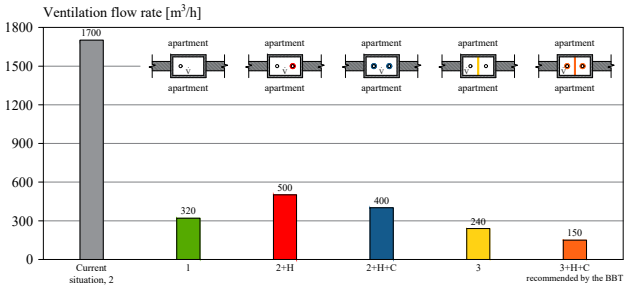

Figure 8 *- Comparison of six CW system scenarios. Scenario analyses demonstrate that the separation of DHW and CW pipes in individual shafts immediately epitomises an enormous optimisation potential since the greater part of transmission, convection and radiation by DHW pipes is blocked immediately. Additional CW pipe insulation (DHW pipe insulation is obligatory) lowers the water temperatures further (orange bar). The scenario recommended by the BBRI proofs to be a best-case scenario.*

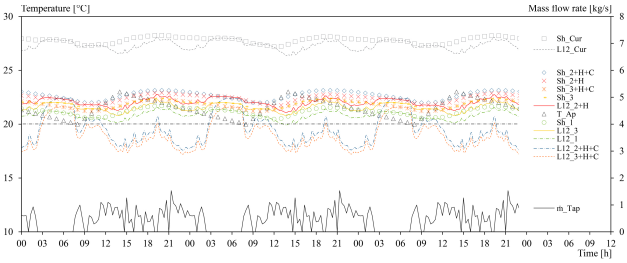

Figure 9 *- Corresponding worst-case cold water and kitchen shaft temperatures for the various scenarios in Figure 8. By adding CW pipe insulation, the water temperatures lower significantly during the greatest part of the day.*

Objective 3

The last research question aims to verify whether the previous proposed best-case optimisation measures also dissolve possible *Legionella pneum.* issues and keep concentrations under control. The risk concentration amounts to 1000 cfu/l. Results for the DHW system are demonstrated in *Figure 10* and *11*, results for the CW system are demonstrated in *Figure 12*. A dead end is inserted to both CW pipes (*i.e.*, kitchen and bathroom).

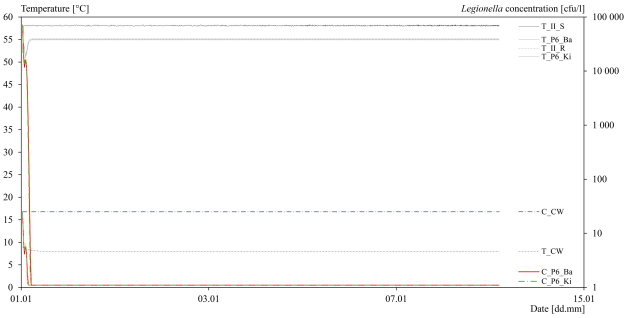

Figure 10 *- Conventional 55 °C regulation in the DHW system (i.e., the energy use is demonstrated in Figure 6 compared to other scenarios). Worst-case Legionella pneum. concentrations are demonstrated in colour (i.e., red and green) on the right ordinate. DHW temperatures are demonstrated in black and grey on the left ordinate. The 55 °C-at-tap regulation proofs to be sufficient to keep Legionella pneum. concentrations under control and for disinfection of the DHW system.*

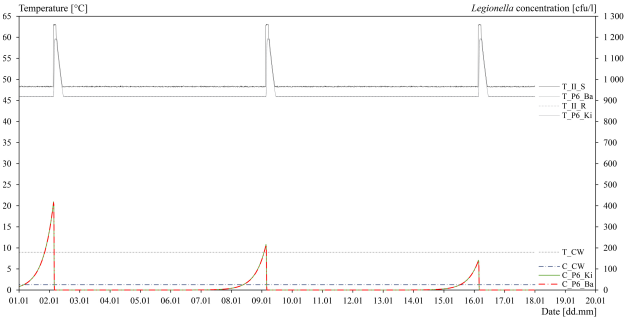

Figure 11 *- Heat shock regulation in the DHW system (i.e., the energy use is demonstrated in Figure 6 compared to other scenarios). Worst-case Legionella pneumophila concentrations are demonstrated in colour (i.e., red and green) on the right ordinate. DHW temperatures are demonstrated in black and grey on the left ordinate. Heat shocks once a week proof to be sufficient to keep Legionella concentrations under control.*

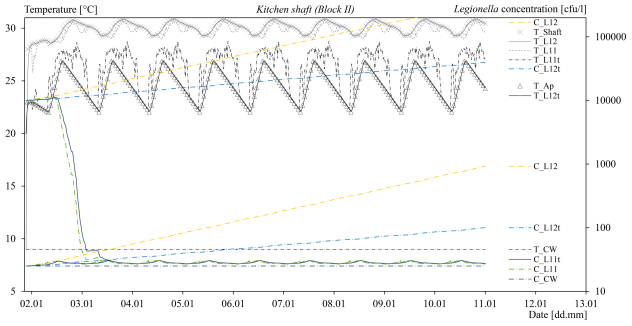

Figure 12 *- Domestic CW system in summer conditions for the kitchen shaft. Temperatures of the worst-case areas in the current system (i.e., floor level 12 in the shaft supplying the kitchens), are demonstrated with corresponding Legionella pneumophila concentrations (in colour, preceded by the character 'C'). DHW temperatures are demonstrated in black and grey on the left ordinate.*

Apparently in the current CW system, *Legionella pneumophila* is not able to grow up to critical concentrations in frequently used CW pipes (in a 9-day simulation). CW sample measurements confirm the low *Legionella* concentrations, but other *Legionella species* were measured, *Legionella pneum.* did not occur. At last, *Legionella pneum.* proliferation occurs in dead pipe ends, which can contaminate the system on the long term.

Discussion and conclusions

Simulation models of domestic water systems (*i.e.*, DHW and CW) can be developed and have the potential to be of great importance in the design, renovation and optimisation of (residential) buildings. Even storage tank stratification can be calibrated and validated, which is proved in a test facility analysis, both thermo-hydraulically and biologically.

For the BBRI test facility, RMSE-values between 0.51 and 2.15 K, MBE-values between -0.010 and 1.199% and CV(RMSE) between 0.158 and 0.734% are achieved for the validation of the thermohydraulic Modelica system simulation model. Furthermore for the *Legionella* growth model RMSE-values between 435 and 714 cfu/l, MBE-values between -0.000527 and -0.000561% and CV(RMSE) between 0.00069 and 0.00133% are achieved.

In case the Modelica software is applied to a *Legionella*-contaminated case study (Breughelpark) analysis, objective 1 demonstrated that energy savings can be obtained in the DHW system by adding 1-3 cm of pipe insulation. For the conventional 55 °C-at-tap regulation with 3 cm of pipe insulation and modified mass flow rates, 28.8% less energy use and much higher DHW temperatures (currently: 36.5-47.0 °C; new: 55 °C everywhere) at taps are obtained in comparison to the current situation. The heat shock regulation corresponded even to 43.4% less energy use and 45 °C at tapping points.

The cold water system analysis (*i.e.*, objective 2) demonstrated that separating DHW and CW pipes is of great importance in order to keep the CW below 20 °C (*Legionella* is in dormant stage below 20 °C). Just as the BBT states, CW insulation can be added, which will lower the CW temperature 3 to 4 °C during the greatest part of the day.

When these best-case optimisation measures are evaluated in terms of *Legionella pneum.* concentration, the DHW conventual 55 °C-at-tap regulation shows no alarming *Legionella pneum.* concentrations. The heat shock regulation also proofs to be suitable when one heat shock is executed every week. The CW system proofs to be safe in the current situation. Although in dead pipe ends, *Legionella pneum.* proliferation occurs, which can contaminate the system in time, but this is not perceived in a 9-day simulation.

In conclusion, the obtained results proof that the Modelica growth model can assist HVAC designers to quantify and decrease the *Legionella* infection risk in the design phase as well as to optimise existing DHW and CW systems. Furthermore, Modelica models are able to reduce the thermal energy use drastically by testing various scenarios (*e.g.*, up to 43.4% in the case study) in existing DHW systems.

FUTURE RESEARCH

By the end of this thesis, the simulation model, which represents the test facility, is considered calibrated and validated in terms of *Legionella pneum*. between the setpoint temperature of 45 °C and a heat shock temperature of 60 °C. Given the importance of the correctness of the model and the possible impact on human health, further model calibration for a broader temperature range can be undertaken in future research. Tests with heat shocks of 65 °C are currently running and in the near future, tests with a setpoint of 40 and 50 °C are planned.

Secondly, model simulation time (CPU time for integration) is an issue, mainly in models with *Legionella* equations (*e.g.*, one single *Legionella* simulation of 17 days (*Figure 11*) was executed, which generated 21 GB of data in a 28 hour simulation and nearly made a powerful computer crash). 9-day simulations proved to be more feasible (*i.e.*, 10-12 hour simulations) in terms of simulation time. However for *Legionella* risk analyses, longer simulation periods are necessary. Therefore, Modelica Dymola model optimisations have to be further examined in order to speed up simulations without sacrificing on accuracy and precision.

Furthermore, the *Legionella pneum*. growth model can still be refined. *Legionella pneum*. is a hardly understandable bacteria, with sometimes unexpected growth results (as confirmed by test rig measurements). By further calibration and validation with other casestudies and water temperatures, the growth will become more understandable and controllable. Also additional *Legionella species* and subgroups can be added to the simulation model with different growth curves to verify more than one *Legionella specie* in the DHW and CW system. Future research is currently ongoing.

At last, one of the main reasons, which is thwarting the model development, is that *Legionella* cannot be monitored continuously. *Legionella* samples have to be taken manually, sent to an accredited laboratory and then it takes another week to obtain the *Legionella* results. Furthermore, it is technically impossible to examine tapping samples of one full day (e.g., every hour) for various locations, simply because this requires too much manual labor. Therefore, the limited amount of *Legionella* measurements makes model development much more difficult.

REFERENCES

[1] Stout J. E., Best M. G., Yu V. L., "Susceptibility of members of the family *Legionellae* to thermal stress: implication for heat eradication methods in water distribution systems", *ASHRAE Journal,* 1986, 46, 52-54.

[2] Rogatty W., "Heizen und Kühlen in Niedrigenergie- und Passichäusern", *IKZ-HAUSTECHNIK*, 2003, 8, 38-42.

[3] Van Kenhove E., Van Hove M., De Backer L., Dinne K., Bleys B., Gerin O., Janssens A., Laverge J., "Model calibration for *Legionella* in domestic hot water system simulation", *Applied Energy*, 2018, in review.

[4] Dinne K., Gerin O., Bleys B., De Cuyper K., "Evaluation of the risk of *Legionella spp*. development in sanitary installations", CIBW062 Symposium 2017.

[5] Coakley D., Raftery P., Keane M., "A review of methods to match building energy simulation models to measured data.", *Renewable and Sustainable Energy Reviews,* 2014, 37, 123-141.

[6] ASHRAE, ASHRAE Guideline 14: Measurement of energy and demand savings, *American Society of Heating, Refrigerating and Air-Conditioning Engineers*, Atlanta, 2002, 165.

[7] EVO, "International performance measurement & verification protocol", *Efficiency Valuation Organisation*, 2007.

[8] US DOE, M&V guidelines: measurement and verification for federal energy projects, *US Department Of Energy*, 2008, 3.0.

[9] Van den Abeele L., Dinne K., De Cuyper K., Bleys B., "*Best Beschikbare Technieken (BBT) voor Legionella-beheersing in Nieuwe Sanitaire Systemen*", WTCB & VITO, 2017.

REHVA
Federation of European Heating, Ventilation and Air Conditioning Associations

Recovery of waste heat from the sewer system in the sanitary equipment

Dominika Juhošová (d.juhosova@gmail.com)
Supervisor: doc. Ing. Jana Peráčková, PhD. (jana.perackova@stuba.sk)
Department of Building Services, Faculty of Civil Engineering, Slovak University of Technology in Bratislava, Slovakia
2018

***Abstract*—This master thesis is dedicated to the recovery of waste heat from the sewer system. Its first part investigates the possibilities of recovery of waste heat from the sewer system as an alternative solution of minimalism of the energy demand of the system of preparation domestic hot water. The second part concerns the design of alternative solutions of the recovery of waste heat from the sewer system in the sanitary equipment of the object of a sports facility which include complete project documentation of the sport complex with application of heat exchangers to direct preheating of cold water. The last part is dedicated to the experimental observation of the waste heat recovery system in order to review its energy and economic efficiency as well as payback period.**

The goal of my thesis is to introduce the possibilities of the recovery of waste heat from sewer systems, apply them in the design of multifunction sport complex and review the economic and energy efficiency under laboratory conditions.

***Index Terms* – Heat exchanger; Recovery of waste heat, Sanitary equipment; Sewer system**

Introduction

Nowadays, more and more energy is consumed in dwelling houses where energy is used for preparing hot water, heating, cooling of the building and thus became very valuable. The energy consumption for heating and cooling purposes decreases thanks to the thermal insulation of the building constructions and replacement of old windows for new plastic windows with triple glazing while the energy consumption for preparing hot water is constantly increasing. How can we reduce the energy needed to heat the potable water? One option is recuperating. We are able to recover waste heat from the sewer system to preheat domestic hot water using heat exchangers.

I. THE RECOVERY OF WASTE HEAT FROM THE SEWER SYSTEM INSIDE OF BUILDINGS PRINCIPLE

Buildings with a constant flow rate of waste water and significant amount of it being drained away are suitable for heat recovery directly inside them. In this case, it is very convenient to use the heat from the sewage for preheating hot water for immediate consumption. The system of the recovery of waste heat from the sewer system inside of buildings is based on heat exchangers, which serve to exchange the heat energy between the waste water and the cold water. There is no contact between the potable water supply and the drain water [1].

Fig. 1 shows the fundamental principle of the system of recovery of waste heat from the sewage inside of the building to direct domestic hot water preheating. Waste water from the shower with a temperature of 38 °C is drained into the sewerage through the heat exchanger. The cold water with the initial temperature of 10 °C flows through the heat exchanger, in the opposite flow direction of the drainage water, and is transported into the thermostatic shower mixture tap via this heat exchanger.

Waste water transfers the heat through the heat exchanger into the cold water in order to preheat it – cold water can reach a temperature of approximately 20 °C. The preheated water is supplied into the thermostatic shower mixer tap. Adding the preheated water into the thermostatic shower mixer instead of cold water, a smaller portion of hot water is mixed with a larger portion of preheated cold water thus reducing the hot water flow. This serves to reduce the hot water consumption and the energy needed for water heating [1].

The recovery of waste heat to direct preheat of hot water is recommended for sanitary appliances where the need for hot water exceeds the need for cold water – the best example are showers and wash basins. In case of bath tubs, this principle does not work because the hot water is swallowed at another time as it flows.

This type of recuperation is not suitable for kitchen sink since the wastewater contains oils which can settle on the wall of the heat exchanger and thus reduce its effectiveness.

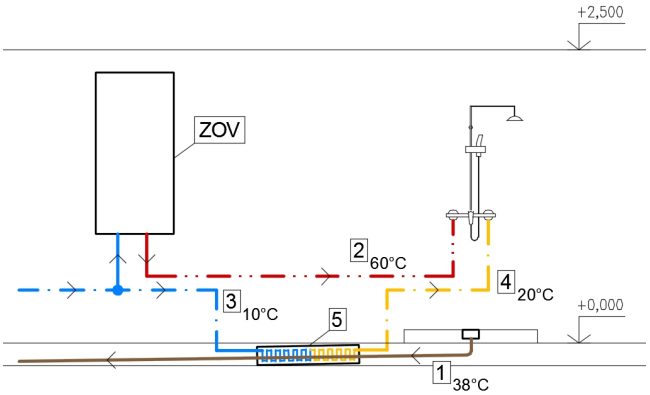

Figure 1. Example of a system of recovery of waste heat using a heat exchanger to direct preheating of hot water for shower

1 – waste water drained from the shower (38 °C), 2 – hot water supply from the storage water heater (60 °C), 3 – cold water supply to the heat exchanger (10 °C), 4 – preheated cold water supply to the shower thermostatic mixer tap (20 °C), 5 – heat exchanger, ZOV – storage water heater

II. METHODS OF INSTALLATION OF HEAT EXCHANGERS

Heat exchangers could be installed in several ways depending on the type of building, the water requirement in the building or the bathroom disposition. The heat exchanger should always be installed as close to the sanitary appliance as possible.

Installation of heat exchangers methods [2]:

- direct connection of the heat exchanger to one sanitary appliance (shower)
- direct connection of the heat exchanger to several sanitary appliances (shower and wash basins)
- combined connection of the heat exchanger with a storage water heater
- parallel connection of the heat exchanger to several sanitary appliances (several showers)

a) direct connection of the heat exchanger to one sanitary appliance (shower):

Principle: The wastewater from the shower flows through the heat exchanger into the sewerage. The cold water flows in the opposite direction of the sewage water and is supplied into the shower mixer tap as the preheated water in order to reduce the hot water flow (Fig. 2).

Application: The connection could be comfortably used for showers in flats, family houses, sanitary equipment of sport facilities, swimming pools, or showers in industrial halls.

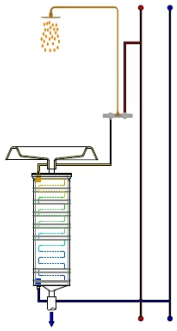

Figure 2. Direct connection of the heat exchanger to one shower [2]

b) direct connection of the heat exchanger to several sanitary appliances (shower and wash basins)

Principle: The wastewater drained from the shower and washbasins flows through one common heat exchanger into the sewerage. The preheated water is supplied into the thermostatic mixer tap of the shower and also into the mixer taps of wash basins (Fig. 3).

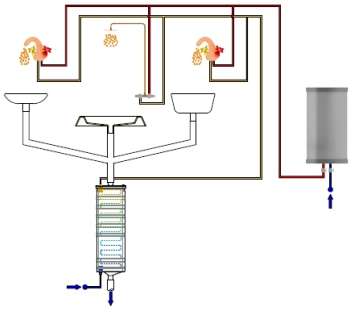

Figure 3. Direct connection of the heat exchanger to one shower and two wash basins [2]

Application: This connection could be used in dwelling houses or apartment flats to direct preheating of the domestic cold water for a sanitary equipment in the bathroom (e.g. a shower and washbasin).

Even though this system installation is one of the useful alternatives, for washbasins preheat water to a temperature above 20 °C I do not recommend from the point of view of hygiene of potable water. Another fact which is necessary take into consideration is that the washing times are too low for this system to be effective.

c) combined connection of the heat exchanger with a storage water heater:

Principle: The preheated cold water is not only supplied into the thermostatic mixture tap, but it is also transported into the storage water heater which serves to save energy needed for hot water preparation (Fig. 4).

Application: This connection could be used in every operation of sanitary equipment where the hot water is prepared locally using a storage water heater. This type of installation is the most effective one in terms of energy savings.

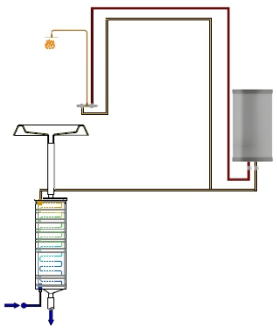

Figure 4. Combined connection of the heat exchanger with a storage water heater [2]

d) parallel connection of the heat exchanger to several sanitary appliances (several showers):

Principle: Sewage from many showers flows into the sewerage through one common sewer pipe into many heat exchangers. With this type of installation, as many heat exchangers are installed as many sanitary appliances there are - heat transfer is more efficient because heat exchangers are able to recover more heat from the sewage water (Fig. 5).

Application: This connection is used in mass showers in objects such as swimming pools, sports facilities, industrial facilities, etc.

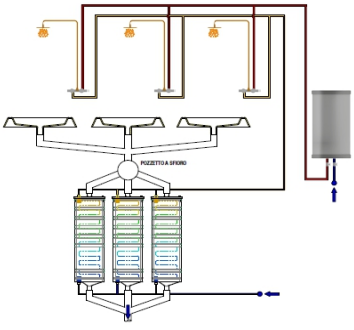

Figure 5. Parallel connection of the heat exchanger to three showers [2]

III. TYPES OF HEAT EXCHANGERS FOR RECUPERATION OF WASTE HEAT FROM THE INTERNAL SEWERAGE SYSTEM

Several types of heat exchangers for recuperation from the internal sewerage systems exist. The rest of this paper aims to introduce alternative solutions of the recovery of waste heat from the sewer system using various types of heat exchangers which were, for the purpose of this thesis, applied in the object of a sports facility.

A. Shower tray with integrated heat exchanger

The recuperation system consists of a special shower tray with the heat exchanger integrated underneath the shower tray (Fig. 6).

Application: If in the object is a shower designed with a shower trays, the first option is recuperation using this special shower tray with an integrated circular heat exchanger in the form of spiral of copper pipes (Fig. 6). The heat exchanger is placed under the shower tray, but the normal height of shower tray is maintained. Combining the heat exchanger with copper or multilayer water pipes is recommended. The energy efficiency depends on the hot water flow, and is around 41% [3].

Figure 6. Shower tray with integrated heat exchanger – cross section and view [3]

Principle: Fig. 7 shows a floor plan of the sanitary equipment in a sports facility where the heat recovery is solved using a shower tray with an integrated circular heat exchanger through which the wastewater flows. The cold water (10 °C) is supplied into the shower tray from the bottom of the heat exchanger. The preheated cold water (20 °C) is transported from the shower tray directly into the thermostatic shower mixer through the heat exchanger.

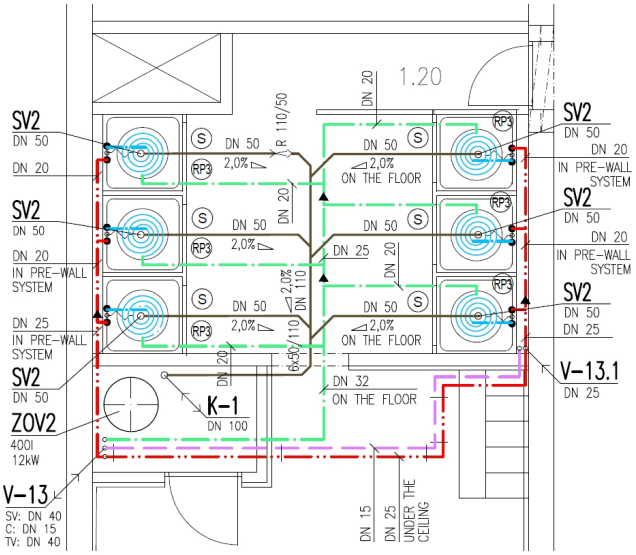

Figure 7. Floor plan with an alternative solution for recovery of waste heat using a shower tray with integrated heat exchanger

V – rising pipe of cold water, hot water and circulation of hot water, K – foul water stack, ZOV – water heater, SV2 – squared shower tray with drain in the middle, RP3 – shower tray with integrated heat exchanger, S – wall-mounted thermostatic shower mixer

B. Heat exchanger in the form of regenerative panel placed under the shower tray

The recuperation system consists of regenerative panel (Fig. 8) designed to recover energy from shower's waste water.

Application: If in the object is a shower designed with a shower tray, the second option is using this regenerative panels. The regenerative panel has a plastic casing and the heat exchanger is made of a copper in the form of a spiral (Fig. 8). The efficiency of these heat exchangers is approximately 30% [4].

Figure 8. Heat exchanger in the form of regenerative panel placed under the shower tray – cross section and view [4]

Principle: Fig. 9 shows the sanitary equipment floor plan where the heat recovery is solved using a regenerative panel placed under the shower tray. The wastewater (38 °C) is drained through the regenerative panel placed under the shower tray on the floor. The cold water with the initial temperature of 10 °C is supplied into the thermostatic shower mixer through the heat exchanger. The heat extracted from the wastewater is supplied into the cold water in order to preheat it, the temperature of preheated water is approximately 20 °C.

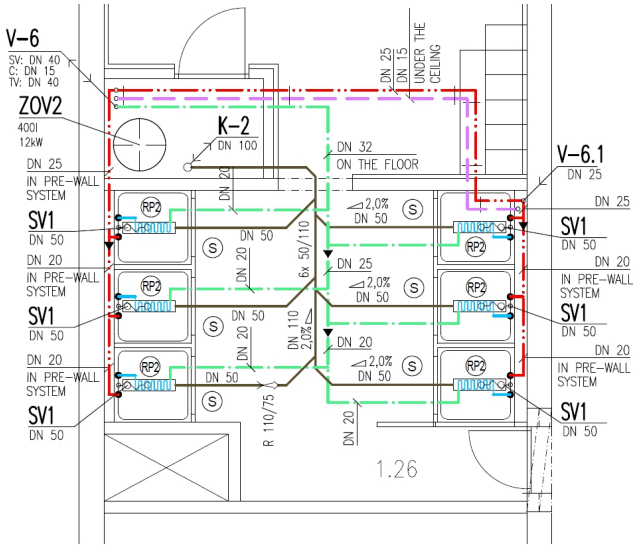

Figure 9. Floor plan with an alternative solution for recovery of waste heat using a heat exchanger placed under the shower tray

V – rising pipe of cold water, hot water and circulation of hot water, K – foul water stack, ZOV – water heater, SV1 – squared shower tray with drain up, in the middle, RP2 – heat exchanger-regenerative panel placed under the shower tray, S – thermostatic shower mixture tap

- cold water (10 °C)
- preheated cold water (20 °C)
- hot water (60 °C)
- waste water (38 °C)
- circulation of hot water (55 °C)

C. Heat exchanger in combination with a floor drain shower system

The recuperation system consists of a heat exchanger designed in combination with a floor drain shower system (Fig. 10).

Application: This alternative is suitable for every sanitary equipment with showers, where a shower with a floor drain system is designed (Fig. 10). This device offers a compact and efficient solution for heat recovery from wastewater inside of a building. Waste water passes through the heat exchanger which is a double walled stainless steel heat exchanger in the form of a spiral. The energy efficiency depends on the water flow - at the flow of a 9 l/min the efficiency is 38,9 % and at the flow of a 11 l/min the efficiency is 38,6% [5].

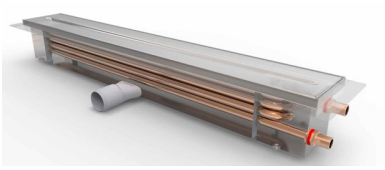

Figure 10. Heat exchanger in combination with a shower with floor drain system [5]

Principle: Fig. 11 shows a floor plan of the sanitary equipment in a sports facility with showers with a floor drain system where the recuperation is provided by a compact heat exchanger. The sewage water from the shower (38 °C) flows into the sewerage through a heat exchanger by a connecting pipe in the floor. The cold water (10 °C) is preheated (20 °C) and supplied into the thermostatic shower mixer.

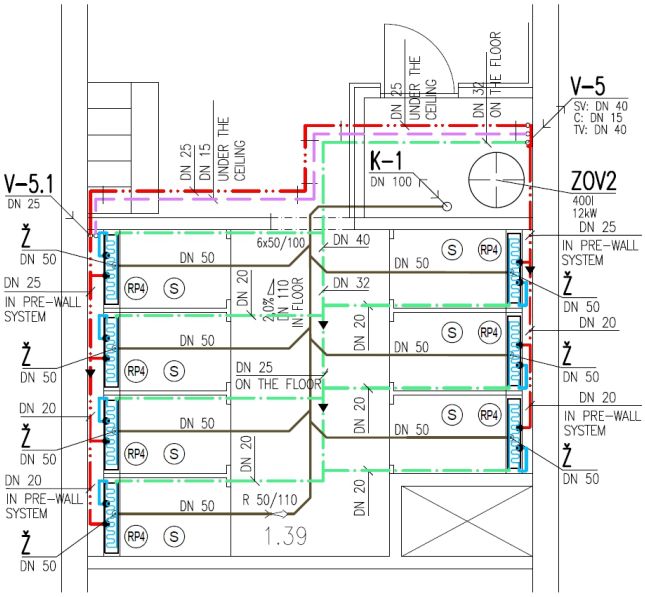

Figure 11. Floor plan with solution for recovery of waste heat using a heat exchanger in combination with a shower with floor drain system

V – rising pipe of cold water, hot water and circulation of hot water, K – foul water stack, ZOV – water heater, Ž – shower with a floor drain system, RP4 – heat exchanger in a combination with floor drain system, S – thermostatic shower mixture tap

- cold water (10 °C)
- preheated cold water (20 °C)
- hot water (60 °C)
- waste water (38 °C)
- circulation of hot water (55 °C)

D. Regenerative panels with stainless steel heat exchanger

The recuperation system consists of a heat exchanger in the form of regenerative panel.

Application: This alternative could be used in sanitary equipment where showers without shower trays are designed. This panel consists of a plastic waterproof case and a stainless steel heat exchanger (Fig. 12). The heat exchanger is placed on the floor, as close to sanitary equipment as possible. The regenerative panel is available in two versions –630 mm long version and 1320 mm long version. The efficiency of these heat exchangers is approximately 30% [2].

Figure 12. Regenerative panel with stainless steel heat exchanger [2]

Principle: The waste water from the shower (38 °C) flows through the heat exchanger placed in the thermal insulation layer of the floor. The cold water is supplied into the thermostatic shower mixer tap through the heat exchanger and heat from wastewater is extracted and transferred into the cold water (10 °C) in order to preheat it (20 °C)*. I suggest using a 613 mm long recuperation panel for one shower and one longer recuperation panel with a 1319 mm length for recuperation of sewage water from two showers.

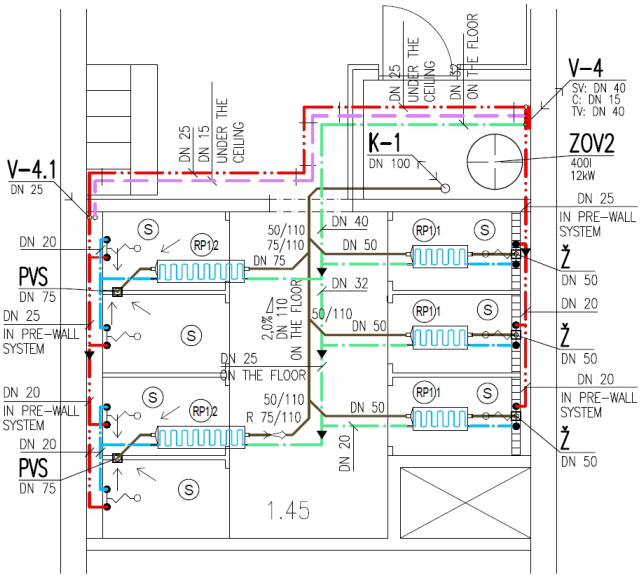

Figure 13. Floor plan with an alternative solution for recovery of waste heat using a regenerative panel with stainless steel heat exchanger

V – rising pipe of cold water, hot water and circulation of hot water, K – foul water stack, ZOV – water heater, PVS – shower floor drain, RP1 –regenerative panel with stainless steel heat exchanger: RP1.1 – length of the panel 613 mm, RP1.2 – length of the panel 1319 mm

- cold water (10 °C)
- preheated cold water (20 °C)*
- hot water (60 °C)
- waste water (38 °C)
- circulation of hot water (55 °C)

*Temperature 20°C of preheated water was experimentally observed

Fig. 15 shows a floor plan with an alternative solution of heat recovery by using heat exchangers with their parallel installation. For three showers I suggest the parallel connection of three heat exchangers through which the water will be preheated for three shower thermostatic mixer taps. In this alternative solution I also suggest supplying the preheated water (20 °C) into the storage water heater.

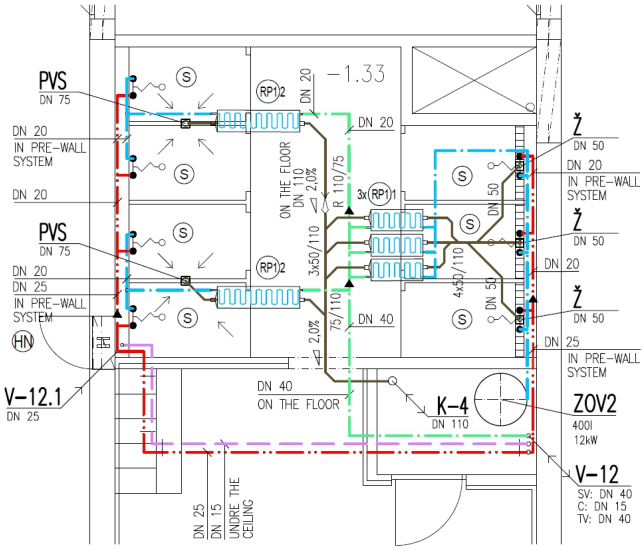

Figure 14. Floor plan with an alternative solution for recovery of waste heat using a parallel installation of heat exchangers

V – rising pipe of cold water, hot water and circulation of hot water, K – foul water stack, ZOV – water heater, PVS – shower floor drain, RP1 –regenerative panel with stainless steel heat exchanger placed in the floor: RP1.1 – length of panel 613 mm, RP1.2 – length of panel 1319 mm

- cold water (10 °C)
- preheated cold water (20 °C)
- hot water (60 °C)
- waste water (38 °C)
- circulation of hot water (55 °C)

IV. EVALUATION OF THE SYSTEM OF RECOVERY OF WASTE HEAT FROM THE ENERGETIC AND ECONOMIC ASPECT

The last part of the thesis is dedicated to the experimental observation of the system of recovery of waste heat from the sewer system inside of the building. This system's energy evaluation is based on the experimental observation results carried out in the Department of Building Services' laboratory at the Faculty of Civil Engineering. The purpose of the experimental observation was to calculate the energy savings and payback period of the heat exchanger.

A. Methodology

The regenerative panel with stainless steel heat exchanger was used in this observation (Fig. 12).

Technical equipment installed in the laboratory was as follows:

- In the laboratory, there was only potable cold water supply installed. It was necessary to provide water heater for the experimental observation - electric water heater with a capacity of 100 liters was installed.
- As the pressure conditions in the system of water supply were insufficient (the laboratory is located on the 23rd floor), it was necessary to increase the pressure using water pressurization system – compact electronically controlled home waterworks was installed in order to provide the required pressure conditions.

The temperature of hot water, temperature of cold water, temperature of mixed water, temperature of waste water, temperature of preheated cold water, flow of hot water and flow of mixed water were the measured values.

The experimental model was based on a direct connection of the regenerative panel to one shower. The experimental model was installed so that the shower could be started with recovery of waste heat and without recovery in order to compare measured values of both cases. Bypasses with shut-off valves allowing the measurements for both recovery and non-recovery system were installed on the cold water route (Fig. 15).

The hot water consumption was measured during a shower with recovery of waste heat and without a heat recovery, values were compared, and the evaluation of system of recovery of waste heat was made.

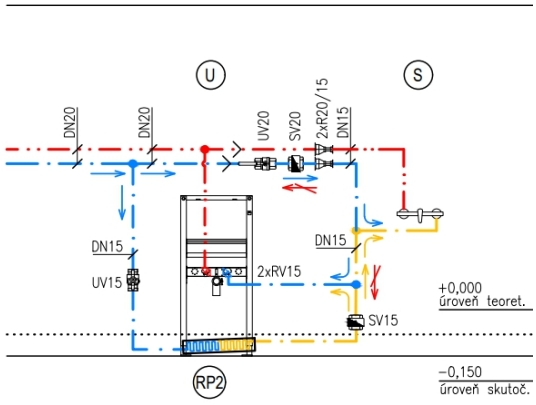

Figure 15. Detail of connection of heat exchanger with bypass of cold water

S – wall-mounted thermostatic shower mixer, U – wall-mounted thermostatic washbasin mixer, RP2 – heat exchanger in the form of regenerative panel of 613 mm length placed in the floor of laboratory, UV – shut-off valve, SV – backflow prevent

- cold water (10 °C)
- preheated cold water (20 °C)*
- hot water (50 °C)

*Temperature 20°C of preheated water was experimentally observed.

The object of a sports facility was chosen for the purpose of the evaluation of system of recovery of waste heat. The input data for evaluation were as follows:

- the object of sport facility's operating hours: 12 hours per day, 350 days a year
- one shower per hour is considered
- one shower's duration: 5 minutes
- totally there are 4,200 showers per year on one shower with one heat exchanger

Shower without recovery of waste water:

- hot water flow: 5.71 l/min
- hot water consumed per 5-minute shower: 28.55 liters

Shower with recovery of waste water:

- hot water flow: 4,407 l/min
- hot water consumed per 5-minute shower: 23.70 liters

The total hot water savings were approximately 5 liters per one shower.

B. Results

It was possible to calculate the cost of shower with and without recuperation using the data obtained in experimental measurement - preparation of hot water using electrical water heater and gas water heater was considered. First, the power consumption was calculated – energy needed for heating cold water multiplied by the price of every type of energy (electricity and gas) equals the price of one shower. I consider totally 4,200 showers per year on one shower with one heat exchanger – prices for one year showering with and without recuperation was determined. When comparing the prices for showering with and without recuperation, the annual savings for each type of energy can be calculated (Fig. 16):

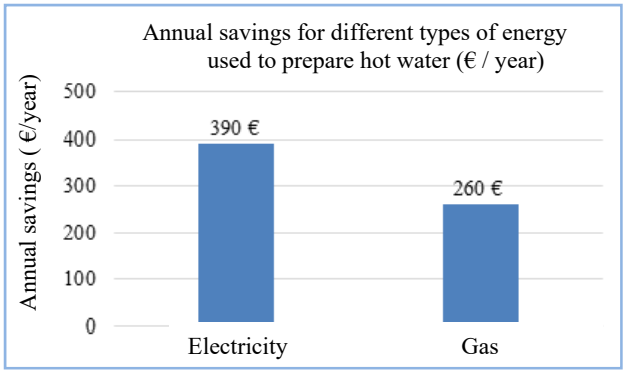

Figure 16. Annual savings for each type of energy used to prepare hot water

The payback period of the installed regenerative panel with stainless steel heat exchanger to one shower is 1.5 years when electricity is used for preparation of hot water and, using gas, the payback period is 2 years and 4 months.

V. DISCUSSION

Heat recovery from sewerage systems could be applied in dwelling houses and apartment flats, sports facilities, swimming pools or factories and the advantage of these systems is their simplicity and price – the payback periods are very favorable.

The aim of this master thesis was to introduce different possibilities of using heat from internal sewerage systems and react to the question of reducing the need for energy used for preparing hot water.

VI. CONCLUSION

I presented various ways and alternative solutions by using recuperation in my thesis. There are many options of recovery of waste heat from sewerage systems and these systems can also be applied in our conditions. Sewage water discharged from dwelling houses, residential, administrative, sport or other buildings is full of unused energy and presents a low-potential source of energy which can be used to prepare hot water.

ACKNOWLEDGEMENT

This work was supported by the Slovak Research and Development Agency and the Ministry of Education, Science, Research and Sport of the Slovak Republic through the grant VEGA 1/0807/17 and VEGA 1/0847/18.

REFERENCES

[1] J. Peráčková and V. Podobeková, "Utilization of heat from sewage", In Budownictwo o zoptymalizowanym potencjale energetycznym, 2013, pp. 79 - 86., ISSN 2299-8535

[2] Innova renewing energies. Bee the heat recovery system for hydro-sanitary systems. Available from: https://www.innovaenergie.com(online)

[3] HEI-TECH, Shower trays - The Recoh tray heat exchanger, Available from: https://www.specifiedby.com/hei-tech/the-recoh-tray (online)

[4] ZYPHO Drain water heat recovery system, Available from: https://www.zypho.eu/products/zypho-standard (online)

[5] RECOUP, Recoup drain+, Drain+Compact Heat Exchanger, Available from: https://recoupwwhrs.co.uk/products (online)

[6] Kasag Langnau AG, Heat exchangers for recovery of waste heat from sewer systems, Available from https://www.kasag.com (online)

[7] Rabtherm energy systems, Heat exchangers for recovery of waste heat form sewers, Available from: http://www.rabtherm.com (online)

[8] SHENOY V.U.: Heat exchanger network synthesis. Proces optimization by energy and resource analysis. Houston: Gulf Publishing Company, 1995. ISBN 0-88145-319-6.

[9] Buri, R., Kobel, B.:"Leitfaden für Ingenieure und Planer," Institut Energie in Infrastrukturan lagen Zürich, ECO.S Energie consulting Stodmeister, Berlin (2005)

[10] J. Peráčková and V. Podobeková, "Jak využít teplo z kanalizace na přípravu teplévody v budovách?," In TZB-info.cz, 2014, ISSN 1801-4399, Vol 16, pp.35-38.

[11] SHENOY V.U.: Heat exchanger network synthesis. Process optimization by energy and resource analysis. Houston: Gulf Publishing Company, 1995. ISBN 0-88145-319-6.

[12] BUZÁS V., PERÁČKOVÁ J.: Sizing and maintaining of wastewater heat exchangers. In: Magyar Épületgépészet. - ISSN 1215-9913. Vol. 64, (2015), pp. 18-21.

REHVA
Federation of European Heating, Ventilation and Air Conditioning Associations

Demand response of space heating using model predictive control in an office building

Aleksi Mäki[1, 2], Juha Jokisalo[1], Risto Kosonen[1]
[1]Aalto University, Sähkömiehentie 4, 02150 Espoo, Finland, firstname.lastname@aalto.fi
[2]Granlund Consulting Oy, Malminkaari 21, 00700 Helsinki, Finland, aleksi.maki@granlund.fi
The master's thesis upon which this article is based was accepted at Aalto University in December 2018

***Abstract*—This work was set to investigate the potential of demand response of space heating in the perspective of thermal comfort, energy flexibility and energy cost savings in an educational office building. A model predictive control (MPC) algorithm was developed to control the space heating temperature setpoints. MPC algorithm used multi-objective optimization to find the optimal control outputs (temperature setpoints) in respect of optimization objectives (thermal comfort, energy flexibility and energy cost). In addition, the draught risk in workstations adjacent to windows during the demand response implementation was studied by performing thermal manikin measurements. The measurement findings were added as constraint to the MPC algorithm. The developed MPC algorithm was tested with case simulations in IDA ICE simulation program (v. 4.8). The simulations showed that the space heating energy cost could be decreased up to 5% in the studied building while maintaining acceptable thermal comfort. The draught risk restriction in the MPC algorithm had minor effect on the energy cost savings.**

***Index Terms*—Demand response, model predictive control, multi-objective building optimization, thermal manikin**

Introduction

Building sector has an important role in the mitigation of the global warming. Globally the building sector consumes over 30% of the total final energy consumption and it produces nearly 30% of the global CO_2 emissions [1]. In EU, the corresponding metrics are 40% and 35%, respectively [2]. Demand response offers one possibility to decrease the CO_2 emissions of the energy production by allowing increasing use of intermitted renewable energy sources (RES) and by decreasing usage of emission intensive peak power plants.

The demand response (DR) can be defined as set of methods which try to optimize the energy system by continually controlling the time and magnitude of the energy consumption at the customer level. The demand response control may be based on for example the hourly energy prizes. In demand response, the buildings energy demand may be shifted to cheaper time periods, the expensive peak demand may be cut, or the demand may be increased during the off-peak periods when the energy is cheaper. These DR actions help to stabilize the energy production and consumption and as a result more intermitted RES can be brought to the energy system. Furthermore, while the peak demand in the energy system is decreased, there's less need to invest and run emission intensive peak power plants such as oil boilers and gas/diesel turbines.

The focus in demand response studies has mainly been in the economic and environmental aspects, while the thermal comfort issues has had only minor role. Since the thermal comfort affects the health and productivity of the occupants [3,4], it should be considered more thoroughly also in demand response studies. Secondly the demand response of electrical loads has been widely investigated while there exist only few studies on demand response of district heating. Thus, this study is focused in the demand response of district heating and the thermal comfort is adhered extensively.

The objectives of this study were twofold. The first objective was to study the local thermal comfort in workstations during the demand response and state a constraint for DR control in order to diminish the draught risk in workstations adjacent to windows. The second objective was to determine the potential of demand response of space heating in a Finnish office building in respect of thermal comfort, energy flexibility and energy cost savings.

I. Methods

A. Case building

The demand response study was conducted in an office building constructed in 1960s locating in the Aalto University campus area in Espoo, Finland. This building was chosen because it resembles typical office building in Finland of that era in respect of structures and HVAC technology. This study was restricted to the 4th floor of the case building which has heated net floor area of 586 m^2. Layout of this floor is shown in Fig. 1.

The envelope and the load bearing structures of the case building were built of reinforced concrete which resulted in relatively high thermal mass. The moderate insulation level and high thermal mass offered great possibilities for DR implementation [5]. The building envelope properties and the average ventilation air flow rate are shown in Table 1. Base floor properties are not shown because only the 4th floor was studied.

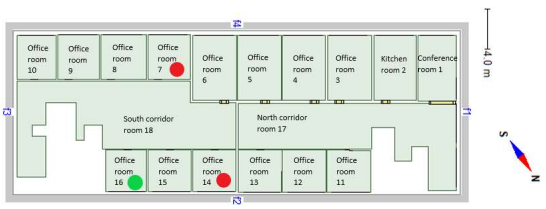

Figure 1. Layout of the studied floor. The RC-modelled rooms are shown with the red dots and the thermal comfort measurement room with the green dot.

This article is sponsored by Granlund Consulting Oy and the original master's thesis was sponsored by Business Finland

TABLE I.
BUILDING ENVELOPE AND VENTILATION PROPERTIES

Structures	U-value ($W/m^2,K$)	g-value
External wall	0.38	
Roof	0.3	
Window, South-West	1.1	0.38
Window, North-West and North-East	1.1	0.59
Window frames, All	2.0	
Air tightness	ACH	
4th floor	1.6	
Ventilation	q_v ($l/s,m^2$)	Schedule
4th floor average	2	24/7

All the heating networks in the case building were heated by the local district heating network. The space heating in the studied office floor was supplied by the hydronic water radiators. The internal gains and the schedules used in the study are shown in Table 2. The maximum occupancy rate was evaluated based on the number of work stations in each office room. The occupancy rate of 40% was assumed in this study. The equipment and lighting heat gains were checked from the product data.

TABLE II.
INTERNAL HEAT GAINS AND SCHEDULES

Internal heat gain	Value	Schedule hours
Lighting	7.5 W/m^2	08 - 16
Equipment	50 W/occupant	08 - 16
Occupancy	40%	
Total number of occupants	16	08 - 16

B. The local thermal comfort measurements

Thermal comfort as a concept can be divided into overall thermal comfort and local thermal comfort. More often, only the overall thermal comfort describing the overall thermal sensation has been considered in the DR studies. The overall thermal sensation is neutral when the heat balance between the human body and the environment is reached without overexcitation of the human thermoregulatory system. The local thermal comfort describes the body thermal sensation in individual body parts. The common phenomenon that causes local thermal discomfort includes draught, asymmetric radiation, cold/hot floors and high vertical temperature differences. The satisfying thermal comfort requires that both overall and local thermal comfort are at acceptable level [6].

Draught is caused by unwanted cooling of one or several body parts due to natural or mechanical airflows. In this study draught risk was evaluated in one office room of the case building by using thermal manikin. The hypothesis was that during the demand response when the heating power is conserved, the convective air flows might develop from the cold window surface and be sensed as draught by the occupant. To investigate this phenomenon the equivalent body temperatures in different body segments were measured at varying radiator thermostat setpoints and different window surface temperatures. Additionally, thermal environment measurements were performed to collect information of room air temperature, air humidity, window and radiator surface temperatures.

The local thermal comfort measurements were performed in one office room of the case floor (shown in Fig. 1). The room had dimensions of 4.2 m (W) x 4.3 m (L) x 2.45 m (H). There were two large windows (1.8 m (W) x 1.55 m (H) and 1.9 m (W) x 1.55 m (H) under which there were two water radiators. The measurement setup is shown in Fig. 2. The thermal manikin was installed in sitting posture in front of the office table.

The office room had constant air volume (CAV) ventilation system and the air handling unit (AHU) was running continually 24/7. Air distribution strategy was mixing ventilation where two supply diffusers supplied air in the room. Supply air diffusers located in the centre of the ceiling panels and the exhaust valves were in the corridor side near the door.

Water radiator heating setpoints were controlled with Fourdeg's electronic IoT thermostat valves. The setpoint temperature for the thermostats were set according to the measurement schedule. Constant setpoints were chosen to be in ascending order starting from 18 °C and finishing to 24.5 °C. Ascending constant temperature setpoints were used to evaluate the local thermal comfort at varying conditions.

Thermal manikin was built by former Helsinki University of Technology [7]. Manikin was size of 50 on European male index and it consisted of 24 heated body parts shown in Fig. 3. Compared to Foda's measurements, some measurement points were combined to form only one measurement point. Total of 20 body parts were used in this measurement. The manikin was dressed in normal office environment clothing. The clothing level was measured according to (EN ISO 9920) resulting in clothing level of 0.6 clo = 0.155 m^2K/W.

Heating of each body part was done with heating foils. The heating was controlled with ON/OFF control build in Labview platform. Timestep of control was 50 ms and deviation ± 0.05 °C. Skin surface temperature was measured in 1 min interval. The surface heat transfer coefficients for each body part determined in the Foda's doctoral thesis [7] were used in the study.

The manikin was controlled by the constant surface temperature mode (CST) in which case the influence by the environment is shown in the required heating power to keep the temperature constant in each body segment. The heating powers at each time step were used to calculate the corresponding equivalent temperatures [8].

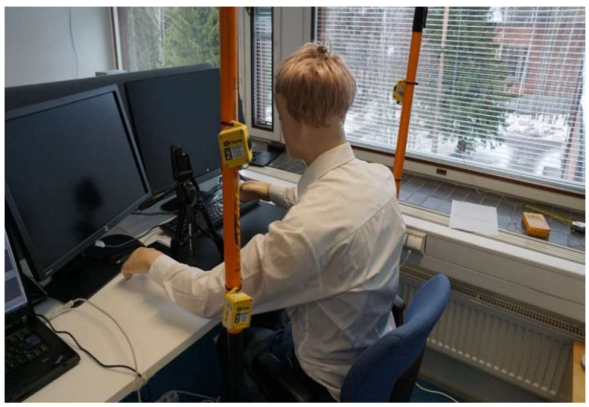

Figure 2. The measurement setup.

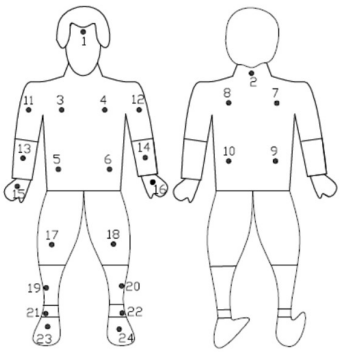

Figure 3. Thermal manikin measurement points.

C. Model predictive control algorithm

A model predictive algorithm (MPC) was developed in this study to implement the DR of space heating. The results from the local thermal comfort measurements were used as constraint in the MPC algorithm (see Table 5 simulation cases B).

The process chart in Fig. 4 presents the idea of DR with the MPC algorithm. First the input data including the weather forecast, dynamic district heating price and predictive usage of the building were imported to the MPC algorithm. The Finnish test reference year (TRY) weather data was chosen since it resembles average annual weather in the Finnish climate. The district heating (DH) marginal cost data utilized in this study was generated by Rinne [9].

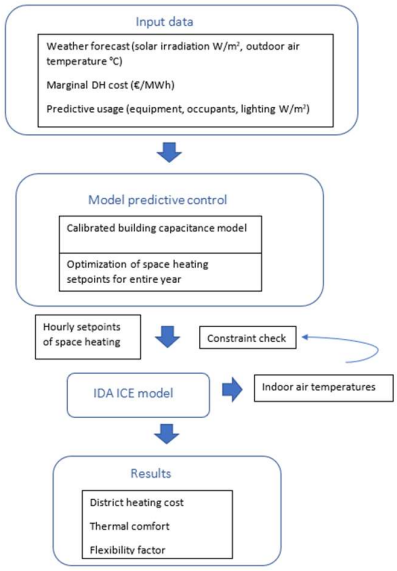

Figure 4. Process chart of the MPC algorithm.

The MPC algorithm written in Matlab composed of the calibrated physical building model and an optimization algorithm. The optimization algorithm used the physical building model in finding the most optimal space heating temperature setpoints over the predicted time spam of either 12 or 24 hours. The optimal setpoints were then exported to IDA ICE simulation software where the efficiency of the MPC algorithm was tested.

In addition, a decentralized feedback control was added to IDA to prevent overheating of spaces. The feedback control replaced the optimized space heating setpoint by the normal setpoint of 21 °C if the room air temperature in any room exceeded 24 °C.

The MPC algorithm was run throughout the year to get the annual space heating temperature setpoints. Therefore, the final simulation results depict the annual DR potential.

D. Calibartion of the RC-model

Simple two capacity RC-model was used to predict the heating demand in the MPC algorithm (Fig. 5). The two-capacity RC-model composes of two temperature node points, first one placed in the room air and the another one in the lumped building mass point. The heat transfer is described by the conductances and the heat gains from occupants, solar, equipment, lighting and space heating units. The heating demand to reach specific indoor air temperature setpoint was solved from the heat balance equations for both air and mass node points.

Two rooms from the studied floor were modelled in the RC-model to get solar radiation values from the opposite facades of the building (marked in Fig. 1). The modelling was limited to two rooms since the modelling of all rooms would have taken more time without giving remarkable benefits in the accuracy of the end-results of the DR potential. The conductances and capacitances were defined by calibrating the RC-model against the more sophisticated and validated IDA ICE room model. The static and dynamic calibration steps resulted in well-performing and accurate RC-model. The calibrated parameters are shown in Table 4.

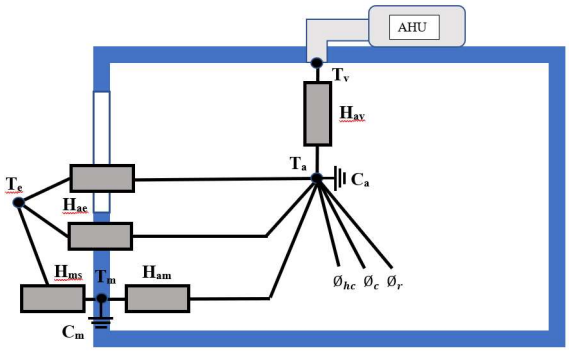

Figure 5. Schematic of the RC-model.

TABLE III.
SYMBOL DEFINITION

Symbol	Description	Unit
C_m	Heat capacitance of the mass node point	J/K
C_a	Heat capacitance of the air node point	J/K
H_{ae}	Combined conductance of the windows and leakage air	W/K
H_{ms}	Conductance between mass node and outdoor air node point	W/K
H_{am}	Conductance between mass node and indoor air node point	W/K
H_{av}	Heat capacity flow through ventilation	W/K
T_e	Exterior/outdoor temperature	°C or K
T_m	Mass temperature node point	°C or K
T_a	Air temperature node point	°C or K
T_v	Supply air temperature node point	°C or K
$\emptyset_{hc}$	Zone heating/(cooling) power	W
$\emptyset_c$	Convective heat loads	W
$\emptyset_r$	Radiative heat loads	W

TABLE IV.
RC-MODEL PARAMETERS AFTER CALIBRATION.

H_{ams}	H_{av}	H_{ae}	H_{ms}	H_{am}	C_a	C_m
W/K	W/K	W/K	W/K	W/K	kJ/K	kJ/K
10.4	51.8	7.7	10.7	372.2	336.3	19290

E. Optimization of space heating setpoints

Model predictive control algorithm involved an NSGA -II optimization algorithm which was used to find out the optimal space heating setpoint trajectories for the upcoming hours. The NSGA-II algorithm was chosen because it belongs to genetic algorithms which can find multiple solutions with one optimization round making the optimization efficient compared to preference-based optimization methods [10]. The original optimization code was developed by Tutum [11].

Optimization dealt with three optimization functions. Optimization tried to minimize the total heating energy cost (1), reach the maximum heating energy flexibility (2) and minimize the thermal discomfort described by the deviation of the air temperature of the RC-model to the preferred air temperature set according to the Finnish indoor air classification level S2 (3) [12]. The energy flexibility factor (FF) describes how efficiently the control algorithm can shift the load from expensive energy price to cheaper energy price periods [5].

$$Min\left\{F1(\boldsymbol{x}) = \sum_{t=1}^{n} heating\ power(\boldsymbol{x}(t)) * DH\ price(t)\right\} \quad (1)$$

$$Max\{F2(\boldsymbol{x}(t)) = flexibility\ factor\} \quad (2)$$

$$Min\left\{F3(\boldsymbol{x}) = \sum_{t=1}^{n} \left(T_a(\boldsymbol{x}(t)) - T_{ref}(\boldsymbol{x}(t))\right)^2\right\} \quad (3)$$

where

$\boldsymbol{x}$	space heating temperature setpoints
t	time instance
n	length of the prediction horizon
T_a	air temperature
T_{ref}	reference air temperature (winter 21.5 °C, summer 24.5 °C).

The optimization variable (x) was restricted to get values between [20-24.5] °C to maintain acceptable thermal comfort level. During the summertime when the 24 h average outdoor air temperature exceeded 0 °C the acceptable range was changed to [20-21] °C preventing overheating. The length of the predicted heating demand (n) was set to either 12 or 24 h, which also defined the length of the optimization variable vector x.

In addition to specifying the acceptable range for the space heating setpoints, the optimization had one constraint for the heating power. The heating power was not allowed to exceed the maximum outdoor air dependant heating power (physical restriction).

F. Simulated cases

The studied simulation cases composed of reference cases R, optimization cases O, parameter analysis cases C and draught risk constraint cases B. The cases are shown in Table 5.

The reference cases (without DR) formed a benchmark for which the DR cases could be compared. The temperature setpoint was constant throughout the year, either 21 °C (R1), which is a normal temperature target value in Finnish building code or 20 °C (R2) which resembles a case where the heat is conserved. In the optimization cases the objective functions and the length of the prediction horizon was changed. In the parameter analysis, different temperature setpoint ranges were studied. In the draught risk constraint cases, the minimum heating power was forced on whenever the simulated window surface temperature dropped below restrictive temperature defined in manikin measurements. Two different power requirements were studied (either 30% or 50% of the maximum power during the specific hour) with two window constructions (the case building windows U=1.1 W/m^{2}K and 2-pane windows U=2.6 W/m^{2}K).

TABLE V. STUDIED SIMULATION CASES.

Case	Optimization objectives	Prediction horizon, [h]	Temperature setpoint range, [°C]	Window surface temperature constraint
R1	-	-	Cons. 21	No
R2	-	-	Cons. 20	No
O1.2	Min (F1)	12	[20-23]	No
O2.2	Max (F2)	12	[20-23]	No
O3.2	Min (F1) Min (F3)	12	[20-23]	No
O4.2	Max (F2) Min (F3)	12	[20-23]	No
O2.3	Max (F2)	24	[20-23]	No
O3.3	Min (F1) Min (F3)	24	[20-23]	No
O4.3	Max (F2) Min (F3)	24	[20-23]	No
C1.2	Max (F2) Min (F3)	24	[20-24.5]	No
C2.2	Max (F2) Min (F3)	24	[20-21]	No
B1[a]	Min (F1)	12	[20-23]	No
B2[a]	Min (F1)	12	[20-23]	Min power 30%
B3[b]	Min (F1)	12	[20-23]	No
B4[b]	Min (F1)	12	[20-23]	Min power 30%
B5[b]	Min (F1)	12	[20-23]	Min power 50%

a = the case building windows U=1.1 W/m^{2}K
b = 2-pane windows U=2.6 W/m^{2}K

II. DATA PRESENTATION AND DISCUSSION

A. Thermal manikin measurements

The hypothesis of this measurement was that during the demand response, if the heat was conserved and the radiator valves were closed, the cold windows surfaces might generate convective downdraughts. Without thermal plumes from the radiators, the downdraughts could not be blocked, and the downdraughts could be sensed as draught. Commonly the draught is sensed in ankles as the air movement is increased at the floor level. However, in these measurements, it was noticed that the air movement was increased especially above the office table. The reason was that the office table was attached to the window side wall and instead of the air flows descending to floor level they were directed above the table. As a consequence, the draught risk was found to be higher at the uncovered hands of the manikin than at ankles.

The draught risk was further analyzed during three chosen measurement periods from the total measurement time. These periods were chosen so that they had different space heating temperature setpoints and window surface temperatures. The three periods analyzed are shown in Table 6. The periods P1 and P2 depict the condition were the temperature setpoint was low and the radiator valves were closed. In P3, the radiator valves were opened, and the radiators supplied heating and thermal plumes. The window surface temperature was higher in period P2 compared to periods P1 and P3.

TABLE VI.
THE MEASUREMENT PERIODS ANALYZED

Period	Room air temperature setpoint (°C)	Average room air temperature (°C)	Average window surface temperature (°C)
P1	18	20.1	15
P2	19	20.5	17
P3	20	20.1	15

The equivalent temperatures at the manikin's left hand (corridor side) and right hand (window side) are shown in Fig. 6. It can be seen that the equivalent temperature of the right hand is lower than that of the left hand during the period P1. This indicates that the downdraughts from the window caused convective heat loss in the right arm. During periods (P2) and (P3), the difference of the equivalent temperature between the right and left hand first decreases and then balances out. Therefore, it can be concluded that the draught risk is increased if the window surface temperature is below 15 °C and the heating is turned OFF. If the windows surface temperature was higher or the radiator heating was ON, the draught risk was decreased.

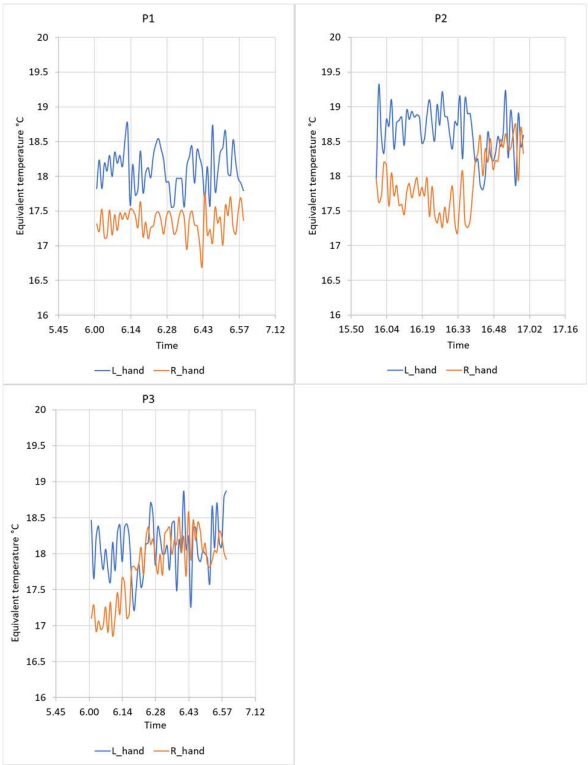

Figure 6. Equivalent temperature of the right- and left-hand during the periods P1, P2 and P3.

B. Results from demand response simulations

The results from the MPC algorithm implemented DR cases are analysed in respect of energy cost savings, energy flexibility and thermal comfort. The annual heating costs and flexibility factors are presented in Table 7. Heating energy consumption and costs are given per heated net floor area allocated form and the relative savings are calculated in reference to case R1.

TABLE VII.
DISTRICT HEATING ENERGY SAVINGS, COST SAVINGS AND ENERGY FLEXIBILITY

CASE	DH energy	Cost	DH energy	Cost	Cost and energy saving ratio	Flexibility factor
	kWh/m²	€/m²	%	%	-	%
R1	128.3	8.2	0.0	0.0	0.0	7
R2	121.2	7.8	-5.5	-4.8	0.9	7
O1.2	121.4	7.8	-5.4	-4.7	0.9	7
O2.2	125.3	7.9	-2.3	-3.1	1.3	10
O3.2	122.3	7.8	-4.7	-4.2	0.9	6
O4.2	126.2	8.0	-1.6	-2.7	1.6	11
O2.3	125.7	7.9	-2.0	-4.0	2.0	13
O3.3	122.5	7.8	-4.5	-4.6	1.0	7
O4.3	127	7.9	-1.0	-3.0	2.9	14
C1.2	127.2	8.0	-0.9	-2.5	3.0	13
C2.2	126	7.8	-1.8	-4.3	2.4	14
B1	121.4	7.8	-5.4	-4.8	0.9	7
B2	121.4	7.8	-5.4	-4.7	0.9	7
B3	144.5	9.3	-4.7	-3.8	0.8	7
B4	145.3	9.4	-4.2	-3.5	0.8	7
B5	147.7	9.5	-2.6	-2.3	0.9	5

The results show that the highest energy cost savings were obtained from the DR case O1.2. However, the cases O3.3 and C2.2 reached almost the same cost savings. The cost savings in these DR cases are close to the savings given by heat conservation in the reference case R2.

The highest flexibility factor of 14% was reached in the cases O4.3, C1 and C2 which all had flexibility factor as one objective. The flexibility was increased considerably compared to the reference cases R1 and R2 which had FF of roughly 7%.

The cost optimized cases and the flexibility optimized cases differed in the strategy they used to modify the heating load. The cases having cost optimization as one objective tried to decrease the energy costs by heat conservation (similarly to reference case R2). In comparison, the cases having flexibility optimization as one objective, utilized the load shifting strategy where the load was shifted from expensive to cheaper energy cost periods. The difference between these strategies can be seen from the cost and energy saving ratios shown in Table 5 and from Fig. 7.

The cases where the thermal comfort acted as one objective resulted in slightly lower heating cost savings compared to cases optimized only by costs or FF. The length of the prediction horizon had significant effect on the results. The longer prediction time increased the cost savings and decreased the heating energy savings in both cost and flexibility optimized cases. The parameter analysis cases (C cases) revealed that the heat loading seems not to be feasible in this case building. In the case

C1.2, the allowed temperature setpoint range was [20-24.5] °C while it was [20-21] °C in case C2.2. The case C2.2 resulted in higher heating cost savings and therefore the heat loading with temperature setpoint above 21 °C seems not to be feasible. The reason for this might be that the relatively high ventilation air flows would flush the heat away before it could be loaded to the building mass.

Adding a draught risk constraint to the MPC algorithm had small influence on the DR potential. With energy efficient windows (B1 and B2), the influence was neglectable. With 2-pane windows (B3-B5), the cost saving potential was dropped by 8% and 40% (compared to B3) when the heating power requirement of 30% (B4) and 50% (B5) were used, respectively. However, in the manikin measurements, it was found out that even small heating power could prevent the draught and therefore, the 50% heating power requirement was regarded unnecessary high and its influence can be neglected.

Thermal comfort level in the simulation cases was analyzed by plotting the air temperature duration curves of the coldest room in the case floor. The duration curves showing cases R1, R2, O1.2, O2,2, O3.2 and O4.2 are presented in Fig. 7. The temperature duration curves showed that the air temperature did not drop below 20 °C in any of the simulated cases. As the 20 °C is regarded as the minimum allowed air temperature in the Finnish indoor air classification [8], it can be concluded that the acceptable thermal comfort was maintained in all studied cases. The cases where the thermal comfort was also optimized resulted in slightly higher room air temperatures and comfort levels. The difference was small because the decision between two optimization objectives (either cost + comfort or FF + comfort) was always done so that either cost or FF was preferred over the comfort.

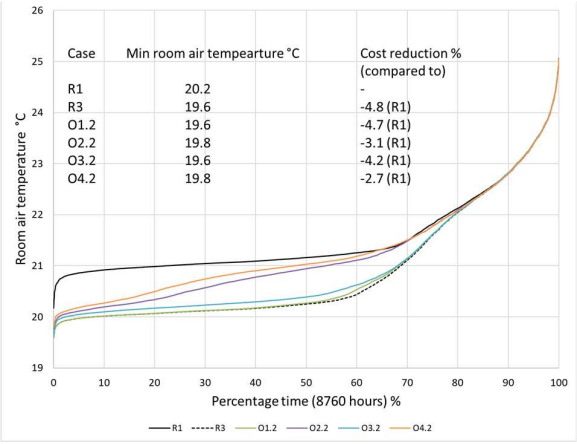

Figure 7. Temperature duration curves of the coldest room of the case floor.

III. CONCLUSIONS

The draught risk measurements with thermal manikin revealed that the draught risk was increased in the office room if the window surface temperature dropped below 15 °C while the heating was turned OFF due to the demand response control. It is suggested that the DR could have constraint that would force heating ON when the window surface temperature is in danger to drop below this restrictive temperature.

The MPC algorithm developed in this thesis, was tested in IDA ICE simulation software by modelling one floor of the case building and simulating different case scenarios. The simulations revealed that the MPC algorithm could reduce the space heating energy costs up to 5 % when compared to the reference case with space heating setpoint of 21 °C. Acceptable thermal comfort was maintained in all the studied cases.

The analysis of the different optimization objectives in MPC algorithm showed that the cases where the heating costs were minimized lead to heat conservation (low temperature setpoints) whereas the cases where the energy flexibility was optimized lead to load shifting (temperature setpoints followed the variations in the energy price). Increasing the prediction horizon, time period within the setpoints were optimized, resulted in both higher energy cost savings and energy flexibility. The window surface temperature constraint tested in the MPC algorithm simulations had no significant effect on the DR potential.

ACKNOWLEDGEMENT

A.M. thanks Juha Jokisalo and Risto Kosonen for the guidance and supervision of the thesis and Simo Kilpeläinen for the help in the manikin measurements.

REFERENCES

[1] IEA. “Building energy performance metrics”, 2015.

[2] European Commission. “Energy efficiency – buildings”, 2017.

[3] O. Seppänen, F. Wisk and Q.H. Lei. “Effect of temperature on task performance in office environment”, Lawrence Berkeley National Laboratory, 2006.

[4] WHO. “Indoor environment: health aspects of air quality, thermal environment, light and noise”, 1990.

[5] J. L. Dreáu & P. Heiselberg. “Energy flexibility of residential buildings using short term heat storage in the thermal mass”, *Energy*, Vol. 111, 2016, pp. 991-1002.

[6] Indoor Climate Quality Assessment: Evaluation of Indoor Thermal and Indoor Air Quality. 2011, *Rehva quidebook No. 14*., Rehva, Brussels I.

[7] E. Foda. “A thermal manikin with human thermoregulatory control: implementation and validation”, *International Journal of Biometeorology*, Vol. 56, no. 5, 2012, pp. 959-971.

[8] H.O. Nilsson and I. Holmer. “Comfort climate evaluation with thermal manikin methods and computer simulation models”, *Indoor Air,* Vol. 13, no. 1, 2003, pp. 28-37.

[9] S. Salo et al. “The Impact of Optimal Demand Response Control and Thermal Energy Storage on a District Heating System”, accepted for publication in Energies-journal.

[10] K. Deb. 2008, “Multi objective optimization using evolutionary algorithms”, John Wiley and Sons, UK. pp. 515.

[11] C.C. Tutum. “Optimization of thermo-mechanical conditions in friction stir welding”. Doctoral Dissertation, (DTU), Copenhagen, 2010, pp. 159.

[12] FiSIAQ. “Finnish indoor climate classification”, Helsinki, 2008, pp. 22.

REHVA
Federation of European Heating, Ventilation and Air Conditioning Associations

Construction and test of a new Distributed Thermal Response Test (DTRT) using heating cable in shallow borehole

Alice GEBER, José ACUÑA

***Abstract*— Sweden is a leading country in shallow geothermal energy usage for heating, cooling and storage. Before the design of a borehole field, a Thermal Response Test (TRT) is usually performed in-situ to determine the ground thermal conductivity of a specific location. A better understanding of the ground proprieties can lead to a better ground source heat pump efficiency. TRTs are conventionally made with a hydraulic equipment. Even though other ways exist they are not yet commercially developed. Nowadays Bengt Dahlgren, a Swedish consultant company, sells TRT and Distributed Thermal Response Test (DTRT) performed with their hydraulic equipment, but the company aims to develop a DTRT using heating cables, a more practical approach from the execution and data evaluation point of view. This paper introduces a design of DTRT equipment using heating cable that could allow to perform tests in boreholes up to 300 meters deep. The construction steps are detailed from the first general concept idea to the construction of the equipment and its installation in the field.**

***Index Terms*— Geo-energy – Distributed Thermal Response Test (DTRT) - Borehole - Heating cable**

Introduction

The geothermal energy is a sustainable energy mostly used to produce heat during the winter. However, ground may not only be used for extracting heat but also for cooling purpose, to store energy and to produce electricity. In geothermal resources the thermal energy exists in the rock, soil and groundwater that fills the boreholes, pores and fractures. Geo-energy can be classified into categories depending of the depth where the energy is exchanged, and they have different applications. This paper focuses on vertical shallow borehole exploited for direct use application combined with or without a ground source heat pump (GSHP).

Shallow ground resources are already widely use in Sweden and the average borehole depth has been growing since 1980. Most of the newly drilled boreholes are between 200 and 300 meters deep [1].

The efficiency of a GSHP system using boreholes heat exchangers (BHE) as a source relies partly on ground characteristics. Since only the first meters of soil are weather dependent, the major part of the immersed pipes is in contact with a stable environment. Therefore, knowing the in-situ ground characteristics of a project localization helps to design an adapted system with the better understanding of the energy source. The most impacting on the heat behavior in a BHE is the thermal conductivity of the ground and the TRT is a method that aims to evaluate this value, among others.

A TRT is performed in a borehole by injecting heat or cold and by monitoring the evolution of the temperature in and out the borehole. The measured data are, for example, inserted in the infinite line source model which considers heat injection (or extraction) on a single infinite line that stands for the BHE [2]. In this model heat is only propagating in one dimension (radially), the heat transfer medium is assumed to be isotropic and constant in time. The heat transfer is purely conductive and the heat rate is assumed constant.

Since the amount of injected heat is known and the temperatures are measured, this model calculates an average thermal conductivity for the tested borehole when applied to a conventional TRT. Even though other models could be used to calculate more precisely the heat transfer in the ground the ILS is fast and simple and suits a commercial purpose.

While conventional TRTs give an average value for the thermal conductivity, a so called Distributed Thermal Response Test (DTRT) gives the thermal conductivity of the ground along the length of the borehole [3]A fiber optic cable is inserted in the borehole to monitor the evolution of temperature along the depth, allowing to identify zones with high and low thermal conductivity, location of fractures and groundwater flow movement along the borehole

Some requirements should be upheld to do a proper TRT: the waiting period between the drilling and the beginning of the test is 3 to 5 days. The temperature measurement and recording devices should have an accuracy of ± 0,3K and the deviation of the applied power should be less than ±1,5%. The heat rate should be between 20 and 80 W/m [4].

Most conventional TRT equipment follow the same design pattern and consist of a hydraulic machine composed of a heating element, a pump, a flowmeter, a couple of sensors. To perform a DTRT, temperatures are often measured with a fiber optic cable that is added to the set up and connected to a Distributed Temperature Sensor (DTS). (**Figure 1**)

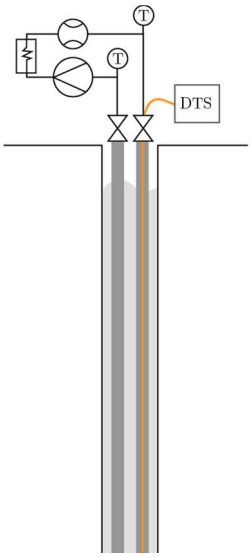

Figure 1 : Hydraulic DTRT

A DTRT could be performed using heating cable instead of through flowing fluid (**Figure 2**). The heating cable is immersed vertically inside the borehole and injects relatively constant power during the desired time. Since the power may fluctuate, a power meter is needed to lead to accurate calculations. Moreover a DTRT performed with a heating cable that stands still rather than a flowing fluid is closer to the theoretical line source model that is used for the ground conductivity calculation.

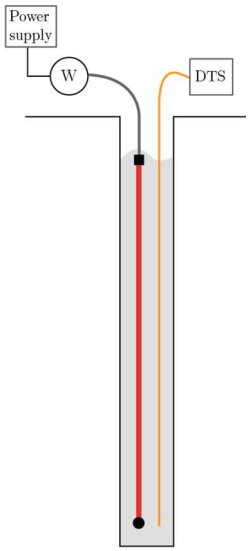

Figure 2 : DTRT using heating cable

Some experiments using heating cable inside boreholes to perform Heat Trace Test (HTT) or DTRT have already been performed earlier. One test using sections of heating cables covered a length of 150 meters deep with a released power of 28,6 W.m^{-1} [5] and another one with a full length of heating cable was conducted onto 100 meters depth in a homogeneous media with a released power of 15 W.m^{-1} which is enough to determine where the ground water flow accelerates the heat dissipation but is insufficient to calculate the thermal conductivity. [6]

The challenge of the work presented in this paper was to design and construct an equipment that could perform DTRT using heating cable in boreholes up to 300 meters deep.

General design

The idea is to use a heating cable to generate constant heat output and then monitor the temperature evolution with a fiber optic cable connected to a DTS device to calculate the ground thermal conductivity using the ILS. Since the equipment is made to be used for commercial applications it needs to be simple and light to be transported and manipulated easily on the field.

It is usual to have on the field a power supply of 3 phases, 230V and 16A. With the requirement of at least 20 W.m^{-1} of released power by the cable a first preliminary calculation was made to ensure enough power is available for our application (Equation 1):

$$P = \frac{U \times I}{L \times 3} = \frac{230 \times 16}{300 \times 3} = 36\ W.m^{-1} \qquad (1)$$

The maximum power output that could be obtained for a 300-meters-long heating cable is 36 W.m^{-1} which is enough to perform a DTRT. However, a power drop in the equipment is inevitable, so a smaller power output is expected for the final equipment.

The cable that is chosen for this application is a constant wattage heating cable that is usually used to melt down snow on pathways. According to the manufacturer it should supply a constant power of 30 W.m^{-1}. It is made of resistances connected in parallel between two copper cables, one phase and one neutral, and it releases the same amount of power along the cable depending of the current. The ground is wrapped around the copper cables and several protection layers make it waterproof. Nonetheless heating cables are not designed to be immersed inside a borehole and no manufacturer would give warranty for an unstandardized use.

Heating cables have a maximum length which depends of the installation general circuit breaker, in our case 16A, and of the power output. The maximum length for single phase heating cable is around 100 meters long.

The idea is to connect the heating cable to two phases so the electric potential rises up from 230V to 400V, thereby the maximum length of the heating cable increases to 200 meters. The remaining phase could be used to get power in a smaller heating cable of 100 meters long. In total the equipment is 300-meter-long.

Since the first 20 meters below the ground surface are usually not evaluate in TRT, the heating cables that were bought are 190 and 95 meters long for a total length of 285 meters (**Figure 3**).

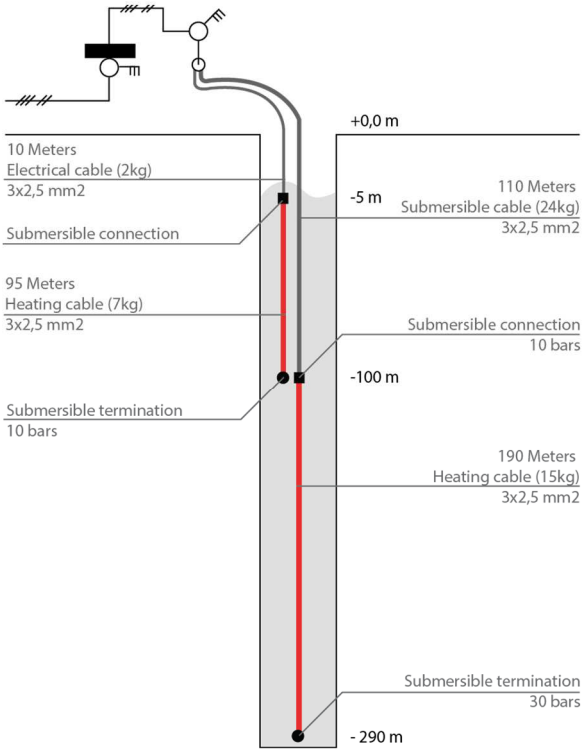

Figure 3: Final Design

This solution reduces the amount of cold cable and connections/terminations to its maximum which were previously problematic in other design ideas.

Moreover, since the longer heating cable is supplied with 400V the voltage drop in the cold cable is not important and a 3 wires/2.5 mm cold cable is used, which is neither too wide nor expensive.

The terminations of the heating cables are the weak points of the equipment. If the test requires it, the termination of the 190 meters long heating cable may be immersed 300 meters below the water surface and therefore it needs to sustain at least 30 bars. Furthermore, to be able to dive down the cable, its termination should weight enough to bring it down.

Electrical box construction

The electrical box **(Figure 4**) stands between the heating cables and the power supply, it should fulfill several requirements. Security-wise it needs to be able to protect the power source and the system if something goes wrong. The main plugs for the power supply, the heating cables and the DTS device are outside the box. The electrical box is made to turn on and off the heating cables via switches. Since the exact power output is needed for the calculation a power meter is added and two temperature sensors are placed in the borehole and outside.

Finally, the command system ensures that the equipment functions correctly. Everything is monitored by a Raspberry Pi which is a micro-computer that can be accessed remotely from a computer or a phone. It allows the user to check at anytime from anywhere if the system is running or if a technical problem occurred.

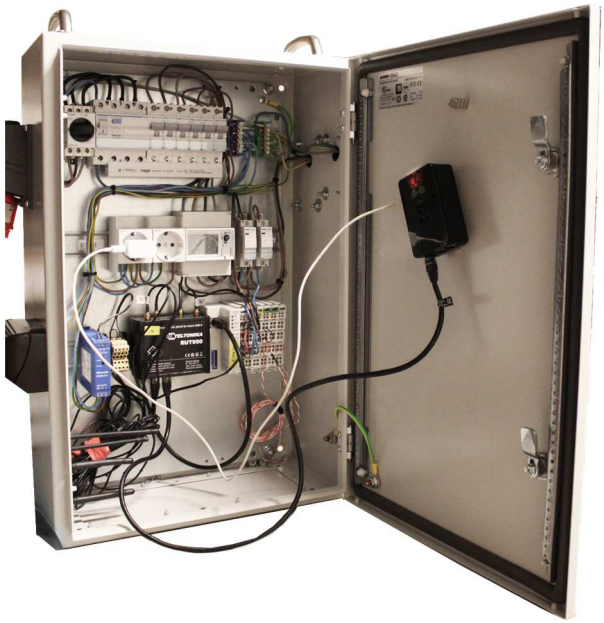

Figure 4: Electrical box

The command system is made with a recycled controller device made from a Beckhoff Bus Coupler with four bus terminals. The first bus terminal controls two contactors that let though 24V DC, these are the switches for the heating cables. The second bus terminal acquires pulse outputs, and is connected to our energy meter. The third bus terminal has two temperature sensor inputs, the last bus terminal is not used in this equipment.

A thread-based python code allows turning on and off the contactors while getting and storing data during the full test time. In addition to showing the command buttons of the contactors the graphic interface shows the sensors measured values, a couple of graphs and the elapsed time of the test.

Set up on the field - Method

Five distinct elements constitute the final equipment (

Figure 6) and the can all be transported independently and then plugged together on site. The two heating cables and the fiber optic cable are rolled on three separate drums and weight less than 40 kg. The DTS computer is contained in a suitcase and the electrical box is easily transportable and weight around 20 kg.

To run the test a 3 phase 230V 16A power supply must be available on site. First all cables have to be rolled down inside the borehole. To ensure no cable would be damaged on the sharp edges of the borehole during this step a little helper was built to smoothly slide the cables down (**Figure 5**).

Figure 5: Helper to slide the cables down

The central element is the electrical box on which the two heating cables and the DTS are plugged. The fiber optic cable is connected to the DTS.

When all the cables and the DTS are plugged the power can be turned on via the main switch, then the Raspberry PI can be accessed from anywhere to start the program and begin the measurements and the calculations. The DTS launches itself independently and can also be accessed through a router and controlled from the office.

It is easy to control the installation and ensure everything is running fine at any time of the test without being permanently on site.

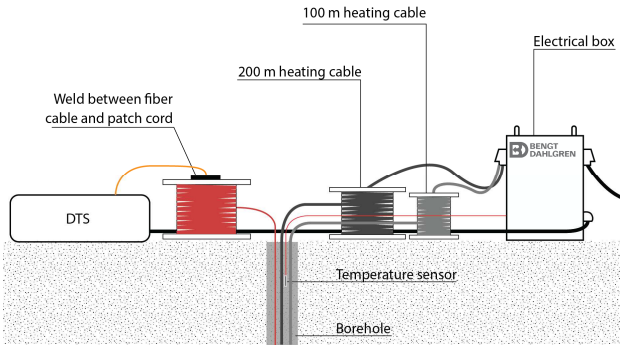

Figure 6: Field set up

DTRT using heating cable is a new technology therefore a specific protocol for this equipment does not exist yet. However, the literature about TRT and DTRT can be used as a basis to set up a protocol. TRT should last between 50 to 72 hours **[3]**. The duration of each test varies from one site to another and depends on the location itself as much as the conditions of the test. Technical problems can increase the duration of the test. If the test must be redone from the beginning one must be careful because when the ground is heated it needs some time to get back to its undisturbed state. Three mains measurements steps should be recorded:

- The undisturbed ground temperature, which gives the undisturbed temperature profile of the ground.
- The heating period during which heat is injected into the ground until the temperature reaches a steady state.
- The recovery period when the heat injection is turned off up until the ground returns to its undisturbed temperature profile.

A first test was performed and completed with the new equipment took. The equipment was installed to test an empty 250-meter-deep borehole. The 190-meter heating cable was rolled down to the bottom of the borehole so the first 60 meters of the borehole were not part of the heating section. The fiber optic cable was also rolled down. The borehole temperature sensor was placed inside the borehole but because of its short length it was unlikely to reach the groundwater level.

The equipment was installed on Friday the 27th of July 2018 which was the day after the drilling. The energy meter showed a consumption of 4,64 kW and 12A. The DTS update time was 600 seconds, and the TRT software update time was 30 seconds. The DTS was launched, as well as the Raspberry PI. Two divers were added to the general set up. The test was redone between the 17th of August and the 27th of August. The monitoring stopped for 24,5 hours after 28 hours for technical reasons, but for a better readability of the results the graphics do not show this gap. The two divers were immersed in the borehole at 10 and 20 meters of depth. They were used to correct the measurements of the fiber optic cable afterwards.

Data presentation

The 3D-Diagram below (Figure 7) shows the evolution of the temperature versus time for each depth of the borehole. The first 60 meters were not part of the heated length. (**Figure 7**)

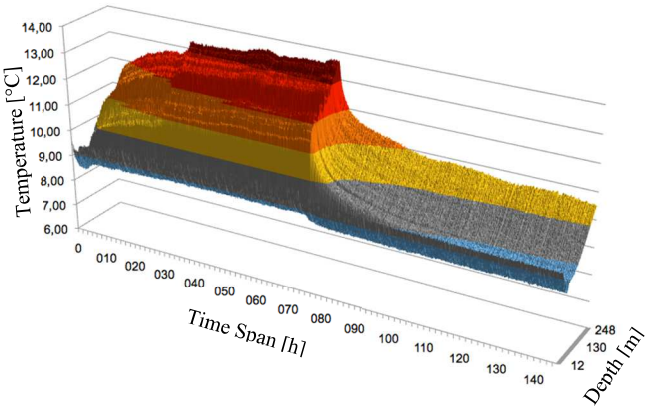

Figure 7: Results of the test in Årsta, 3D-Diagram showing the temperature VS time VS depth

These values are close to the theoretical line source model and can be used to make calculation of the ground thermal conductivity. As an example, the following graphic (**Figure 8**) shows the evolution of the temperature through time for a depth of 150m inside the borehole. The discontinuity at 28 hours corresponds to a loss in the monitoring for one day and two hours.

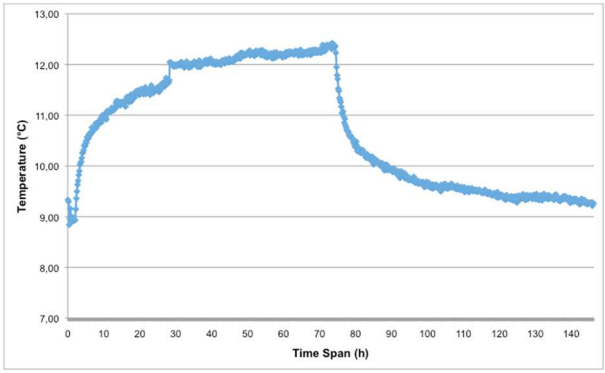

Figure 8: Temperature vs time for a depth of 150 meters

The calculations were made on the recovery period. Which begins at 72 hours of continuous test. The rock was homogeneous with an average calculated thermal conductivity value of 4,09 $W.m^{-1}.K^{-1}$ (**Figure 9**) This value is above the average for the Stockholm area where the ground is mainly granite

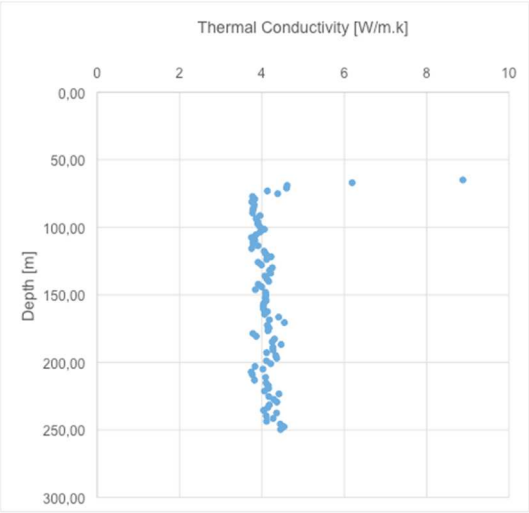

Figure 9: Thermal conductivity VS depth

Discussion

This new type of DTRT equipment presents some advantages compared to the hydraulic DTRT. The hydraulic machine can cover boreholes up to 300 meters deep but with a power supply of 3 phases 230V and 32 A which are not always easy to find on the field. It is more common to have a 3 phase 230V and 16A power supply. Moreover, its installation requires to tighten up the pipe connections on the field, to pressurize the system and to insure all the air is removed before the test can start. The new DTRT using heating cable reduces the time on the field to set up the installation. It could even be installed by the drillers while they are on the field which could optimize the consultant's time. However, the hydraulic TRT also permit to perform a flow check of the collector to detect any leakage since it is hydraulically connected to the borehole, which is not possible when using heating cables. The DTRT using heating cables is though lighter and it can be transported and manipulated on the field by a single person since it is composed of five elements that are independent and weighs less than 40 kg each.

The termination of the cable set up should be, if measuring inside the heat exchanger pipes, smaller than the regular size of a collector. If bigger, measurements should be performed in boreholes without a collector. Smaller terminations exist but they are more expensive. However, the termination only corresponds to a plastic hollow pipe that is poured with resin, it should therefore be possible to construct a termination with piping elements that fit together and then pour it with electrical resin. This solution will probably be cheaper and the perfect size for the termination could be selected.

To widen the range of available tests, a complementary 50-meter-long heating cable could be bought. Then tests could be conducted in boreholes of 50, 100, 150, 200, 250 and 300 meter deep. However, to be able to do all these configurations an adaptor from a blue single-phase plug to a red single-phase plug should be made, therefore the 50 meters long heating cable could be plug on both single phase and two phase plug of the electrical box.

The helper could be modified to add a wheel and a revolutionary counter. The heating cable and the fiber optic cable would roll on the wheel just before being pulled down. Then with a correct calibration of the counter the length of rolled down cables could be known.

The electrical box was designed to make Thermal Response Tests with heating cables. Nevertheless, it can also be used to proceed to other types of tests in boreholes.

A Heat Trace Test cable can be designed with a short and powerful heating element at the end on a new reel. It would be plugged instead of the 95-meter-long heating cable. The DTS would be plugged as for a DTRT. Since it would be convenient to be able to roll down the heating cable while the test is running a slip ring should be mounted on the reel to make the power supply loose from the rotation of the reel.

A pump can be plugged instead of the DTS and a diver could monitor the drawdown to realize a pump test. According to the site, the pumped water can be either rejected farther away or collected in a bucket.

Conclusion

In the geothermal field the introduction of the Thermal Response Test was an important step toward a better understanding of the ground behavior. This test allows to determine experimentally the effective ground thermal conductivity and therefore design borehole fields that correspond better to their localization. With the introduction of the fiber optic to monitor the temperature along the whole length of the borehole the thermal conductivity could be determined at each depth. The temperature profile of the ground was more precise and could led to better calculation of the heat exchange during simulations of a borehole field usage. The Distributed Thermal Response Test using heating cable is a new progress since it can show where the groundwater flow has a significant influence on the thermal conductivity profile. Indeed, the flowing fluid in a hydraulic TRT machine homogenizes the temperature response although the heating cables are still in the water and impact very little the groundwater behavior. This paper introduces a new technology to do DTRT using heating cable instead of a flowing fluid. A new equipment was developed to be able to perform tests in shallow boreholes up to 300 meters deep. The design and the construction of this new equipment stand for a major part of this work, since no such equipment exists already.

In comparison to the hydraulic TRT machine, this new DTRT equipment has several advantages. From a practical point of view the equipment is easier to set up on the field since there are no need for pressurizing the system or even have water supply on site. There are only electrical plugs to connect. No hydraulic connection require to be fastened and it needs only a 3 phase 16 A power supply to work. The five parts of the equipment could be transported individually and assembled on the field by a single person. It is possible to reach locations that would be hard to get to with a trailer. Tests could be conducted in boreholes between 100 and 300-meter-deep, it can also work to test an open loop well. The measured temperatures inside the

borehole are not influenced by the outside ambient temperature fluctuation if the DTS device is auto-calibrating correctly and/or well insulated.

However, in the final new equipment the termination of the heating cable is wide, and tests can only be conducted in empty boreholes or within collectors that are wider than 40 mm inner diameter, which is not common. But this is not a main issue since the drillers can install the collector afterwards when they will be drilling the complete borehole field.

The first test using the equipment was conducted and the experimental data was used to calculate the effective thermal conductivity for each depth of the borehole and gave an average value of 4,09 $W.m^{-1}.K^{-1}$.

This work resulted in an operational and user-friendly equipment that fulfills the requirements to perform commercial DTRT on the field while being closer to the mathematical model used for the thermal conductivity calculation. It is therefore a step forward in determining the ground characteristics. [7]

ACKNOWLEDGEMENT

1. I would like to thank José Acuna for this master thesis opportunity and being a trustful and motivation supervisor and a great teacher.
2. I am grateful to Johan Andrén for assisting me with the construction of the equipment and everything he taught me about electricity and how to build things.
3. Finally, I am very thankful to my brother Olivier who was a fantastic Python programming teacher and a great support throughout all this work.

REFERENCES

[1] S. Gehlin and O. Andersson, "Geothermal Energy Use, Country Update for Sweden," in *European Geothermal Congress*, Strasbourg, 2016.

[2] P. Monzo, "Comparison of different Line Source Model approaches for analysis of Thermal Response Test in a U-pipe Borehole Heat Exchanger," KTH, Stockholm, 2011.

[3] J. Acuña, "Distributed Thermal Response Test: New insights on U-pipe and Coaxial heat exchangers in groundwater-filled boreholes," Doctoral thesis KTH Energy Technology, Stockholm, 2013.

[4] S. Gehlin, "Riklinjer för Termisk Responstest (TRT)," Svenskt Geoenergicentrum, Stockholm, 2015.

[5] J. Raymond and L. Lamarche, "Development and numercial validation of a novel thermal response test with a low power source," *Geothermics,* pp. 434-444, 2014.

[6] T. Colman, B. Parker, C. Maldaner and M. Mondanos, "Groundwater flow characterization in a fractured bedrock aquifer using active DTS tests in sealed boreholes," *Journal of Hydrology,* pp. 449-462, 2015.

[7] A. Geber, "Construction and test of a new experimental Distributed Thermal Response Test using heating cable in shallow borehole," Master thesis INSA, Strasbourg, 2018.

REHVA
Federation of European Heating, Ventilation and Air Conditioning Associations

Design and application of air/water heat pumps of apartment buildings

Ing. Jan Vitouš

Abstract— **The thesis deals with the design and evaluation of air/water heat pumps for apartment buildings using dynamic building simulation. In the introductory parts of the thesis, individual approaches to design and evaluation of air/water heat pumps are shown.**

The air/water heat pump is designed for a specific apartment building according to the design practice and evaluated with several approaches. For each approach, the input parameters and results obtained by calculation are described. The partial conclusion includes a comparison of these evaluation approaches according to the obtained results.

The second part is dedicated to a parametric study proposing 4 variants of the main heat source for heating and hot water supply based on results from the evaluation approaches in the first part of the article. These variants are designed with different heat pump technologies used and meeting different percentage of energy needs. For a comparison with conventional heat source, a variant with heat gas condensation boiler is also designed. Based on the designed variants, an economic evaluation is performed. The evaluation consists of the calculation of operating costs, investment costs and total cost of each system. The resulting comparison is shown by using cash flow for the monitored lifetime of 30 years. The conclusion of the article provides information about the complexity of the designed systems in terms of the investment and operating costs of individual heat sources for possible future decisions by investors.

Index Terms — Air-water heat pump, apartment house, balance interval method, CO2 heat pump

Introduction

The current development of constructions in the Czech Republic and overall in the European Union is now very thoroughly regulated in terms of energy management of buildings. For building permits, it is necessary to submit a building energy rating (BER) to the Building Authority, which evaluates the building in terms of the thermal properties of the building envelope and assess the technical systems used in the building. To meet this requirement, it is often necessary to install technical systems with alternative or renewable energy sources. There are many possibilities for choosing renewable sources, however, each source has its advantages and disadvantages and is suitable for different applications. To solve this issue with using renewable and alternative sources in apartment buildings, the design is often limited by the usability and requirements for the operation of individual systems.

The big advantage of heat pumps are their low requirement for system operation, the compliance with the legislation and the possibility of installation in buildings only with electric grid connection.

How does the design and evaluation of heat pumps for apartment buildings, especially the evaluation of their economic benefits works in reality? To clarify this issue a study of the apartment building, where design approaches and individual evaluation methods were used, will be presented. Based on these conditions a variant design of the main heat source for this object will be performed. Then designed options will be assessed in terms of investment, operating and total costs.

I. Apartment Building

A specific example of individual design and evaluation approaches is presented at an apartment building where the main source for heating and hot water supply is the heat pump. An object as apartment building was chosen from the point of view for the specific design of the heat pump system, in particular the energy component for hot water heating to its high temperature request and its amount for the apartment building. This request is almost stable throughout the year.

The design and evaluation of the heat pump will be shown in various levels of detail and everything will be determined on the specific apartment building, which is located on the outskirt of Prague.

A. Building description

The apartment building is a detached building with plan dimensions 18x18m with a floor to ceiling height of 2.62 m and the floor height of 2.92 m. The building has 5 floors, four of them are above ground and intended for residential purposes. The basement is partially situated underground and is unheated.

From the parameters of apartment units, the number of inhabitants was estimated as 41. According to these parameters, the need of hot water supply was determined.

Fig. 1 - Apartment building

II. Heat Pump Design by Project Practice Using ČSN EN 12 831

In the project documentation, the heat loss of the building is calculated according to ČSN EN 12 831 for the design of the heating system. The total heat loss of the building is 44 302 W. In the project documentation was also determined hot water sampling curve

for an apartment building constructed according to ČSN 06 0320. The curve was constructed according to the number of people in the object. The specific hot water supply need for the tank design was determined according to the standard value for apartment buildings of 82 l/person/day and 40 l/person/day for the calculation of the hot water supply balance.

A. *Choice of heat pump performance*

The choice of heat pump performance in project practice is most often carried out on a proposal of 70% of the required performance of the building. In our case, the source design is at least 0,7 * 44,3 = 31,01 kW. For this study and a demonstration of the difference in evaluation methods were chosen two heat pumps from Stiebel – Eltron as cascade for energy source, specifically a pair of Stiebel - Eltron WPL 34 heat pumps, which achieve a power of around 30 kW with cascade connection and calculation temperature of -13 ° C, i.e. approximately 70% of the calculated heat loss of the object. Alternatively, air/water heat pumps are also designed for full heat loss, but the performance of the source is determined for the A2/W35 source parameters.

III. EVALUATION OF THE DESIGNED SOURCE

In the previous chapter, the main source of heat in the building was designed. Now we will show, based on individual evaluation approaches, how to evaluate this source in terms of thermal energy.

A. *Table values using energy need according to ČSN EN 12831*

When choosing source of 70% heat loss covering and using air/water heat pump, annual energy need will be covered by heat pump in 92% [1]. The day-to-day method calculates the annual heat balance of the building and divides it by 92% for the heat pump and last 8% energy needs to be covered by a bivalent heat source.

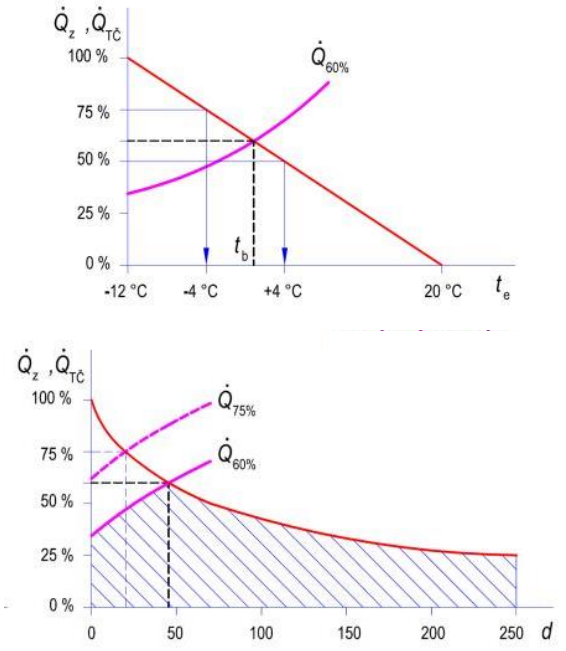

Fig. 2 - The relation between heat pump performance and cover of annual energy needs [1]

B. *Evaluation of designed source and calculation of energy need according to TNI 730531: 2014*

According to TNI 73 0531: 2014, the need for energy to be covered by a heat pump was calculated. This energy need was calculated based on the heat loss of the building (based on the previous calculation procedure), based on the internal and external designed temperature and the temperature gradient of the heating system. Furthermore, in energy need calculation is taken into account heat loss surcharge and a correction factor based on the building's energy standard (as it is). The calculation of the energy need also includes the calculation of the energy needs for hot water preparation, which was based on the input data from the project documentation.

The evaluation of the heat pump by this method can be carried out with specific heating performances and heat pump factors stated in the technical parameters of the products based on the ČSN EN 14 511 test methodology. The values for the balance calculation are for the selected heat pump WPL 34.

C. *Evaluation of the designed source and calculation of energy need according to the producer's design program*

Another tool to evaluate the choice of heat pump is to use computational programs directly from the producer. Stiebel - Eltron has a computational tool in Excel. To carry out the balance calculation in this program, input data are required - heat loss, average internal calculation temperature, external calculation temperature (it is possible to use pre-set offer of climatic values), type of selected heat pump, number of heat pumps, calculation temperature of heating system and its temperature gradient, attenuation coefficient, daily hot water supply need.

D. *Evaluation of the designed source and calculation of the energy need by the interval methodology according to the results of dynamic simulation*

It is also possible to use the interval methodology based on the ČSN EN 15316-4-2 procedure for the evaluation of the designed source. For this methodology, you must first determine the interval length. Then, based on the selected interval length, obtain the necessary input data for the calculation. For more detailed evaluation (possible comparison) of the designed air heat pumps, it is necessary to determine the amount of energy needed to operate the object in greater detail than just obtaining the annual energy need. The rate of detail is given by the dependence of the heat pump performance parameters on ambient conditions. Sufficient details can be achieved by dynamic simulation.

The advantage of dynamic simulation is the use of measured climatic data in the building locality and the design of the building's schedule so the model is as close as possible to the actual building's behavior. As a result, you can obtain the necessary data for each need with the appropriate details.

For these reasons, a dynamic simulation of the monitored apartment building was created. The simulation was created in the DesingBuilder software and building data was obtained for the subsequent evaluation of the heat pumps in the hourly interval.

The energy need values for the individual heating intervals are shown in the graph depending on the outdoor

temperature. The graph also shows the performance dependence of the designed heat source (Stiebel Eltron WPL 34) on the outdoor temperature. The obtained values of the heating energy need from the dynamic simulation are not linearly dependent on the outdoor temperature. Therefore, a point cloud corresponding to an energy need at each interval and outdoor temperature is interspersed with a curve. The selected curve corresponds to the highest possible reliability value.

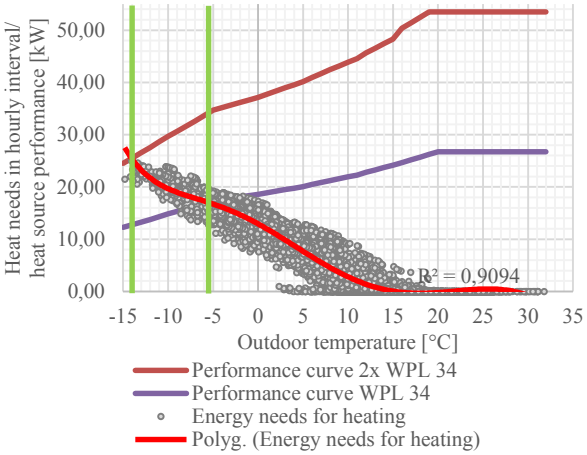

Fig. 3 – Energy need for heating corresponding to the outdoor temperature, STE WPL 34 heat pump performance curve

You can see the generated bivalence point on the graph above. This is the point of intersection of the heating need curve and the heat pump performance. From this point of intersection, the energy need for heating can be covered by an additional source - alternative bivalence, or the heat pump can operate in parallel with an additional heat source - parallel bivalence. The bivalent point temperature for the heat pump WPL 34 is around -5.5 ° C outdoor air, for the cascade of two heat pumps 2x WPL 34 the whole energy need of the building for heating is covered (the point of intersection is - 14.5 ° C but energy need for heating occurs under the heat pump's performance curve). Based on the data from the dynamic simulation, the cascade of 2 STE WPL 34 heat pumps can cover the entire energy need for heating in apartment building.

From the set of individual points corresponding to the hourly need of the building for heating, the frequency of occurring values of need during the evaluation of one year was compiled.

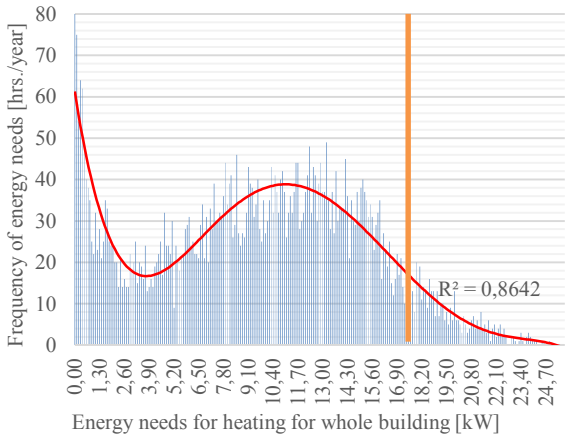

Fig. 4 – Frequency of the energy need for heating per year

E. Evaluation of Design Approaches

The most unfavorable results for designed heat pumps were based on an approach based on a simpler evaluation apparatus - ČSN EN 12831 with using tables. The results of this approach have allocated 8% to the bivalent energy source, while the interval method approaches have evaluated the proposed source as monovalent. Interesting are results from the dynamic simulation, when the annual energy need for heating in apartment building is based on the glazed areas, the orientation of the building, operation in the building, etc. about 37% less than the energy calculation according to the ČSN EN 12 831 methodology. The effect of profits in current buildings is not negligible at all, however, the issue of differences in dynamic simulation and normative approaches is not the subject of the article.

According to the results shown in the table, we can compare individual balance approaches more closely. Using the TNI 73 0531: 2014 methodology, the annual heat need for heating is the highest. When using the interval method based on energy need data from dynamic simulation, the heat balance is almost half. Balance values calculated according to other approaches are close to those calculated by TNI 73 0531: 2014. In particular, the simplified methods for calculating the energy need for heating do not consider the actual use of the building and internal profits from users, equipment, lighting. Furthermore, the solar profits of the glazed areas, which are significant in the case of our building, are not taken into account. Next, the dynamic simulation uses measured climate data and takes into account the mass and accumulation of the building, through which the energy need for heating is inversely proportional to the outdoor air temperatures.

TABLE I.
SUMMARY OF EVALUATION APPROACHES

annual energy need		Ch. III. A	Ch. III. B	Ch. III. C	Ch. III. D 2xHP	Ch. III. D 1xHP
for heating	[MWh]	86,40	100,5	92,66	54,27	54,27
for hot water s.	[MWh]	40,98	39,00	34,81	32,51	32,51
for both	[MWh]	127,38	139,50	127,47	86,78	86,78
heat pump	**[MWh]**	**117,19**	**138,90**	**120,15**	**86,76**	**82,47**
bivalent source	**[MWh]**	**10,19**	**0,60**	**7,32**	**0,014**	**4,31**
percentage share of bivalent	**[%]**	**8,0**	**0**	**5,74**	**0**	**4,96**

IV. TECHNICAL DESIGN OF THE MAIN HEAT SOURCE

Subsequently, I carried out a technical-economic study with a design of 4 variants of the heat source. I made the evaluation from the point of view of the total costs, which are decisive when choosing an object user.

A. Variant 1 - Gas condensing boiler

In the first variant as heat source is one 45 kW gas condensing boiler which represents a conventional heat source. Which can be placed in a technical room and is designed in type C with a concentric smoke outlet above the roof.

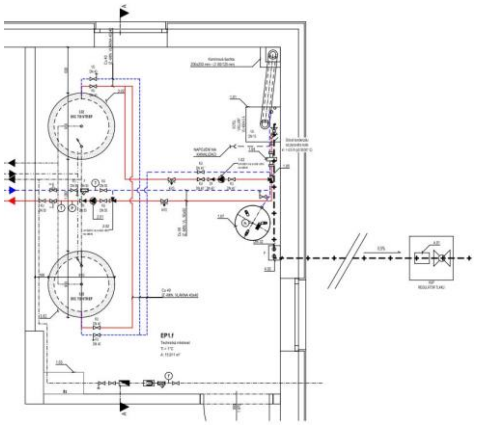

Fig. 5 - floor plan of a technical room with gas boiler

B. Variant 2 - Monovalent cascade of heat pumps with bivalent preparation of hot water supply

In the second variant, the previously mentioned cascade of two heat pumps WPL 34 is designed. According to the evaluation of the interval method, this source covers the monovalent need of the building for heating and preparation hot water supply with the help of bivalence.

The bivalent source is designed here not only to complement but also to achieve the required temperature of the hot water supply to be prepared. Heating cartridges are located in the hot water supply tanks.

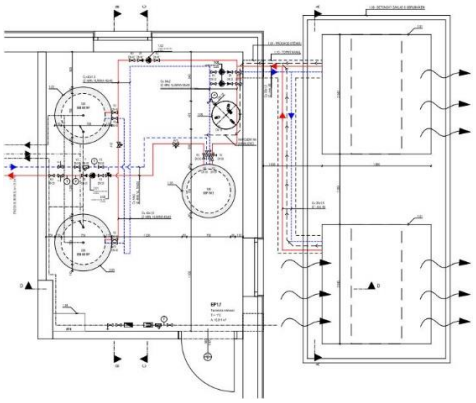

Fig. 6 - floor plan of a technical room with outdoor heat pumps variant 2

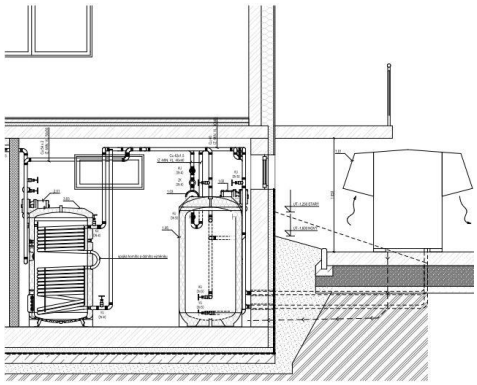

Fig. 7 – Cross section of a technical room with outdoor heat pumps

C. Variant 3 - Bivalent heat pump for heating, separate bivalent heat pump for hot water supply preparation

In the third variant, the cascade is replaced by only one STE WPL 34 source, which provides heating in bivalent mode. Other performance is covered by the designed cartridge in the storage tank. Hot water supply production is ensured by a second heat pump, which is designed according to ČSN 060320 standard and it is possible to consider continuous supply of thermal energy.

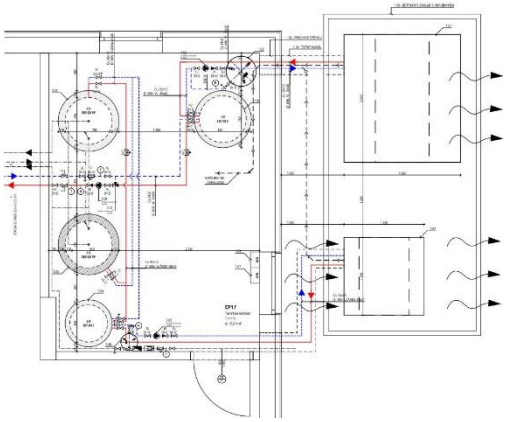

Fig. 8 - floor plan of a technical room with outdoor heat pumps variant 3

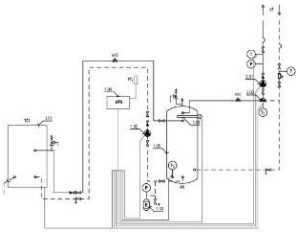

Fig. 9 - heating systems diagrams

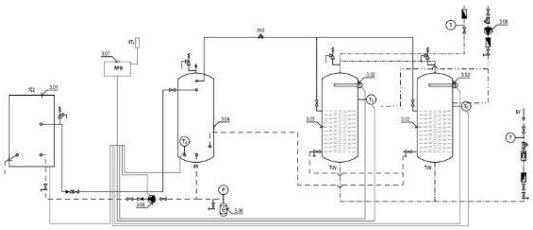

Fig. 10 - hot water supply systems diagrams

D. Variant 4 - Bivalent heat pump for heating, separate high temperature CO2 heat pump for hot water supply preparation

The further and last designed variant is the heating system from the previous variant and a high-temperature heat pump with CO2 refrigerant is designed for the hot water supply system. These heat pumps have their own specifics and are mainly used for hot water preparation.

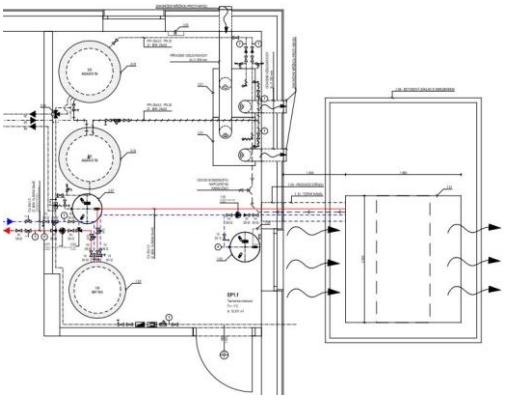

Fig. 11 - floor plan of a technical room with outdoor heat pumps, separate high temperature CO2 heat pump - variant 4

The specificity of these heat pumps is due to the properties of the CO 2 refrigerant shown in the P-h working diagram. Where the heat pump condensation zone does not cross the boundary curves, the thermal energy is not an isothermal process.

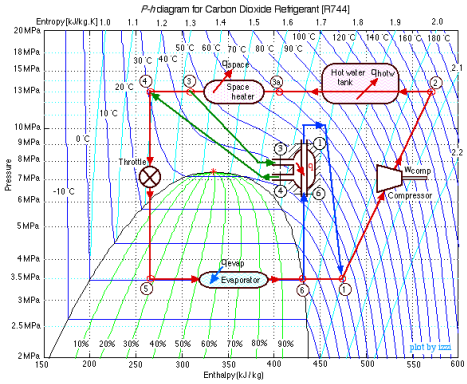

Fig. 12 - P-h working diagram with CO2 refrigerant [6]

Therefore, to achieve high efficiency, it is necessary to ensure sufficient cooling of the condenser with the help of the lowest inlet temperature of the heated substance on the hot side. For this reason, I designed the water connection straight from water supply thought stratification hot water supply storage tank.

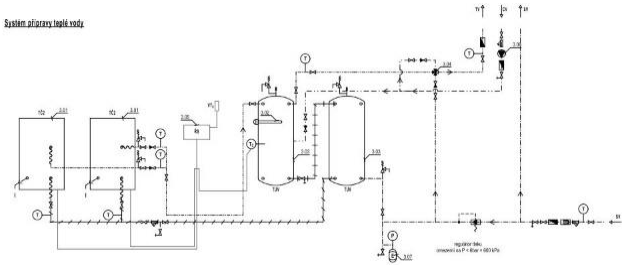

Fig. 13 - hot water supply systems diagrams with CO2 heat pumps

E. Summary results of the designed variants by the interval method

To determine the efficiency of designed heat pump sources and consequently the cost of consumed fuel, I performed a balance calculation using the interval method. The table shows the summary results of the individual variants with the used heat pumps. The lowest need for electricity requires a variant with a high temperature CO2 heat pump. Here we can also see the excellent seasonal heating factor of the hot water supply system. The difference is mainly due to the absence of the necessary electricity for reheating and the thermal disinfection required in the previous variants.

TABLE II.
SUMMARY RESULTS OF THE DESIGNED VARIANTS BY INTERVAL METHOD

		Variant 2	Variant 3	Variant 4
period	[year]	1	1	1
electrical energy need	[kWh]	39199	40949	32109
SCOP – heating system	[-]	-	2,34	2,34
SCOP – hot water system	[-]	-	1,56	3,75
SCOP – unified system	[-]	2,12	-	-
energy need for heat pump drive – heating system	[kWh]	-	20842	20842
energy need for heat pump drive – hot water supply system	[kWh]	-	10704	9 179
energy need for heat pump drive	[kWh]	31424	31546	30021
energy need for bivalent source – heating system	[kWh]	0	1628	1628
Energy needs for bivalent source reheating – hot w.	[kWh]	7224	7224	0,73
bivalent source energy need for thermal disinfection	[kWh]	551	551	459
Heat pump operational hours in hot water mode	[hr.]	682	1766	4020
Heat pump operational hours in heating mode	[hr.]	1482	2855	2855

V. ECONOMIC EVALUATION

For individual heat sources, I then quantified the investment costs depended on the acquisition of technical facilities. The most favorable option in these variants is the variant with a gas condensing boiler. In other variants, we can see a significant increase in costs, especially for heat pumps.

TABLE III.
INVESTMENT COSTS

		Variant 1	Variant 2	Variant 3	Variant 4
Heat source	CZK	70 800,-	804 800,-	623 000,-	636 400,-
	EUR	2 766,-	31 438,-	24 336,-	24 859,-
additional equipment	CZK	231 716,-	352 585,-	399 970,-	354 421,-
	EUR	9 051,-	13 773,-	15 624,-	13 845,-
other equipment	CZK	45 520,-	0,-	0,-	0,-
	EUR	1 778,-	0,-	0,-	0,-
other adjustment costs	CZK	54 002,-	53 627,-	53 627,-	47 289,-
	EUR	2 109,-	2 095,-	2 095,-	1 847,-
project documentation and engineering	CZK	24 122,-	72 661,-	64 596,-	62 284,-
	EUR	942,-	2 838,-	2 523,-	2 433,-
total investment costs without VAT	CZK	**426 160,-**	**1283672,-**	1141193,-	1100333,-
	EUR	**16 647,-**	**50 143,-**	44 578,-	42 982,-
total investment costs inc. VAT	CZK	**512 413,-**	**1550026,-**	1377626,-	1328569,-
	EUR	**20 016,-**	**60 548,-**	53 814,-	51 897,-

Furthermore, the cost of consumed fuel and mandatory inspections and service inspections are also determined.

TABLE IV.
THE COST OF CONSUMED FUEL AND MANDATORY INSPECTIONS AND SERVICE INSPECTIONS

		Variant 1	Variant 2	Variant 3	Variant 4
the cost of mandatory inspections and service inspections lifetime of 30 years	CZK	141 038,-	223 197,-	223 197,-	156 647,-
	EUR	5 509,-	8 719,-	8 719,-	6 119,-
the cost of consumed fuel per year	CZK	155 309,-	114 687,-	118 599,-	98 842,-
	EUR	6 067,-	4 480,-	4 633,-	3 861,-
total operating costs lifetime of 30 years	CZK	5185425,-	4401331,-	4460126,-	3784074,-
	EUR	202 556,-	171 927,-	174 224,-	147 815,-

From investment and operating costs, I then compiled economic models of cash flow. The first model evaluates the cash flow as simple without taking into account the discount rate. In the second, the discount rate is already taken into account, which is determined by the inflation rate of 2%. The order of convenience is the same in both variants.

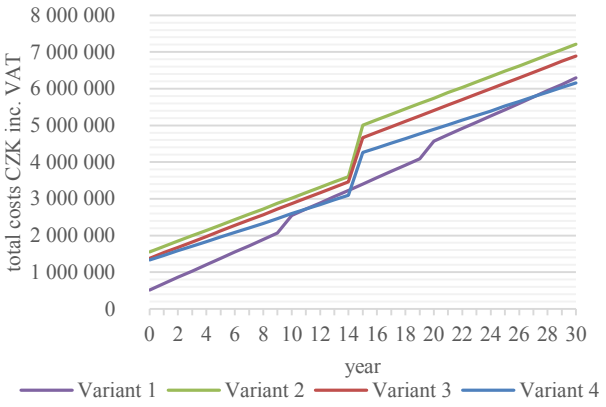

Fig. 13 - cumulative cash flow

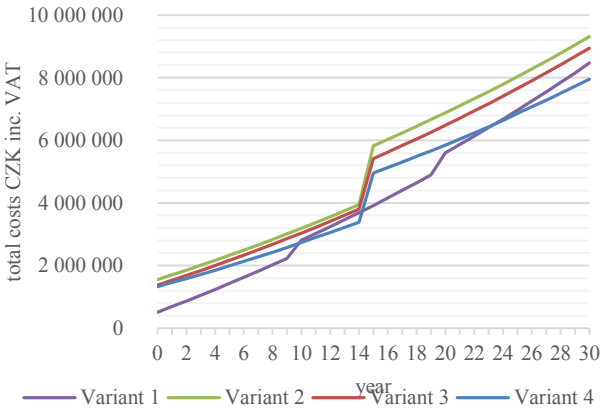

Fig. 14 - Discounted cash flow

Then I converted the resulting values to a price related to the specific need of the object. This interpretation of the resulting variants has the advantage especially in simple comparison with other heat sources such as long district energy.

TABLE V.
EVALUATION OF VARIANTS USING SPECIFIC COSTS

Annual energy need for building				327,39	GJ
Evaluated lifetime				30	years
		Var. 1	Var. 2	Var. 3	Var. 4
Specific cost of fuel related to the annual need of the building	CZK/ GJ	**474,-**	350,-	362,-	**302,-**
	EUR/ GJ	**18,5,-**	13,7,-	14,1,-	**11,8,-**
Specific cost from cumulative cash flow related to the need of the building for the evaluated lifetime	CZK/ GJ	641,-	**734,-**	702,-	**627,-**
	EUR/ GJ	25,0,-	**28,7,-**	27,4,-	**24,5,-**

VI. CONCLUSION

For the small apartment building was created the parametric study with four variants of the main heat source for heating and hot water supply production. Based on the evaluation methodology of the interval method it is possible to get a view about behavior of systems and design components for each variant.

Thanks to the designed elements and obtaining a detailed energy distribution among the heat pump and any bivalent energy source can be made economical evaluation, which is often the decisive factor in choosing between individual variants.

The most advantageous of the designed variants for the solved apartment building is the installation of high temperature heat pump with CO2 refrigerant for the hot water supply system preparation and a conventional heat pump with a bivalent source operating in parallel mode. The system designed in this way has an investment costs higher than a conventional source - a gas boiler, but operating costs during its lifetime of this system can save more than it investment costs difference. All designed heat source variants are under cost charged for the supplied heat energy from the long district energy system in 2016.

The operating and total costs for building heating by a heat pump are particularly affected by their design. This study showed that the design based on current design practice is the most costly variant. To save both investment and operating costs is necessary emphasize the quality of design work and the chosen assessment approach.

REFERENCES

[1] MATUŠKA, Tomáš. Alternativní zdroje energie. Praha: Evropský sociální fond, 2010. Skriptum. ČVUT v Praze, Fakulta strojní.

[2] ČSN EN 12831. Tepelné soustavy v budovách: Výpočet tepelného výkonu. 2005. Praha: ÚNMZ, 2005.

[3] TNI 73 0351. Energetické hodnocení soustav s tepelnými čerpadly: Zjednodušený výpočtový postup. Praha: ÚNMZ, 2014.

[4] Tepelná čerpadla Stiebel Eltron. In: STIEBEL ELTRON [online]. Praha: STIEBEL ELTRON spol. s r.o., 2015, 2015

[5] ČSN EN 15316-4-2. Energetická náročnost budov – Výpočtová metoda pro stanovení potřeb energie a účinností soustavy – Část 4-2: Výroba tepla pro vytápění, Tepelná čerpadla, Modul M3-8-2, M8-8-2. Praha: ÚNMZ, 2017.

[6] P-h diagram for Carbon Dioxide Refrigerant. In: Chapter 9: Carbon Dioxide (R744) The New Refrigerant (updated 3/17/2013) [online].

REHVA Federation of European Heating, Ventilation and Air Conditioning Associations
DIE PLANER. NETZWERK FÜR ENERGIE, UMWELT UND GEBÄUDETECHNIK
Lucerne University of Applied Sciences and Arts HOCHSCHULE LUZERN

Low temperature thermal network for heating and cooling purposes

Timotheus Zehnder, Msc in Business & Economics, BSc HVAC Engineer
Gregor Jeker, draftman in building technologie in subject heating, BSc HVAC Engineer
Professors: Prof. Dr. Zoran Alimpic, PhD, MBA, dipl. HVAC-Eng. FH
Stefan Mennel, BSc HVAC Engineer

***Abstract*— A low temperature thermal network can supply the heating and the cooling demand at the same time for a suitable geographical area. In a modern complex of buildings from a hospital such a solution could make sense from both ecological and economical perspective. With the example of the University Hospital Zürich, this article researches how such a thermal network solution could look like.**

***Index Terms*—low temperature thermal network for heating and cooling, maximized synergies, bidirectional energy flow, non-directed fluid flow, decentralized pumps**

I. Introduction

The basis for this scientific article is the paper "low temperature thermal network for heating and cooling purposes", which was written as a bachelor thesis in the course of the studies “Building Technology with Specialization in Heating-Ventilation-Cooling-Sanitary Engineering” at the Lucerne University of Applied Sciences and Arts in Switzerland.
The University campus in the centre of Zürich houses the University Hospital Zurich (USZ), the medical institutions of the University Zurich and the ETH Zurich, a technical University. The tight collaboration between them results in a great location advantage and gives Zurich and a national and international leading position in medicine. But some infrastructure deficiency could threaten this status. Therefore buildings of the USZ will be gradually renewed or renovated over the years 2024 to 2050. During the construction activities, the thermal energy supply will be renewed. A high efficient network solution is targeted. Therefore, a low-temperature thermal network should be investigated as a possible energy supply system.
This paper assesses the possible structure and functionality of a «low- temperature thermal network» for the completely renewed USZ-area. The goal is to formulate a network solution that allows for thermal integration with maximised synergies between heating and cooling as well across seasons. Since the cooling demand is becoming more and more dominating in the coming years, a high free-cooling proportion is targeted.

II. Preresiquites

A low temperature thermal network could be a suitable solution for the energy supply, if:

- the area has heating and cooling consumers, with little geographical distance between each other.
- high percentage of permanent heating and cooling demands are present that often coincide.
- the energy balance has significant heating and cooling demands and is ideally reasonably balanced over the year.
- a seasonal storage is feasible (e.g. with geothermal probes) or a full-year source or sink (as required) close to network temperature is available.
- optimal conditions are available to realize pipes with large diameters in the supply perimeter, where the ambient temperature is close to the average network temperature (to avoid expensive insulation).
- The necessary secondary temperature levels for heating and cooling purposes are close to the temperature of the main network (for both new and existing buildings)

For the completely renewed USZ area most of this preresiquites are fulfilled. Therefore, a low temperature thermal network can represent a suitable solution.

III. Energy and Power Analysis

The suggested form of thermal integration is ideal for the USZ area because despite seasonable fluctuations both constant heat and cooling demands occur (Figure 1: the heat demand is shown positive, the cooling demand negative, the grey shading shows the monthly residual demand). The energy and capacity analysis shows that for the year 2050, the year of completion, the cooling demand will be about twice as high as the heating demand.
This raises the question of how to deal with the excess heat.

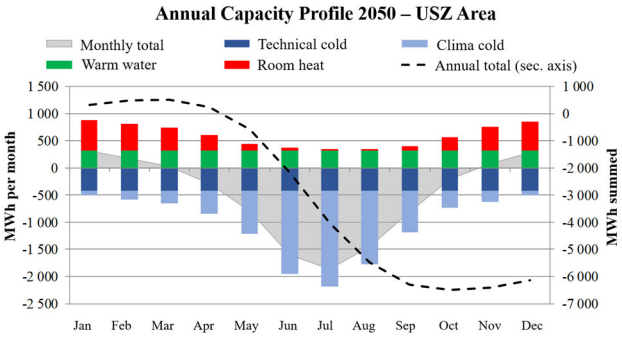

Figure 1: Energy and power analysis USZ area

IV. FUNCTIONALITY

A possible thermal grid solution is a non-directed two-pipe distribution network which's functionality does not rely on one main pump but on many decentralized pumps. This setting allows for self-supply of local network participants, that are equipped with heat-pumps and refrigerating machines, from the warm or the cold pipe, however necessary. In this system, the energy flows bidirectionally which means that network participants can function as both energy source or sink, thereby partially supplying each other. The network temperature varies seasonally between 3°C-19°C and is regulated through two geothermal probe fields and two central cooling stations. The authors formulate an operating strategy, through which, depending also on the size of the geothermal storage fields, the refrigeration can take place cost and energy efficient at low outside temperatures. The schematics below compare a conventional directed distribution network at the top to a non-directed distribution network with decentralized pumps at the bottom.

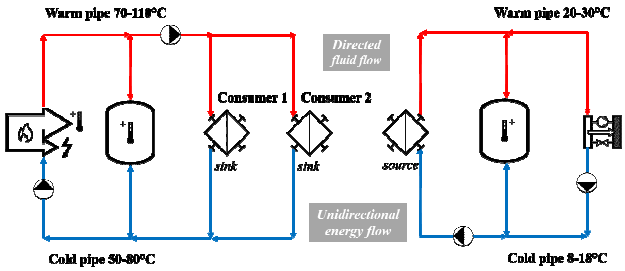

Figure 2: conventional directed distribution network

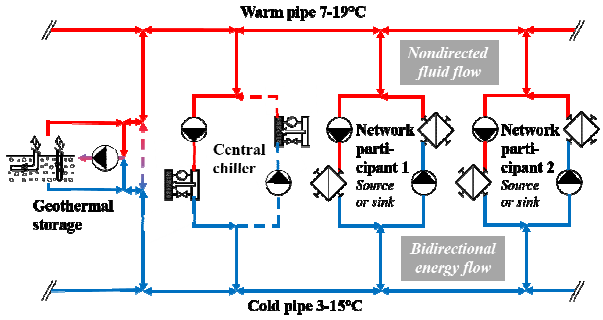

Figure 3: Non-directed distribution network

V. TEMPERATURES

Decisive for the functionality, the dimensioning of the pipes and the primary energy demand of the proposed low temperature thermal network are the following variables: system temperatures of the consumers, temperature level of the main network, temperature spread between warm and cold pipe and geothermal storage capacity. These variables are closely related and should not be considered in isolation.

A. System Temperatures of the Consumers

In principle, the supply temperatures for heating purposes should be as low as possible and the supply temperatures for cooling purposes as high as possible. If there is enough temperature spread across the consumers, little (by heat pump or refrigeration machine) to no (direct use) additional preparation is necessary to achieve the required system temperatures of the consumers.

B. Temperature Level of the main Network

If geothermal storage is used to compensate the seasonal demand fluctuations, network temperatures in the range of the average earth temperature shall be used to minimize losses in the ground. In order to run the system with water and minimize the risk of freezing evaporators, a minmum temperature of 2-4°C is recommended. The maximum temperature is selected so that a large proportion of the cooling demand can be supplied directly from the cold pipe without using a decentralized refrigeration machine.

C. Temperature spread between warm and cold Pipe

If the limits of the main network temperatures are defined, the storage capacity, and thus the size of the geothermal storage required, depends on the temperature spread between the warm and cold pipe. The following applies to the network: the greater the temperature spread, the smaller the mass flow for the transfer of the heating or cooling power. This gives smaller dimensions of the pipes and a lower required electrical pump power.

D. Geothermal storage capacity

The following applies to the geothermal storage: the greater the difference between the minimum outlet temperature for heating purposes and the maximum outlet temperature for cooling purposes, the greater the capacity per probe meter. Where the ecological and energetic optimum is, must be examined case-by-case. The selected four Kelvin in the case of the investigated network option represent only one possibility and can be further analyzed using a dynamic simulation tool.

Due to the above mentioned interrelationships, the system temperatures of the consumers hold a large optimization potential for the dimensioning and the energy demand of the entire low temperature thermal network. Especially for cooling consumers, modern devices and systems with high supply temperatures and maximum "free-cooling" proportion should therefore be used.

VI. GEOTHERMAL STORAGE

For the proposed low temperature thermal network, geothermal probes are investigated as a storage option. There are basically two options for determining the size of these geothermal probe fields:

A. Small Size Option: Heating

The geothermal probes are dimensioned to function as a heat source throughout winter. Thus the ground is cooled down during the heating period. Since cooling demand in summer ist larger than the heating demand in Winter, this means that some but not all consumers can be cooled directly from the cold pipe in summer. The rest is produced with air-cooled central refrigeration machines.

B. Large Size Option: Cooling

The geothermal probes are dimensioned in such a way that a large proportion of the cooling demand can be covered in summer. The waste heat can be sold to outdside consumers or exchanged efficiently via external coolers to the outside air in winter.
The advantages and disadvantages of the two options are shown in the following table:

Table 1: Advantages and disadvantages two size options

	Option Heating	Option Cooling
Advantages	• Low investment costs • Clear and simple management strategy of the probes • Expansion possible at any time	• Low operating costs due to better coefficients of performance of the refrigeration machine in winter • Excess waste heat can be sold more easily in the winter • Lower chiller capacity required
Disadvantges	• Operation of coolers and chillers in summer results in lower coefficient of performance and higher operating costs • Waste heat highly unlikely to be usable in summer • Higher performance of the central refrigerating machines in summer	• High investment costs • Management of the probes requires experience and good planning • Many probe fields in a thermal network are a big operating challenge

In order to make a decision regarding storage size, cost analyses, a simulation of the probes as well as clarifications regarding potential heat consumers and sales prices must be carried out. In the case of the USZ, it is generally recommended to start with the heating option, but to plan additional reserves for the final expansion.

VII. INTEGRATION OF THE NETWORK PARTICIPANTS

The schematic design in Figure 4 shows a possibility of how the hydraulics could look like for a network participant. Components shown in grey are optional.
The decentralized pumps are arranged in series. With complementary heat and cooling loads, only the residual energy demand of the network participant is drawn from the network.
The required heat and cooling energy is regulated via the mass flow at the heat and cooling consumers. The controlled variable is the temperature difference across the consumers.
On the cold side, the group pumps draw the required cold from the technical storage unit. The upstream pump serves as a control element for the temperature difference on the secondary side.
On the warm side, the warm water and the heat delivery systems are integrated in parallel. A high degree of efficiency is achieved by separating and optimizing the individual heat consumers. Not illustrated in the schematic design are the detailed group circuits and possible decentralised storage units.

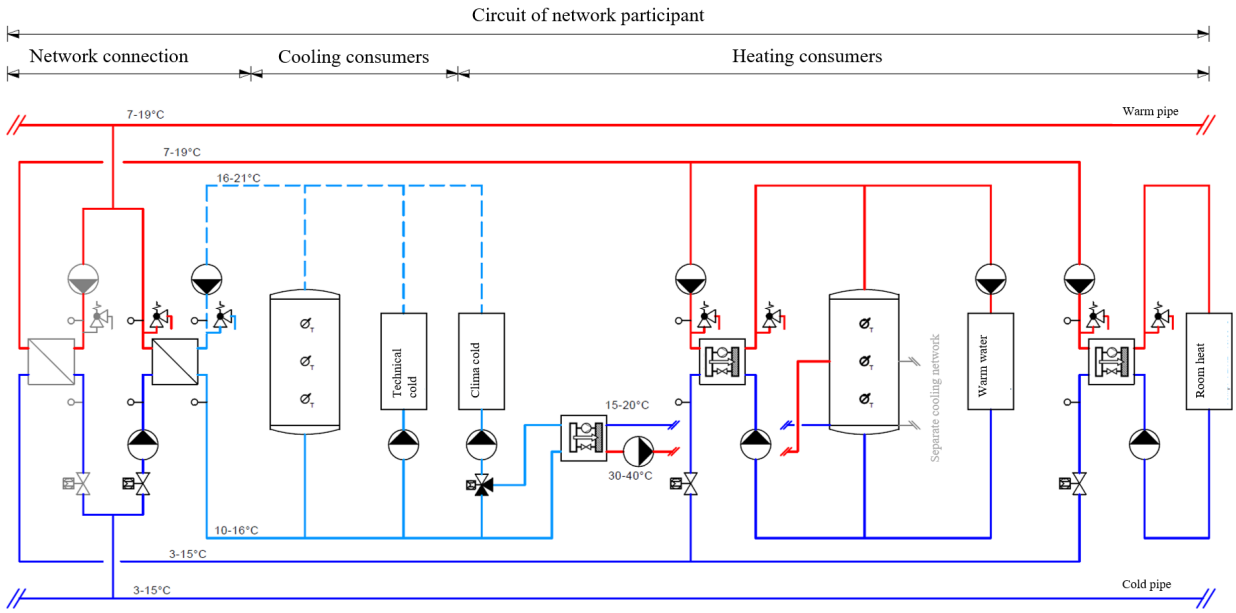

Figure 4: scheme of the intergration of network participants

VIII. SUMMARY INVESTIGATED LOW TEMPERATURE NETWORK

Figure 6 below shows a network option for the investigated USZ area. By using the network funcionality described above and the seasonal storage (GTP 1 & 2), the waste heat generated in summer can cover the entire heat demand throughout the year. This means that no additional central source is required (the excess heat from summer is the only heat source). With decentralized heat preparation, a high degree of efficiency is targeted by differentiating the consumers according to system temperatures and keeping these as low as possible. Chilled water is supplied most efficient by using centraslised refigeration machines with turbo compressors (CRM 1 & 2). The waste heat from these cooling plants is either discharged to adjacent areas in a hydraulically separated recooling network or to the environment via hybrid coolers. The aim is to achieve the highest possible "free-cooling" proportion within the low temperature thermal network. Due to the low maximum cold pipe temperature of 15°C, only dehumidification operation requires the use of decentralized refrigeration machines, whose high-quality waste heat is used directly for warm water preparation.

IX. TOPOLOGY INVESTIGTION

The optional realization of sections 11 and 12 (see Fig. 6) allows various topology options to be investigated. Using the network calculation and simulation tool STANET, an energetic and economic comparison between the realization of a tree, ring or mesh structure is carried out by simulating the electrical pumping energy of different load cases (winter, summer, spring).

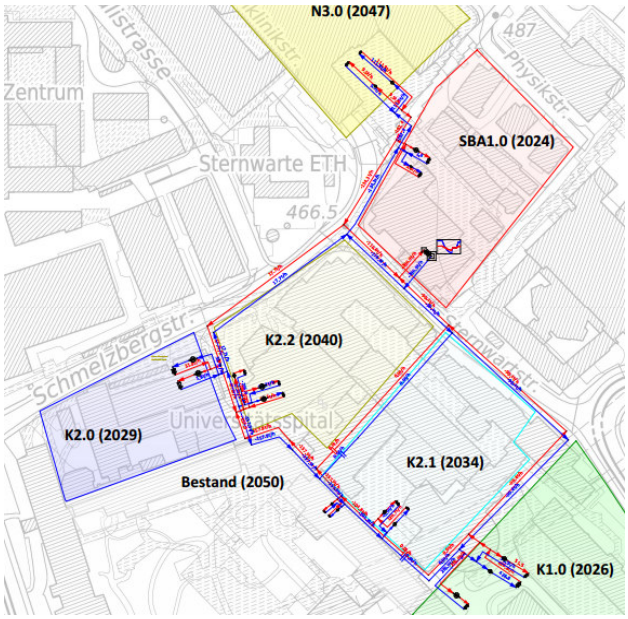

Figure 5: STANET topologie

The mapping and simulation in STANET (see Fig. 5) allowed for appropriate dimensioning of the network and for the various load cases to be investigated and confirmed.

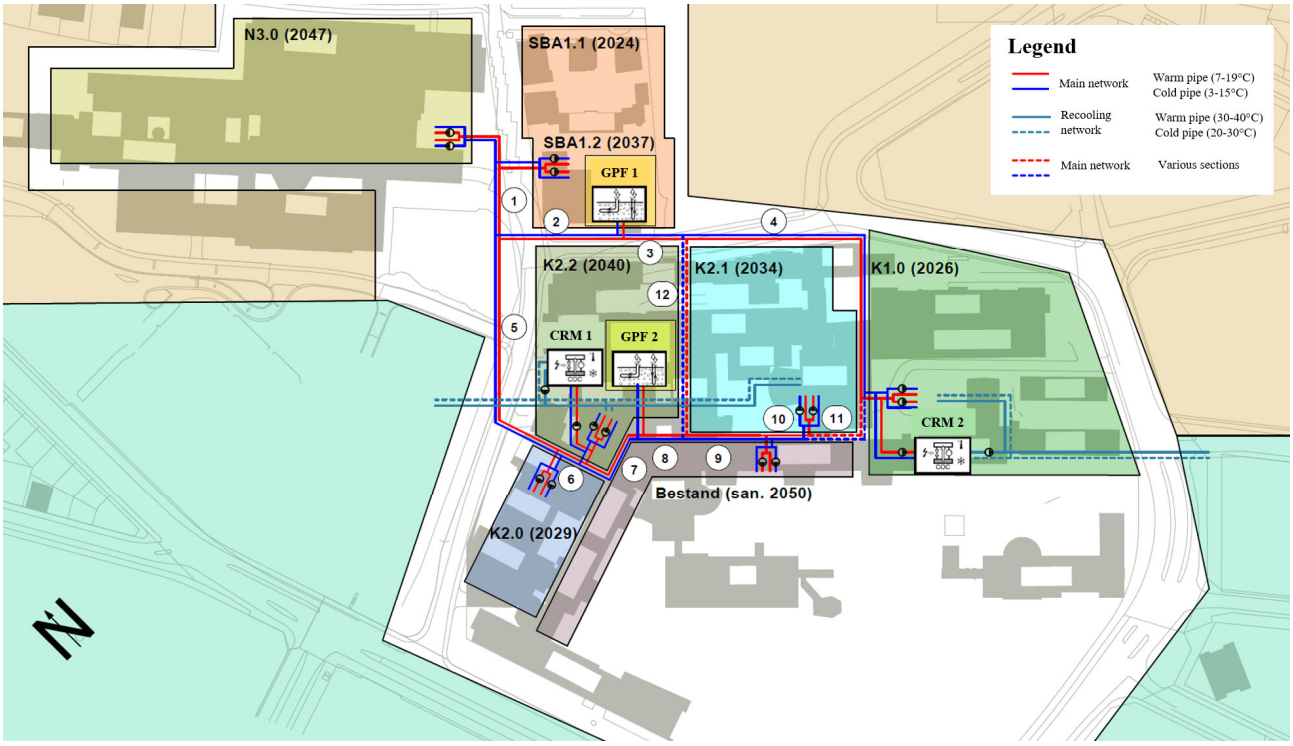

Figure 6: network option for the investigated USZ area

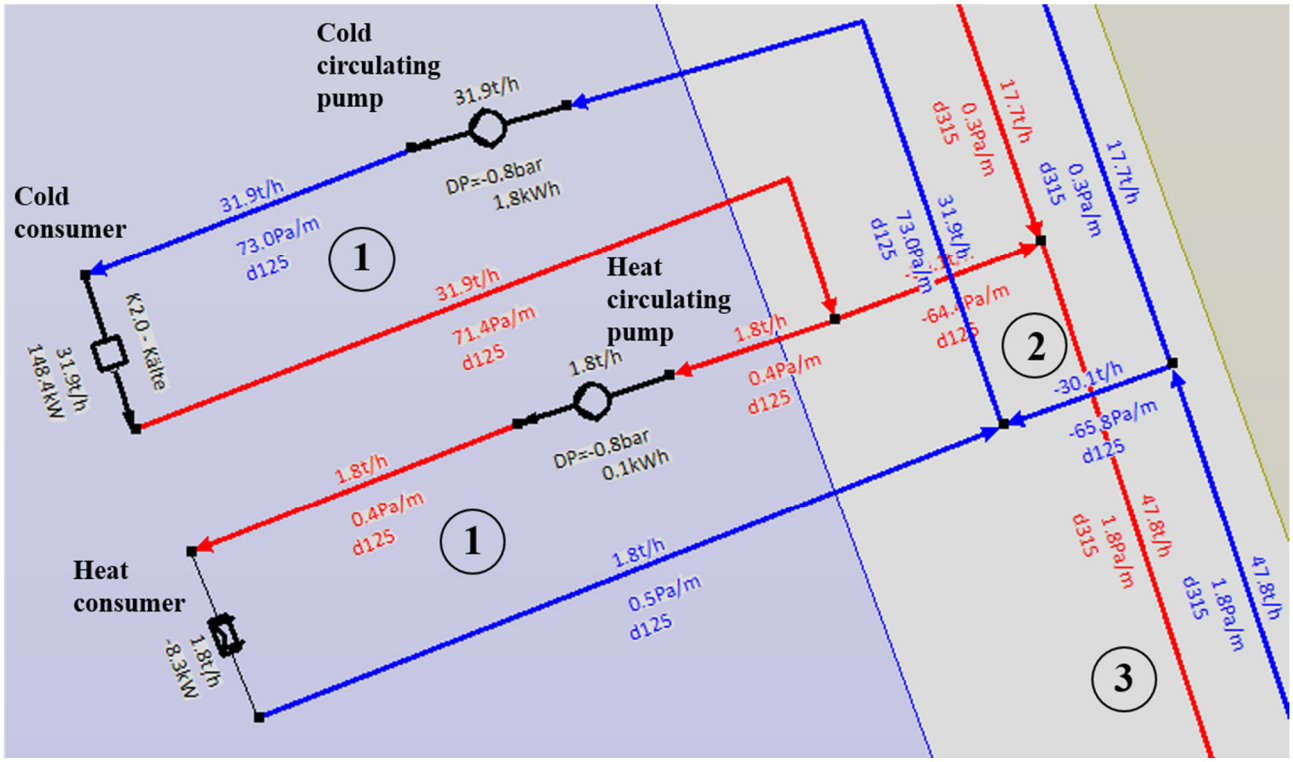

Figure 7 STANET-Extract of a participant for a summer case

The figure above shows a simulation result of a network participant in a summer case. There is an excess cooling demand. A small part of the waste heat from the cooling consumer supplies the heat consumer. The non-usable waste heat is led into the main network. The different network options (tree, ring or mesh structure) were realized and analyzed in sections 11 and 12 by means of an optionally opened or closed gate valve.

As Table 2 shows, a tree structure makes the most economic sense in this application. Nevertheless, a simple ring structure with various ramifications is recommended for redundancy and energy considerations. A mesh structure, realized by an additional ring closuare, offers hardly any advantages with regard to the required electrical pumping energy, but is associated with considerable additional investments.

The simulation also shows that the choice of topology (tree, ring or mesh structure) has no effect on the hydraulic functionality of the network. This means that the supply of all consumers is guaranteed at all times with all investigated network structures. A structural change or a network expansion, for example supplying the University or ETH Zurich, is thus possible.

Table 2: Results of the topologie investigations

Results of the topologie investigations ***Electrical pump power***	**Tree structure (11 & 12 not realized)**			**Ring structure (11 realized, 12 not)**			**Mesh structure (2 rings) (11 & 12 realized)**			
Load case	Summer	Winter	Spring	Summer	Winter	Spring	Summer	Winter	Spring	
Thermal energy	94	73	51	94	73	51	94	73	51	*[MWh/d]*
Electrical pump energy (excl. probepump)	2'215	1'613	1'079	2'184	1'603	1'073	2'182	1'592	1'072	*[kWh/d]*
Ratio electrical / thermal	2.35	2.21	2.09	2.32	2.19	2.08	2.32	2.18	2.08	*[%]*
Annual energy savings				**-4'700**			**-6'024**			***[kWh/a]***
Annual cost savings (0.15 CHF/kWh)				**-705**			**-904**			***[CHF/a]***
Additional investment (1500 CHF/meter)				**105'000**			**262'500**			***[CHF]***
Amortization (0% interest)				**149**			**291**			***[years]***

X. Energy flow analysis

The energy flow analysis of the investigated network option shows that due to the thermal network and the seasonal storage, about half of the used energy can be converted within the system. Maximum use of synergies and short supply routes allow an overall ecological picture to be drawn. However, challenges such as temperature and pressure fluctuations caused by decentralized pumps still have to be mastered before such energy networks can be implemented.

XI. Challenges

Based on findings from existing networks and the current state of research, there are still some challenges to overcome for the proper operation of low temperature thermal networks. As an example, the decentralized pumps can cause pressure fluctuations in the network, which can result in supply shortage of consumers. In order to avoid this supply shortages, suitable pressure conditions in the network should be sought. Temperature islands can also occur in the network. The temperature level in a network section swings in one direction if insufficient media flow is guaranteed. For a sufficient energy flow at the consumers, this can result in massively increased electrical energies of the pumps. Ongoing new research results are published on the challenges mentioned above.

XII. Conclusion

The investigation of a low temperature thermal network as an energy supply system for the USZ shows that a non-directed two pipes, bidirectional network with a geothermal storage for a modern hospital area is a realistic alternative to conventional heating and cooling by means of a directed four pipe system.

Due to a high degree of synergy utilization, the energy balance is positive and enables a very good eco-balance with the corresponding type of electricity generation. Since the USZ is a large source of waste heat over the year, nothing stands in the way of expansion in the sense of thermal area integration.

It should not be overlooked, however, that the unbalanced annual balance means that a large proportion of the waste heat has to be discharged and that an exergetically high degree of utilisation is not always achieved.

Although the cool main network temperature is ideal for cooling purposes and for geothermal probes, it also leads to lower efficiency in decentralized heat pumps. However, since the cooling requirement predominates and the waste heat at an exergetically high level is generated primarily when it can hardly be used (summer half-year), the solution presented with low network temperatures for a high proportion of free-cooling appears to be the most sensible.

Should the solution for the University Hospital Zurich be pursued further, the challenges mentioned in the paper must be tackled step by step in the next planning phases. In particular, the integration of the network participants and the system temperatures have a significant influence on the functionality and efficiency of the low temperature thermal network. The considerations and investigations presented in this paper ideally offer solid support.

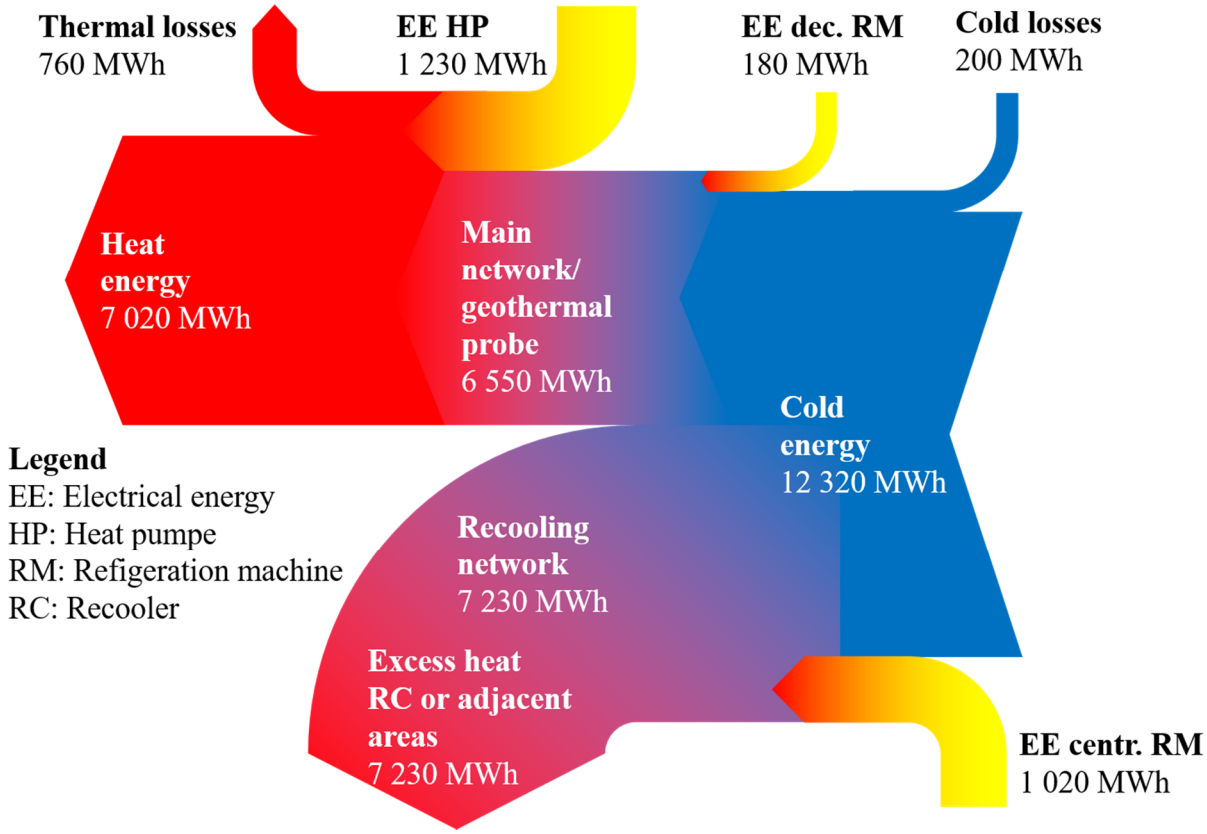

Figure 8: Energy flow analysis of the investigated energy network

REHVA
Federation of European Heating, Ventilation and Air Conditioning Associations

Data-Driven Predictive Control for Heating Demand in Buildings: Method Development and Implementation

Cristina Jurado López[1], Laure Itard[2], Paul Stoelinga[3]

[1]Delft University of Technology
Delft, The Netherlands
Cristina.Jurado.L@gmail.com

[2]Delft University of Technology
Delft, The Netherlands
L.C.M.Itard@tudelft.nl

[3]Deerns Nederlands
Rijswijk, The Netherlands
Paul.stoelinga@deerns.com

***Abstract*— The prediction of heating demand in buildings is normally performed by physic-based simulation tools which require a large number of input parameters, which are difficult to estimate accurately in practice. This results in a very time-consuming task that requires tedious expert work, in addition it reduces the accuracy of the heating demand prediction. This research aims to simplify the collection and estimation of parameters by using simple, flexible and fast data-driven statistical models to obtain the heating demand. This increases the flexibility of the controller towards future changes in the energy systems such as building- or installation renovations or placing external shadings or the introduction of new energy sources. This last characteristic is specifically relevant in the current context demand side management and integration in smart networks. Several regression models are developed, validated and compared. The simplicity, high accuracy and physical meaning of these models make it possible to automate the self-training of the model (machine learning) and use the model for the purposes of prediction of thermal energy demand at building and district level, predictive control, failure prediction of installations and parametric analysis.**

***Index Terms*—Data-driven predictive control, failure prediction of installations, machine learning, multivariate regression models, parametric analysis, prediction thermal energy demand, Smart Energy Networks.**

NOMENCLATURES

Symbols

C_i	Parameters' coefficients [-]
i	Sub index for each of the parameter coefficients [-]
T_{ground}	surface ground temperature [ºC]
T_{indoor}	indoor air temperature [ºC]
$T_{outdoor}$	outdoor air temperature [ºC]
$T_{out\ AHU}$	Outlet air temperature Air Handling Unit (AHU) being introduced in the building [ºC]
$T_{indoor\ surfaces}$	Indoor surface temperature of the surfaces with major thermal mass [ºC]
t	Upper index for variables used at real time instant.
t-n	Upper index for variables used at 'n' hours before the real time instant variables.
V_{wind}	Wind velocity [m/s]

I. INTRODUCTION

The built environment consumes more than 40% of the global energy used and contributes up to 30% of the global greenhouse gasses emissions [1]. Space and water heating in European households accounts for 79% of the total final energy use (192.5 Mtoe) and 84% of that heating is still generated from fossil fuels while only 16% is generated from renewable energy [2]. In order to realise the European climate and energy goals, the heating sector in buildings must sharply reduce its energy consumption and cut its use of fossil fuels [2].

The transition from current energy systems (based on fossil fuel and nuclear energy) towards future energy systems (based on renewable energy systems) leads to an increase in the fluctuation of energy supply. As a result, the current energy system needs to be transformed into a smart energy system which focuses on the integration of electricity, heating, cooling and transport sectors, and on utilising energy demand fluctuation together with the storage of energy [3]. This implies the integration of different energy grids (electricity grids, district heating and cooling grids, gas grids and other fuel infrastructures) and the coordination between these grids to achieve the optimal solutions for each individual sector and for the overall system storage [3].

The coordination and integration of the different energy grids is done through smart controllers. These controllers need to have enough flexibility to be able to allow more renewable energy sources to be integrated in the energy system, as well as to cope with building renovations which affect the demand side (buildings changing from high to low temperature supply).

Data-driven controllers allow a higher flexibility than rule-based or physics-based controllers since the algorithm can be readjusted to the building and/or system characteristics (eg. new renewable energy sources incorporated in the grid/building, building renovations, changing outdoor conditions affecting the demand of the building such as heat island effect or external shadings, etc.). This research focuses on the development and implementation of a data-driven model for the predictive control of the heating demand in buildings.

The prediction of heating demand is normally performed by physic-based simulation tools which give good estimations of the thermal energy demand of the building but require a large number of input parameters (a minimum of 200 parameters), which are difficult to estimate accurately in practice. At a district level, the number of buildings involved increases, which grows the number of parameters to be estimated. This results in a very time-consuming task that requires tedious expert work, in addition it reduces the accuracy of the heating demand prediction. This research aims to simplify the collection and estimation of parameters,

getting a better insight of the influence of the different parameters in the building response and increasing the flexibility of the controller towards future changes in the energy system.

This research uses emulated and measured data from 2 different building typologies. The study is subdivided in the following 2 parts.

Part 1: development of two theoretical models based on an emulated data set using 3 different university buildings.

Part 2: validation, adjustment and implementation of the theoretical model based on actual (measured) data set using an office building.

In part 1, two multivariate linear models are developed based on a simulated data set obtained by a physics-based simulator. The first model is defined by the outdoor air temperature and the indoor surface temperature. This last parameter is normally not available in real data sets, therefore this first model was upgraded towards its implementation into practice by replacing the indoor surface temperature by other available data. This led to a second model defined by measurable weather data, indoor air temperatures and the occupancy of the building. Both equations show a high predictive potential and accuracy level.

In part 2, the theoretical model is adjusted to a specific building by using actual measured data set. In a later research, the adjusted model is used to make a parametric analysis where the occupancy influence on the heating demand of an office building is quantified.

A. *Prediction model classification and comparison techniques*

There are several categorisation systems to classify the different existing prediction methodologies [4]–[8]. Most of the authors classify these methods into white-box models (law-driven models based on physical methods), black-box models (data-driven models based on statistical methods) and grey-box models which use limited building physics in combination with statistical methodologies [6], [7], [9], [10]. The selection of the optimal prediction technique for buildings is determined by the optimal complexity level which is defined by the information available (building, installation and operating characteristics) [11]. The selection of a more complex model (higher number of physical equations) does not mean a better outcome. The more complex the model, the higher the amount of parameters needed. When these parameters are unknown, they need to be estimated, increasing the input data errors which reduces the output accuracy. Therefore, a more complex model will only be more accurate than a simpler one when all the required parameters are known. This limits the complexity of the building model to the information available.

B. *Case studies*

The first part of the study was developed within the framework of Smart Grid Innovation Programme (IPIN) in collaboration with Delft University of Technology (TU Delft) and Deerns. Three TU Delft buildings with different characteristics were used to build the model on emulated data sets. These buildings are: (1) 3mE (Faculty of Mechanical, Maritime and Materials Engineering), (2) IO (Industrial Design) and (3) TPM (Technology, Policy and Management). 3mE is the oldest of the three buildings, it was built in 1953 and renovated in 2003 (TU Delft Energy Monitor, 2017). It has an architectural design where facades and large windows are dominant. IO is dating from 1973 and was renovated in 2000 (TU Delft Energy Monitor, 2017). Its shape is more compact and the facades have less windows. TPM is the newest building and has the most compact shape of the three buildings, it was built in 2001. The three buildings are modelled as heavy buildings with a specific thermal mass in the range of 300-600 kg/m2 floor. The resulting emulated data are needed to develop and test the method.

The second part of this study was developed with measured data of an office building. This is a light and compact building with a façade composed of glass and wooden panels. The climate control system is semi-automated with limited user influence.

II. METHODOLOGY

A. *Statistical method*

The statistical method used in this study is a multivariate regression. This method is used in several publications to build models for the energy demand prediction [12]–[14] and to analyse the most influencing parameters on actual heating demand [15]. The functional form of this approach is expressed in equation 1. These models combine the different independent variables according to a linear or polynomial relation between the independent and dependent variable.

$$Q(h) = constant + \sum_{i=1}^{n} C_i \cdot X_i \quad (1)$$

Where $Q(h)$ is the hourly thermal energy demand of a specific building in a specific operation mode, C_i are the corresponding coefficient of the dependent variable, X_i is the dependent parameter and i the index of dependent variables selected for the model.

B. *Statistical validation*

Each model is statistically validated to analyse the significance of the model and avoid an over-fitted model. The validation is done by applying a statistical search procedure, at each step a variable is introduced. FIGURE 1 summarizes the search procedure and criterion used for a correct selection of predictor variables. At each step, the residuals of the data set are analysed, and the significance level of both the variables' coefficients and the total model are quantified [16].

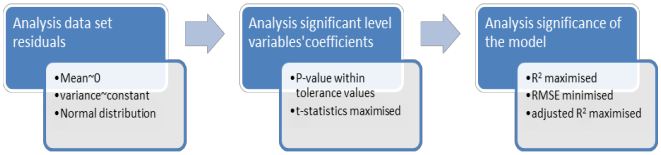

FIGURE 1 FLOW SCHEME OF THE SEARCH PROCEDURE AND STATISTICAL CRITERIA USED FOR PREDICTOR SELECTION

C. *Definition of the number of models and equations*

Within this paper the terms models and equations are used with a different meaning. One model will differ

from another when different independent variables are considered. Each model will lead to different building-specific and operating mode-specific equations which will have the same independent variables but different coefficients. This is because buildings, system characteristics or operating modes affect the correlation between the variables. Therefore, every building and operating mode will have a characteristic equation for each model. The characteristic equation is obtained by calibrating the model with the corresponding data set. The simplicity of the calibration procedure makes it possible to automate the process and readjust the equation to possible internal or external changing conditions. The buildings studied present three different operating modes: (A) weekdays during opening hours, (B) weekends during opening hours, (C) closing hours.

Every season may need a different multivariable model. Two different models are differentiated for heating demand prediction: (1) moderate weather months (heating and cooling operating during the same day) and (2) cold weather months (only heating). This is because during moderate weather months, different variables may influence when both heating and cooling are operating during the same day (due to the thermo-dynamic effect on the wall and humidity influence). This phenomenon needs to be further investigated. This study considers only cold months.

The variables can be easily adjusted for buildings that are affected by other indoor (such as building or installations renovations) or outdoor phenomena (such as heat island effect, external shadings or new energy sources). This makes the model very flexible to changes. This is shown in model 3.

D. Data set selection

The model developed in the first part of the study uses the emulated data set generated by the physic-based tool corresponding to the buildings being tested in IPIN at TU Delft campus. The advantage of using emulated data is the possibility of simulating and studying different scenarios. The emulated data set selected corresponds to the season when only heating is required, avoiding the influence of cooling. For the sake of simplicity we present in this paper only the results corresponding to operating mode (A) which is built by selecting only the hours corresponding to weekdays during opening hours. This data set corresponds to a total of 1096 hours which corresponds to the total opening hours during weekdays from October 2015 until January 2016. From this data set, the first 75% (~2 months) are used to train the model and the last 25% (~3.5 weeks) are used to validate the model.

The models in the second part of this study are built on the measured data set corresponding to an office building. The actual data set selected also corresponds to the winter season (only heating mode operative) and accounts for 126 hours. The model presented in this paper correspond to operating modes (A) weekdays during opening hours.

E. Model development and selection of parameters

The building's heating demand depends on the amount of heat transferred through the building, produced and accumulated in the building. In order to make a physically meaningful model, the selection of parameters is based on the thermal energy balance of a building. The heat fluxes can be divided in 6 main categories: internal heat gains (Q_{int}), solar heat gains (Q_{sol}), envelop losses/gains ($Q_{gr} + Q_{env}$), ventilation (Q_{vent}), infiltrations (Q_{inf}), and the heat accumulated in the indoor thermal mass ($Q_{th\,mass}$). The thermal mass accumulates the heat absorbed by the solar radiation, internal heat gains and indoor temperature. For insulated buildings, this heat flux can be assumed to be transferred only with the indoor climate through the total surface of the indoor thermal mass. The thermal energy balance described is expressed by equation 2.

$$Q_h = Q_{gr} + Q_{env} + Q_{inf} + Q_{vent} + Q_{th\,mass} + Q_{sol} + Q_{int} \quad (2)$$

This equation is expressed partly as function of the temperature differences corresponding to each heat flux as expressed in equation 3.

$$\begin{aligned} Q_h \left[\frac{W}{m^3}\right] &= constant \\ &+ C_a \left(T_{ground} - T_{indoor}\right) + C_b \left(T_{outdoor} - T_{indoor}\right) + C_c V_{wind} \\ &+ C_d \left(T_{out\,AHU} - T_{indoor}\right) + C_e \left(T_{indoor\,surfaces} - T_{indoor}\right) + C_f\, Q_{sol} \\ &+ C_g\, Q_{int} \end{aligned} \quad (3)$$

Equation 3 can be transformed towards independent temperatures according to equation 4.

$$\begin{aligned} Q_h \left[\frac{w}{m^3}\right] &= constant + C_1 \left(T_{outdoor}\right) + C_2 \left(T_{indoor}\right) + \\ C_3 (V_{wind}) &+ C_4 \left(T_{ground}\right) + C_5 \left(T_{out\,AHU}\right) + C_6 \left(T_{indoor\,surfaces}\right) + \\ C_7\, Q_{sol} &+ C_8\, Q_{int} \end{aligned} \quad (4)$$

Where T_{ground} is the surface ground temperature, T_{indoor} indoor air temperature, $T_{outdoor}$ outdoor air temperature, Tout AHU the outlet air temperature coming from the Air Handling Unit (AHU) and $T_{indoor\,surfaces}$ the temperature of the indoor surfaces. C_i are the coefficients corresponding to each parameter which now differs from the ones indicated in equation 3. For this reason are indicated with a difference index.

The resulting model is defined by weather data and measurable temperatures. The coefficients of the variables correspond to the building and systems characteristics and they are obtained by training the model with historical data at building level. In this way, the model limits the demand of measured data to a few measurable parameters, leaving out all parameters related to building & system characteristics (which are unknown in most of the cases). Note that parameters related to building & system characteristics are left out as an input, but their influence is included in the coefficients of the characteristic equation. This means that each building has a characteristic equation for each operating mode. Moreover, the equation can be easily recalibrated (coefficient adjustments) when there are external or internal characteristic changes (eg. improvement of insulation value, installation changes or different energy sources).

III. RESULTS

The general model described in equation 4 is adjusted to different models with different independent variables.

Model 1: dependent on 2 parameters

This model, using only outdoor and indoor temperatures shows that, using emulated data with only 2 parameters, the heating demand can be well predicted, showing a high fitting profile with respect the data set. In actual cases one of the parameters (indoor surface temperature) is generally not available/measured. Therefore, a second model is developed by replacing the indoor surface temperature by other relevant and available parameters.

Model 2: Towards implementation into practice

The indoor surface temperature is replaced by past (a few hours before) and present internal heat gains and solar radiation. These variables are known to have an high impact on the thermal behaviour of the building and are therefore proposed as replacement of the indoor surface temperatures. This model is tested on emulated data.

Model 3: model tested on actual data

Model 2 is used as basis, but the independent parameters are modified in order to match the types of data measured. The coefficient of the model are determined using actual data for an office building.

A. *Model 1: Model dependent on 2 parameters.*

This model is used to generate three equations, one for each of the emulated data set of the three TU Delft buildings (IO, 3mE and TPM). In the three buildings, the variables $T_{indoor\ surfaces}$ and $T_{outdoor}$ are the most influencing parameters on the hourly heating demand profile. Only including these two variables in the model, the three buildings reach a goodness of the fit (adjusted R^2) with respect to the simulated data set between 96 – 99%. Equation 5 shows the general equation of model 1 for the three buildings.

$$Q_h\left[\frac{w}{m^3}\right] = constant + C_1\left(T^t_{outdoor}\right) + C_2\left(T^t_{indoor\ surfaces}\right) \quad (5)$$

This model shows that the most influencing parameters on the hourly heating demand of the building are the envelop characteristics and the thermal mass of the building. The high accuracy of this model makes this equation able to be implemented into practice. However, the temperature of the indoor surfaces is a parameter which is generally not available in the real case study. When the variable $T_{indoor\ surfaces}$ is neglected from the equation, the fitting profile for the three buildings decreases to 79.42% for IO, 52.9% for 3mE and 63.52% for TPM with respect to the emulated data set, respectively. As a result, the indoor surface temperature should be replaced by known variables to be able to reach enough accuracy for the potential applications.

B. *Model 2: Model towards implementation into practice*

In order to build a model that could be applied using actual data instead of emulated ones, the selection of parameters is restricted to the most commonly measured data. Equation 6 presents the general equation for model 2 for the three TU Delft buildings.

$$Q_h\left[\frac{w}{m^3}\right] = constant + C_1\left(T^t_{outdoor}\right) + C_2\left(T^t_{indoor}\right) + C_3\left(V^t_{wind}\right) + C_4\left(T^t_{ground}\right) + C_5\left(T^t_{out\ AHU}\right) + C_6\left(Q^{t-1}_{int}\right) + C_7\left(Q^{t-3}_{sol}\right) + C_8\left(Q^t_{sol}\right) + C_9\left(Q^t_{int}\right) \quad (6)$$

In this case, the indoor surface temperature is replaced by the internal heat gains and solar radiation a few hours before. In this case study, the internal heat gain is delayed by 1 hour. When using the global horizontal solar radiation, this parameter is delayed by 3 hours (as it simulates the solar radiation profile on the inclination plane at 14PM). The delay time of these variables will vary on every case study and will depend on the thermal mass of the building (lower thermal mass, less delay time). This replacement will be more significant in buildings where the internal heat gains and solar radiation have a higher influence.

This model shows a fitting profile (adjusted R^2) of 83.2% for 3mE, 73.5% for TPM and 90.7% for IO with respect to the simulated data set, respectively. Figure 2 shows the fitting profile corresponding to this model (model 2) for both historical (the emulated data used to determine the coefficients) and predicted data (the emulated data used only for validation). For 3mE and TPM, the mismatch increases on Mondays. This is because the building cools down further during weekends than during weekdays, leading to a higher influence of the indoor surface temperature (parameter replaced). Therefore, the fitting can be improved by making 2 different regression equations: (1) including only Mondays and (2) including all weekdays from Tuesday until Friday.

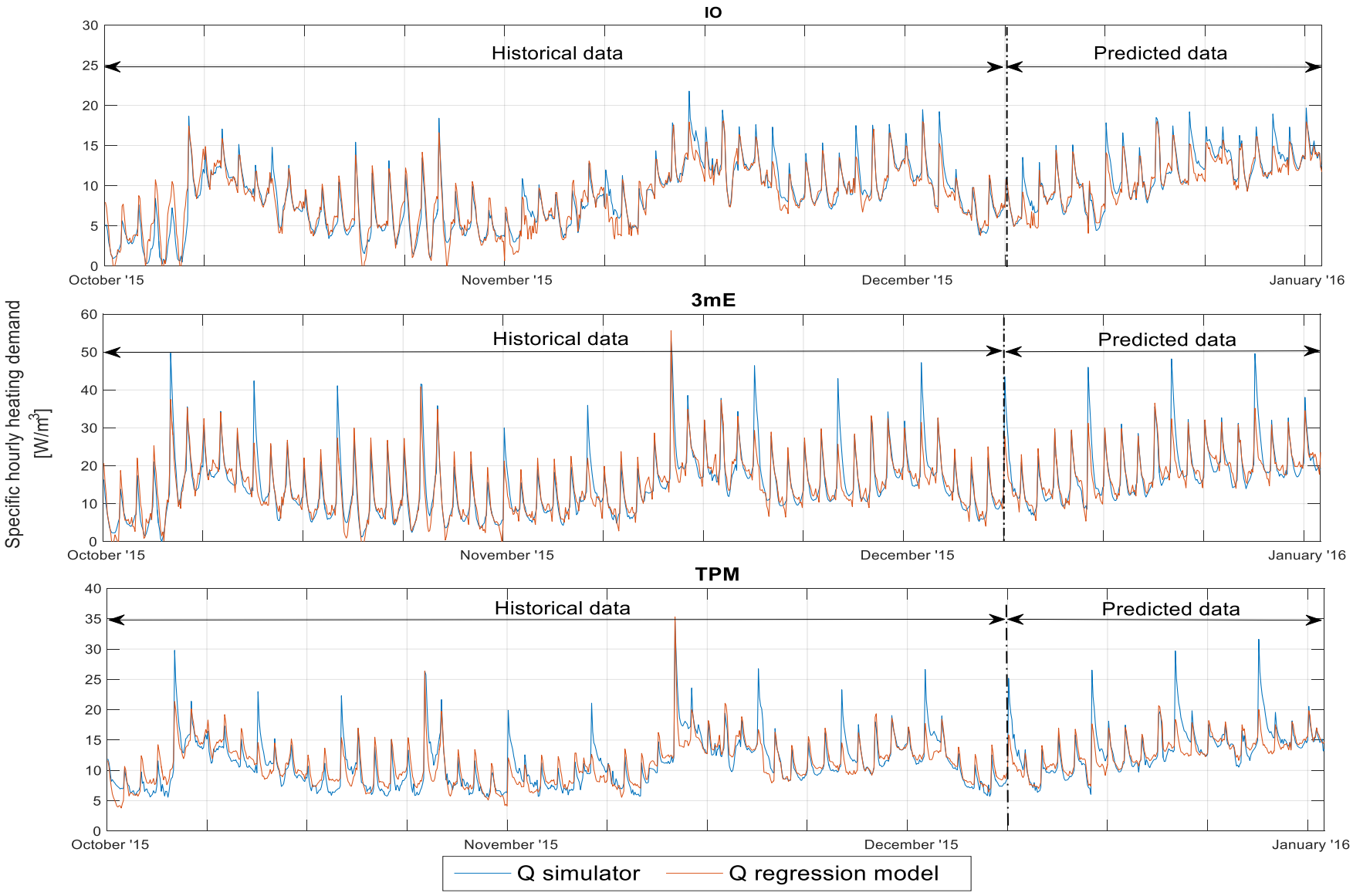

FIGURE 2 FITTING PROFILE OF MODEL 2 ON THE DATA SET OCTOBER 2015-JANUARY 2016 FOR IO, 3ME AND TPM, RESPECTIVELY.

Model 3: Model implemented into practice

The model expressed in equation 6 is modified to quantify the occupancy influence on the heating usage of the building. This is because occupancy influence is expected to be much more important on actual data than on emulated data.

Model 3 is expressed in equation 7. The following modifications are done with respect to the original model:

- Internal heat gains (people + lighting + equipment) are replaced by the occupancy. The data set does not provide the internal heat gains corresponding to lighting and equipment. Nevertheless, the real time occupancy of the building is available for one-month time. Therefore, the occupancy (related to internal heat gains of people) is used instead. This simplification will lead to inaccuracies in the regression model.
- Two different outdoor temperatures are included. The building studied has a dark roof which creates a micro-climate on the roof. This causes different outdoor surface temperature on the roof. In order to account for this factor, both outdoor temperatures are introduced in the model: (1) predicted by KNMI (Dutch meteorology institute) and (2) measured temperature on the roof of the building.

$$Q_{\mathrm{h}}\,[kW.h] = Constant + C_1\,(T^t_{outdoor\ KNMI}) + C_2\,(T^t_{outdoor\ roof}) + C_3(Q^{t-3}_{sol}) + C_4\,(Occupancy^t) + C_5\,(Occupancy^{t-3}) + C_6\,(T^t_{indoor\ air}) \quad (7)$$

This model shows that at least 77% of the actual heating demand can be explained by the outdoor temperature, solar gains, indoor air, and related presence variables such as internal gains. This accuracy is measured with respect to the actual (measured) data set, for more details see [17].

IV. Conclusions

This research concludes that the proposed linear regression models show a promising performance in order to become a fast, flexible and simple to use tool for predicting the heating demand in buildings. Being more suitable than other physics-based or ruled-based models.

The first part of the study shows that emulated data from the previous season (~2 months) are able to predict the next month with an accuracy in the range of 96-99% in the first model and 73-91% in the second model. This model limits the demand of measured data required to a few easy-to-measure parameters and the weather.

The second part proves that the model can be easily adapted to the available data and new influencing parameters (roof micro-climate in this case). A slightly modified model was applied on actual data, showing a 77% accuracy. Nonetheless, it is advisable to use a larger amount of data set to check the predictive potential of the model over a larger amount of time and avoid possible over-fitting.

The model flexibility in combination with the relatively small amount of monitored data needed, makes the model easy to implement in existing buildings and for large-scale implementation (from campus to national level). Moreover, it shows a physical relation with the input coefficients, making it possible to get a better insight in the influence of the different parameters in the building response.

The above-mentioned characteristics make this model suitable to automatize the training (machine learning) and use the model for the purposes of prediction of thermal energy demand at building or large-scale level, predictive control, failure prediction of installations and parametric analysis.

References

[1] "UN Environment Programme - Environment for Development : Buildings and Climate Change: Summary for Decision Makers |." 2009.

[2] "Heating and cooling - Energy - European Commission," Energy. [Online]. Available: /energy/en/topics/energy-efficiency/heating-and-cooling. [Accessed: 01-Feb-2017].

[3] H. Lund et al., "4th Generation District Heating (4GDH): Integrating smart thermal grids into future sustainable energy systems," Energy, vol. 68, pp. 1–11, Apr. 2014.

[4] E. H. Borgstein, R. Lamberts, and J. L. M. Hensen, "Evaluating energy performance in non-domestic buildings: A review," Energy and Buildings, vol. 128, pp. 734–755, Sep. 2016.

[5] D. Coakley, P. Raftery, and M. Keane, "A review of methods to match building energy simulation models to measured data," Renewable and Sustainable Energy Reviews, vol. 37, pp. 123–141, Sep. 2014.

[6] Z. Li, Y. Han, and P. Xu, "Methods for benchmarking building energy consumption against its past or intended performance: An overview," Applied Energy, vol. 124, pp. 325–334, Jul. 2014.

[7] T. A. Reddy and K. K. Andersen, "An Evaluation of Classical Steady-State Off-Line Linear Parameter Estimation Methods Applied to Chiller Performance Data," HVAC&R Research, vol. 8, no. 1, pp. 101–124, Jan. 2002.

[8] H. Zhao and F. Magoulès, "A review on the prediction of building energy consumption," Renewable and Sustainable Energy Reviews, vol. 16, no. 6, pp. 3586–3592, Aug. 2012.

[9] J. Bai, "Estimation of a Change Point in Multiple Regression Models," The Review of Economics and Statistics, vol. 79, no. 4, pp. 551–563, Nov. 1997.

[10] S. Chib, "Estimation and comparison of multiple change-point models," Journal of Econometrics, vol. 86, no. 2, pp. 221–241, Oct. 1998.

[11] M. Trčka and J. L. M. Hensen, "Overview of HVAC system simulation," Automation in Construction, vol. 19, no. 2, pp. 93–99, Mar. 2010.

[12] T. Catalina, V. Iordache, and B. Caracaleanu, "Multiple regression model for fast prediction of the heating energy demand," Energy and Buildings, vol. 57, pp. 302–312, Feb. 2013.

[13] J. C. Lam, S. C. M. Hui, and A. L. S. Chan, "Regression analysis of high-rise fully air-conditioned office buildings," Energy and Buildings, vol. 26, no. 2, pp. 189–197, 1997.

[14] T. Olofsson and S. Andersson, "Long-term energy demand predictions based on short-term measured data," Energy and Buildings, vol. 33, no. 2, pp. 85–91, Jan. 2001.

[15] A. Ioannou and L. C. M. Itard, "Energy performance and comfort in residential buildings: Sensitivity for building parameters and occupancy," Energy and Buildings, vol. 92, pp. 216–233, Apr. 2015.

[16] J. P. M. de Sá, Applied Statistics Using SPSS, STATISTICA, MATLAB and R. Springer Science & Business Media, 2007.

Stepwise regression - MATLAB stepwisefit - MathWorks Benelux. Retrieved January 23, 2017, from https://nl.mathworks.com/help/stats/stepwisefit.html

[17] C. Jurado López, L. C. M. Itard and P.Stoelinga "Heating Prediction and Control in Buildings: Demonstration of the Accuracy of Simple Multivariate Statistical Models and its use to quantify the Occupant Influence on Heating Energy Use in Buildings," Submitted to IBPSA, Sept. 2019.

REHVA
Federation of European Heating, Ventilation and Air Conditioning Associations

Product-specific set-point variation calculation method for EN15306-2

Karl-Villem Võsa, Jarek Kurnitski
Tallinn University of Technology, Department of Civil Engineering and Architecture
Ehitajate tee 5, 19086, Tallinn
karl-villem.vosa@taltech.ee
Master's thesis 2018

***Abstract* — In this paper, a temperature set-point variation method is imposed on annual energy calculations to account for heating system losses. This method complements the energy calculation method present in EN15306-2 and provides the possibility to use product-specific values of set-point variations instead of tabulated values. A specific enclosure definition in the form of a European Reference Room is used for this calculation process, which enables precise and comparable determination of the total set-point variation. An experimental study is carried out with several different emitter configurations, from which simulation input parameters such as vertical temperature gradients and controller parameters are measured. These values are then used in the annual simulation model of the European Reference Room along with the developed method to specify the total set-point variation. We find that the total set-point variation to compensate for system losses is up to 1.76 °C in the old building and 1.20 °C in the new building type. This represents an increase of up to 20% and 22% in total heating energy used, respectively.**

***Index Terms* — Energy calculation, emission efficiency, operative temperature, European Reference Room**

I. Introduction

The building sector is generally considered to be the largest individual contributor to global energy consumption. Faced with continuous population growth and increased primary energy usage per capita, a global shift towards energy efficiency is required for a sustainable building sector [1]. Heating energy used in buildings can account for a considerable fraction of overall energy usage, especially in colder climates where the heating period spans for many months annually, therefore it is only rational to maximize the efficiency of heating emission systems.

In Europe, EN15306-2 currently defines emission efficiency values for various configurations of heat emission systems [2]. Previous redactions of the same document used a more common approach in form of efficiency components was in use. With the latest revision, this method was discontinued and now a method which uses an increased temperature set-point is specified instead. In principal, this increased set-point results in higher energy consumption than with the initial set-point. The difference in the used heating energy represents the energy lost due to system inefficiency.

The standard specifies tabular values as conservative default set-point variation components, with the option to use product-specific values instead. In [3], emission efficiency of radiant systems under dynamic conditions was studied, and the authors found that the current standard over-estimates the embedded and control losses by up to 2 °C. As with many other European standards, EN15306-2 also states that a national annex can provide different values for use in local legislation. However, the standard does not provide a standardized method for calculation of these values. Without common criteria for evaluation of these parameters, the use of product-specific values cannot be regulated.

The method developed in this study for determination of product-specific set-point variation makes use of a specified European Reference Room, which defines the boundary conditions for the calculation of product-specific values from experimental measurement or simulation results [4]. This room specification in conjunction with validated simulation software is used to calculate the total set-point variation from annual energy consumption in relation to a reference configuration.

An experimental study of different heat emitter configurations, such as radiators, underfloor heating (UFH), ceiling panels and air heating, is carried out to specify additional input parameters such as vertical temperature gradients, heat transfer coefficients and controller parameters. Measured and calculated values are then used in the annual simulation model of the European Reference Room and the total set-point variations are obtained with the developed method.

II. Methods

Standard EN15306-2 accounts for heating system losses as a room air temperature set-point variation that increases the total heating energy consumed by the system when compared to the initial set-point:

$$\theta_{int,inc} = \theta_{int,ini} + \Delta\theta_{int,inc} \,, \tag{1}$$

$$\Delta\theta_{int,inc} = \Delta\theta_{str} + \Delta\theta_{ctr} + \Delta\theta_{emb} + \Delta\theta_{rad} + \Delta\theta_{im} + \Delta\theta_{hydr} + \Delta\theta_{roomaut} \,, \tag{2}$$

where $\theta_{int,ini}$ – initial air temperature set-point

$\theta_{int,inc}$ – increased air temperature set-point

$\Delta\theta_{int,inc}$ – total set-point increase due to stratification, imperfect control, embedded losses, radiation, imperfect hydronics, intermittent heating and room automation

This is a different formulation for the same additional energy expenditure as was defined in previous version of the standard, which used a more conventional method of individual efficiency coefficients:

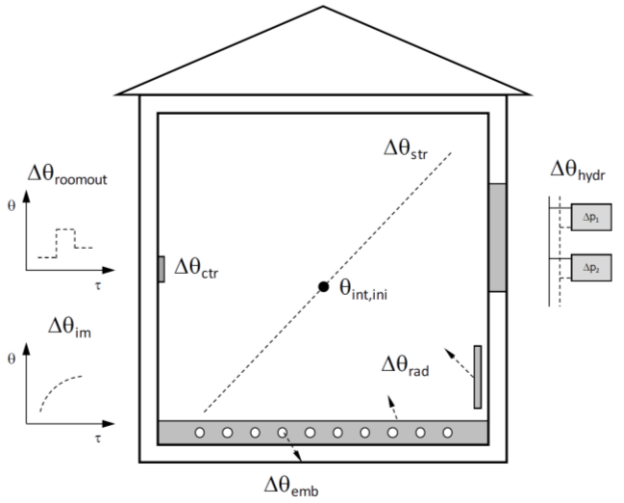

Figure 1 - System losses in heating systems [4].

$$Q_{em,ls} = \left(\frac{f_{hydr} \cdot f_{im} \cdot f_{rad}}{\eta_{em}} - 1\right) \cdot Q_H \quad (3)$$

$$\eta_{em} = \frac{1}{(4 - (\eta_{str} + \eta_{ctr} + \eta_{emb}))} \quad (4)$$

Both formulations address several components which account for most of the system losses within a system, as seen in Figure 1:

- Control accuracy
- Embedded losses
- Stratification losses
- Thermal comfort (operative temperature)
- Hydronic imbalance
- Intermittent heating and zone automatics

A. *European Reference Room*

ISO/DIS 52031 specifies a European Reference Room for the purposes of product-specific value calculation [4]. The room lies on the southern façade of a multi-storey building and has a single external wall with windows, see Figure 2. The amount of heating energy needed within this enclosure depends on the amount of heat lost through these external components. On the other hand, the windows allow heat from solar radiation to reach the room. Additional heating energy is needed to heat up the ventilation supply air. The standard specifies two different operating conditions and construction layer materials for this room (Table 1):

- New building – a well-insulated building, which represents an average building built from 2000 onwards
- Old building – built before year 2000 but after 2nd World War

Table 1 - Main boundary and operating conditions of the European Reference Room.

Building type	New building	Old building
Dimensions x/y/z (m)	4/4/3	
Windowed area (m^2)	3	
Ext. wall U-value W/(m^2K)	0.25	0.90
Window U-value W/(m^2K)	1.08	2.34
Frame U-value W/(m^2K)	1.20	2.00
Window frame fraction (%)	30	
Window g-value	0.64	0.76
Air exchange rate (h^{-1})	1	1
Supply air temperature (°C)	18	t_{out}
Heat recovery efficiency	0.8, t_{exh}>0 °C	-
Internal gains (W/m^2_{floor})	3.8	
Supply/return temp. for radiator (°C)	55/45	70/55
Supply/return temp. for UFH °C	35/28	40/30
Control	t_{op}=20 °C middle of room at h=0.60 m	
Gradient (K/m)	Measured value	

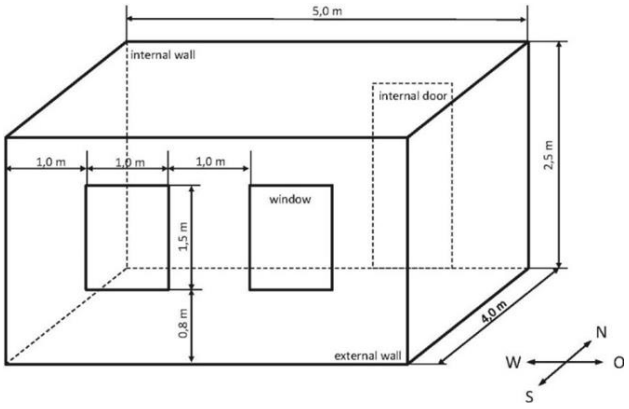

Figure 2 – Geometry of the European Reference Room.

The main differences between the two scenarios are the thermal properties of the enclosing layers and windows, presence of mechanical ventilation with heat recovery in the new building and higher supply and return temperatures for the heating systems.

Operative temperature control with a set-point of 20 °C is imposed on both building types in the middle of the room at a height of 0.6 m. For a full description of the room, see [4].

B. *Operative temperature*

The operative temperature t_{op}, by definition, is the uniform temperature of an enclosure in which an occupant would exchange the same amount of heat by radiation plus convection as in the existing non-uniform environment. For this reason, it constitutes a crucial parameter of thermal comfort standards [5]. In most practical cases where the relative velocity is small (<0.2 m/s) or where the difference between mean radiant and air temperature is small (<4 °C), the operative temperature can be accurately calculated as the mean value of air and mean radiant temperature (MRT):

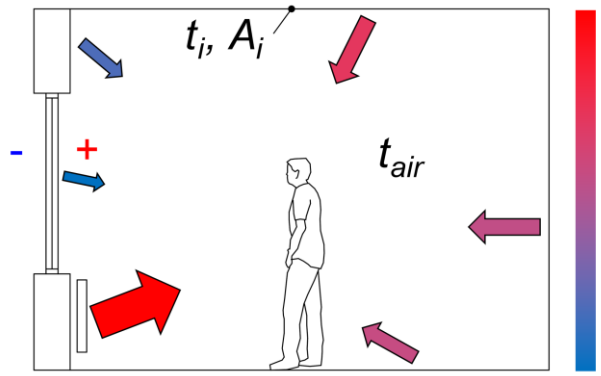

Figure 3 – Effect of mean radiant temperature on occupant.

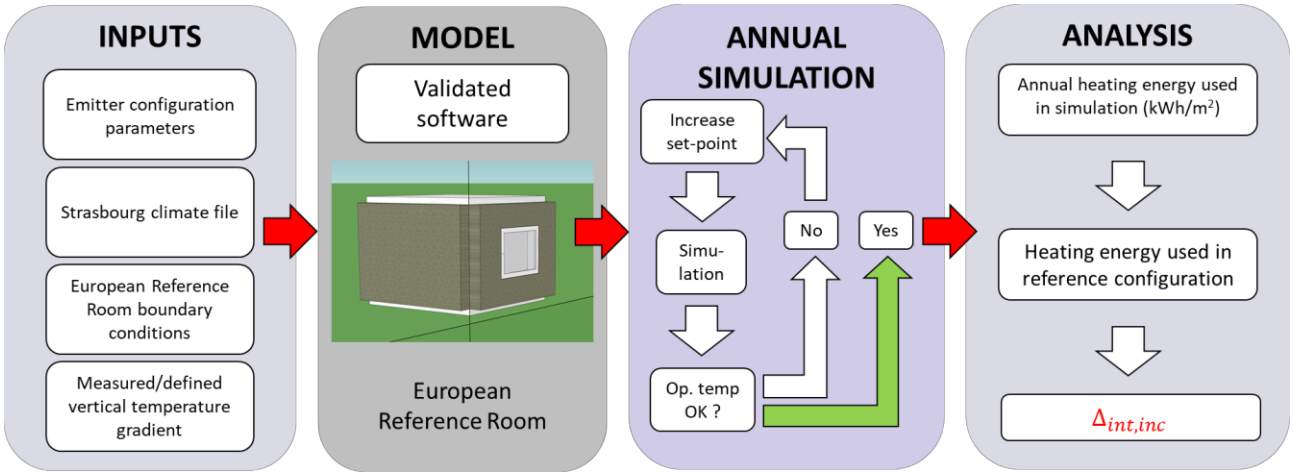

Figure 4 -Developed calculation method for total set-point variation calculation.

$$t_{op} = \frac{t_{air} + t_{mrt}}{h}. \quad (5)$$

The mean radiant temperature is calculated from enclosing surface temperatures,

$$t_{mrt} = \sqrt[4]{\sum T_n F_{p \to n}}, \quad (6)$$

where T_n is the n-th surface temperature and $F_{p \to n}$ is the view factor from the n-th surface to the point of occupancy.

Higher mean radiant temperatures allow the air temperature to be lowered within the room and vice versa at the same operative temperature. This presents a possibility to save (or expend more) energy and is accounted for in the standard with the $\Delta\theta_{rad}$ component, which can take both positive and negative values depending on the surrounding surface temperatures.

C. Developed calculation method

Using the geometry, boundary and operating conditions established for the European Reference Room, the total set-point variation can be calculated with an annual simulation in a validated software package. Parameters specific to the emitter and controller system, such as size, heat transfer coefficients and controller parameters (deadband width, integration time, gain *etc*) are inserted into the modelled room along with the common parameters from the room specification. The model is simulated at Strasbourg with its respective climate file. The calculation method is visualized in Figure 4.

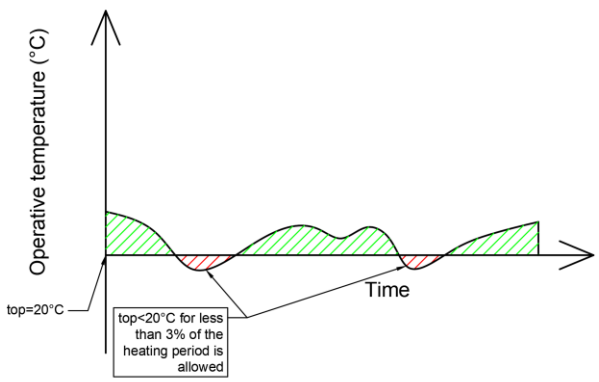

Figure 5 - Operative temperature constraint.

This initial simulation uses a room air temperature set-point of 19 °C and is incrementally raised until a constraint set with an objective function is satisfied. This constraint arises from the operative temperature requirement of 20 °C that must be maintained within the room. For 3% of the length the heating period, the temperature can drop under the specified operative temperature, see Figure 5. This eliminates the need to artificially increase the air temperature for most of the year to satisfy the temperature requirement when the temperature dips rapidly for a short period of time.

The air temperature set-point is increased until the constraint is satisfied. Annual heating energy used in that simulation is then compared to the energy used by a baseline reference configuration. From this comparison, the total set-point variation is determined.

D. Reference configuration

The reference configuration consists of a purely convective point heat source that exhibits no embedded, stratification or control losses. Such an ideal heat source serves as a great baseline to benchmark other systems, as real systems have losses and will always expend more energy. Energy consumption of such a reference system in an annual simulation is shown in Figure 6 and Figure 7.

E. Experimental study

The proposed method was tested with an experimental study in the Tallinn University of Technology nZEB test facility, shown In

Figure 8 and Figure 9. In this study, radiators, underfloor heating (UFH), ceiling panels and an air heating system coupled with ON/OFF and PI-type controllers were measured. The measurements provided heat emitter and controller input parameters as well as vertical temperature gradient values for the simulation model.

These parameters were then then used to configure the model of The European Reference Room within the IDA ICE simulation software package. Annual simulations were then run with these configured models and the process described in the previous subsections was followed to produce the total set-point variations for the tested emitter configurations.

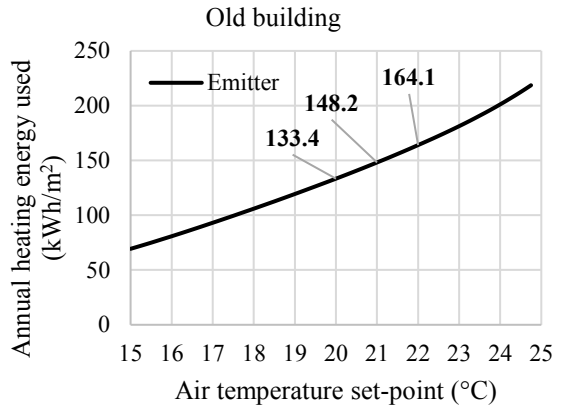

Figure 6 - Energy expenditure of old building in reference configuration

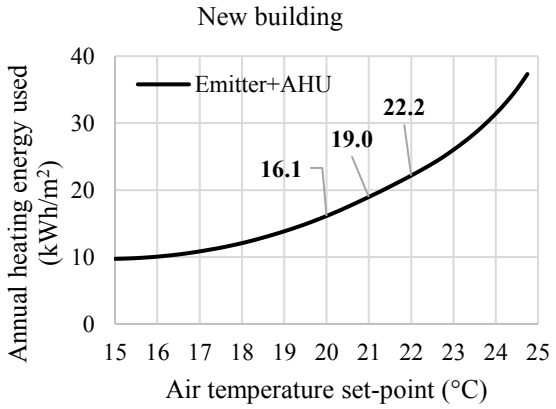

Figure 7 - Energy expenditure of new building in reference configuration

Table 2 – Vertical temperature gradients from measurements.

Type	Gradient (°C/m)
Radiator ON/OFF R5	0.15
Radiator PI R5	0.16
Radiator ON/OFF R9	0.08
Radiator PI R9	0.10
UFH ON/OFF R5	0.06
UFH PI R5	0.08
UFH ON/OFF R9	0.02
UFH PI R9	0.04
Ceiling panel ON/OFF R5	0.52
Ceiling panel PI R5	0.70
Air heating ON/OFF R9	0.36

III. RESULTS

The experimental study provided vertical temperature gradients as the input for annual simulations. These results are visualized in Figure 10 and Table 2. Radiator and underfloor heating have considerably lower vertical temperature gradients than air and ceiling panel heating. Both ceiling panels and air heating through the ventilation system first heat air at the higher part of the room, which due to a higher air pressure does not mix well with the rest of the air in the room. This explains the much higher temperature gradient when compared to the radiator and underfloor heating, in which heat is heated in the lower half of the room. In case of air heating, we noticed a strong linear correlation between the air supply temperature and the induced vertical temperature gradient, shown in Figure 11. For example, a 5 °C increase in the supply temperature increases the vertical temperature gradient by 0.25 °C/m. For other parameters also calculated and included in the annual simulations, see [6] and [7], which describe the experimental measurements and calibration procedure in detail.

The results from the annual simulations according to the developed calculation method are shown in Figure 14 and Figure 13. Systems with PI-type controller outperform those with proportional controls, with ON/OFF type controllers performing the worst, both in new and old building type. The temperature variation required to account for the system losses is higher in the old building, where the effects of stratification and embedded losses is more prominent.

Figure 8 - Outside view of the test facility.

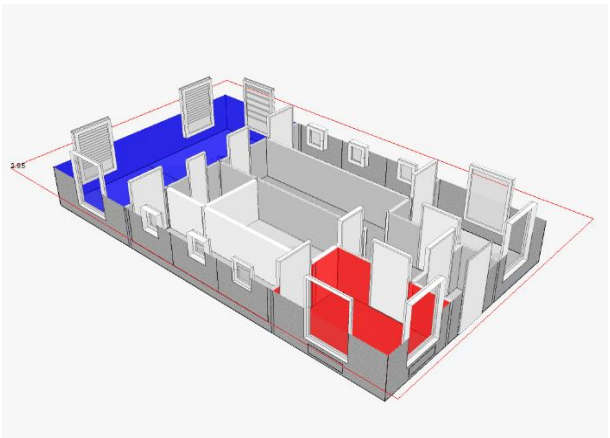

Figure 9 - Section cut of the test facility. R5 in red, R9 in blue.

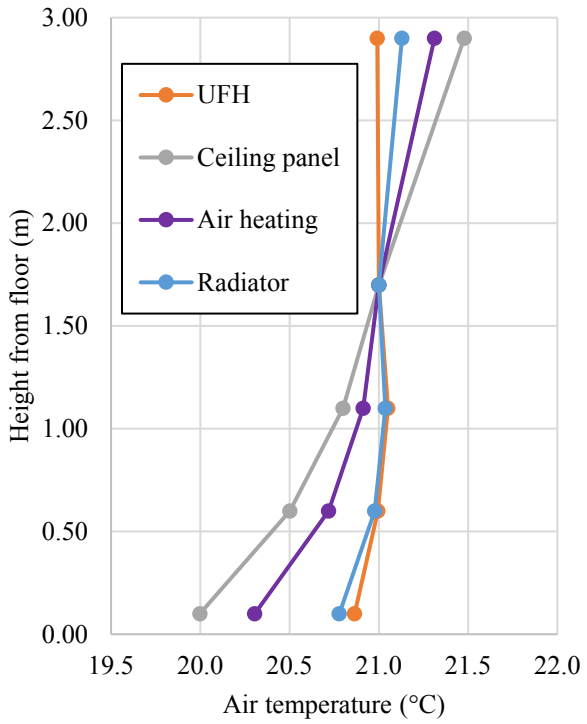

Figure 10 – Measured vertical temperature profiles. These results are averaged values and are normalized at h=1.70 m

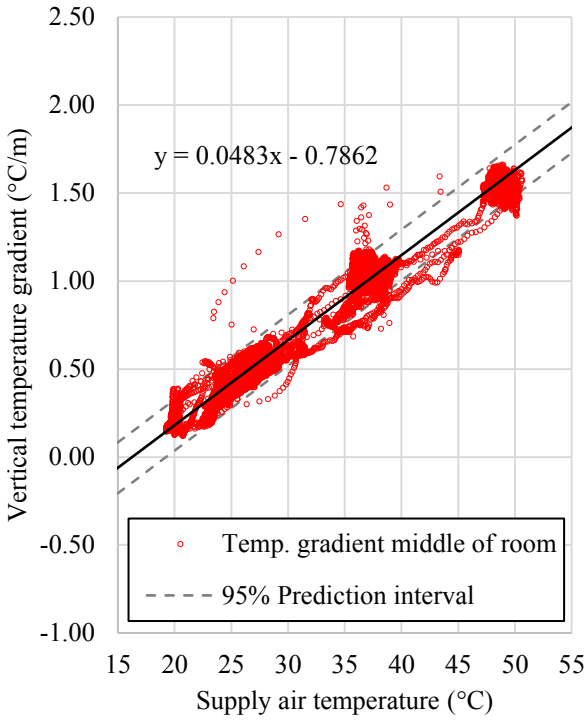

Figure 11 - Air heating: supply air temperature and vertical temperature gradient correlation.

The total set-point variation to compensate for system losses is up to 1.76 °C in the old building and 1.20 °C in the new building type. This represents an increase of up to 20% and 22% in total heating energy used, respectively. Internal gains from occupants, equipment, lighting and solar radiation have a considerably higher impact on the room temperature and heating energy in a new building, which results in a higher sensitivity to the temperature set-point.

In Figure 12, duration graphs of air and operative temperature are shown for select cases. For underfloor heating, the operative and air temperature are very close to each other and no significant additional energy is needed to maintain the required operative temperature with air temperature control. In case of radiators, this is not true as the air temperature set-point must be increased to compensate for the lower operative temperature. This difference between the operative and air temperature causes and additional system loss when a conventional air temperature control is used.

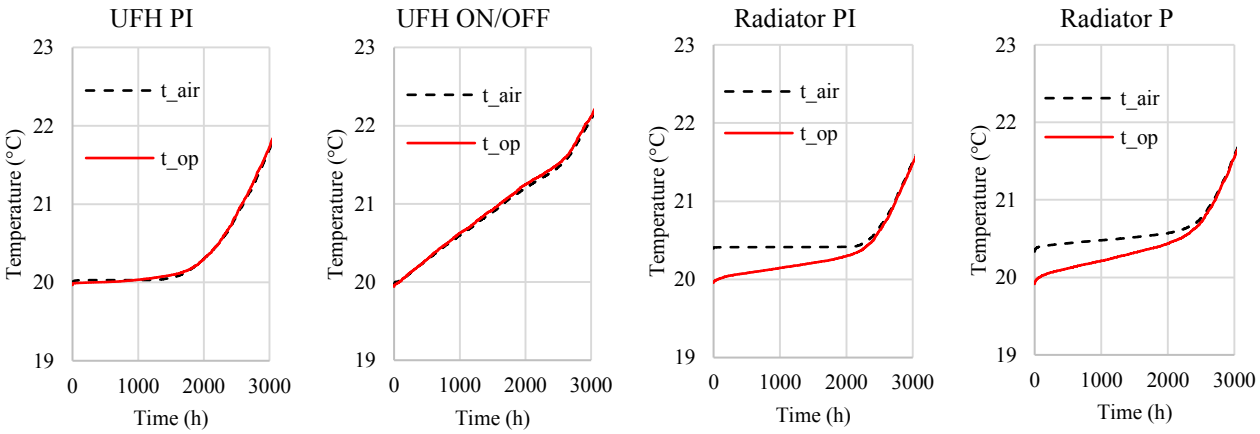

Figure 12 - Air and operative temperature duration graphs.

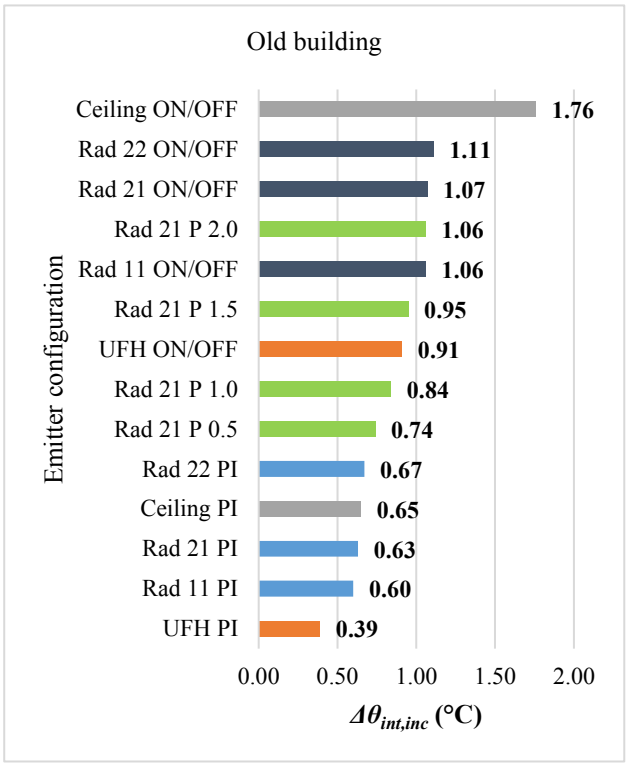

Figure 13 - Calculated set-point variation of old building type for tested emitter configurations. Conclusions

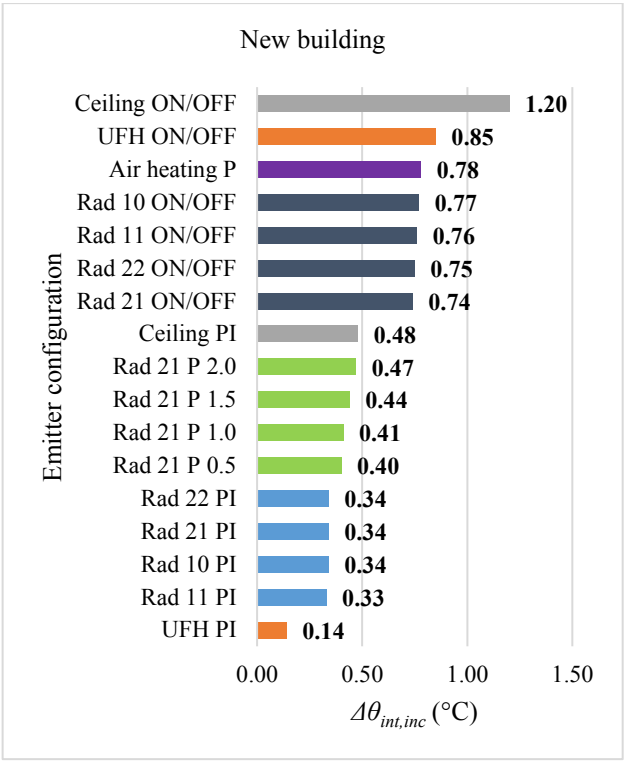

Figure 14 - Calculated set-point variation of new building type for tested emitter configurations.

IV. CONCLUSIONS

In this study, a method was developed to calculate product-specific total set-point variations for use in EN15316-2 standard. This method uses the definition, specification and boundary conditions of a European Reference Room included in the ISO/DIS 52031 along with developed criteria to obtain the total set-point variation from annual simulations. The main criterion requires an operative temperature of 20 °C to be maintained within the room for at least 97% of the duration of the heating period. The air temperature set-point in the simulation is increased until this constraint is satisfied. Annual heating energy use in the simulation is then compared to a lossless reference configuration's energy consumption, and a total set-point variation is achieved from this comparison.

An experimental study was also carried out to provide proof of concept for the method. In this experimental study, numerous heat emitter configurations were measured, and data obtained was used as input for the model in the annual simulations. One of the measured parameters was the vertical temperature gradient, which was measured to be 0.04 and 0.13 °C/m for UFH and radiators, and 0.36 and 0.62 °C/m for air heating and ceiling panels, respectively.

Applying the developed method in the European Reference Room along with the input parameters from the experimental data, total set-point variations of up to 1.20 and 1.76 °C were obtained for the new and old building types. This resulted in 20 and 22% increases in annual heating energy consumption due to system losses, respectively. Overall, the method provides a reliable, accurate and transparent way to calculate the total set-point variation for specific product configurations.

ACKNOWLEDGEMENT

This master's thesis is part of the research supported by the Association of the European Heating Industry EHI member companies Irsap Spa, REHAU AG + Co, Stelrad Radiator Group Limited, Uponor Corporation, Vasco Group, Wavin B.V., Rettig Austria, Zehnder Group International AG, and Estonian Centre of Excellence in Zero Energy and Resource Efficient Smart Buildings and Districts, ZEBE, grant 2014-2020.4.01.15-0016 funded by the European Regional Development Fund

REFERENCES

[1] A. Allouhi, Y. El Fouih, T. Kousksou, A. Jamil, Y. Zeraouli, and Y. Mourad, "Energy consumption and efficiency in buildings: Current status and future trends," *J. Clean. Prod.*, 2015.

[2] EN 15316-2:2017, "Energy performance of buildings - Method for calculation of system energy requirements and system efficiencies - Part 2: Space emission systems (heating and cooling), Module M3-5, M4-5," *Eur. Stand.*, 2017.

[3] G. Alessio, M. De Carli, A. Zarrella, and A. Di Bella, "Efficiency in Heating Operation of Low-Temperature Radiant Systems Working under Dynamic Conditions in Different Kinds of Buildings," *Appl. Sci.*, vol. 8, no. 12, 2018.

[4] "ISO/DIS 52031, Energy performance of buildings - Method for calculation of system energy requirements and system efficiencies - Soace emission systems (heating and cooling)," *ISO Stand.*, 2019.

[5] "ISO 7726, Ergonomics of the Thermal Environment, Instruments for Measuring Physical Quantities," *Geneva Int. Stand. Organ.*, 1998.

[6] K.-V. Võsa, A. Ferrantelli, and J. Kurnitski, "Experimental study of radiator, underfloor, ceiling and air heater systems heat emission performance in TUT nZEB test facility," in *CLIMA 2019*, 2019.

[7] K.-V. Võsa, A. Ferrantelli, and J. Kurnitski, "Annual performance analysis of heat emission in radiator and underfloor heating systems in the European reference room.," in *CLIMA 2019*, 2019.

REHVA
Federation of European Heating, Ventilation and Air Conditioning Associations

Grey wastewater heat recovery for heating of sanitary hot water in hotels

Master's thesis, October 2018

M. Sc. Danijel Todorović
Faculty of Technical Sciencies
Department of Energy and Process Engineering
University od Novi Sad, Serbia
danijeltodorovic3@gmail.com
Affiliations: renewable energy; heat transfer; BIM;

Ph D Mladen Tomić
Faculty of Technical Sciencies
Department of Energy and Process Engineering
University od Novi Sad, Serbia
mladen.tomic@uns.ac.rs
Affiliations: heat transfer; mass transfer; CFD;

***Abstract* - In this paper it is described system and shown method for dimensioning of the system for sanitary hot water heating (SHW) in hotels using heat from grey waste water as heat source, that is collected from hotel rooms, apartments and rain water and then heated by heat pumps. Also, it was carried out techno economic analysis between mentioned system, system that uses gas boilers as only heat source and system with solar plate collectors supported by gas condensing boiler.**

***Index Terms* – sanitary hot water, grey wastewater, rainwater.**

I Introduction: Potential for new investments in hotel industry

Tourism is considered to be the largest single economy branch in world, with more than 200 millions of people employed worldwide [1] with thousands of hotels and accommodation facilities worldwide as crucial part of branch. Hotels are in basics real estates, thus there are two ways for growth of profit: first one is large investments for larger capacities and entertainment content and second one is to make savings in operational costs . Costs for energy are considered to go up to 50% of total operational costs [8], with potential for frequent increase of energy price, cut of energy costs comes as obvious first choice in manner of gaining larger profit. Estimated hotels revenue worldwide will go up to 141,588 millions USD in 2018 and will go up to 186,000 millions USD in 2022 [2], so there is massive potential for relatively low investments that cuts costs and increases profit.

One of the challenges in process of designing system for sanitary hot water, for hotels and tourism facilities in general, is to predict number of occupants because it is very fluctuant through the year and it depends on many factors. Of course, there are some periods of year for every region of world when hotels are almost full but those periods are usually short so HVAC systems are most often designed to have lowest costs per unit of delivered energy on average occupancy level. According to Eurostat – statistical office of EU, average occupancy level of hotels in Southern Europe is around 70% and in East Europe is around 65% [9]. Since analysis and design of system will be carried out for hotel in Novi Sad, one of the most developed regions in Serbia, reference occupancy in this case will be 68%.

II Demands for sanitary hot water in hotel: methods and methodology. Investment systems

System sizing and calculation of SHW requirements, energy consumption and sizing of system elements is carried out according to DIN 4800-4804, DIN 4753-1, DIN 4708-1-3, DIN 1988-1 to DIN 1988-8 that is sublimated in [3]. Also, SHW demands are carried out for hotel/motel facilities, according to Standard 90.1-2004, used in ASHRAE 2007 HVAC applications handbook, chapter 49, for SHW requirements and it showed similar quantity since both handbooks are using data from 40's to 60's of twentieth century, therefore are not applied possibility of reducing needed hot water, regarding using newly designed low flow shower heads and sink aerators.

For hotel category of four stars, located in Novi Sad, Serbia, that is consisted of 144 double-bed rooms with bathroom, nine apartments, restaurant capacity of 76 people, café-restaurant capacity of 60 people, according to [3], it is calculated daily demand of SHW and shown in table I and table II.

Total daily demand for SWH is 17,690 litres of hot water. In this case, SHW demands are dimensioned according to accumulation method for average daily occupancy of 68%. For total SHW accumulation needs are selected three water tanks, two tanks of 5,000 l volume and one tank of 3,000 l volume, constructed for SHW propositions, with total accumulation volume of 13,000 l in cell configuration. Daily energy demands for SHW accumulation heating is 482.66 kWh for cold water temperature of 25 °C and hot water temperature of 60 °C. With 5% heat losses through pipelines, tanks, e.g. [3], total daily energy consumption is 506.79 kWh that comes to yearly energy consumption of 184,978.35 kWh. Energy demand calculation is based on simplified energy balance method showed in [3].

TABLE I
SHW demand in rooms and apartments

Space description	Quantity of accommodation units	Daily demand of SHW at 60°C for single accommodation unit in liters [l]	Total daily demand of SHW at 60°C in liters for accommodation units [l]
Double-bed room	144	100	14.400
Apartments	9	130	1.170

For base cases are chosen two most common systems we can find in hotels in our region, first one that use only boilers as heat source and second one that uses solar plate collectors with bivalent configuration with boilers.

Hotel that has been used as subject for this paper is business type hotel, so its main target clients are people that travel mostly for business, minimum period for heating SHW is 2 hours [3]. In that manner, for base first case as energy source are selected two gas boilers Remeha Gas 310 Eco Pro 285/5, each capacity of 261 kW and yearly efficiency of 88%.

For second base case are selected 37 plate solar collectors, Vaillant VFK 145 V, with total solar absorber area of 77.7 m^2, with inclination angle of 30° and azimuth angle of 40°. The best orientation of collectors is south-west, regarding hotel position, technical solution of roof and available area for placing of collectors. As support for heating SHW is selected gas boiler Viessmann Vitoplex 100 345, capacity of 345 kW. Simulation for this case is carried out using T- sol 5.5 software. Result of simulation are show in table III:

TABLE II
SHW demand in rooms and apartments

Space description	Number of people	Daily demand of SHW at 60°C per person in liters [l]	Total daily demand of SHW at 60°C in liters [l]
Restaurant	76	20	1.520
Café restaurant	60	8	600

In table III are shown simulation results for system with solar plate collectors and in table IV are shown costs per year and costs during estimated exploitation period for natural gas costs, electricity costs of auxiliary elements like circulation pumps and investments costs for both systems.

TABLE III
Simulation results for system with solar collectors per year

Description	Value
Installed collector power	65.01 kW
Irradiation on to collector surface (active)	128.74 MWh
Energy delivered by collector loop	45.45 MWh
Energy delivered by auxiliary source	141.7 MWh
SHW solar fraction	23.7%

TABLE IV
Investment and operational costs of base case systems

Description	System with boilers	Solar plate collectors system
Investment expenses [eur]	55,230.00	78,500.00
Natural gas costs [eur/year]	7,002.62	5,364.22
Electricity costs [eur/year]	58.25	77.95
Total operational costs in exploitation period of 20 years [eur]	141,216.53	108,843.43

III SYSTEM WITH HEAT RECOVERY FROM GREY WASTEWATER: METHODOLOGY AND DIMENSIONING

As proposed case there is system that uses grey wastewater from hotel rooms, apartments, sink from café restaurant and rainwater. Prerequisite for applying this system is to separate grey wastewater – wastewater from bathtubs, shower cabinets, washbasins and black wastewater – wastewater from toilets. Usage of water can vary very much from person-to-person so calculation of quantity for grey wastewater is made using average temperature of SHW in moment of using and mass and energy balance. In table V are shown average temperatures of hot water in moment of using at faucets. Quantity of grey wastewater is calculated using values of hot water at faucets, shown in table V, mass balance, energy balance and data based in experience that around 30% of hot water in hotel rooms and apartments is used on washbasins.

Mass balance:

$$m_{gww} = m_{SHW} + m_{cw} \quad (1)$$

m_{gww} – mass of grey wastewater;

m_{SHW} – mass of SHW for rooms, apartments and café restaurant sinks at 100% occupancy;

m_{cw} – mass of cold water on average temperature a year of 12 °C in Novi Sad;

Energy balance:

$$m_{gww} \cdot c_{p\ gww} \cdot t_{gww} = m_{SHW} \cdot c_{p\ SHW} \cdot t_{SHW} + m_{cw} \cdot c_{p\ cw} \cdot t_{cw} \quad (2)$$

$c_{p\ gww}$ – specific heat of grey wastewater [kJ/kgK];

t_{gww} – temperature of grey wastewater [°C];

$c_{p\ SHW}$ - specific heat of SHW [kJ/kg];

t_{SHW} – temperature of SHW [°C];

$c_{p\ cw}$ - specific heat of cold water [kJ/kg] at temperature of 12 °C;

t_{cw} - temperature of cold water [°C];

TABLE V
Temperature of hot water at faucet in moment of usage [4]

Faucet position	Temperature of water
Shower cabinet	38 °C
Washbasin	35 °C
Hot tube	37 °C
Bar	35 °C

Total mass of grey wastewater at 100% occupancy of hotel is 28.943,6 kg. For business type of hotel there are, usually, two daily peak consumption, first one in the morning from 7 am to 10 am and second one in the evening from 6 pm to 10 pm, so we can say minimum daily consumption period is 2 hours, therefore grey wastewater tanks are selected to have total capacity of 15.000 l. For space and positioning reason, grey wastewater accumulation is consisted of 6 tanks, each has capacity of 2.500 l. For filtration of grey wastewater are selected four coalescing filter. Filters are the most sensible and ''the weakest'' element of the system, so it should be carried out with engineer of technology and wastewater treatment.

Beside grey wastewater, there is possibility to collect rainwater and use, also, as heat source, but only in some periods of year, when temperature of rainwater is higher than minimum water temperature possible to use as heat source of 9 °C. According to Republic Hidrometeorogical Service of Serbia average daily data for atmospheric precipitation, it is possible to collect 1240 litres of rainwater a day [5]. Unfortunately, there is no data about rainwater temperature, so as reference temperature is used value of 12 °C that is temperature of cold water from faucets. In table VI are shown average atmospheric precipitations for Novi Sad, for period from May to September 2017.

TABLE VI
Quantity of rainwater in Novi Sad from May to September 2017 [5]

Month	**Total amount of rainwater [mm/m²]**	**Number of days with rain**	**Average rainwater quantity a day [mm/m²]**		**Quantity of rainwater for 700 m² roof area [mm/m²]**
May	82.9	13	2.67		1,869
June	65.7	9	2.19		1,533
July	12.0	8	0.39		273
August	17.4	5	0.56		392
September	91.5	14	3.05		2,135
Average	53.9	9.8	1.77		1,240

Average yield of grey wastewater at 68% a day is around 19.700 kg and about 1240 litres of rainwater, totally 20.940 litres of water per day.

For period of one week, during Exit festival days in Novi Sad, temperature of grey wastewater (GWW) is recorded from 11th to 17th of July, 2018 in hotel in Novi Sad. Temperature values for mentioned period shown in table VII. As reference temperature for this case is selected value from 14th of July, 2018, because it was possible to observe changes for few hours, during morning peak consumption. Because of relatively low yield of GWW three-way valve should be installed on water return pipe on heat exchanger, on side of GWW so it can be returned to GWW tanks and re-used again, because of relatively high temperature of water. By re-using water, daily exploitation period of unit is much longer and since using heat pumps for water heating is much cheaper than heating it using gas boilers. In this case heat pumps should be selected to source side water flow, because system is dimensioned on available potential, not only on energy demands, so this system must have some additional source like boiler, to help when fast heating of water is needed and also to be back-up source in case of accident situation. For this purposes is selected same boiler that is selected for system with solar plate collectors, Viessmann Vitoplex 100 345, capacity of 345 kW, that has enough power to heat SHW accumulation in two hours.

To select heat pumps, first of all, available daily water flow must be calculated. Since water temperature difference of user side of heat pumps should be 4-7 °C, ideally 5 °C, so elements of system, like pumps and pipelines at GWW side of system are selected and to average temperature difference 5 °C.

TABLE VII
Temperature of grey wastewater in hotel in Novi Sad

Date	**Temperature of grey wastewater [°C]**	**Hotel occupancy [%]**
11th of July 2018	11.5	33
12th of July 2018	17.8	62
13th of July 2018	24.3	88
14th of July 2018	25.1	86
15th of July 2018	20.8	88
16th of July 2018	23.0	62
18th of July 2018	17.73	45

Average temperature difference between two water flows is 5 °C, so minimum inlet temperature of GWW is 9 °C because water is changing its physical state from liquid to solid state at 4 °C. If GWW temperature is lower than 9 °C, water diverts by three-way valve to sewer system. Scheme of mentioned system shown in figure 1.

Calculation of daily GWW water flow regarding reference temperature, minimum temperature on inlet side of heat exchanger and temperature difference between inlet and outlet water flows:

$$\dot{V}_{max} = n \cdot \dot{V}_{25.1} \quad (3)$$

V_{max} – the maximum average water flow regarding reference temperature, minimum temperature on inlet side of heat exchanger and temperature difference between inlet and outlet water flows [l/day];

n – GWW water flow re-circulations [-];

$V_{25.1}$ – water flow of GWW at temperature of 25.1 °C [l/day];

$$n = \frac{t_{ref} - t_{min}}{\Delta t_{sr}} \quad (4)$$

t_{ref} – reference temperature of GWW [°C];
t_{min} – minimum temperature of GWW on heat exchanger inlet [°C];
Δt_{sr} – mean temperature difference of GWW intel/outlet at heat exchanger [°C];

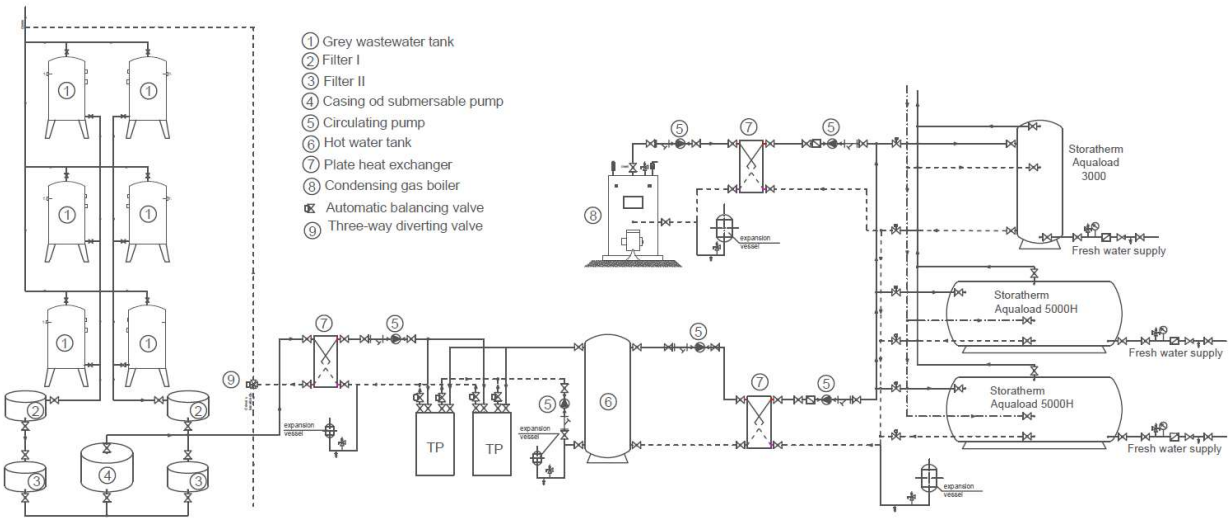

Figure 1: Hydraulic scheme of system for heating sanitary hot water using grey wastewater as heat source

The maximum possible recirculation number is n = 3,22 based on starting GWW temperature and lowest acceptable temperature, max water flow is calculated with three re-circulations, so maximum average GWW water flow is 62,820 litres per day. For protection of heat pump's evaporator from impurities and to have maximum temperature of fluid on user side of heat pump 23 °C – that is maximum temperature that heat pump can work with, there is plate heat exchanger.

Regarding maximum temperature of fluid on user side of heat pump, mean temperature difference of fluid inlet/outlet, minimum GWW inlet temperature, difference on GWW maximum temperature and heat pump user side fluid maximum temperature, it is calculated average temperature regime on user side of heat pump and it is 17/12 °C. With user side fluid as mixture 85% water and 15% ethylene glycol.

User side water temperature regime of heat pump is 60/55 °C, therefore temperature regime on SHW side of plate exchanger is 25/58 °C. Besides basic heating of SHW, also there should be protection against legionella bacteria, so every Sunday to Monday night, total accumulation of SHW should be heated to 68 °C (Δt = 10 °C) for period of two hours every week by gas boiler. Also, there could be expected interruptions for filter cleaning once in 30-45 days and possible needs for faster SHW heating, so it is calculated that gas boiler delivers 16.586,6 kWh of energy. Rest of needed energy, 168.192,85 kWh, is delivered from heat pumps with average working time of 13.5 h a day. Investment and exploitation costs are show in table VIII in chapter IV.

IV TECHNO-ECONOMYC ANALYSIS

When it comes to final decision which system to install in hotel, naturally it comes to investor, company's CEO or company owner to make final decision. There are lot of criteria that will affect decision, first of all, reliability and functionality of system are mandatory and criteria that implies, but then it comes to financial part of criteria that is usually ''decision maker''. Of course, CO_2 foot print is very important for environment and community in general, but usually it comes as extra value of system and very good data for hotel marketing.

Hotel that is subject of this case study is newly built and all the solutions are considered for installation, techno-economic analysis is carried out for differences in investment costs. Investment costs, exploitation costs, difference in exploitation costs per year and difference of investments costs are shown in table VIII and in table IX are shown data for PBP – payback period, POP- period of dynamic payback, IRR – internal rate return and MIRR – modified internal rate return, since first result in IRR iterations for system with solar plate collectors is show for 29th year of exploitation (-12%), but since estimated life span of equipment is 20 year, result is not considered for this analysis. For analysis is used reference discount rate for 2018, of 4.39%, announced by Serbia's Commisson for control of government's subventions [6].

TABLE VIII
Investment and exploitation costs difference

System	Invest-ment cost [eur]	Exploita-tion costs per year [eur]	Diffe-rence in invest-ment costs [eur]	Diffe-rence in exploita-tion cost per year [eur]
System with boilers as only heat source	*55,230,00*	*7,060.00*	-	-
Solar plate collectors system	*78,500.00*	*5,442.17*	*23,270.00*	*1,618.65*
GWW heat recovery system with heat pumps	*65,090.00*	*4,792.70*	*9,860.00*	*2,206.78*

TABLE IX
Results of comparative techno-economic analysis system with gas boiler as only heat source and systems with renewable energy source

System	PBP [years]	POP [years]	IRR [%]	MIRR [%]
Solar plate collectors system	14.38	23.23	-12*	-100.00
GWW heat recovery system with heat pumps	4.47	5.09	16.00	13.00

* IRR value is for at least 29 years of lifespan;

In figure 2 and figure 3 are shown cash flows for systems with solar plate collectors and system with GWW as heat source.

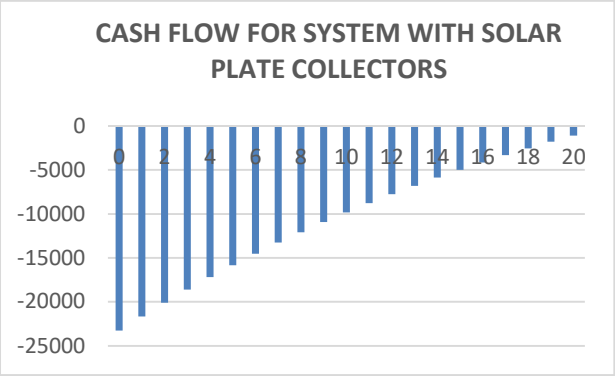

Figure 2: Chart of cumulative cash flow for system with solar plate collectors

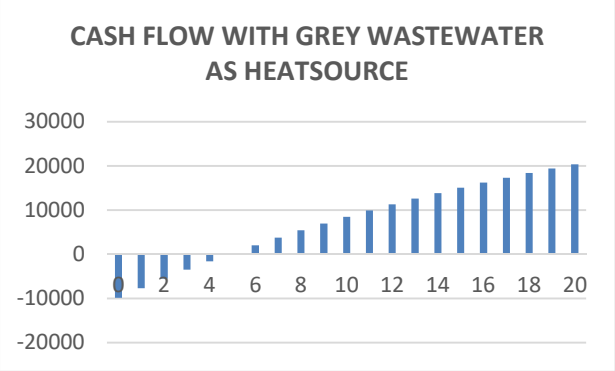

Figure 3: Chart of cumulative cash flow for system grey wastewater as heat source

V CONCLUSION

As it is shown in this paper grey wastewater has great potential as energy source, but it must have additional heating source for faster SHW heating and for greater occupancy than average, but still this system is the most sustainable of all presented systems. Usage of fossil fuels in hotels in this way is cut in minimum for heating of SHW. It is very important because hotels are usually using commercial boilers that, with just basic filtration and cleaning of waste combustion gases, unlike power plants that has already special filters for combustion gases cleaning or will have in near future.

System with solar plate collectors is shown as very unprofitable, even it is calculated for hotel located in Serbia that has very large solar yields. Of course main reason for this is low price for electricity and natural gas. Beside, low prices of electricity and natural gas, there is no any subsides and regulations in Serbia that could help mass installation of solar plate collectors.

The main reason why solar plate collectors are so unprofitable is the same one why system with heat recovery from GWW are profitable and shown as very good investment, in terms of payback period, sustainability and also very good image for hotel and for company that manages hotel facility. That good image creates impression of very modern place that attracts people and increases hotel's revenue, profit and makes good position for new investments, what creates space for applying new engineering ideas and gains possibility for technology development.

Financial analysis is carried out using current prices of equipment, installation costs, design costs, gas and electricity costs with officially announced discount rate. If discount rate was calculated, it would be value around 2%, with current interest rates on loans for renewable energy sources and stable inflation rate that we have in Serbia currently. Applied discount rate also take risks in to consideration for fluctuant and small market, as one we have in Serbia. For example, if one of the largest international companies decides to move their production away from country, like Fiat could do, inflation will rise and it will also affect interest rates on loans. Scenario like this will make large impact to economy. Another reasons for applying larger discount rate is exploitation period of 20 years that is period when lot of changes can happen, especially in small countries like Serbia.

VI REFERENCES

[1] Paulina Bohdanowicz, Angela Churie – Kallhauge, Ivo Martinec - Energy-Efficiency and Conservation in Hotels – Towards Sustainable Tourism – Royal Institute of Technology, Stockholm Sweden, 2001

[2] Statistics portal statista.com - web site accessed in 4th of September 2018.

[3] Reckngel, Sprenger, Schramek, Čeperković - Grejanje i klimatizacija 2012

[4] Engineering toolbox – engineering web site accessed on 7th of September 2018.

[5] Republic Hidrometeorogical Service of Serbia yearly meteorogical report for 2017 – web site access on 10th of September 2018.

[6] Obaveštenje o objavljivanju referentne kamatne stope za 2018. godinu – Komisija za kontrolu državne pomoći – Notice on the publication of the reference interest rate for 2018 - Commisson for control of government's subventions;

[7] 2007 ASHRAE handbook - HVAC applications

[8] Internationa Hotels Group engineering design guide

[9] European comission statistics portal Eurostat ec.europa.eu – web site web site accessed in 3rd of September 2018.

REHVA
Federation of European Heating, Ventilation and Air Conditioning Associations

Experimental and numerical analysis of a Closed Loop Air Ground Heat Exchanger Prototype System

Student: Daniel BUTUCEL **Coordinators:** Assoc. Prof. Tiberiu CATALINA & Assoc. Prof. Catalin LUNGU
Technical University of Civil Engineering – Faculty of Building Services Bucharest
Blvd. Pache Protopopescu no66, sect.2, Bucharest, ROMANIA
Email: danielbutucel@gmail.com / tiberiu.catalina@gmail.com / clungu@yahoo.com
Year of paper acceptance: 2018 – Bachelor Thesis of student Daniel BUTUCEL

***Abstract*—In this study a new ventilation strategy is proposed to be used for residential buildings. Compared to a classic Canadian well heat recovery ventilation system who has multiple inconveniences (cost, risk of bacteria, condensation) the proposed prototype is cheap, easy to implement and with high impact on energy efficiency and indoor air quality. These advantages are demonstrated using an extended experimental campaign and the economical benefits are confirmed using numerical simulations. Overall, the proposed system was proven to be technically and economical feasible contributing to a clean and low energy indoor environment.**

***Index Terms*—air ground heat exchanger, passive house, energy efficiency, indoor air quality.**

Introduction

In the EU, the buildings sector is responsible for about 40% of the total energy consumption and due to the energy sources, the amount of CO2 emissions exceeded by far 30%. Therefore, the EU issued several directives related to reducing the energy consumption in buildings. But just as important as the energy efficiency is the **indoor air quality**, especially in the residential buildings due to the lack of mechanical ventilation systems. In Europe, **15% of lung cancer diseases are related to Radon exposure [1]** and concerning the IAQ, people spend more than 80% of the time indoors and therefore the quality of the air is very important for preventing the possible health risks. Consequently, the mechanical ventilation becomes a must for residential buildings [2] and therefore there is a need for low energy systems that ensure a good air quality at low costs. There are low energy ventilation systems available on the market, such as the heat recovery ventilation especially if it is combined with an air ground heat exchanger which pre-cool or pre-warm the outdoor fresh air through the ground before entering the heat recovery ventilation system. This „classic„ system is mainly supported by an an earth–air heat exchanger who was found to be a very good solution to passive heating and cooling buildings [3]. The study of Flaga et al. [4] reports the experimental and numerical analyses conducted on air ground source heat exchanger for a passive house placed in a cold climate while Congedo et al. [5] presented the experimental validation of a mathematical model implemented by the CFD Fluent for the simulation of heat exchange that takes place within a HAGHE for geothermal heat pumps.

But this system has some inconveniences, especially when used with an HRV system: **high investment and installation cost** of the **piping system** (silver particles treatment) which must prevent bacteria's formation and at the same time it has evacuate the condensation/maintenance (filters, etc).

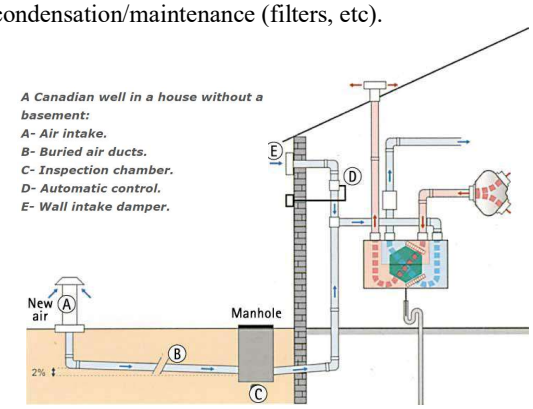

Figure 1. Classic low energy efficient ventilation system for passive houses [6]

Objectives of the study

The main goal of this study is to achieve the proper indoor air quality using an **innovative prototype called CLAGHE** and at the same time to **demonstrate its technical and economic feasibility** through the **experimental and numerical analyses** conducted throughout this year, hence raising awareness and contributing to the development of the institution.

Experimental campaign

For experimental analysis, the measurements have been conducted by using sensor for monitoring the air temperature, CO2 and Radon concentration as well as the humidity and air velocity sensors for measuring the proper distribution of the air in the rooms. For numerical analysis, the simulation software Design Builder has been used.

The ventilation prototype system was monitored in real conditions on an existing house, as shown in figure 2. It is an **ecological house** where the studied system was monitored. It was designed and built following the 5 principles of passive house and the certification is in process. The built-up area of the building is 250 m2 and the useful area is 195 m^2. From a constructive point of view, the resistance structure is made of load-bearing walls made

in "frame" system of wooden panels and wood-portal wooden assemblies assembled by pressing joints of corrosion-resistant and wooden side walls. The wood structure is stiffened by a network of longitudinal and transverse contours that make a rigid bolt at the shell level. Structures and spacers are provided to stiffen the structure.

The thickness of the outer panels is 19 cm. Inside, the partition walls are made of shutters with vegetable fiber plates, mechanically attached to the wood structure, having a thickness of 25 cm. Outside the plaster is decorative, white. The carpentry is made of PVC with three-ply glass. Inside the finish is made of plaster mortar with decorative painting on walls and plasters with plaster and washable paint on the ceilings.

As far as the thermal insulation of the house is concerned, it is made of **heat-insulating sheets of straw of approximately 35 cm (eco-friendly material)**. From the point of view of the installation systems, the dwelling is equipped with an underfloor heating system with an ionizing power plant as a heating source. About the cooling system. there is no proper system in this regard, the air conditioning of the house being achieved through the mechanical heat recovery system coupled to the ground-to-air heat exchanger without an active cooling source.

Figure 2. Eco-passive house in Chitila, Romania

It is an ecological house because it is build mainly with environmental friendly materials such as wood structure, wheat straw insulation, interior rammed earth walls as thermal mass, it is well sun oriented, it has installed a thermal solar system, and is equipped with a Heat Recovery Ventilation System combined with the studied system the **Closed Loop Air to Ground Heat Exchanger (CLAGHE).**

The system is divided in 2 major elements: CLAGHE on the right, and the HRV (Heat Recovery Ventilation) on the left. CLAGHE consists primarily of the geothermal exchanger – a closed loop 50 m length made of 110 mm diameter PVC pipe buried at 2,3 m depth. The loop closes in the air to air heat exchanger and at this point the fresh intake air gets pre-cooled or pre-heated by the air that flows through the geothermal exchanger, moving forward to the heat recovery unit. The fresh air is distributed and collected in/from the house through special HDPE antibacterial flexible tubes.

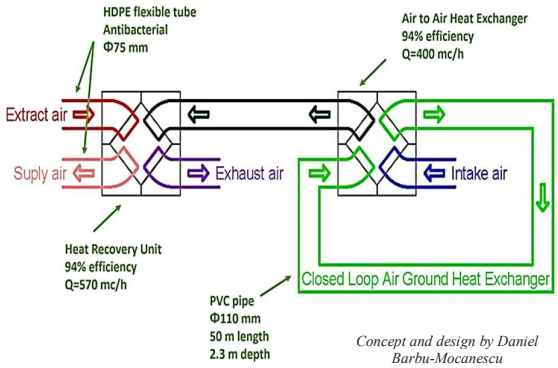

Figure 3. Functional scheme of CLAGHE prototype

The studied system has a **certain particularity, the most important one**. The ground-to-air heat exchanger is not directly connected to the heat recovery system but is connected in the first phase with an air-to-air heat exchanger. At this level, by heat transfer, the outside air is preheated or pre-cooled by the air conveyed into the buried tubing into the ground, and is subsequently directed to the heat recovery, as can be seen in Figure 3. This solution has been chosen for both economic and air quality considerations. At a total geothermal collector surface of about 50 meters, the price for 1 m linear bactericidal tubing is at least 2 times higher as the price of one linear meter of plain PVC tubing. Moreover, it is wanted to avoid the introduction of the air in the house from the soil, in order to avoid contact with radon and other possible harmful gases resulting from soil infiltration.

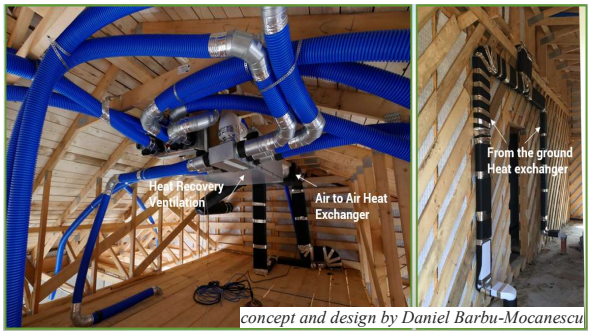

Figure 4. CLAGHE system – HRV and Air Heat Exchanger (left) and the Pipes from the ground (right)

At the heat recovery level, depending on the inlet temperature, it can: 1) exchange heat with the extracted indoor air; or 2) it can be set to bypass mode and thus the outside air is distributed directly into the rooms of living. The first case is specific to the cold season when the outside temperature is low and heat input is needed with indoor air to bring it to comfort. If the indoor temperature does not correspond to the interior conditions specific to the cold season (20-22˚C), the ventilation system has not been fitted with a heating battery, which is why the underfloor heating of the house will take over the load thermal insulation and will ensure the optimum level of thermal comfort inside the house. The second case is called free-cooling and occurs when the outside temperature is at the comfort indoor temperature and is specific to the intermediate periods of the year (spring and autumn).

As for the summer period, when the outside temperature exceeds 30 °C, the system was designed so that the heat exchange between outdoor air and the ground, the temperature at which the air will be introduced inside does not exceed the thermal comfort level associated with the summer period (24-26°C). For this reason, from the experimental analysis presented in this paper we will find out whether the system works in the projected parameters and what improvements it can bring to optimize its operation in the three scenarios: winter, spring, summer.

Throughout the measurements, the air-to-air heat exchanger was set to 90% of its maximum flow rate of 430 m^3/h while the heat recovery at 60% of its maximum flow rate of 570 m^3/h. It should be noted that the fan in the air-to-air heat exchanger required to extract the outside air has been shut down and replaced by the heat recovery fan. To determine the total air flow of the building, we estimated, according to the national Romanian Norms an air change rate of 0.75 ach. This results in a total air flow of approximately 400 m^3/h. No measurements have been made to determine the air flow velocity in the geothermal collector, but we calculated from the modelling part an approximate speed of 3.5 m/s, considering the operation of the air-to-air heat exchanger.

The experimental campaign was meant to demonstrate the effectiveness of the proposed system. Small temperature sensors have been installed in different positions of the air flow. The sensors are made by Kimo France and have a good endurance and accuracy (±0.2°C).

Figure 5. Photos with the sensors and during the experimental campaign

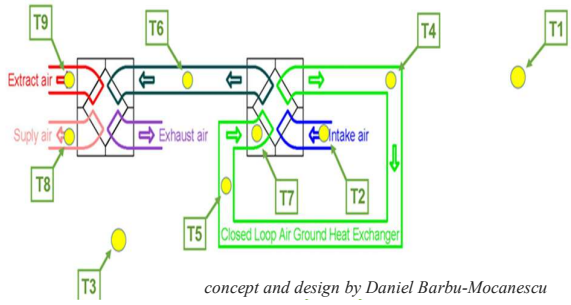

Figure 6. Temperature sensors positions in the CLAGHE prototype

The experimental analysis consists mostly of temperature measurements and the sensors have been placed in every important point of the system, in order to measure the temperature variation from the outside to the inside. Four different scenarios were set up, according to the data obtained: winter (21 March - 16 April), spring (20 April - 18 May), summer (25 May - 5 September), autumn (10 September - 10 October).

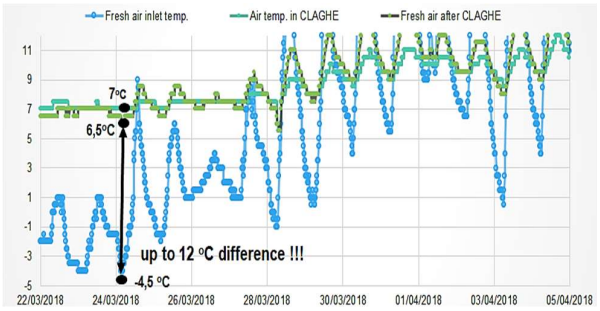

Figure 7. Winter campaign results on air temperatures

Fresh air inlet gets pre-warmed with up to 12°C, which means 1,6 kW gain from the ground at -4,5 °C. For -15°C outdoor temperature, the economies can reach up to 2,5 kW.

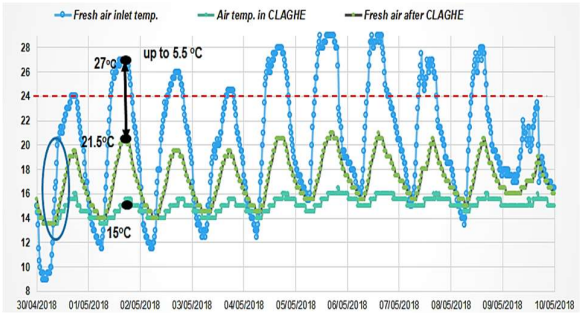

Figure 8. Spring campaign results on air temperatures

The air inlet is cooled down with 5°C, the optimum indoor air inlet temperature. During some periods the CLAGHE should not function and that means a **necessity of an automation system**.

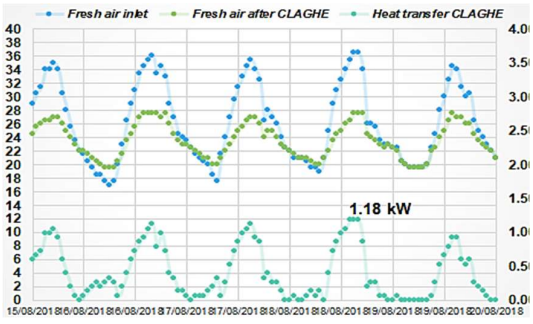

Figure 9. Summer campaign results on air temperatures

The fresh air inlet gets pre-cooled with up to 10 oC during hot summer periods. More than 1,2 kW saved during summer period -» **high energy reduction.**

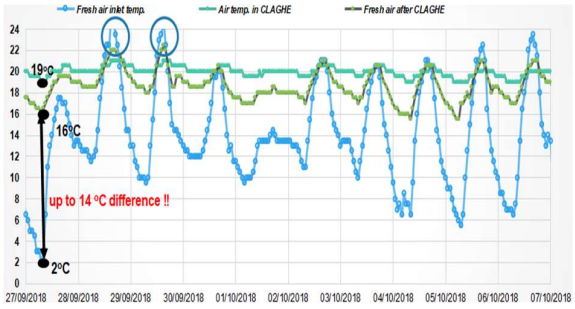

Figure 10. Autumn campaign results on air temperatures

The fresh air inlet gets heated with **up to 14°C** during this period and the maximum energy savings is **1,8 kW** in one hour. For the entire week, it reached **132 kWh/week or 20 EUR/week**.

Numerical campaign

The modelling software Design Builder was used for calculating the heat gains and losses through the envelope as well as the energy consumption for heating, cooling and ventilation. The main goal of this analysis is to compare the case study, namely the HRV combined with CLAGHE for cooling, with a reference case consisting of the same HRV but this time combined with an ordinary split system in order to demonstrate the technical and economic feasibility of the system.

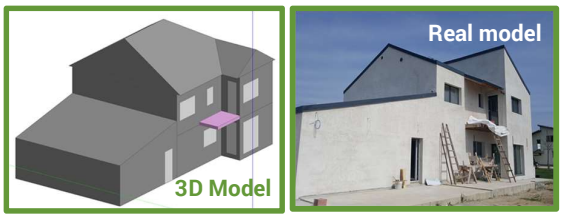

Figure 11. 3D Model realized in Design Builder versus Real House

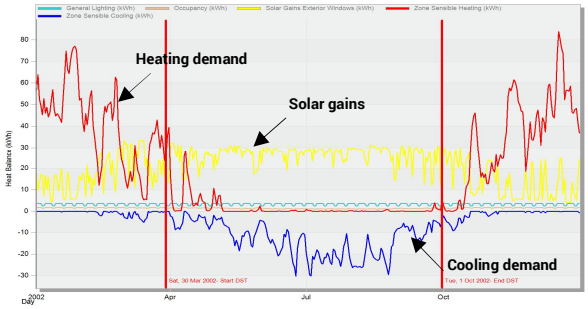

Figure 12. Heating/Cooling demand and outdoor/indoor heat gains

For the reference case, the heating demand was 7275 kWh/year and the cooling demand resulted in 1010 kWh/year. After simulating the case study, the heat demand was **5634 kWh/year** and the cooling demand was 0 kWh/year as the CLAGHE system could supply cooled air that maintained the indoor air temperature below 27°C.

CLAGHE versus STANDARD Heat Recovery Ventilation System (no cooling)

Heating consumption economy up to 33% !	**Cooling consumption economy 100 % !**

Financial impact

We have obtained using simulation a heating consumption economy = 1641 kWh/year or 215 EUR/year and Cooling consumption economy = 1010 kWh/year or 131 EUR/year. This is translated in 346 EUR/year. The costs of the system are presented below:

TABLE I.
TOTAL COSTS OF THE PROPOSED PROTOTYPE SYSTEM

CLAGHE System Price		
PVC piping system	130	EUR
Rectangular piping	43	
Drilling work	130	
Air heat echanger	1200	
Insulation material	98	
Workmanship	43	
Other small parts	50	
TOTAL	**1696**	

Using the Simple Payback Time we can achieve a **remarkable 4.9 years !.**

Modelling campaign

In order to determine an optimal system to ensure a reduction in energy consumption for heating / cooling, it is necessary, in view of the above-mentioned recommendations, to calculate the heat flow transmitted or discharged to the tube as well as the total transfer area heat that will later determine the required length of the geothermal collector. Determining these values will be done starting with the airflow required for the building.

In this regard, we will continue to present a mathematical model used in the GAEA software by Heidl and Benkert [7] and used in our case:

- the influence of the Canadian well on reducing the energy consumption in a passive house;
- determining the optimal geometry of the Canadian well (length and diameter of tube, number and distance between tubes, depth of burial) to ensure a given air flow.

To begin with, the following information is required: distribution of external air temperature and distribution of ground temperature:

$$\theta_a(t) = \theta_m + (\theta_{\max} - \theta_m)\cos\left(2\pi\frac{t}{t_0}\right) \qquad (1)$$

where:

- θa (t) - the outside air temperature at hour t, [° C];
- θm - annual average outdoor air temperature, [° C];
- θmax - annual max. external air temperature, [° C];
- t - time [s];
- t_0 - the duration of the year [s] (31.5x106 s).

In addition to the annual variation in soil temperature at a certain depth, the application also allows the annual variation in the air temperature across the Canadian well and annual variations in the soil temperature. The variation of the soil temperature in contact with the wall of the

geothermal collector, unaffected by it, is calculated as a function of the annual average temperature in the outside air and its maximum annual value:

$$\theta_s(t) = \theta_m + (\theta_{\max} - \theta_m) \cdot e^{-\zeta} \cdot \cos\left(2\pi \frac{t}{t_0} - \zeta\right) \quad (2)$$

where:

- θs (t) - the soil temperature in contact with the tube wall, unaffected by the tube [°C];
- thermal depth [m] (calculated according to the depth and thermal properties of the soil):

$$\zeta = S_0 \sqrt{\frac{\pi \rho c}{t_0 \lambda}} \quad (3)$$

where:

- S_0 - the depth, [m];
- λ - thermal conductivity of the soil, [W/mK];
- δ_c - volumetric soil capacity, [J/m3K].

The temperature of the soil in contact with the tube wall is influenced by both the heat transfer between the tube and the air in the tube, the two influences being included in the coefficient U* defined as follows:

$$U^* = 2\pi \frac{\lambda}{U_{a,p}} \frac{1}{\ln\left(\frac{S_0}{R_0} + \sqrt{\left(\frac{S_0}{R_0}\right)^2 - 1}\right)} \quad (4)$$

where:

- $U_{a,p}$ - the thermal transfer coefficient between the air and the wall of the tube, [W/mK];
- R_0 - tube radius [m].

Knowing the air temperature inside the tube (θ_a), the correct soil temperature at the contact with the pipe walls (θs, p) will be calculated using the formula:

$$\theta_{s,p} = \frac{U^* \cdot \theta_s + \theta_a}{U^* + 1} \quad (5)$$

To determine the heat flow transferred from the ground to the air in the Canadian well, we will divide the total length of the well into 100 segments (with constant air temperature on a segment), and the heat exchange will be calculated for each segment:

$$\dot{Q} = \Delta z \cdot U_{a,p} (\theta_{s,p} - \theta_a) \quad (6)$$

where:

- Q - the heat flow transferred to the air by the soil, [W];
- Δz - segment length, [m].

The heat transfer coefficient between the air and the wall of the tube depends on the heat transfer coefficient at the inner surface of the pipe:

$$U_{a,p} = \pi (2R_0) h_i \quad (7)$$

where:

hi - heat transfer coefficient between the air and the wall of the tube, [W / m2K]; shall be calculated according to the air and material parameters of the tube and its geometrical characteristics:

$$h_i = \frac{\lambda_a}{l_c} \cdot Nu \quad (8)$$

- Nu - Nusselt number;
- lc - characteristic length; in this case - the diameter of the pipe ($2R_0$), [m];
- λ_a - the thermal conductivity of the air in the tube, [W/mK]; is determined from the air characteristics table as a function of its temperature.

The Nusselt number is calculated as a function of the Prandtl number (Pr - is determined from the air properties table as a function of its temperature and Reynolds (Re):

$$\mathrm{Re} = \frac{w}{\nu_a} \cdot l_c \quad (9)$$

- υa -kinematic air viscosity, [m2/s]; is calculated from the air characteristic table as a function of its temperature;
- w - air velocity in the tube, [m/s]:

$$w = \frac{D}{\pi \cdot R_0^2} \quad (10)$$

where:

- D - the airflow to be supplied, [m^3/];

For the turbulent state, based on the Gnielinski model, Nusslet is determined as:

$$Nu = 0.024(\mathrm{Re}^{0.8} - 100) \cdot \mathrm{Pr}^{0.4} \quad (11)$$

Knowing the air temperature at the entrance to the tube (equal to the outside air temperature) based on the heat flow of each tube segment, taking into account the limit conditions for preserving the heat flow, can determine the variation of the air temperature along the Canadian well, as well as the heating / cooling potential of the house using this system.

As the type is important as well as the soil proprieties (conductivity, diffusivity, thermal capacity, type, etc) it was necessary to gather this data either using ThermoMap software or by geological measurements

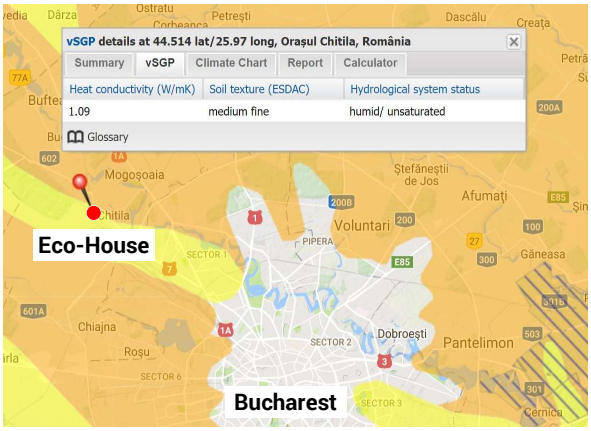

Figure 13. ThermoMap for Bucharest and its surrondings

The soil heat capacity was found to be 2.06 MJ/m^3K while the heat conductivity of 1.09 W/mK.

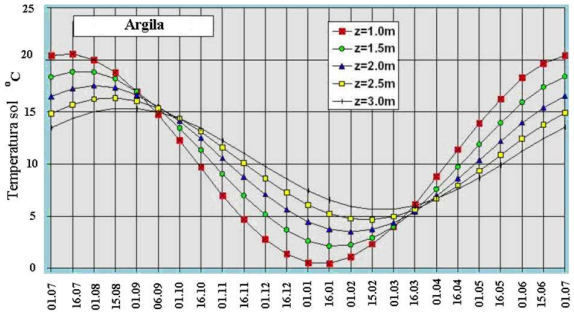

Figure 14. Soil temperature variation for clay soil

The mathematical model was afterwards implemented in a „home made,, Excel sheet that can help us with different parametric studies on different variables like soil type, air change rate, pipe conductivity and other. A screen shot of this model is illustrated in the following figure:

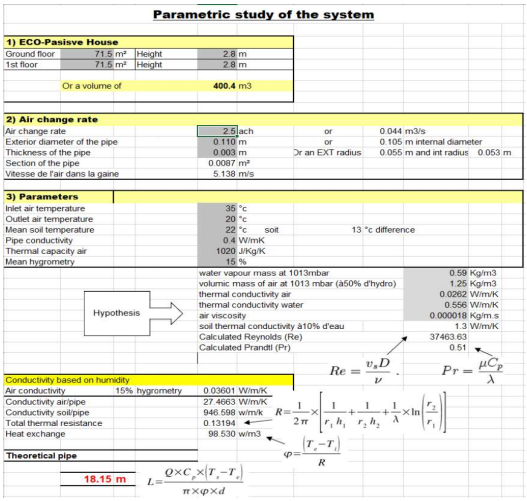

Figure 15. Excel „home made,, calculation sheet for parametric study and sizing of air/ground heat exchangers

Conclusions

The proper indoor air quality is directly related to reducing the risk of health problems from pollutants associated with building use. Regarding the economical impact, after one year of operation, the studied system would reduce the energy consumption for cooling and heating with more than 2500 kWh/year which would mean a total **economy of about 350 EUR/year**. Considering the cost of approximately 1700 EUR, the investment would pay back in 5 years. The are multiple conclusions at the enf of the study: perfect indoor air quality (CO_2 < 850 ppm during whole year, RADON level < 100 Bq/m3, low air velocities, good air distribution in the whole house and good indoor air temperatures)

And finally, according to the evaluation criteria we consider that:

- The subject responds to **European objectives** on **reducing health problems** related to air quality and **increasing building energy efficiency,**
- **The results covered all the targeted objectives**: air quality, energy efficiency and economic impact,
- The **prototype ventilation system** was tested in-situ and proved to be **technical feasible and ready for mass production,**
- Using an **extended experimental campaign** and **detailed simulations** it was proven the ***benefits*** and ***innovation*** of the subject,
- Excellent Institution development using Mass Media and future research projects potential
- The social benefits of sustainable design are related to improvements in the **quality of life, health, and well-being**,
- Knowledge transfer, improved environmental quality, neighborhood restoration, and **reduced health risks** from pollutants associated with building energy use,
- **Institutional development:** publicity on national television, top international journal under submission, acquisition of equipment's

ACKNOWLEDGEMENT

The team would like to thank architect Daniel Barbu MOCANESCU and the owner of the house, Cornel IOSIV, for their support in realizing this study.

REFERENCES

[1] Elío J, Crowley Q., Scanlon R., Hodgson J., Zgaga L., Estimation of residential radon exposure and definition of Radon Priority Areas based on expected lung cancer incidence, Environment International Volume 114, May 2018, Pages 69-76

[2] Dayi Lai, Yue Qi, Junjie Liu, Xilei Dai, Lei Zhao, Shen Wei, Ventilation behavior in residential buildings with mechanical ventilation systems across different climate zones in China, Building and Environment, Volume 143, 1 October 2018, Pages 679-690

[3] Bisoniya, Trilok Singh, Kumar, Anil, Baredar, Prashant, 2013. Experimental and analytical studies of earth–air heat exchanger (EAHE) systems in India: a review. Renewable Sustainable Energy Rev. 19, 238–246. https://doi.org/10.1016/j.rser. 2012.11.023. ISSN 1364-0321.

[4] Flaga-Maryanczyk, A., Schnotale, J., Radon, J., Was, K., 2014. Experimental measurements and CFD simulation of a ground source heat exchanger operating at a cold climate for a passive house ventilation system. Energy Build 68, 562–570

[5] Paolo Maria Congedo, Caterina Lorusso , Cristina Baglivo , Marco Milanese , Luca Raimondo, Experimental validation of horizontal air-ground heat exchangers (HAGHE) for ventilation systems, Geothermics, 80, 78-85, 2019.

[6] Canadian Well for ventilation and air conditioning https://www.siberzone.es/ and http://www.tectonica-online.com/products/2310/conditioning_air_ventilation_canadian/

[7] Benkert, St., Heidt, F.D., Scholer, D. - Calculation tool for earth heat exchangers GAEA, Proceeding of Building Simulation, Fifth International IBPSA Conference,Prague, 1997, Vol. 2

REHVA
Federation of European Heating, Ventilation and Air Conditioning Associations

Influence of Climate and Control Strategies on the Visual and Energy Performance of a Dynamic Component for Office Buildings

Manuela Baracani

Abstract—
The dynamic facade components, such as Venetian blinds and Smart Windows, are components capable of modifying their properties to adapt to different needs. In particular, Smart Windows are windows that can change their properties in response to an external stimulus and therefore adapt to the instantaneous needs of the environment. The control of these dynamic components makes it possible to greatly improve both visual and energy performances compared to those obtained with traditional glasses, as long as the control logics that dominate them are carefully studied. The control startegies present in the literature are almost all mono-objectives, due to the fact that visual and energy requirements are often in contrast with each other. The following paper, born from the work developed in a master's thesis in Architecture Construction and City at the Polytechnic of Turin, investigates the performance of a particular dynamic component: an electrochromic glass that with the changing of its color is capable of varying its thermo-optical properties in response to one electrical stimulation. The aim of the paper is to verify the possibility of implementing control strategies based on multiple objectives and multiple control criteria organized with decision trees, to investigate their effectiveness compared to traditional technologies and the variation of the results obtained based on the location considered for numerical simulations . It has been considered a standard-sized office with a south-facing glass facade located in three cities with different climates: Turin, Rome and Abu Dhabi. The risk of glare, the availability of natural light and the annual energy consumed were examined as evaluation parameters.

Index Terms— **Electrochromic glazing, smart window, adaptive façade, energy performance simulation, visual comfort simulation.**

Introduction

The global energy consumption and CO_2 emission strictly depends on the energetic performance of buildings, responsible for 20% to 40% of the global energy use [1]. Most of the energy consumption of buildings is caused by the high transmission of the transparent envelope and by its features of permeability to daylight and solar radiation. This is positive in winter period, when solar gains contribute to the heating of the indoor environment and reduce energy demand, but become strictly negative in summer period, when it increases the energy demand for cooling. Moreover transparent component affects visual comfort permitting daylight availability and the view to the outside, but also causing glare phenomena (if not properly shadowed) in some times of the year. And ideal window should reflect shortwave infrared and ultraviolet radiation coming from the outside in a hot climate and minimize the transmission of longwave infrared radiation from indoor to outdoor in a cold climate[2]. Traditional windows cannot change their properties depending on internal and external conditions; conversely the so-called "Smart Windows" can vary their thermo-optical properties depending boundary conditions and user needs. Passive Smart Windows change their properties spontaneously in response of environmental conditions; active Smart Windows are controlled by an external and usually electrical stimulus and so they can be controlled by a user. This type of windows can have extremely positive benefits on visual comfort and energy performance, but this strictly depends on the control logic that dominates the changing of properties of the glazing. [3]. These control strategies usually follow a hierarchy of objectives, that can require contradictory actions (for example the need of shadowing to reduce glare in winter is in contrast with the need to maximize solar gains): the priority given to them deeply affects final results. A Building Performance Simulation (BPS) software that consider all these differents parameters and objectives is necessary to verify and study design choices of control strategies, but this is rarely the case [4].

The thesis on which this paper is based investigated the visual comfort and energy performance results of different control strategies implemented on an electrochromic window in comparison with static technologies. The electrochromic window is an active transparent façade component able to vary its thermo-optical properties, passing from a transparent bleached state to a tinted one, depending on the difference of potential applied. It also investigated the difference of results related to the choice of the location, so the analyses were performed for a south oriented enclosed office located in three different cities: Turin, Rome, Abu Dabhi.

Methodology

A. *Performance evaluation parameters*

Following parameters were consider in the evaluation:

Energy Performance Index (EP_{GL}):

Calculated according to the equation (1)

$$EP_{GL} = EP_h + EP_c + EP_l \quad (1)$$

it is the amount of primary energy annually consumed per unit area for heating (EP_h), cooling(EP_c), and lighting(EP_l), and it is expressed in kWh/(m^2·year).

Daylight Glare Probability (DGP):

This metric quantifies the percentage of people dissatisfied with the visual environment in a point in the

space placed 3 m away from the window, on the centerline of the room, at a height of 1.2 m [5]. Ref [5] identifies four daylight glare comfort classes characterized by a DGP range. Glare is considered disturbing when DGP range exceed 0,4.

Daylight glare comfort class	Threshold
Imperceptible glare	DGP < 0.35
Perceptible glare	0.35 ≤ DGP < 0.40
Disturbing glare	0.40 ≤ DGP < 0.45
Intolerable glare	DGP ≥ 0.45

Daylight Autonomy (DA): this metric is defined as the percentage of hours of occupation of a space over a year in which daylight alone is sufficient to meet the minimum illuminance (E) requirement (in this case 500 lx) [6].

$$DA = \frac{\sum_{i=1}^{8760} t(E \geq 500)}{\sum_{i=1}^{8760} i}\Bigg|_{occupied} \qquad [\%] \ (2)$$

The DA was assessed for a grid of points positioned at 0.75 m above the floor and spaced 0.25 m from each other, for a total number of 130 points.

B. Description of the case study climate

Energetic and visual performance of dinamic glazing stricly depends on the location: their functioning is as much more performing as the climatic conditions are subject to winter and summer variations. So three differents climate where considered:

Turin (45.06°N 7.68°E): sub-continental climate, heating dominated. Its geographical position also means that in winter the solar path is low on the horizon, intercepting the visual field of users for most of the day and thus causing glare.

Rome (41.88°N 12.47°E): mediterranean climate, the energy requirement for winter heating is still greater than that for summer cooling, which in any case is significant.

Abu Dhabi (24.37°N 54.37°E): arid subtropical climate, the energy requirement for summer heating is predominant, and the energy requirement for winter heating is completely negligible.

C. Reference office characteristics and glazing considered

The case study considered is an enclosed office 3.6 m large, 4.5 m deep, and 2.7 m high, as shown in Fig.1. The short wall south oriented is the transparent one, alternatively equipped with the static or dynamic glazing (Window to wall ratio=1). The other surfaces, as the office is considered part of a building, were assumed to be adiabatic. The heating system guarantees a temperature higher than 21°C in winter period; the cooling system guarantees lower than 26° C in summer period.

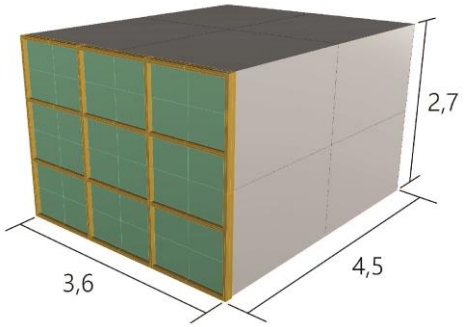

Figure 1. 3d view of the standard office used in numerical simulation

The lighting system was designed to guarantee a minimum illuminance on the workplane equal to 500 lx, with dimmable lighting controlled by photosensors. The office was assumed to be occupied from 8.00 to 17.00.

In the present study glazing with different optical properties were compared: an electrochromic glazing (EC) and two traditional selective glazing were alternatively used as external layer of a Double Glazing Unit (DGU). The internal layer of the DGU was a clear glazing with a low-emissivity coating, while the cavity was 16 mm and filled with argon 90/10. In Table I the thermo optical properties of the glazing are shown.

For some control strategies analyzed, internal or external Venetian blinds were also considered. They were both considered with the following angles of rotation of the slats: 0 ° (horizontal), 15 ° and 30 °.

TABLE I.
VISIBLE TRANSMISSION (T_{VIS}), SOLAR TRANSMISSION (T_{SOL}) AND SOLAR FACTOR (G-VALUE) OF THE DOUBLE GLAZING UNITS CONSIDERED, INCLUDING THE DGU WITH THE EC FOR THE PRINCIPLE STATES

Double Glazing Unit		T_{vis} [-]	T_{sol} [-]	g-value [-]	U [W/(m^{2}K)]
Reference glazing	U62/30	0.62	0.28	0.30	1.1
	V72/38	0.72	0.36	0.38	1.1
Electrochromic glazing states	EC 10 (bleached)	0.52	0.29	0.35	1.1
	EC 8	0.39	0.16	0.23	1.1
	EC 7	0.33	0.12	0.20	1.1
	EC 6	0.26	0.09	0.16	1.1
	EC 4	0.21	0.07	0.15	1.1
	EC 1 (tinted)	0.10	0.03	0.11	1.1

D. Control strategies

Starting from the literature analysis, different control strategies were selected for the electrochromic component under examination. Both control strategies aimed at optimizing energy performance and strategies designed with the aim of maximizing visual comfort for

the occupant were chosen and subsequently modified in order to improve the performance of the component even in the non-optimized aspects.

ML = minimizing loads: the electrochromic glazing is totally bleached (EC 10) in presence of a heating load and totally or partially tinted (EC 1 or EC 6) in presence of a cooling load.

ML1: the glazing switches from state EC 10 to EC1;

ML6: the glazing switches from state EC 10 to EC6.

MG_L = minimizing glare risk with a linear switching: the electrochromic glazing switches to the clearest state ensuring a DGP lower than 0.4.

MG_L_1: the glazing switches from state EC10 to EC1;

MG_L_1_w: the glazing switches from state EC10 to EC1 maintaining a totally bleached state from the 15th of December to the 15th of January (in order to improve winter energy performance).

MG_L_6_w-s: in order to minimize the glare condition and maximize the daylight availability the glazing switches from state EC 10 to EC6; it is also set to totally bleached state from the 15th of December to the 15th of January and in order to improve the summer energy performance. EC6 is used as minimum transparency limit state from the 15th of June to the 15th of September, while EC1 is used when the office is not occupied (control strategy used in Turin climate).

MG_L_1_9: same as *MG_L_1;* when there is a cooling need the glazing is set on state EC9 (control logic simulated in the case of Rome).

MG_B = minimizing glare risk with blinds: internal venetian blinds are coupled to a selective glazing to ensure a DGP lower than 0.4. When DGP exceeds this limit value the internal blinds are adjusted to the lowest slat angle (between 0°, 15°, 30°) able to ensure a DGP lower than 0.4.

U62/30_B_I: Internal venetian blinds coupled with selective glazing characterized by T_{vis}= 0.62 and g = 0.30.
V72/38_B_I: Internal venetian blinds coupled with selective glazing characterized by T_{vis}= 0.72 and g = 0.38
U62/30_B_E: External venetian blinds coupled with selective glazing characterized by T_{vis}= 0.62 and g = 0.30.
V72/38_B_E: External venetian blinds coupled with selective glazing characterized by T_{vis}= 0.72 and g = 0.38

E. Simulation strategy

To reach a global valuation of the performance of dynamic glazing we followed an ad-hoc simulation strategy based on the implementation and integration of several existing simulation tools, developed by Politecnico of Turin and collaborators [7].
It was based on the following steps:
1. Discretization of the switching range of the dynamic glazing in a number of static states with defined thermo-optical properties. After that an annual simulation is carried out and an annual profile of daylight availability and glare prediction is obtained. In this step different simulation tools are used: *Rhinoceros, Diva4Rhino* plugin, *Grasshopper* and add-on *Honeybee*)
2. The thermo-optical properties of the glass and the annual profiles are imported in *Energy Plus*, and thanks to the implementation of a *EMS (Energy Mangement System)* code an annual simulation is carried out. This follows a decision tree that can use as simultaneous inputs the properties of the glass and visual and energy aspects. The simulation identifies at every timestep the required state of the glazing and carries out an accurate energy simulation and the switching profile of the glazing.
3. Thanks to the switching profile previously obtained the glare and daylight results are calculated with Excel and this allows to obtain Climate-Based Dynamic Metrics.

Data Presentation

In this section the results of the simulations are presented in three main sections: static glazing (selective glazing and the principle state of the electrochromic glass), minimizing load strategies and minimizing glare strategies. For each section the results concerning the tree cities considered are presented.
Visual and energy aspects are often in contrast and they influence each other, so in order to examine all of them at the same time we're going to introduce two particular type of graph. The first graph present the correlation between glare probability and daylight availability: the optimum is on the upper right corner of the graph (DGP always under the disturbance threshold and full daylight availability). The second graph present the correlation between glare probability and Global Energy Performance index. In this case the optimum is on the up-left corner (DGP always under the disturbance threshold and minimum energy consumption).

A. Performance of static glazing properties

As we can see in Fig. 2 both the selective and the electrochromic static glazing delineate a curve shaped line that represent the maximum performance that a static component can reach. This curve is associated with the intrinsic characteristics of the transparent components. From the graph it's clear that glare risk increase with daylight availability and inversely, to avoid glare risk you have to largely sacrifice the entering of daylight. The location of the simulation influence both daylight availability and glare risk; in particular we can see that in Abu Dhabi, due to the fact that the transparent facade is South oriented and the sun almost reach the zenit in its

daily path, there is total absence of glare with a glazing even partially tinted. This means that a control logic suitable for this location doesn't need the use of darker states to avoid glare. The two traditional selective glazing allows a major quantity of daylight to enter, but are very poor in avoiding glare.

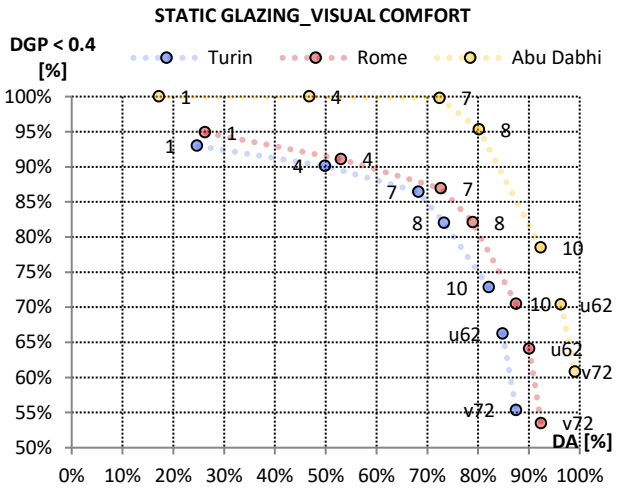

Figure 2. DA and DGP <0.4 correlation for the static glazing

Looking at Fig. 3 we can see that also when we consider energy performance and glare probability the performance of selective glazing form a curve shaped line, that this time has very different trends depending on the location: in the case of Turin we can see that with the darkening of the glass we decrease glare risk but we largely increase energy consumption due to the reduction of solar gains. The traditional selective glazing and the totally bleached state of the EC reach the best performance. In the case of Rome, where heating need and cooling need are more balanced, the best performance is reached by the medium tinted state of EC: moreover, the traditional selective glazing cause consumption similar to medium tinted states, while totally bleached and tinted states causes higher consumptions. This is very important because denotes that these climates are the ones that require more variation of thermo-optical properties of the glazing to adapt to winter and summer season.
In the case of Abu Dhabi static glazing don't define a well-shaped curve: consumption of the darker states are higher than the medium ones because the darkening of the glazing increase the energy need for lighting.

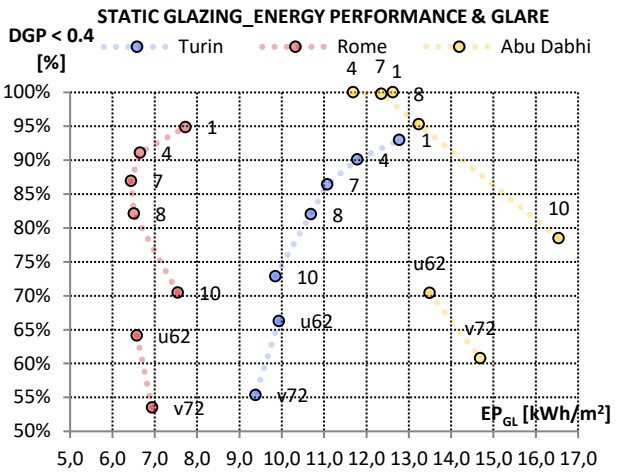

Figure 3. EP_{GL} and DGP <0.4 correlation for the static glazing

B. *Minimizing load strategies (ML)*

As we can see from Fig. 4 the binary strategies aiming to minimize loads have very different results depending on the location considered. In the case of Turin they result less convenient than many static states of the glazing on both visual and energy aspects. In the case of Rome ML strategies slightly improve the performance of the static glazing but almost always just for one aspect.
In the case of Abu Dhabi, were the cooling need is almost always present, to implement this strategy is equivalent to set the glass on the static state chosen as darkening limit.

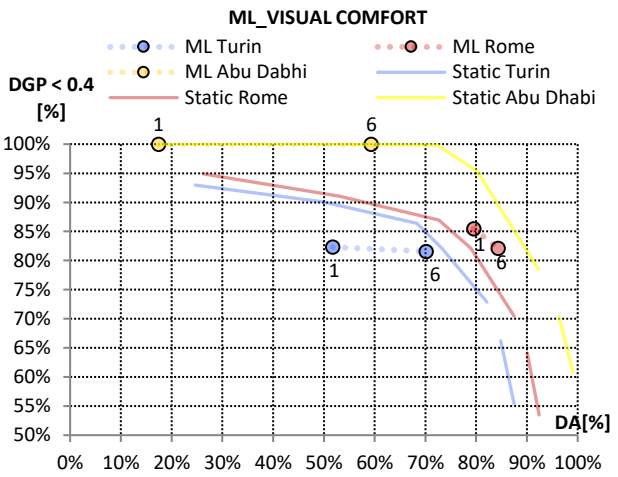

Figure 4. DA and DGP <0.4 correlation for minimizing loads strategies

Analysing Fig. 5 we can see that ML strategies in Turin and Rome are always convenient for at least one aspect between glare probability and energy performance compared to static glazing. In the case of Abu Dhabi, as already noticed in Fig. 4, they are equal to the performance of the static state chosen as darkening limit.

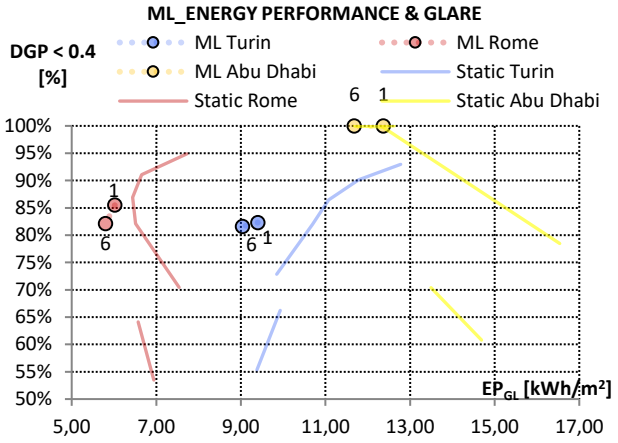

Figure 5. EP_{GL} and DGP <0.4 correlation for minimizing loads strategies

C. *Minimizing glare linear strategies (MG_L) and Venetian blinds (MG_B)*

Talking about visual comfort it is clear that a linear switching of the dynamic transparent components improves the visual results. This is clearly shown in Fig. 6: all the strategies increase glare interdiction compared to the static glazing. We can see once again that the location influences very much the results: all the strategies improve at least one of the two parameters considered and in the case of Rome and Abu Dhabi the related points in the graph are very near to the optimum; In the case of Rome there is a big distance between the points related to MG strategies and the curve of the static glazing, and this is because the strategies are very effective. In the case of Turin and Abu Dhabi we can see a substantial improvement, but the gap between the points and the static curve is shorter.

In some cases MG_L strategies are comparable with strategies that include the use of Venetian blinds (see Turin MG_L_1_w and v72/38_B_I). Blinds are always effective in reducing glare risk and in the case of Abu Dhabi yield better results even from the daylight point of view. Selective glazing u62/30 coupled with blinds is more efficient tahn v72/38 in avoiding glare but not the same talking about daylight. MG_L and MG_B strategies never outperform daylight performance of selective glazing v72/38, but they reach anyway very good results, and simultaneously strongly reduce glare risk in comparison to that.

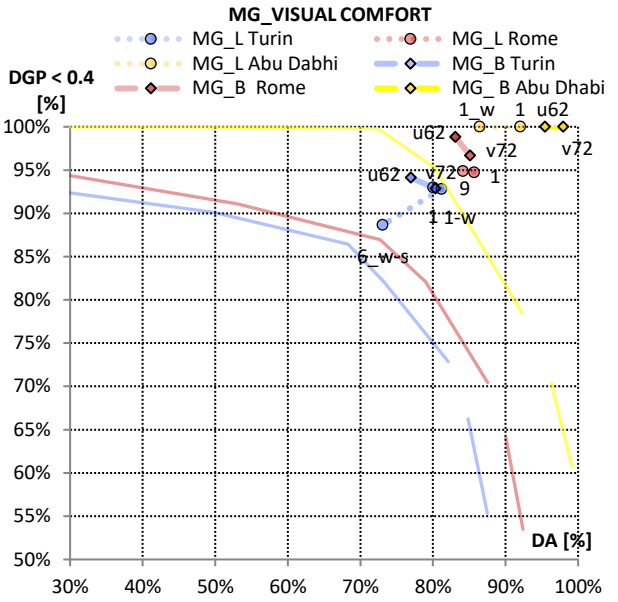

Figure 6. DA and DGP <0.4 correlation for minimizing glare strategies

In Fig. 7 we can see again how the changing of the location deeply influence the energy performance results: the points referring to Rome climate are the nearest to the optimum. However we can notice that in every city - from the energy point of view - some of the MG_L strategies allow to nearly reach the best results of the static glazing. These strategies are the ones modified thanks to a analysis of the location and of the monthly behavior of the visual and energy performance. In the case of Rome MG_B reach better results than both static glazing and MG_L on the visual and energy point of view. In the case of Turin there is a little difference between MG_L and MG_L and each one result convenient from one of the two aspects investigated. In the case of Abu Dhabi MG_L and MG_B strategies make an improvement in comparison to bleached static glazing but they don't if compared to medium tinted states of EC.

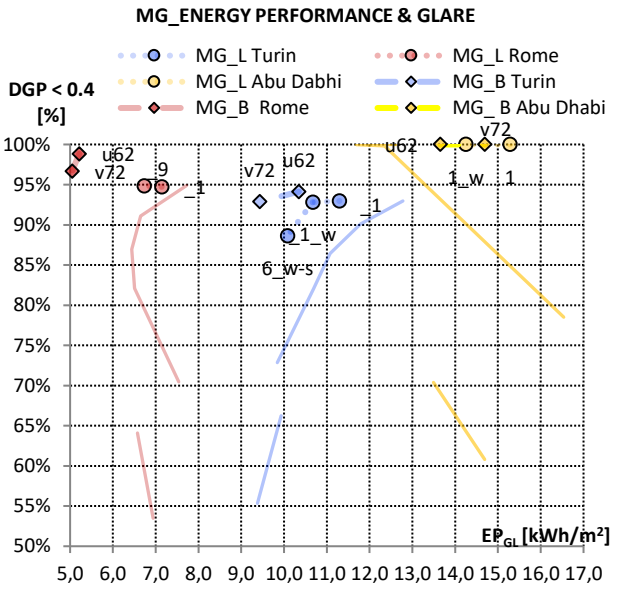

Figure 7. EP_{GL} and DGP <0.4 correlation for minimizing glare strategies

Discussion

Wanting to collect the fundamental observations of the work presented above we can say that:

- The location is fundamental in the choice of the strategy and in its articulation;
- It is therefore necessary to study strategies case by case analysing the external environment;
- To ensure real energy and visual comfort, decision trees can no longer focus on just one goal, but must be able to consider multiple goals simultaneously;
- The minimizing loads strategies extracted from the literature are strongly penalizing from the point of view of the comfort; minimizing glare strategies allow instead to reach absolutely interesting results for both visual comfort and energy performance.
- Tendentially the use of venetian blinds on selective glazing brings the best results on visual and energy aspects, but the use of a minimizing glare strategy with linear switching of the electrochromic component get close to these results without sacrificing the vision of the outside.
- It would be interesting to identify the thresholds of DA and DGP to ensure visual comfort.

Conclusions

This paper collects part of the thesis work developed by the author on the topic of the control of transparent dynamic components. The performance of an electrochromic glazing capable of modifying its thermo-optical properties was analyzed using numerical simulations in comparison with the performance of two high-performance selective glasses. It was also introduced the use of internal and external Venetian blinds applied to selective glazing. The energy and visual results were analyzed by applying this technology to a standard office with a totally transparent window south oriented and analyzed in three different locations: Turin, Rome, Abu Dhabi. The window was alternatively equipped with two selective glazing and with the electrochromic glazing both maintaining static coloring states, and controlled with different startegies based on one or multiple criteria.
The results show that control strategies studied depending on the location and based on multiple objectives allows to obtain better results than traditional static glazing on both the visual and energy aspect. However, it is always necessary to create a hierarchy of objectives that guides the articulation of the control strategy. The considerable change in performance depending on the location shows that it is necessary to develop control logics strongly linked to the context in which they are applied, to avoid the risk of canceling the positive results expected from the application of a dynamic technology.

ACKNOWLEDGEMENT

First of all, I would like to thank the Aicarr association which allowed me to attend to this competition. I would also like to thank the Tebe group of the Polytechnic of Turin, the work team thanks to which the thesis was developed and which was a parameter of comparison and correction along the way. Finally, I thank Valentina Serra, Luigi Giovannini and Fabio Favoino for the great support and professional help always given to the development of this work.

REFERENCES

[1] L. Pérez-Lombard, J. Ortiz, C. Pout, "A review on buildings energy consumption information", *Energy and Buildings,* vol 40, Issue 3, pagg 394-398, 2008.

[2] Hong Ye, Xianchun Meng, Linshuang Long, Bin Xu, "The route to a perfect window", *Renewable Energy*, vol 55, pagg 448-449, 2013.

[3] Favoino F., Fiorito F., Cannavale A., Ranzi G., Overend M., Optimal control and performance of photovoltachromic switchable glazing for building integration in temperate climates, *Applied Energy*, vol 178, pagg 943–961, 2016.

[4] Giovannini L, Serra V, Lo Verso VRM, Pellegrino A, Zinzi M, Favoino F. A novel methodology to optimize visual comfort and energy performance for transparent adaptive façades, "*Proceedings of the 18th International Conference on Environment and Electrical Engineering (IEEE EEEIC)*", 12th – 15th June 2018, Palermo, Italy. in press on IEEE XPlore digital library, June 2018.

[5] Wienold, J. and Christoffersen, J., 2006. Evaluation methods and development of a new glare prediction model for daylight environments with the use of CCD cameras. *Energy and Buildings*, 38(7): 743-757, Wienold, 2006.

[6] Wienold, J., 2009. Dynamic daylight glare evaluation. "*Proceedings of the 11th International IBPSA (International Building Performance Simulation Association) Conference – Building Simulation",* Glasgow, Scotland, 944-951, 2009.

[7] Reinhart C. F., Mardaljevic J. & Rogers Z., Dynamic Daylight Performance Metrics for Sustainable Building Design, *"LEUKOS",* 3:1, 7-31, 2006

[8] M. Baracani, L. Giovannini, V. Serra, F. Favoino, Control of dynamic glazing in heating dominated climate for office buildings: contrasting occuopant visual comfort requirements with energy use, *"51th AiCARR Int. Conf. - Hum. Dimens. Build. Energy Perform."*, Associazione Italiana Condizionamento dell'Aria Riscaldamento e Refrigerazione (AiCARR), Venice, Italy, 20-22 February 2019.

Event Pictures

The REHVA Community of Young Professionals brings together participants from past editions of the student competitions to share knowledge and best practices.

This Book of Papers aims at concentrating the knowledge of each edition of the competition and serves to commemorate the occasion.

REHVA warmly thanks all the people involved in the organization of, and participation to, the events.

Join the discussion on the @RCYP Linkedin group!